PRELIMINARY INVESTIGATION INTO THE USE OF GAS HYDRATE TECHNOLOGY FOR THE TREATMENT OF VINASSE

By

Nadia Croeser

BSc. Eng. (Chemical)

University of KwaZulu-Natal

This dissertation is submitted in fulfilment of the academic requirements for the degree of Master of Science in Engineering (Chemical) at the School of Engineering, University of KwaZulu-Natal

Supervisor: Prof. Paramespri Naidoo

Co-Supervisors: Prof. Deresh Ramjugernath, Prof. Amir H. Mohammadi, and Dr. Wayne Nelson

May 2017

DECLARATION

I, Nadia Croeser, declare that:

(i)   The research reported in this thesis, except where otherwise indicated, and is my original work.

(ii)   This thesis has not been submitted for any degree or examination at any other university.

(iii)   This thesis does not contain other persons' data, pictures, graphs or other information, unless specifically acknowledged as being sourced from other persons.

(iv)   This thesis does not contain other persons' writing, unless specifically acknowledged as being sourced from other researchers. Where other written sources have been quoted, then: a) their words have been re-written but the general information attributed to them has been referenced; b) where their exact words have been used, their writing has been placed inside quotation marks, and referenced.

(v)   Where I have reproduced a publication of which I am an author, co-author or editor, I have indicated in detail which part of the publication was actually written by myself alone and have fully referenced such publications.

(vi)   This thesis does not contain text, graphics or tables copied and pasted from the Internet, unless specifically acknowledged, and the source being detailed in the thesis and in the References sections.

_____   _____

Nadia Croeser   Date

As the candidate's supervisors I agree/do not agree to the submission of this thesis.

_____   _____

Prof. Paramespri Naidoo   Date

_____   _____

Prof. Deresh Ramjugernath   Date

_____   _____

Prof. Amir H. Mohammadi   Date

_____   _____

Dr. Wayne Nelson   Date

ABSTRACT

Worldwide, sugar based industries are moving towards an integrated biorefinery approach where sugarcane is viewed as a source of biomass that can be processed to produce multiple value-added chemical and energy related products, in order to generate additional revenue and maintain profitability. A key hurdle limiting the potential of South African sugar companies from taking advantage of the bioethanol opportunity is the safe and cost-effective handling and disposal of the high strength wastewater, termed vinasse. One of the challenges associated with vinasse is the very high concentration of dissolved solids, largely in the form of potassium salts. Desalination technologies can be employed in the separation of salts from high salinity wastewaters such as vinasse to produce purified water, however, traditional desalination technologies such as evaporation and distillation are energy intensive. The application of a novel technology known as gas hydrate technology can make the process of desalination less energy intensive. This study investigates gas hydrate technology as possible desalination for the treatment of vinasse.

Gas hydrates, or clathrate hydrates, are non-stoichiometric crystalline structures that are formed through the combination of water, known as the host molecules, and gas molecules, known as the former (or guest molecules), under suitable conditions of temperature and pressure. Gas hydrates are considered a nuisance in the petroleum industry due to the problems they cause with the blockage of pipelines, but they have the potential for positive application in various engineering fields such as gas separation, carbon dioxide sequestration, gas storage and transportation as well as seawater and industrial wastewater desalination.

The objective of the research is to obtain hydrate dissociation data for systems representative of vinasse, with a suitable former. The criteria for choosing the most suitable former include the former to be: environmental acceptable, non-toxic, non-flammable, chemically stable, compatible with standard materials, available, low cost compared to other hydrate formers, and have suitable operating conditions of temperature and pressure. Taking the above criteria into account, carbon dioxide was chosen as the most suitable hydrate former for application in this research.

The hydrate-liquid-vapour (HLV) phase equilibrium measurements were performed in a static high-pressure stainless steel equilibrium cell, using the isochoric pressure search experimental method. The combined expanded uncertainties for the 0 - 10 MPa pressure transducer and the Pt-100 temperature probe are $\pm$ 0.01 MPa and $\pm$ 0.1 K respectively. The experimental apparatus, technique and calibrations were verified by conducting HLV equilibrium measurements on known test systems. These include the CO_2 (1) + water (2), CO_2 (1) + water (2) + 5 wt % NaCl (3), CO_2 (1) + water (2) +

5 wt % KCl (3) and CO_2 (1) + water (2) + 5 wt % NaCl (3) + 5 wt % KCl (4) system. New systems measured include the CO_2 (1) + water (2) + 5 wt % Na_2SO_4 (3), CO_2 (1) + water (2) + 5 wt % KCl (3) + 5 wt % Na_2SO_4, (4), CO_2 (1) + water (2) + mixed salts A (3), CO_2 (1) + water (2) + mixed salts B, and CO_2 (1) + water (2) + synthesised vinasse (3) system. The salt mixtures termed *mixed salts A* and *mixed salts B* contained [3 or 5] wt % KCl + 1 wt % Na_2SO_4 + 0.5 wt % $MgCl_2$ + 0.5 wt % $CaCl_2$. The *synthesized vinasse* sample contained 5 wt % KCl + 1 wt % Na_2SO_4 + 0.5 wt % $MgCl_2$ + 0.5 wt % $CaCl_2$ + 2.2 wt % ethanol + 0.5 wt % propionic acid + 0.3 wt % acetic acid.

For the measurements performed in this study, it was found that the presence of salts and organic components, such as ethanol and acetic acid, exhibit an inhibition effect on the formation of gas hydrates. This was seen by the shift of the HLV equilibrium phase boundary to a lower temperature or higher pressure. The average temperature shifts, from the CO2 (1) + water (2) system, for the new systems measured were: -0.9 K for the 5 wt % Na_2SO_4 system, -2.9 K for the 5 wt % KCl + 5 wt % Na_2SO_4 system, -1.9 K for the *mixed salt A* system, -2.4 K for the *mixed salt B* system, and -3.4 K for the *synthesized vinasse* system.

The solid solution theory of van der Waals and Platteeuw (vdW-P) (Van der Waals and Platteeuw, 1959) was used to model the hydrate phase. The Peng-Robinson-Stryjek-Vera (1986) equation of state (PRSV EOS) with the classical mixing rule was used to describe the fluid phases. The model developed by Aasberg-Petersen et al. (1991) was used to account for the salts present in the system as well as for the solubility of carbon dioxide in the aqueous electrolyte solutions. In the Aasberg-Peterson model (Aasberg-Peterson et al., 1991), the aqueous phase was first treated as a salt-free mixture and the PRSV EOS was used to determine the fugacity coefficient. The calculated fugacity coefficient was than corrected with the Debye-Hückel electrostatic term. The water-salt interaction coefficients were accounted for using the parameters reported by Tohidi et al. (1995). The experimental data compared well to the predicted data.

A process for the desalination of vinasse using gas hydrate technology is presented. This is based on the proposed process of Javanmardi and Moshfeghian (2003) which was first presented by Knox et al. (1961). An approximate cost analysis for the proposed process was conducted. The shortcut method put forward by Douglas (1988) was used to perform the economic evaluation which involved determining the total capital investment. This was dependent on the total sum of the installed equipment cost as well as the operation and maintenance cost. The cost correlations proposed by Guthrie (1969) were used to determine the installed equipment costs. The results of the economic analysis, based on a 2012 basis, indicated a total product cost of $ 6.09/ton for the proposed process, which is higher than total product cost for multi-stage flash distillation, multi-effect distillation and

reverse osmosis. The final products of hydrate-based desalination are concentrated brine and potable water. Possible uses and disposal options for the concentrated brine and potable water are outlined.

In order for hydrate-based treatment technologies to be implemented into industry, crystal size and quality of the gas hydrates need to be determined. Therefore, investigations regarding such properties should be conducted. Possible methods for such investigations include Spectroscopy, X-ray Diffraction and Laser Scattering. In addition, techniques to determine the concentration of the final solution, such as centrifugation of the hydrate slurry, need to be established.

ACKNOWLEDGEMENTS

TABLE OF CONTENTS

LIST OF FIGURES

LIST OF PHOTOGRAPHS

LIST OF TABLES

NOMENCLATURE

a	Attractive volume parameter
a_w	Activity of water
A	Area
Å	Angstrőm unit
A_{mj}	Fitted constant for component j in cavity m (K)
A_p	Hydrate surface area per particle
b	Excluded volume parameter
B_{mj}	Fitted constant for component j in cavity m (K)
°C	Degree Celsius
C_{mj}	Langmuir constant for component j in cavity m
C_p	Heat capacity (J/mol.K)
d	Density
f	Fugacity
F	Degrees of freedom
G	Gibbs free energy
h	Enthalpy
h_{ws}	Interaction coefficient between dissolved salt and non-electrolyte component
I	Ionic strength
k	Boltzmann's constant
k_{ij}	Binary interaction coefficient
K	Kelvin
K*	Combined rate constant (m/s)
K_d	Dissociation rate constant
M_m	Salt-free mixture molecular weight
N	Number of species
P	Pressure (MPa)
Q	Quadruple point
Q_t	Quintuple point
r	Core radius (m)
R	Universal Gas Constant (J/mol.K)
$\bar{R}$	Average radius of cavity
S_i	Ionic strength fraction of electrolyte i
t	Time
T	Temperature (K)

u_c	Combined standard uncertainty
u_i	Standard uncertainty
U	Combined expanded uncertainty
v	Molar volume
W	Weight
w(r)	Spherically symmetric cell potential (J)
x	Liquid mole fraction
x_N	Salt free mole fraction
y	Gas mole fraction
Z	Coordination number of each cavity

Symbols

Δ	Delta/Change

Greek Letters

α	Stryjek-Vera temperature dependency
β	Interaction energy parameter
ε_m	Salt free mixture dielectric constant
ε_N	Dielectric constant of water
γ	Activity coefficient
γ_i	Water-free mole fractions of component i
μ	Chemical potential (J/mol)
π	Number of phases
∅	Fugacity coefficient
θ_m	Fraction of the type m cavities
ν_m	Number of cavities of type m
ω	Acentric factor

Subscripts

A	Component A
B	Component B
b	Bulk
c	Critical
eq	Equilibrium
F	Former
g	Gas

HC	Hydrocarbon
i	substance
mix	Mixture
P	Particle
tr, H_2O	Triple point of water
w	Water

Superscripts

α	Pure water
β	Empty hydrate
a	Additive
A-P	Aasberg-Peterson
EL	Electrolyte
EOS	Equation of state
H	Hydrate
i	adjustable parameter
k	Number of coexisting phases
L	Liquid
MT	Hypothetical empty hydrate
N	Integer
V	Vapour
o	Reference point

Abbreviations

AA	Anti-agglomerates
AC	Activated carbon
%AAD	Percent absolute average deviation
%AADp	Percent absolute average deviation on pressure measurement
bhp	Brake horse power
BOD	Biochemical oxygen demand
COD	Chemical oxygen demand
CMS	Concentrated molasses solids
DSC	Differential scanning calorimetry
DTA	Differential thermal analysis
EOS	Equation of state
GWP	Global warming potential
H	Hydrate

HLV	Hydrate-liquid-vapour
HVOS	Huron-Vidal-Orbey-Sandler
I	Ice
KI	Kinetic inhibitors
L	Liquid
LDHI	Low dosage hydrate inhibitors
LTX	Low temperature extraction
MED	Multi-effect distillation
MD	Membrane distillation
MW	Molecular weight
MM	Million
MOC	Material of construction
M&S	Marshall and Swift cost index
MSF	Multi-stage flash distillation
NGH	Natural gas hydrate
NIST	National Institute of Standards and Technology
NDD	Non-density dependent
ODP	Ozone depletion potential
O&M	Operational and maintenance
PR	Peng-Robinson
PRSV	Peng-Robinson-Stryjek-Vera
PT	Patel and Teja
PTFE	Polytetrafluoroethylene
QCM	Quartz crystal microbalance
R&D	Research and development
RO	Reverse osmosis
rpm	Revolutions per minute
sI	Structure I
sII	Structure II
sH	Structure H
SMRI	Sugar Milling Research Institute
SRK	Soave-Redlich-Kwong
Std	Standard
STEP-Bio	Sugarcane Technology Enabling Programme for Bio-Energy
TDS	Total dissolved solids
TRU	Thermodynamics Research Unit
TSS	Total suspended solids

US	United States
V	Vapour
vdW-P	van der Waals and Platteeuw
VLE	Vapour-liquid equilibrium
VLSE	Vapour-liquid-solid equilibrium
VPT	Valderrama modification of the Patel and Teja equation of state
wt	Weight

<div align="right">

1

</div>

<div align="right">

CHAPTER ONE

</div>

INTRODUCTION

The South African sugar industry is both a strategically important agro-processing industry and one of the world's leading producers of high quality sugar (Phillips, 2011; SMRI, 2014). It is however a mature industry showing signs of decline, and it is facing a changing and increasingly competitive marketplace (SMRI, 2014).

In the recent past, there has been a discernible decline in sugarcane production in South Africa. Unfavourable weather conditions, economic factors such as poor return on investment, rising costs, and high fertilizer prices as well as socio-political factors such as urban development in the coastal regions, land claims, and unsuccessful land reform projects have all contributed. Furthermore, the industry suffers from the disorder of the world sugar market conditions, which stem from subsidy-induced overproduction, high tariffs and preferential trade agreements between the major sugar producing countries (Parker, 2009; Phillips, 2011).

It has become clear that in order for the sugar industry to remain competitive and sustainable into the future, *breakthrough and disruptive technologies* are required. The industry has already broadly identified how this can be achieved. It will be necessary to both reduce costs and improve profitability by means of novel processing technologies and strategies, and to generate additional revenue streams through adoption of an integrated biorefinery approach.

In 2014, in an effort to achieve the required change, the South African sugarcane processing industry and the Department of Science and Technology's Innovation Partnership Initiative established the Sugarcane Technology Enabling Programme for Bio-Energy (STEP-Bio). The basis of the STEP-Bio

programme was to explore opportunities for additional revenue generation. The major objectives of the STEP-Bio programme were to (SMRI, 2014):

1. Significantly increase sugarcane processing research and development (R&D) in South Africa;
2. Ensure that R&D is aligned with the industry's strategic objectives;
3. Create a sugarcane biorefinery research unit in KwaZulu-Natal;
4. Fund research in sugarcane processing;
5. Facilitate a technologically advanced agro-processing industry and;
6. Increase the industry's overall competitiveness.

Global trends indicate that sugar industries are addressing sustainability by moving away from only producing sugar, to having three revenue streams (sugar, electricity and bioethanol) (SMRI, 2014). For the South African sugar industry to maximise its competitiveness, it also needs to develop new sugar-based products, such as electricity and bioethanol. But, any such interventions have their associated by-products/waste streams. These, in turn, need to be investigated for further potential beneficiation and environmentally friendly disposal. To this end, the treatment and beneficiation of vinasse, the waste stream (effluent) from bioethanol production, forms the focus of this investigation.

There are currently three bioethanol distilleries in South Africa: the Glendale Distilling Co., situated in the Umvoti River valley in northern KwaZulu-Natal, Illovo Sugar SA - Merebank plant, and NCP Alcohols, both situated in Durban, KwaZulu-Natal. Some of the vinasse produced at these three facilities is used for the production of concentrated molasses solubles, and the remainder is sent to the municipal wastewater works for treatment (Zulu, 2016). With a potential drive towards the production of bioethanol, the problem of how to treat and dispose of increasing quantities of vinasse will become increasingly important.

There are considerable technical challenges associated with the treatment of vinasse. The solution applied in many cane-growing countries that produce bioethanol is to distribute the vinasse back into the cane fields during irrigation, or to pump it directly out to sea. For various environmental, technical, and economic reasons these are not viable options in many parts of the South African sugarcane-growing region and alternative solutions must be sought. While there are a number of technology vendors that are able to supply equipment for the treatment of vinasse (SMRI, 2014), the general view is that none of the options provide a universal solution. Furthermore, the design of the vinasse management system is viewed as the bottleneck in the design of new facilitates for the production of bioethanol.

Vinasse does however have significant revenue generating opportunities as it contains high concentrations of dissolved solids, largely in the form of potassium salts. Annually, South Africa spends approximately R 0.5 billion (SMRI, 2014) on importing potassium based fertilizer for sugarcane cultivation. This potassium can potentially be recovered from the effluent for reuse in sugarcane cultivation.

1.1 Background into vinasse

Vinasse, also referred to as stillage, is the aqueous by-product generated during the production of bioethanol. For each litre of bioethanol produced, between 9 and 20 L of vinasse may be generated (Wilkie et al 2010; España-Gamboa et al., 2011; Ortegón et al., 2016).

Bioethanol may be produced from a wide range of feedstocks. These feedstocks include sugar-based, starch-based, and cellulose-based materials. Sugar-based feedstocks include sugarcane juice, cane molasses, and beet molasses, and fruit crops such as grapes. These feedstocks contain readily available fermentable sugars and are therefore the most easily fermented feedstocks. Grains, such as corn and rice; and root crops such as potatoes and cassava are examples of starch-based feedstocks. Cellulose-based feedstocks include biomass, industrial waste, and municipal solid waste. Starch-based and cellulose-based feedstocks require a pre-treatment step in order to convert the starch and cellulose to fermentable sugars. The processes applied to the various feedstocks used in the fermentation and distillation steps of bioethanol production yield vinasse with differing physico-chemical compositions.

The use of sugarcane for direct conversion into bioethanol has been limited. This is due to the relatively high market value of sugar. Cane molasses, a by-product of the sugar production process, is therefore the most commonly-used sugar-based feedstock for the production of bioethanol (Wilkie et al., 2000). This research is focused on vinasse derived from sugarcane molasses. The reader is referred to the works of Wilkie et al. (2000) and España-Gamboa et al. (2011) for further information regards the various types of vinasse.

1.1.1 The production of bioethanol and generation of vinasse.

The production of bioethanol using cane molasses as the feedstock is carried out via four key steps: feed preparation, fermentation, distillation, and packaging (Satyawali and Balakrishnan, 2008). Figure 1-1 provides a process description of bioethanol production from sugarcane molasses.
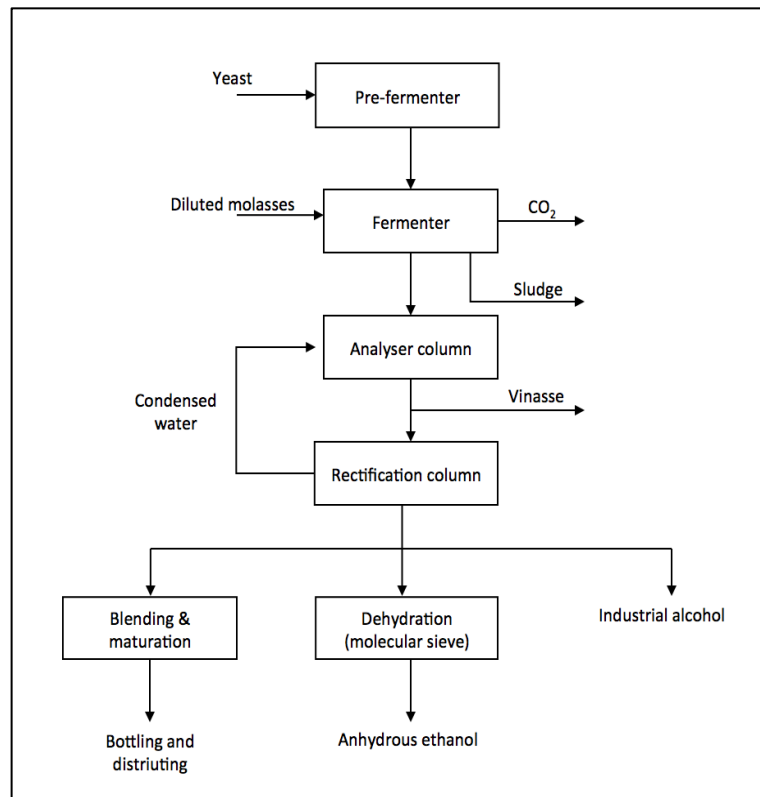
Figure 1-1: Process description of bioethanol production from sugarcane molasses (Satyawali and Balakrishnan, 2008).

As previously mentioned, cane molasses contains readily available fermentable sugars and does not require a pre-treatment step. Firstly, the cane molasses is diluted to 20-25 brix and, if required, the pH adjusted before fermentation (Satyawali and Balakrishnan, 2008). In the fermentation step, the sugars are converted into bioethanol and carbon dioxide by means of yeasts. The process is usually operated in batch mode, however, continuous mode may be adopted (Prasad et al., 2007).

In a conventional batch process a yeast culture is prepared and propagated in a series of pre-fermenters. An inoculum of the yeast culture is added to the feed. Fermentation occurs over 24 - 36 h with an efficiency of 95 % (Satyawali and Balakrishnan, 2008). The resulting fermentation broth contains 6 - 8 % alcohol. Through settling, the sludge (mainly yeast cells), is separated and discharged from the bottom of the fermenter, and the fermented broth (free from yeast cells) is sent for distillation. Fermentation is an anaerobic process that is carried out under controlled conditions of temperature and pH. The reaction is exothermic. Plate heat exchangers are used to maintain the temperature at approximately 25 - 32℃. Several organisms have been proposed for use in the fermentation step. Different strains of the yeast, *Saccharomyces cerevisiae*, are most widely used due to their robust growth rate and high tolerance to ethanol (Wilkie et al., 2000; Satyawali and Balakrishnan, 2008).

The distillation stage involves a two-stage process. An analyser column is used for the first stage, and the second, a rectification column. The fermentation broth is preheated to 90 ℃. Thereafter it is sent to the degasifying section of the analyser column where the broth is heated by live steam, and fractionated to produce 40 - 45 % alcohol. The bottom discharge from the analyser column is the effluent, vinasse. The ethanol-enriched vapours are led to the rectification column. In the rectification column, by reflux action, 96 % alcohol is obtained, cooled, and collected (Satyawali and Balakrishnan, 2008). The condensed water from the rectification column is pumped back to the analyser column.

The collected ethanol can be used in the production of chemicals such as acetic acid, acetone and oxalic acid; modified by the addition of other substances (denaturants), to produce denatured ethanol, or blended with other forms of alcohol, such as malt alcohol, to attain a desired type of liquor (Satyawali and Balakrishnan, 2008).

1.1.2 Characterisation of vinasse derived from sugarcane molasses

Before it can be treated, it is important to ascertain the characteristics and composition of the stream that requires treatment. The characteristics of vinasse are extremely variable and complex and are dependent on the feedstock used for the production of bioethanol. The soil characteristics, variety of sugar cane, period of harvest, and the industrial process used for the production of bioethanol, will also impact the composition of vinasse (Wilkie et al., 2000; Salomon and Lora, 2009; España-Gamboa et al., 2011; Christofoletti et al., 2013). The wash water used to clean fermenters, as well as the cooling and boiler water blow down may be combined with the vinasse, contributing to its variability (Wilkie et al., 2000).

Molasses contains a variety of chemical constituents which include cations such as Ca^{2+}, Mg^{2+}, and K^+, anions such as sulphates, phosphates, chlorides, and a variety of organic components such as sucrose, glucose, fructose, and acids (Bernhardt, 1998). It is estimated that during the production of bioethanol, approximately 88 % of constituents in molasses end up in vinasse (Jain et al., 2002).

In general, vinasse which is derived from molasses is essentially a mixture of water and inorganic and organic compounds. It is strongly acidic (pH: 3.5 - 5) and dark brown in colour (España-Gamboa et al., 2011), with a total solids concentration between 5 - 10 % (Christofoletti et al., 2013; Vadivel et al., 2014; Ortegón et al., 2016). It has high levels of biochemical oxygen demand (BOD), and chemical oxygen demand (COD) (Satyawali and Balakrishnan, 2008; España-Gamboa et al., 2011). Due to the components present in molasses, vinasse contains a variety of chemical constituents in the form of ions, such as potassium (high levels), calcium, magnesium, sulphate, and chlorides; and low

molecular weight (MW) compounds such as lactic acid, glycerol, ethanol, and acetic acid (Wilkie et al., 2000).

As a result of the nutrient intake from the soil during the growing season, vinasse contains low levels of nitrogen and phosphorus as well as trace elements such as iron, zinc, and copper. Furthermore, vinasse contains 2 % melanoidins. Melanoidins are dark brown, high MW polymers which provide vinasse with its characteristic dark colour (Kalavathi et al., 2001). Melanoidins are one of the final products of the Maillard reaction; a non-enzymatic browning reaction resulting from the reaction of reducing sugars and amino compounds (Martins and Van Boekel, 2005).

Table 1-1 presents some of the main parameters that define the chemical composition of sugarcane molasses derived vinasse. An illustration of the variation of sugarcane molasses derived vinasse from various origins was presented by Cortez and Brossard Pérez (1997), and can be seen in Table 1-2. A more comprehensive literature survey on the characterisation of vinasse is presented in Table A-1 of Appendix A.1.

Table 1-1: Composition and yield of vinasse derived from sugar cane molasses (Salomon and Lora, 2009).

Parameter	Unit	Range
pH	-	4.46 - 4.8
BOD	$g.L^{-1}$	39.5
COD	$g.L^{-1}$	48.9 - 95
Nitrogen	$mg.L^{-1}$	153 - 1230
Phosphorus	$mg.L^{-1}$	1 - 190
Potassium	$mg.L^{-1}$	4893 - 11000
Sulphur	$mg.L^{-1}$	1500 - 3480
Copper	$mg.L^{-1}$	0.27 - 1.71
Cadmium	$mg.L^{-1}$	0.04 - 1.36
Lead	$mg.L^{-1}$	0.02 - 0.48
Iron	$mg.L^{-1}$	12.8 - 157.5
Phenols	$mg.L^{-1}$	34
Vinasse yield	$LL_{ethanol}^{-1}$	12 - 20

Table 1-2: Comparative composition of vinasse derived from sugar cane molasses from different origins (Cortez and Brossard Pérez, 1997).

	Unit	Brazil	Australia	Australia	India	USA
Potassium	$mg.L^{-1}$	4893	8767	10704	4078	9073
Phosphorous	$mg.L^{-1}$	102	20	12	5097	1
Nitrogen	$mg.L^{-1}$	408	3160	1835	1019	153
Calcium	$mg.L^{-1}$	714	1121	2039	n.a	143
Magnesium	$mg.L^{-1}$	204	1529	1325	n.a	61
Ash	$mg.L^{-1}$	19879	32622	n.a	n.a	50972
Organic solids	$mg.L^{-1}$	47200	n.a	n.a	n.a	n.a
Total solids	$mg.L^{-1}$	n.a	n.a	91750	69322	n.a
pH	-	4.8	n.a	n.a	4.3	4.5

n.a: not available

1.1.3 Environmental issues of vinasse

Vinasse has an extremely high polluting ratio: 100 times more powerful than domestic sewage (Salomon and Lora, 2009); and its direct disposal into the environment can be extremely hazardous to both soil and underground water. The high levels of organic content and dissolved solids in vinasse are not only toxic, but under certain conditions can become contaminants. Vinasse also contains phytotoxic, antibacterial, and recalcitrant compounds, such as phenols, which have an adverse effect on the plants and microorganisms at disposal sites (España-Gamboa et al., 2011).

If discharged untreated to surface water, the melanoidins present in vinasse lead to a reduction in the sunlight penetration in rivers, lakes, and lagoons that reduce the photosynthesis activity and dissolved oxygen concentration, which results in hazardous conditions for aquatic life (Prasad and Srivastava, 2009). The high nutrient and organic content of vinasse may result in eutrophication of water bodies, leading to undesirable changes in the ecosystem.

The uncontrolled disposal of vinasse on land may be hazardous to vegetation if applied above the recommended limits and can reduce the soil alkalinity and manganese availability, thus inhibiting seed germination (Kumar et al., 1997; Meyer et al., 2016). In addition, land availability, odour generation, and putrefaction are associated problems with direct land disposal.

1.1.4 Current methods of vinasse treatment

Numerous treatment technologies have been explored to reduce the contaminating characteristics of vinasse. In some countries, such as Brazil, vinasse is applied directly to the soil as a fertilizer and potassium source. Due to the environmental concerns outlined in section 1.1.3, for this practice to be carried out successfully, without adverse environmental effects, necessary analysis of the soil characteristics is performed so that the appropriate amount is used. Meyer et al. (2016) recently reviewed past research on the impact that vinasse disposal has on sugarcane yield, soil properties, and the environment and proposed a soil property matrix that could be utilized to classify the potential suitability of applying vinasse and condensed molasses solubles (CMS) to fields under Southern, Central and East African irrigated conditions. The authors concluded that the proposed soil property matrix will enable distillers to select fields that are best suited for vinasse and CMS treatment and to asses the long-term effects on soil, crop and environmental quality as a result of repeated application. In addition, Meyer et al. (2016) concluded that the suitable rate of vinasse and CMS application to fields depends on the potassium content of the vinasse and CMS as well as the standard rate of potassium for the particular field concerned.

Deep well disposal is a possible option, however this alternative is limited due to the availability of underground storage as well as specific geological location. Other disposal methods, such as evaporation of vinasse to produce animal feed additives, and incineration of vinasse for potash recovery, have been explored (Wilkie et al., 2000).

Biological treatment has been recognized as an effective method for dealing with high concentration industrial wastewaters, such as vinasse. Anaerobic, aerobic systems, or a combination of both, are often employed. Anaerobic treatment is usually the first step, as it has been proved the most effective at lowering the contaminant compounds (Pant and Adholeya, 2007; Satyawali and Balakrishnan, 2008; Mohana et al., 2009). Anaerobic treatment, using different high-speed reactors, has been used on a pilot scale and full-scale operation. Aerobic treatments, using different microbes such as fungi and bacteria, have also been explored. Various physico-chemical methods, such as adsorption, coagulation-flocculation, and oxidation processes have also been tried for the treatment of vinasse.

Aerobic and physico-chemical processes perform well as post-treatment options following anaerobic treatment (Prasad and Srivastava, 2009; Mohana et al., 2009; España-Gamboa et al., 2011) and have proven the most suitable as the first and only treatment step when vinasse is diluted (Sreethawong and Chavadej, 2008; Prasad and Srivastava, 2009).

The individual use of only one of the aerobic, anaerobic or physico-chemical method tends to not result in satisfactory treatment of vinasse. Often a two or three part treatment process, using a combination of aerobic, anaerobic and physico-chemical methods would be employed. The final treatment method used is dependent not only on the characteristics and quantity of the vinasse but also on the intended post treatment disposal location.

These three treatment methods are discussed, in detail, in Appendix A.2. Instances where the different treatment methods have been applied, as well as the level of treatment achieved, is also presented. The reader is referred to the articles by Pant and Adholeya (2007), Satyawali and Balakrishnan (2008), Mohana et al. (2009), and España-Gamboa et al. (2011) for a more detailed review of the methods employed for the treatment of molasses derived vinasse, as well as of vinasse derived from other feedstocks.

There are various associated disadvantages with the treatment methods listed above such as excess use of chemicals, sludge generation with subsequent disposal concerns, high operational costs, as well as variable water input (Pant and Adholeya, 2007; Satyawali and Balakrishnan, 2008; Mohana et al., 2009). In addition, these treatment methods are concerned only with the reduction of organic load and colour. Even after primary and secondary treatment, the vinasse still contains considerable amounts of dissolved solids, in the form of salts.

This study set out to investigate a feasible method for the treatment of vinasse and the recovery of salts for potential reuse in the fertilizer industry. Due to the nature of vinasse (high levels of organic content and dissolved solids) and the desired outcome of the treatment (salt recovery), the method would fall in the physico-chemical treatment category. As a result, desalination of previously treated vinasse (either anaerobic or aerobic methods) by means of gas hydrate technology is proposed.

Gas hydrate technology is not a new processing technique. One of the first processes for desalination (of seawater) through gas hydrate technology was investigated in 1961 by Knox et al. (Knox et al., 1961). A considerable amount of research has been undertaken since then in order to improve the technology. Gas hydrate based desalination is promising because of its potential lower energy requirements, compared to processes such as evaporation and distillation (Sloan and Koh, 2008).

In this study, in order to ascertain the suitability of hydrate-based technology for application in vinasse desalination, hydrate dissociation conditions of temperature and pressure were first measured. These measurements were performed on single salt systems, mixed salt systems and on solutions representative of vinasse. The experimental results were reproduced using appropriate thermodynamic methods. Thereafter, an economic and feasibility study, which included a preliminary design, was conducted in order to determine the feasibility of implementing the treatment technology, in the sugar industry, for the treatment of vinasse.

But what is gas hydrates and how can they be applied in the desalination of vinasse? In this dissertation the second chapter introduces the reader to gas hydrates. This includes a brief description of gas hydrates; their classification and molecular structure; the formation and dissociation of gas hydrates; the phase behaviour of hydrate forming systems; the role of hydrate formers, inhibitors and promoters, and, finally; the industrial application of gas hydrates, with emphasis placed on gas hydrate based desalination.

The fundamentals of phase equilibrium and the thermodynamic modelling of the phases in a hydrate forming system are considered and discussed in chapter three.

In chapter four, the experimental methods for measuring gas hydrate dissociation conditions are discussed. These methods include the isobaric temperature search method, the isothermal pressure search method, and the isochoric pressure search method. In addition, the different types of equipment that can be used for conducting hydrate measurements are presented.

In chapter five, the experimental setup and technique, based on the isochoric pressure search method, is described. In addition, calibration results for testing the reliability of the experimental method are presented.

The results are presented and discussed in chapter six. This includes the experimental results, the results of the thermodynamic modelling, and the results of the feasibility study.

The conclusions of the study are presented in chapter seven and finally recommendations are offered in chapter eight.

<div align="right">

2

</div>

<div align="right">

CHAPTER TWO

</div>

REVIEW OF HYDRATE LITERATURE

Gas hydrates or clathrate hydrates are non-stoichiometric crystalline solid structures consisting of water and smaller molecules such as CO_2, N_2, CH_4, etc. that are formed under suitable conditions of low temperature and (generally) high pressure (Sloan and Koh, 2008; Carroll, 2014). These small molecules are referred to as guest molecules or formers. Gas hydrates are a subset of inclusion compounds and during their formation the water molecules, through hydrogen bonding, link together to form a cavity that physically entraps, without the aid of any chemical bonding, the guest molecule. Van der Waals forces exist between the water and the guest molecule, which ensures hydrate stability.

Hydrate structures were first discovered by Sir Humphry Davy and later confirmed by Michael Faraday in the 19th century (Englezos, 1993; Sloan and Koh, 2008). Throughout the 19th Century, the interest in hydrates remained purely academic and researchers focused their efforts on identifying the compounds required, and the conditions, for hydrate formation. Today there are more than 130 known species capable of hydrate formation (Sloan and Koh, 2008). The industrial significance of hydrates was demonstrated in the 20th Century (Sloan and Koh, 2008; Carroll, 2014) when it was discovered that the plugging of natural gas pipelines was due to the formation of hydrate plugs rather than the formation of ice (Hammerschmidt, 1934; Sloan and Koh, 2008). Even though gas hydrate formation has negative implications in the petroleum and gas industry, they have the potential for beneficial application in numerous technologies such as: CO_2 capture and sequestration (Lee et al., 2003), storage and transportation of gas (Sloan, 2000), concentration of dilute aqueous solutions (Li et al., 2015), separation of different gases from their corresponding gas mixtures (such as flue gas streams) (Tajima et al., 2004; Naeiji et al., 2014), and, for the purpose of this dissertation, desalination of

industrial wastewaters and seawater (Gaarder, 1993; McCormack and Andersen, 1995; Park et al., 2011). Gas hydrates have also been discovered in vast quantities in the earth's crust and thus have the potential for use as an energy source (Makogon, 1965). The publication by Eslamimanesh et al. (2012) provides a review of the numerous applications of gas hydrates in separation technologies and should be consulted for further information.

This chapter presents a concise background in order to gain an understanding on the fundamentals of gas hydrates. Firstly the classification of hydrates, their formation, and dissociation, as well as the phase behaviour of various hydrate-forming systems are discussed. Thereafter, the effect of various hydrate formers, inhibitors, and promoters on phase equilibrium is discussed. The criteria used in the selection of a former for this work is also outlined. Lastly, the technical aspects and industrial applications are discussed, as well as the technologies for a hydrate-based desalination process.

2.1 Hydrate formation and structural theory

The majority of gas hydrates are known to form one of three structures, namely; cubic structure I (sI), cubic structure II (sII), and hexagonal structure H (sH). Each hydrate structure contains different sized cavities, which are classified as either small or large for hydrates of sI and sII, and small, medium or large for sH hydrates (Mohammadi and Richon, 2009a). The type of crystal structure formed is dependent on the nature and size of the guest molecule (Sloan and Koh, 2008).

Molecules with diameters less than 3.8 Å do not form hydrates. Molecules with a diameter between 4.2 and 6 Å, such as methane, ethane and carbon dioxide, form sI hydrates. Molecules with a diameter between 3.8 and 4.2 Å (such as argon) as well as diameters between 6 and 7 Å (such as propane) form sII hydrates. Molecules that have a diameter between 7 and 9 Å, such as cycloheptane, form hydrates of sH. The relationship between the size of the guest molecule, and the type of structure formed, is well represented by a chart first reported by Von Stackelberg (1949), and can be viewed in Appendix B.1.

All hydrate structures contain a pentagonal dodecahedron cavity that is formed by the hydrogen bonded water molecules. This cavity, the basic cavity, is known as the building block of all hydrate structures. The orientation of these cavities and how they link together to form different cavities determines which structure is formed. The pentagonal dodecahedron is a polyhedron structure with 12 pentagonal faces. Figure 2-1 depicts the crystal structure of the different cavities, the crystal notation, and the names of the crystal structures, and the number of water molecules per unit cell for each hydrate structure. The numbers above the arrows in Figure 2-1 represents the number of each respective cavity that make up one unit cell of a specific hydrate structure. For example, the unit cell

of sI hydrates will contain 2 pentagonal dodecahedron cavities and 6 tetrakaidecahedron. The nomenclature used for describing hydrate structures is n_i^{mi} where "n" is the number of edges in face type "i" and "mi" is the number of faces with "ni" edges (Sloan and Koh, 2008). Using the proposed notation, these two cavities of sI hydrates would be described as 5^{12} (pentagonal dodecahedron) and $5^{12}6^2$ (tetrakaidecahedron).

The stability, pressure, and temperature of a hydrate is determined by the fit of the guest molecule within each cavity (Sloan, 2004). A hydrate will not form in the absence of a guest molecule. It is not necessary for the crystal to be completely filled with guest molecules for hydrate formation to occur, however, for hydrate stability, all cavities would need to be occupied. In the absence of guest molecules, the hydrate structure is unstable. Without the guest molecules to keep the cavities in position, the expanded hydrogen-bonded water structure will collapse. For a guest molecule to enter a cavity, it must meet its specific dimensional, physicochemical, and morphological criteria. An important criterion for determining whether a guest molecule will form a stable hydrate is the ratio of the guest diameter to cavity diameter (Sloan and Koh, 2008). If the size ratio is less than 0.76, the guest molecule will not contribute enough van der Waals forces to stabilise the cavity. If the ratio is greater than 1, the guest molecule is too large to fit within the cavity without distorting it (Sloan and Koh, 2008).

Structure I is the simplest hydrate structure. Structure II is significantly more complex than sI. Both sI and sII hydrates are able to form with only one guest filling either the small or large cavities. If a guest molecule is able to occupy and stabilise a small cavity it will also be able to enter the large cavity. In the case where two guest molecules, or a guest molecule and a *hydrate promoter* (discussed in section 2.4.3) are used, both the small and large cavities can be filled. In this event, the hydrate structure has increased stability compared to having only one cavity filled. This increased stability allows hydrates to form at a lower pressure for a given temperature (Sloan & Koh, 2008). Hydrates of structure H are a relatively new discovery and are less common than sI and sII. They are unique, as their formation requires two formers to be present; a small molecule and an sH former (Carroll, 2014). Hydrates of sH are always double hydrates. A list of sH formers as well as other known hydrate formers is presented in Appendix B.2.

A summary of the hydrate structures and their properties is provided in Table 2-1. Detailed descriptions about the different hydrate structures, and their physicochemical properties have been well established by Sloan and Koh (2008) and Carroll (2014) and should be consulted for more information.
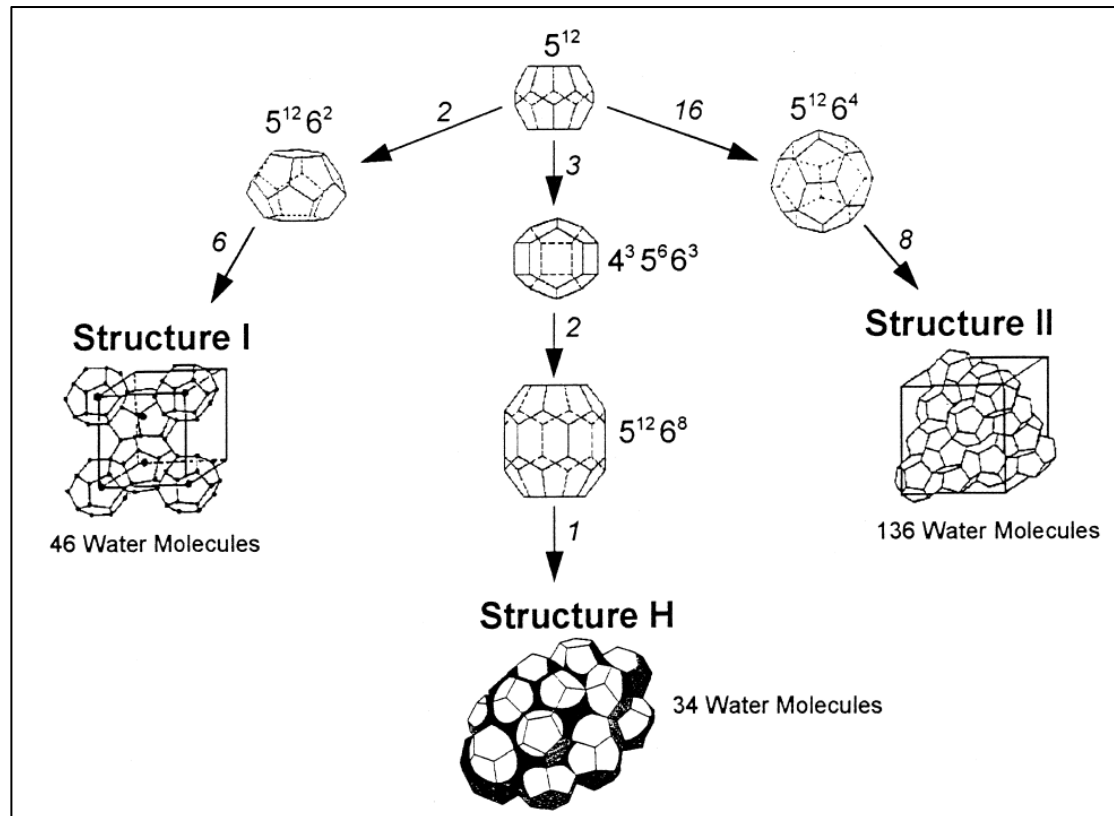
Figure 2-1: Three hydrate unit crystals and their cavity arrangement (Khokhar et al., 1998).

Table 2-1: Properties of hydrate structures.

Hydrate crystal type	I		II		H		
Cavity size [a]	Small	Large	Small	Large	Small	Medium	Large
Spatial arrangement [a]	5^{12}	$5^{12}6^2$	5^{12}	$5^{12}6^4$	5^{12}	$4^35^66^3$	$5^{12}6^8$
Number of cavities per unit cell [b]	2	6	16	8	3	2	1
Average cavity radius (Å) [b]	3.95	4.33	3.91	4.73	3.91	4.06	5.71
Number of water molecules per unit cell [b]	46		136		34		
Volume of unit cell (m³) [c]	1.728×10^{-27}		5.178×10^{-27}				

[a] Sloan and Koh (2008), [b] Sloan (2004), [c] Carroll (2014).

2.2 Hydrate kinetics

The kinetics of gas hydrate formation is far less understood than the well-established thermodynamic properties such as the dissociation temperature and pressure. A contributing factor is the *stochastic nature of hydrate formation*, which makes it difficult to measure kinetic data that is reproducible and independent of the instruments used. Even under identical test conditions, kinetic measurement may result in drastically different formation times (Koh et al., 2011).

The lifecycle of gas hydrates is comprised of three kinetic phenomena. The first two are hydrate nucleation and crystal growth, and are analogous to the crystallization process (Bishnoi and Natarajan, 1996). During hydrate nucleation, critical-sized stable nuclei are formed. These nuclei serve as the seed for the growth phase, in which they grow to form stable hydrates. The third kinetic phenomenon is hydrate dissociation. When equilibrium is disturbed by an increase in temperature or a decrease in pressure, the hydrates dissociate and the trapped guest molecules within the cavities are released. Hydrate formation is regarded as path-dependent, and hydrate dissociation as path-independent (Sloan and Koh, 2008). For this reason, some experimental methods choose to take the equilibrium pressure based on the dissociation trace (Sloan and Koh, 2008; Petticrew, 2011).

The kinetics of gas hydrates are important for industrial purposes as they dictate the time required for hydrate formation and as a result, the time required for hydrate-based industrial processes. In addition, the longer the time given for hydrate formation, the better the separation between the hydrate and the salt (Petticrew, 2011). This section provides a brief overview of these kinetic phenomena. The work of Bishnoi and Natarajan (1996) and Sloan and Koh (2008) should be consulted for more information on the kinetics of gas hydrates.

2.2.1 Hydrate nucleation

Hydrate nucleation occurs in a supersaturated environment formed by excess dissolved guest molecules in the aqueous (or pure water) solution. The water molecules position themselves around the guest molecules, forming gas-water clusters. These clusters constitute the nuclei. If the size of these clusters is less than the critical size, they are unstable and may either continue to grow or dissolve in the aqueous solution (Bishnoi and Natarajan, 1996). Once these clusters reach critical size, they are stable nuclei and instantly form hydrate crystals (Bishnoi and Natarajan, 1996). Experimental and calculated results indicate that stable hydrate nuclei have a radii ranging from 25 - 170 Å (Englezos et al., 1987).

Supersaturation is the driving force of nucleation. The location where stable nuclei first appear is dictated by the availability of supersaturation in the solution. For a non-agitated system, the hydrate nucleation site is located at the vapour-liquid interface: the highest concentration of dissolved gas. For an agitated system, the nuclei may form at any point in the solution where the highest concentration of dissolved former is present (Bishnoi and Natarajan, 1996). The pressure-temperature trace of hydrate formation and dissociation in an isochoric system is shown in Figure 2-2. The nucleation process occurs between points A and B.
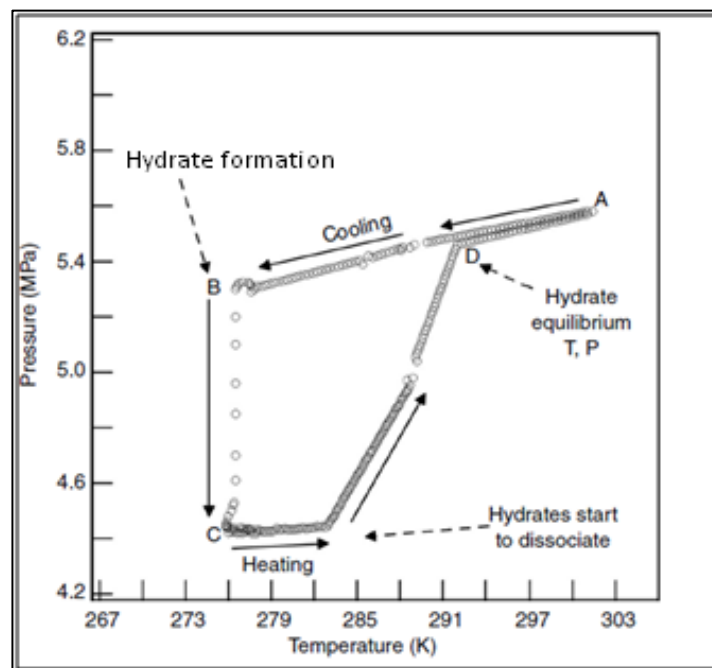
Figure 2-2: Schematic representation of the hydrate formation and dissociation process (Sloan and Koh, 2008).

The time elapsed during the nucleation process (formation of clusters and their growth to critical-sized stable nuclei) is known as the induction time. It is one of the important parameters used to characterize hydrate nucleation, and is dependent on: (a) history of water (Natarajan et al., 1994); (b) degree of supersaturation (Bishnoi and Natarajan, 1996; Jensen et al., 2008); (c) stirring rate (Englezos et al., 1987); (d) temperature and pressure (Sloan and Koh, 2008); (e) molecular diameter to cavity size ratio (Sloan and Koh, 2008); and (f) surface area of contact between gas and water (Sloan and Koh, 2008). Three models have been developed to describe the nucleation process. Further information of these models can be found in the work of Sloan and Koh (2008).

2.2.2 Hydrate growth

The hydrate growth process occurs between points B and C in Figure 2-2. Once the nuclei have reached critical size, they continue to grow to form hydrate crystals. During the crystal growth, a large pressure drop is experienced. This is due to the diffusion and adsorption of guest molecules into the cavities of the hydrate structure, in order to make them stable. Mass and heat transfer play important roles in the hydrate growth process. Mass transfer may be the dominating process, as gas molecules require transportation to the hydrate surface in order to enter the hydrate crystal. In addition, the nucleation parameters, such as displacement from equilibrium conditions, surface area, and stirring rate, continue to play an important role in the process. Three types of models have been developed in order to describe crystal growth. These models are based on (i) growth kinetics, (ii) heat transfer, and (iii) mass transfer. For more details on these models the reader is referred to the work of Sloan and Koh (2008).

At equilibrium, the growth rate per particle can be described as (Bishnoi and Natarajan, 1996):

$$\left(\frac{dn}{dt}\right)_p = K^* A_p \left(f_b - f_{eq}\right) \tag{2-1}$$

where A_p is the hydrate surface area of each particle is, f_b is the fugacity of the dissolved gas in the bulk solution, f_{eq} is the fugacity at equilibrium, and K^* is the combined rate constant.

2.2.3 Hydrate dissociation

Hydrate dissociation is an endothermic process that involves the destruction of hydrate crystals and the release of the trapped guest molecules. The dissociation process occurs between points C and D in Figure 2-2. Heat is required to break the hydrogen bonds between the water molecules and the van der Waals forces that exist between the guest and water molecules. The heat transfer that occurs during this processed is analogous to the nucleate boiling phenomena described by Kamath et al. (1984).

Hydrate dissociation occurs via a two-step process: the destruction of the hydrate lattice at the particles' surface, followed by desorption of the guest molecule from the surface (Bishnoi and Natarajan, 1996). At extremely low temperatures, the molecular motion within the hydrate lattice stops, resulting in a very rigid hydrate lattice. As the temperature increases, the motion, due to water molecule reorientation and diffusion, results in the dissociation of the hydrate, and the release of the gas trapped within the cavities of the hydrate. This release of gas results in an increase of the system pressure.

At equilibrium, the dissociation rate for a hydrate particle is given by (Bishnoi and Natarajan, 1996):

$$-\left(\frac{dn}{dt}\right)_p = K_d A_p \left(f_{eq} - f_g^{\,V}\right) \tag{2-2}$$

where K_d is the dissociation rate constant and $f_g^{\,V}$ is the fugacity of the gas obtained at the particle surface temperature and the experimental pressure.

2.3 Phase behaviour of gas hydrate systems

Understanding the phase behaviour of gas hydrates is essential for their effective application in industrial processes. One can attain this understanding through the study of phase diagrams. The phase behaviour of hydrates change considerably depending on the size, shape, and nature of the guest molecules. This section provides a brief description of the phase behaviour of hydrate forming systems.

2.3.1 The Gibbs phase rule

According to the Gibbs phase rule (Smith et al., 2005):

$$F = 2 - \pi + N \tag{2-3}$$

where π is the number of phases, N is the number of species, and F is the degrees of freedom of the system.

The degrees of freedom represent the number of fixed, independent, and intensive variables needed to specify the system. Such variables include temperature, pressure, phase amounts, volume, density, and concentration. Density, volume, and phase amounts are difficult to measure. Temperature, pressure, and composition are therefore mostly used to determine phase equilibrium. More specifically, the intensive state of hydrate phase equilibrium is determined from the system pressure, temperature, water free former phase composition, and water free phase composition. The remaining properties are calculated (Sloan and Koh, 2008). For a more detailed discussion on phase diagrams the reader is referred to Harmens and Sloan (1990), Huo et al. (2003), Mooijer-van den Heuvel (2004), and Wierzchowski and Monson (2006).

The maximum number of degrees of freedom is represented by:

$$F_{max} = N + 1 \qquad\qquad (2\text{-}4)$$

where F_{max} represents the number of dimensions required to represent the complete phase behaviour of a system (Mooijer-van den Heuvel, 2004).

2.3.2 The phase diagram

Systems containing gas hydrates consist of two or three components and are referred to as binary and ternary systems respectively. For a binary system, these components are water and one guest molecule; and water, one guest molecule, and an additive such as a promoter/inhibitor comprise a ternary system. All systems investigated in this study are multicomponent in nature (comprising water, carbon dioxide, and salt/s). Only water and CO_2 make up the gas hydrate structure, with the salts remaining in the liquid solution. Only binary systems (former/gas and water) will be discussed here. For more information on ternary systems, the reader is referred to Appendix B.3.

According to the Gibbs phase rule, for a binary system, F_{max} is 3. Full representation of the phase behaviour cannot be achieved in a two dimensional P-T plane and must be projected onto a third axis that shows the dependency of composition on the equilibrium conditions, i.e., P, T, and x. Due to this increased complexity, the phase behaviour is often presented in a planar cross-section of the equilibrium conditions at a fixed value of one of the variables. Figure 2-3 demonstrates a P-T phase diagram for a binary system at a specified composition.
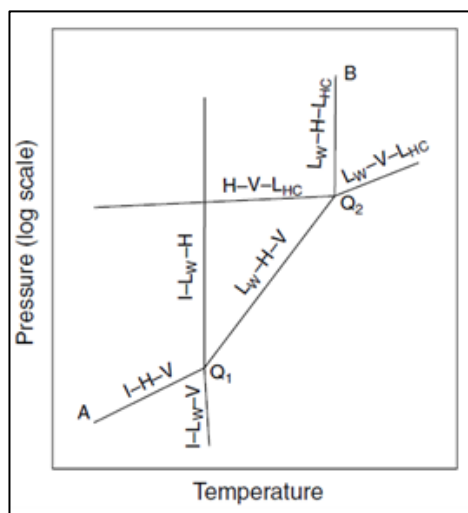
Figure 2-3: Pressure-temperature phase diagram for a binary system at a specific composition (Sloan and Koh, 2008).

The phases that occur in a binary system of gas hydrates are: ice (I), liquid water (L_w), vapour (V), hydrate (H), and liquefied guest (L_{HC}). Two-phase regions are bound by three-phase equilibrium curves (I-H-V, Lw-H-V etc.). Four three-phase equilibrium curves intersect at a quadruple point, i.e., the point where four phases coexist in equilibrium (Q1 and Q2) (Figure 2-3).

Two variations of the phase diagram presented in Figure 2-3 are encountered. The distinction between the phase diagrams is related to the critical temperature (T_c) of the gas, and its proximity (lower or higher) to the triple point of water (T_{tr,H_2O}). Gases with T_c lower, or close to T_{tr,H_2O}, are referred to as *gas-like*, while gases with T_c above T_{tr,H_2O}, are referred to as *liquid-like*. The triple point temperature of water is 273.16 K. The former used in this study, carbon dioxide (discussed in detail in section 2.4.1), has a critical temperature of 304.25 K, appreciably above the triple point of water. The systems investigated in this study exhibits a *liquid-like* behaviour in the hydrate formation region. The P-T diagram for such systems (guest molecule with high critical temperature) is shown in Figure 2-4.
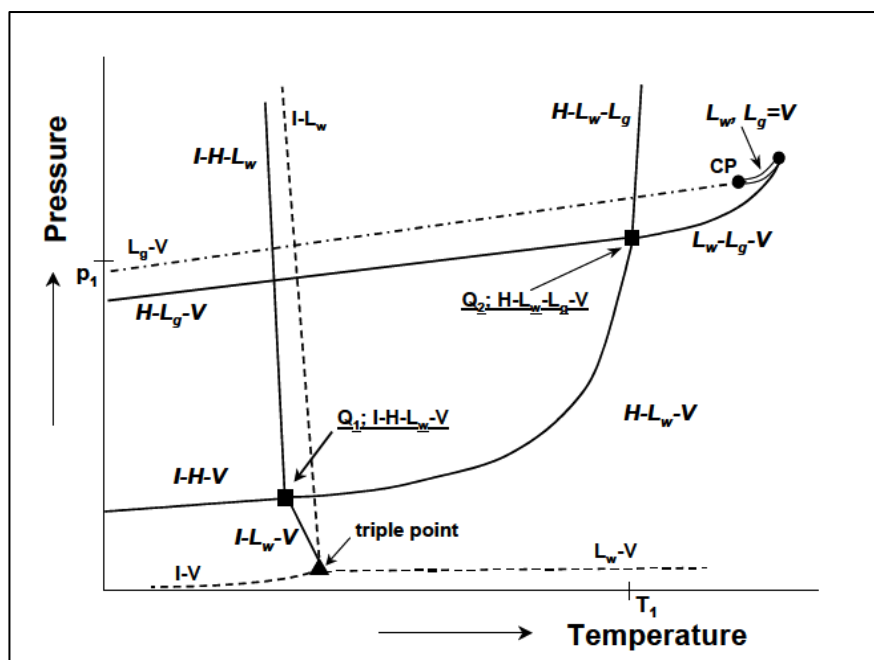
Figure 2-4: Pressure-temperature phase diagram for a binary system of water + gas (−). The phase behaviour of the unary system of water (---) and gas (-.-.-) is included as a reference, as well as the triple point of water (▲), the critical point of the gas (●) (Mooijer-van den Heuvel, 2004).

The H-L_g-V equilibrium curve in Figure 2-4 proceeds to higher temperatures and intersects with the H-L_w-V curve at a quadruple point (Q_2). The four phases that coexist at Q_2 are H-L_w-L_g-V. The equilibrium curves that intersect at Q_2 are H-L_w-V, H-L_g-V, H-L_w-Lg and L_w-L_g-V. The I-H-V equilibrium line at conditions below Q_1, the H-L_w-V equilibrium line between Q_1 and Q_2 as well as the H-L_w-L_g equilibrium line at conditions above Q_2 bind the hydrate region. Hydrates are able to form at conditions of lower temperature or higher pressure to the left of this region enclosed by the three lines. To the right no hydrate formation is possible. Due to the fact that the H-L_w-L_g equilibrium curve is so steep, the temperature of Q_2 is often taken as the maximum temperature for gas hydrate existence (Mooijer-van den Heuvel, 2004). The L_w-L_g-V equilibrium curve continues to higher temperatures above Q_2 and terminates at the critical end point.

For more information of the phase behaviour of low critical temperature gases, the reader is referred to Appendix B.3. The application of the Gibbs phase rule for binary and ternary systems can also be found in Appendix B.3. The work of of Mooijer-van den Heuvel (2004) should also be consulted.

2.4 Formers, promoters and inhibitors

Hydrate formers are the type of guest molecule that is required for hydrate formation. Promoters and inhibitors are chemicals that affect hydrate formation and dissociation respectively. Promoters increase the temperature, or reduce the pressure, at which the hydrate forms, while inhibitors have the opposite effect. In addition to a brief description on formers, promoters, and inhibitors, this chapter outlines the criteria and method used in selecting a former for this study as well as the type of inhibitors present in the hydrate systems studied.

2.4.1 Formers

As previously mentioned, the small guest molecules that occupy the cavities within the hydrate crystal are hydrate formers. Hydrates cannot form in the absence of the former. The hydrate structure is stabilized through the intermolecular interactions between the former and the molecule. Formers exist in either liquid or gaseous form, are either organic or inorganic, are usually hydrophobic, and have various degrees of toxicity and flammability.

The most important characteristics of the former are its chemical nature, size, and shape. As previously mentioned, the types of structure formed, and the stability of the formation, are dictated by these characteristics. Once hydrates have formed, the former should not interfere with the hydrogen bonding that has occurred between the water molecules. The exception to this is in the formation of semi-clathrates. Semi-clathrates are a type of clathrate that has some broken bonds in the hydrogen bonded water frame work (Jeffrey, 1984). Semi-clathrate hydrates have the same properties as conventional gas hydrates however the guest molecule not only occupies the hydrate cavity but contributes to the lattice structure (Bouchemoua et al., 2011). If an intended former has hydrogen bonds, hydrates will not form. An example of such is methanol (Carroll, 2003).

Several criteria were used to determine which of the more than 130 known hydrate formers (Sloan and Koh, 2008) would be most suitable for this study. The first step, in narrowing down the field of choice, was to determine which were environmentally acceptable. The initial criteria used included selecting hydrate formers that were non-toxic, had low ozone depletion potential (ODP), low global warming potential (GWP), low explosion potential, and were non-flammable. Flammability could be considered less of a major concern provided extensive knowledge on how to properly handle the particular hydrate former on an industrial scale was available.

Hydrate dissociation data for the environmentally suitable hydrate formers in pure water was then used to determine which of these possible formers were capable of forming hydrates at temperatures

well above 0 ℃ and pressures as close to atmospheric pressure as possible, in order to reduce the energy required for hydrate formation and the corresponding separation process.

The other criteria used included the solubility of the hydrate former in water, its cost, and availability. The solubility of the hydrate former in water assists in determining what type of separation step will be required to recover the hydrate former from the water phase, once the hydrate has been dissociated. The cost of the hydrate former, and the degree of purity that will be required for the recovered water, will dictate the extent to which the hydrate former must be recovered. The economic feasibility of the process depends largely on the cost and availability of the selected formers. An overview of the selection criteria is presented in Table 2-2.

Common hydrate formers, found in literature, which included methane, ethane, propane, and carbon dioxide, were initially selected as possible hydrate formers for this study. Based on the above-mentioned criteria, a detailed analysis was conducted on each of these potential formers. This analysis can be found in Appendix B.4. These common formers were further investigated to determine the effect an inhibitor would have on hydrate formation. The hydrate forming conditions of these potential formers, in pure liquid water and in the presence of salts, have been measured extensively in literature.

Figure 2-5 shows the gas hydrate dissociation data, compared to pure water, of each former in a 5 wt % sodium chloride solution. From Figure 2-5 it can be seen that propane experiences the least effects of an inhibitor and would, thermodynamically, be the most suitable former. Propane however is flammable and has an explosion potential if not handled properly. For these reasons, propane was not selected as a suitable former for this application, despite its widespread use in industry.

Carbon dioxide is more soluble than the other hydrate formers of interest; it is a known greenhouse gas, and requires pressures of up to 4.5 MPa to form. It is, however, non-flammable, and can form hydrates at temperatures of up to 282 K. Most importantly, CO_2 is generated as a by-product during the fermentation of molasses to bioethanol, making it readily available for use as a hydrate former, and thereby, reducing the operating costs.

Table 2-2: List of specific criteria used to determine suitable hydrating agents (McCormack and Andersen, 1995; Smith, 2015).

Characteristic	Criteria
Environmentally acceptable	The former must have low ozone depletion and greenhouse effect and if applicable, be approved by the Montreal Protocol.
Non-toxic	The former should have low toxicity, is non-carcinogenic and non-mutagenic.
Non-flammability	The former should have a high flash point in order to reduce the fire risk.
Chemical stability	The former should react slowly with chemicals.
Compatibility with standard materials	The former has low chemical activity.
Low cost	Lower operating costs.
Availability	Commercially available quantities
Water solubility	The former should have low water solubility. This will increase the degree of recovery of the former from water.
Structure of unit cell	Either sI, sII, sH, or semi-clathrate
Suitable operating temperature and pressure	In order to reduce operating costs, formers should have operating conditions close to ambient temperature and atmospheric pressure.
Quadruple point	Operation near the upper quadruple point is recommended for energy intensity of the process.
Critical point	The heat of vaporization should be considerable. The upper quadruple point should be, as much as possible, far from its critical point.

Fluorinated hydrocarbons are able to form hydrates at substantially lower pressures compared to common hydrocarbon formers (formation conditions between 277.5 - 282.5 K and 2.048 - 4.020 MPa respectively when CO_2 is used as a former (Mohammadi et al., 2005) compared to formation conditions between 277.1 - 282.6 K and 0.114 - 0.382 MPa when R134a is used as a former (Petticrew, 2011)). If hydrates are able to form at temperatures and pressures closer to ambient

conditions, the cost associated with their use for desalination may be reduced. For this reason they were also considered as possible formers. When selecting a fluorinated hydrocarbon for use, the Montreal Protocol needed to be considered. The Montreal Protocol addresses greenhouse effects and ozone depletion due to the presence of chlorine. A list of the commercially available fluorinated compounds was obtained (Petticrew, 2011) and compared to the chemicals listed in the Montreal Protocol. Due to the intended industrial application of this technology, only the refrigerants that were not banned, nor could potentially be banned, were considered for this study. The refrigerants considered were R14, R116, R134a, R152a, R218, R404a, R407c, R410a, and R507a. A list of commercially available fluorinated formers can be found in Appendix B.5.

The detailed analysis of each property and criteria, for each potential fluorinated hydrate former, is available in Appendix B.6. From the analysis performed, the most suitable fluorinated hydrate formers were found to be R134a, R410a and R507. Significant research has been done within the Thermodynamics Research Unit (TRU) at the University of KwaZulu-Natal, investigating the possible use of fluorinated refrigerants in the application of gas hydrates for desalination. Petticrew (2011) investigated the use of R134a and conducted hydrate measurements on R134a (1) + water (2) + [5 wt %, 10 wt %, and 15 wt % NaCl] (3). The author's results indicated an average shift in temperature between the system R134a (1) + water (2) containing no salt and the systems containing [5, 10, and 15] wt % NaCl of -1.9 K, -4.8 K and -8.1 K respectively. Petticrew (2011) concluded that the use of R134a as a hydrate former was insufficient to ensure gas hydrate technology was competitive with other desalination technologies and recommended the use of a promoter such as cyclopentane to shift the hydrate-liquid-vapour (HLV) equilibrium phase boundary closer to ambient conditions. Ngema (2014) investigated the potential use of R134a, R410a, and R507. The author conducted measurements on the following systems:

Table 2-3: Systems measured in the study conducted by Ngema (2014).

System	Salt concentration
R134a (1) + water (2) + NaCl (3)	5.0, 10.0, and 15.0 wt %
R134a (1) + water (2) + CaCl$_2$ (3)	3.8, 6.0, and 7.5 wt %
R134a (1) + water (2) + MgCl$_2$ (3)	2.3, 4.7, and 7.0 wt %
R410a (1) + water (2) + NaCl (3)	5.0 and 10.0 wt %
R410a (1) + water (2) + CaCl$_2$ (3)	3.8 and 7.5 wt %
R410a (1) + water (2) + MgCl$_2$ (3)	2.3 and 4.7 wt %
R507 (1) + water (2) + NaCl (3)	5.0 and 10.0 wt %
R507 (1) + water (2) + CaCl$_2$ (3)	3.8 and 7.5 wt %
R507 (1) + water (2) + MgCl$_2$ (3)	2.3 and 4.7 wt %

The results of the study conducted by Ngema (2014) showed that the hydrate dissociation temperature data for the [R134a or R507] + water systems were 10 K lower than ambient temperature and therefore the [R134a or R507] + water + [NaCl, CaCl$_2$ or MgCl$_2$] systems may require a water insoluble promoter such as cyclopentane to shift the temperatures closer to ambient conditions. The hydrate dissociation temperatures for the R410a + water system were close to ambient temperature indicating that R410 would not require a water insoluble promoter. Ngema (2014) concluded that R410a was a suitable refrigerant for use in a hydrate-based desalination process.

Due to the cost of the fluorinated hydrate formers, the results of previous studies, and the accessibility of CO$_2$, it was decided that, for the purpose of this study, CO$_2$ would be selected as the hydrate former, with further testing on fluorinated hydrocarbon and vinasse systems to be done as a continuation of this study, within the Thermodynamics Research Unit.
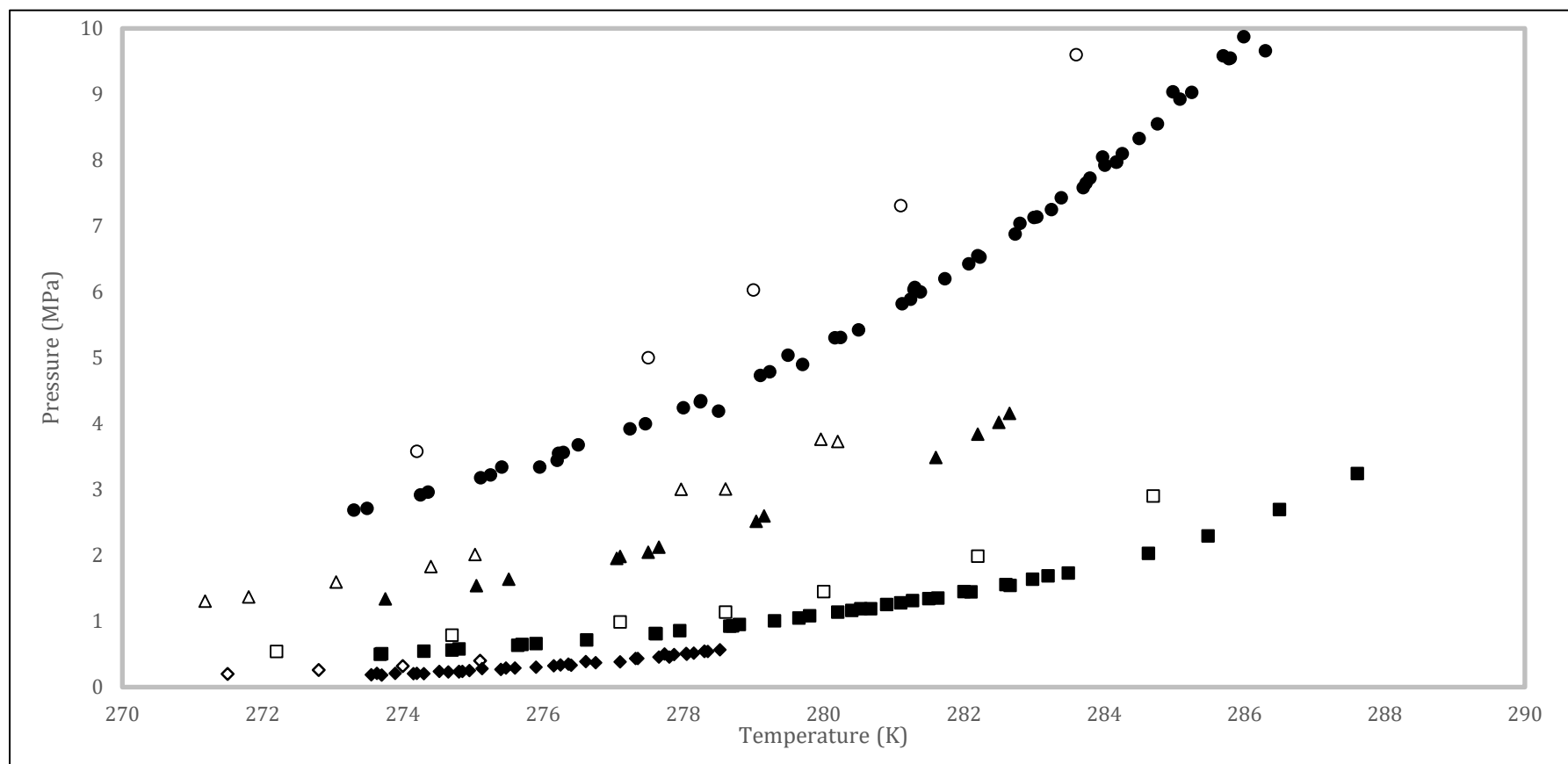
Figure 2-5: Comparison of hydrate dissociation points between hydrate formers and hydrate formers with 5 wt % NaCl. (●) CH₄ (Mohammadi et al., 2005), (Nakamura et al., 2003), (Yang et al., 2001), (Nixdorf and Oellrich, 1997), (De Roo et al., 1983); (o) CH₄ and NaCl (Mohammadi et al., 2008b); (■) C₂H₆ (Nixdorf and Oellrich, 1997), (Deaton and Frost, 1946), (Englezos and Bishnoi, 1991), (Holder and Hand, 1982); (□) C₂H₆ and NaCl (Mohammadi et al., 2008b); (♦) C₃H₈ (Nixdorf and Oellrich, 1997), (Englezos and Ngan, 1993), (Robinson and Metha, 1971), (Deaton and Frost, 1946), (Kubota et al., 1984), (Bishnoi and Dholabhai, 1993); (◊) C₃H₈ and NaCl (Mohammadi et al., 2008b); (▲) CO₂ (Mohammadi et al., 2005), (Englezos and Hall, 1994), (Dholabhai et al., 1993); (Δ) CO₂ and NaCl (Mohammadi et al., 2008b).

2.4.2 Inhibitors

Thermodynamic inhibitors prevent hydrate formation by shifting the equilibrium conditions to lower temperatures or high pressures, making it more difficult for hydrates to form. Inhibitors are used in the oil and gas industry to prevent hydrate formation. There are two classifications of inhibitors that exist: thermodynamic inhibitors such as alcohols, glycols, and salts and low dosage hydrate inhibitors (LDHI). There are two groups of LDHI's: kinetic inhibitors (KI) and anti-agglomerates (AA). Kinetic inhibitors delay hydrate nucleation and decrease the speed of crystal growth where AA control the agglomeration of the hydrates crystals. The salts, organic compounds, and alcohols present in vinasse thermodynamically inhibit hydrate formation. This section is therefore focused on thermodynamic inhibitors. For more information of LDHI's, the reader is referred to the work of Sloan and Koh (2008) and Shahnazar and Hasan (2014). A list of common thermodynamic inhibitors is presented in Table B-8 in Appendix B.7.

Thermodynamic inhibitors are required in larger quantities compared to LDHI's; 10 - 50 wt % for thermodynamic inhibitors versus 0.1 - 1.0 wt % for LDHI's (Katz et al., 1959; Karaaslan and Parlaktuna, 2002); and are added to the aqueous solution in order to reduce the activity of water. Reducing the activity of the water increases the pressure, or decreases the temperature at which the hydrate dissociates, thus reducing the hydrate formation region.

Alcohols inhibit hydrate formation through direct competition with the hydrate for guest and water molecules. This occurs in two ways: the hydroxyl group on the alcohol hydrogen bonds to the water molecules (the major effect); and the hydrocarbon end of the alcohol causes water molecules to cluster around it, in the same way a former would (lesser effect). The glycol-based inhibitors have more hydroxyl groups compared to alcohols, and provide more hydrogen bonding opportunity with water. The approximation of the temperature depression that can be expected from alcohols and glycols is given by the following equation (Sloan and Koh, 2008):

$$\Delta T = \frac{2335W}{100M - MW} \tag{2-5}$$

where ΔT is the hydrate depression (ºF), M is the molecular weight of inhibitor (alcohol or glycol), and W is the weight percent of the inhibitor in the liquid phase.

For further information on this equation, the work of Sloan and Koh (2008) should be consulted.

The action of salts as inhibitors is different from that of alcohols and glycols. The salts ionize in solution and the resulting ions form Coulombic bonds with the dipoles of the water molecules (Sloan & Koh, 2008; Petticrew, 2011; Ngema, 2014). These Coulombic bonds are considerably stronger than the hydrogen bonds between the water molecules, or the van der Waals forces between the crystal

structure and the guest molecule (Sloan and Koh, 2008). This stronger attraction of water to ions inhibits hydrate formation (water is attracted to ions more than the hydrate structures), which results in a higher pressure or lower temperature, at which the hydrates form.

The greater the increase in salt concentration, the greater the temperature shifts. In addition, the strong forces between the salt and water molecules result in a "salting-out" effect, in which the solubility of the guest molecule is reduced (Sloan and Koh, 2008). The strong interaction between water and salt depresses the water freezing point and inhibits liquid from vaporising. As a result, the upper and lower quadruple point for the systems containing salt are at lower temperatures compared to the systems containing no salt. The higher the salt concentration, the lower the temperature of the upper and lower quadruple point (refer to Table 2-4 for freezing point depression data of NaCl in water). Mixed-salt solutions have a generally greater inhibitory effect on hydrate dissociation compared to single salt solutions. These effects can be seen in Figure 2-6, which shows the hydrate dissociation data for carbon dioxide as the former gas in pure water, at various concentrations of NaCl, and in a mixed salt solution.

Table 2-4: Freezing point depression data for sodium chloride (Petticrew, 2011).

Wt % NaCl	Freezing point ΔT (K)
5	3.05
10	6.56
15	10.92 (by linear interpolation)
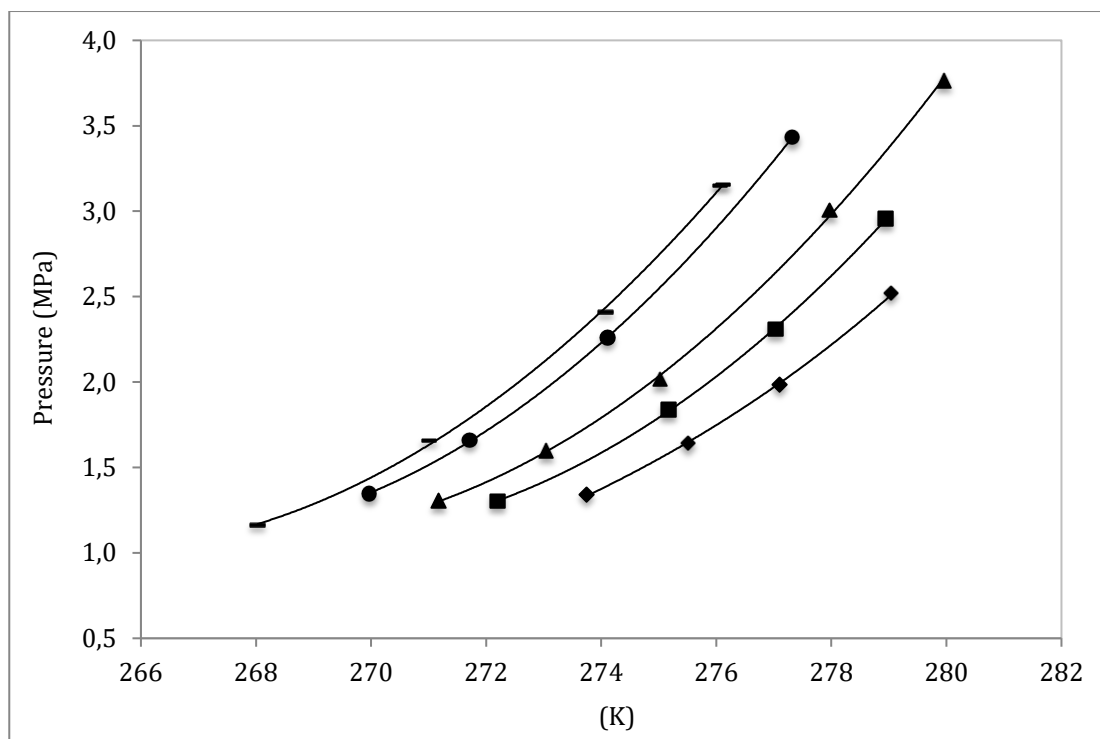
Figure 2-6: Comparison of hydrate dissociation points for carbon dioxide in pure water and at various concentrations of NaCl. (♦) Pure water (Dholabhai et al., 1993); (■) 3.0 wt % NaCl (Dholabhai et al., 1993); (▲) 5.0 wt % NaCl (Dholabhai et al., 1993); (—) 10.0 wt % NaCl (Dholabhai et al., 1993) (●) 5 wt % NaCl and 5 wt % KCl (Dholabhai et al., 1993).

An extensive literature review of previously measured hydrate dissociation data was conducted on systems containing thermodynamic inhibitors. Due to the constituents present in vinasse, pure and mixed salt systems, systems containing organic components such as alcohols and glycols, and systems containing a combination of thermodynamic inhibitors, with various formers, were investigated.

The measured HLV equilibrium data (temperature and pressure ranges) for the systems containing CO_2 and single salt aqueous solutions, and CO_2 and mixed salt aqueous solutions are shown in Table 2-5 and Table 2-6 respectively. The measured data cited in literature for CO_2 as the former covers a salt concentration range of 3.0 wt % to approximately 20.0 wt %. The salts measured were: NaCl, KCl, $CaCl_2$ and $MgCl_2$. From the tables it is evident that extensive HLV measurements have been done on systems containing CO_2 and salt(s). The reader is referred to Tables B-10 and B-11 in Appendix B.8 for the measured HLV equilibrium data for single and mixed salt systems containing formers other than CO_2. It should be noted that Table 2-5 and Table 2-6 are first grouped by salt and then arranged in increasing salt concentration. From Table 2-5 and 2-6, it can be seen that in a system containing salt inhibitors, CO_2 requires pressures up to approximately 4.4 MPa to form.

Table 2-5: Measured HLV equilibrium data for the CO_2 (1) + water (2) + single salt (3) systems cited in literature.

Salt system	T range (K)	P range (MPa)	Reference
3.000 wt % NaCl	272.2 - 279.0	1.30 - 2.96	Dholabhai et al. (1993)
3.020 wt % NaCl	273.2 - 280.9	1.43 - 3.91	Dholabhai et al. (1993)
5.000 wt % NaCl	271.2 - 280.0	1.31 - 3.77	Dholabhai et al. (1993)
	278.1 - 280.2	1.37 - 3.73	Mohammadi et al. (2008b)
10.000 wt % NaCl	268.0 - 276.1	1.16 - 3.16	Dholabhai et al. (1993)
	268.8 - 277.4	1.15 - 3.70	Englezos and Hall (1994)
	271.9 - 276.1	1.86 - 3.23	Tohidi et al. (1997)
10.020 wt % NaCl	277.0 - 277.2	3.67 - 3.78	Dholabhai et al. (1993)
15.000 wt % NaCl	265.4 - 273.0	1.21 - 3.24	Dholabhai et al. (1993)
15.200 wt % NaCl	267.5 - 274.5	1.39 - 3.14	Englezos and Hall (1994)
20.000 wt % NaCl	263.2 - 268.8	1.52 - 3.12	Tohidi et al. (1997)
20.030 wt % NaCl	263.3 - 266.9	1.61 - 2.63	Dholabhai et al. (1993)
3.000 wt % KCl	272.7 - 281.1	1.33 - 3.83	Dholabhai et al. (1993)
5.010 wt % KCl	272.1 - 280.5	1.33 - 3.91	Dholabhai et al. (1993)
10.000 wt % KCl	273.5 - 278.4	1.94 - 3.61	Tohidi et al. (1997)
	273.8 - 278.0	2.010- 3.35	Mohammadi et al. (2008b)
10.020 wt % KCl	269.0 - 277.9	1.130- 3.49	Dholabhai et al. (1993)
14.970 wt % KCl	269.0 - 276.0	1.42 - 3.58	Dholabhai et al. (1993)
3.030 wt % $CaCl_2$	272.6 - 280.9	1.30 - 3.70	Dholabhai et al. (1993)
5.020 wt % $CaCl_2$	271.1 - 280.1	1.18 - 3.66	Dholabhai et al. (1993)
9.990 wt % $CaCl_2$	268.1 - 277.9	1.10 - 3.82	Dholabhai et al. (1993)
10.570 wt % $CaCl_2$	267.4 - 278.1	0.94 - 3.65	Englezos and Hall (1994)
14.970 wt % $CaCl_2$	263.4 - 273.2	0.96 - 3.22	Dholabhai et al. (1993)
15.000 wt % $CaCl_2$	270.2 - 274.7	2.10 - 3.60	Mohammadi et al. (2008b)
19.960 wt % $CaCl_2$	259.2 - 266.7	1.05 - 2.69	Dholabhai et al. (1993)
3.000 wt % $MgCl_2$	273.6 - 281.6	1.54 - 4.35	Kang et al. (1998)
5.000 wt % $MgCl_2$	274.0- 280.4	1.78 - 4.22	Kang et al. (1998)
10.000 wt % $MgCl_2$	272.5 - 276.3	2.13 - 3.78	Kang et al. (1998)

Table 2-6: Measured HLV equilibrium data for the CO_2 (1) + water (2) + mixed salt (3) systems cited in literature.

System	T range (K)	P range (MPa)	Reference
2.020 wt % NaCl + 8.000 wt % $CaCl_2$	267.8 - 277.5	1.05 - 3.70	Dholabhai et al. (1993)
3.010 wt % NaCl + 3.010 wt % KCl	271.5 - 279.9	1.33 - 3.98	Dholabhai et al. (1993)
3.030 wt % NaCl + 3.030 wt % $CaCl_2$	271.0 - 279.2	1.26 - 3.60	Dholabhai et al. (1993)
5.000 wt % NaCl + 5.010 wt % KCl	267.0 - 277.3	1.35 - 3.43	Dholabhai et al. (1993)
5.020 wt % NaCl + 14.700 wt % $CaCl_2$	259.2 - 267.3	1.04 - 2.95	Dholabhai et al. (1993)
6.990 wt % NaCl + 10.000 wt % KCl	267.6 - 274.1	1.48 - 3.46	Dholabhai et al. (1993)
8.010 wt % NaCl + 2.030 wt % $CaCl_2$	267.8 - 276.0	1.09 - 3.09	Dholabhai et al. (1993)
15.010 wt % NaCl + 5.030 wt % KCl	262.9 - 269.8	1.22 - 3.05	Dholabhai et al. (1993)
15.010 wt % NaCl + 5.030 wt % $CaCl_2$	259.0 - 267.4	0.91 - 2.67	Dholabhai et al. (1993)
Synthetic sea water [a]	272.14 - 281.0	1.29 - 4.07	Dholabhai et al. (1993)

[a] Synthetic sea water: 2.931 wt % NaCl + 0.069 wt % KCl + 0.011 wt % KBr + 0.401 wt % Na_2SO_4 + 0.507 wt % $MgCl_2$ + 0.115 wt % $CaCl_2$ + 0.005 wt % NaF + 0.002 wt % $SrCl_2$

As already stated, fluorinated hydrocarbons are able to form hydrates at substantially lower pressures compared to common hydrocarbon formers. This can be seen when comparing the HLV equilibrium data in Tables B-10 and B-11 of Appendix B.8 to the data in Table 2-5 and 2.6. Compared to common hydrate formers and other fluorinated hydrate formers, R410a has dissociation conditions closest to ambient conditions. This is attractive in hydrate-based desalination processes as it reduces the operating pressure and the associated energy costs and is thus the more favourable fluorinated hydrate former.

The literature review conducted on systems containing CO_2 and alcohols, glycols and glycerol is shown in Table 2-7. The reader is referred to Table B-12 in Appendix B.8 for measured HLV equilibrium data for alcohol/glycol/glycerol systems containing formers other than CO_2.

Table 2-7: Measured HLV equilibrium data for the CO_2 (1) + water (2) + alcohol/glycol/glycerol (3) systems cited in literature.

System	T range (K)	P range (MPa)	Reference
10.0 wt % methanol	269.5 - 274.9	1.59 - 3.48	Ng and Robinson (1985)
	269.5 - 275.4	1.37 - 2.82	Dholabhai et al. (1996)
	266.7 - 274.7	1.01 - 2.56	Mohammadi and Richon (2012a)
20.0 wt % methanol	260.3 - 270.7	0.90 - 3.16	Mohammadi and Richon (2012a)
20.0 wt % methanol	264.0 - 268.9	1.59 - 2.94	Ng and Robinson (1985)
30.0 wt % methanol	253.8 - 265.5	0.89 - 3.82	Mohammadi and Richon (2012a)
35.0 wt % methanol	242.0 - 255.1	0.38 - 1.77	Robinson and Ng (1986)
40.0 wt % methanol	250.2 - 256.0	1.39 - 2.91	Mohammadi and Richon (2012a)
50.0 wt % methanol	232.6 - 241.3	0.50 - 1.31	Robinson and Ng (1986)
	241.1 - 248.2	1.21 - 3.00	Mohammadi and Richon (2012a)
10.0 wt % glycerol	272.9 - 279.3	1.39 - 3.35	Breland and Englezos (1996)
5.0 wt % ethanol	272.4 - 280.1	1.31 - 3.41	Mohammadi et al. (2007)
10.0 wt % ethanol	271.3 - 278.3	1.39 - 3.37	Mohammadi et al. (2007)
20.0 wt % glycerol	270.4 - 277.1	1.50 - 3.56	Breland and Englezos (1996)
25.0 wt % glycerol	269.6 - 276.8	1.480- 3.96	Ng and Robinson (1994)
30.0 wt % glycerol	270.1 - 273.2	2.03 - 2.98	Breland and Englezos (1996)
10.0 wt % ethylene glycol	271.4 - 277.8	1.35 - 2.86	Mohammadi and Richon (2010a)
20.0 wt % ethylene glycol	267.5 - 274.5	1.22 - 2.79	Mohammadi and Richon (2010a)
35.0 wt % ethylene glycol	261.6 - 267.4	1.31 - 2.66	Mohammadi and Richon (2010a)
50.0 wt % ethylene glycol	249.9 - 256.4	1.19 - 2.67	Mohammadi and Richon (2010a)

From Table 2-7, it is evident that significantly higher concentrations (up to 50 wt %) of the organic thermodynamic inhibitor are present compared to salt systems. Pressures up to approximately 3.9 MPa are required to form hydrates in systems containing CO_2 as the former and organic thermodynamic inhibitors.

The literature review conducted on systems containing CO_2 and mixed inhibitors is shown in Table 2-8 below. The reader is referred to Table B-13 in Appendix B.8 for measured HLV equilibrium data

for mixed inhibitor systems containing formers other than CO_2. The measured data cited in literature for the systems presented in Table 2-8 covers a salt concentration range of 10.0 wt % to approximately 20.0 wt % and pressures up to approximately 3.0 MPa are required for hydrate formation.

Table 2-8: Measured HLV equilibrium data for the CO_2 (1) + water (2) + mixed thermodynamic inhibitor (3) systems cited in literature.

Salt system	T range (K)	P range (MPa)	Reference
5 wt % methanol + 5 wt % NaCl	270.6 - 276.2	1.48 - 3.04	Dholabhai et al. (1996)
5 wt % methanol + 15 wt % NaCl	263.4 - 269.2	1.27 - 2.71	Dholabhai et al. (1996)
5 wt % methanol + 10.01 wt % KCl	265.5 - 274.7	0.91 - 2.90	Dholabhai et al. (1996)
4.96 wt % methanol + 10.0 wt % CaCl$_2$	265.9 - 274.2	0.99 - 2.81	Dholabhai et al. (1996)
5 wt % methanol + 14.97 wt % CaCl$_2$	265.2 - 270.7	1.33 - 2.72	Dholabhai et al. (1996)
9.96 wt % methanol + 9.96 wt % NaCl	264.0 - 270.8	1.18 - 2.87	Dholabhai et al. (1996)
10.0 wt % methanol + 5.0 wt % NaCl	266.3 - 272.5	1.22 - 2.51	Mohammadi and Richon (2012a)
10.0 wt % methanol + 10.01 wt % KCl	265.6 - 271.9	1.25 - 2.77	Dholabhai et al. (1996)
9.95 wt % methanol + 9.93 wt % CaCl$_2$	264.7 - 270.9	1.14 - 2.55	Dholabhai et al. (1996)
15.14 wt % methanol + 5.0 wt % NaCl	264.8 - 270.8	1.24 - 2.73	Dholabhai et al. (1996)
15.03 wt % methanol + 5.02 wt % CaCl$_2$	264.7 - 270.8	1.16 - 2.46	Dholabhai et al. (1996)
15.0 wt % ethylene glycol + 5 wt % NaCl	264.4 - 268.8	0.10 - 1.60	Mohammadi and Richon (2012a)

From the data presented in Tables 2-5 to 2-8, it is evident that as the concentration of the inhibitor increases, the temperature required for hydrate formation decreases, which increases the associated energy costs.

2.4.3 Promoters

The application of gas hydrate technology for industrial use is hindered by the slow formation of gas hydrates, and the energy costs associated with the low temperature and/or high-pressure formation conditions. Promoters, used in conjunction with formers, enable hydrates to form at reduced pressures or increased temperatures. This is due to a stabilization effect caused by the promoter on the hydrate structure (Mooijer-Van den Heuvel, 2002a). The stabilization effect arises from the promoter molecule occupying the small or large hydrate cages that the former itself could not fill (Kuo, 2010). Promoters thereby reduce mass transfer and kinetic challenges during hydrate formation (Mandal and Laik, 2008).

Promoters can be solid, liquid, or gas. They are usually hydrophobic, and are classified, like formers, according to their shape, size, chemical nature, and their water solubility (Petticrew, 2011). Hydrates are unable to form with only the presence of promoters (Carroll, 2014). According to the Gibbs phase rule, the amount of promoter added will not affect the dissociation point. A list of common promoters is shown in Appendix B.7.

2.5 Technological aspects and industrial applications of gas hydrates

Gas hydrates have generally been considered a nuisance by the oil and gas industry as their presence can lead to the plugging of pipelines. However, gas hydrates have the potential for positive application in various engineering fields such as gas separation, carbon dioxide capture and sequestration, gas storage and transportation, and desalination. In addition, naturally occurring gas hydrates can potentially be used as an energy source. The sections presented below provide a brief overview of the application of gas hydrates in various industrial sectors with emphasis placed on the use of gas hydrates for desalination and industrial effluent treatment.

2.5.1 The oil and gas industry

During the extraction of natural gas, water is often present. At specific conditions of temperature and pressure, hydrates may form. The formation of hydrates lead to the plugging of pipelines; reducing the cross sectional area in which the fluid flows and increasing the pressure drop across the line. Hydrates may also form with the liquid phase of hydrocarbons in drilling muds and oil reserves. In industry, hydrate formation is prevented by mechanical methods (physical removal of hydrates), thermal methods (heating the pipelines), thermodynamics (predicting under which conditions hydrates will form), and adjusting the activity of water by introducing inhibitors (Eslamimanesh et al., 2012).

The plugging of pipelines, pose a significant economic and safety risk. A hydrate plug separates the pipe into a high-pressure section between the wall and the plug, and a low-pressure section between the plug and the recovery division (Chatti et al., 2005). A pipe blast can occur in the upper section due to the increase in pressure. The hydrate plug can behave as a projectile that destroys the pipe. Once a hydrate plug has formed it can take weeks, even months, to dissociate it safely (Atilhan et al., 2012).

2.5.2 Gas hydrates as an energy source

Approximately 10^{16} m^3 methane exists in hydrate form on land in the Polar Regions and offshore around the globe. By dissociating these hydrate deposits into gas and water, the methane can be recovered and used as an energy source. This can be done by reducing the pressure of the reservoir, increasing the reservoir temperature to conditions outside the hydrate stability zone, or by the addition of inhibitors. The use of hydrate technology to produce methane from gas hydrate reserves has not yet been implemented on an industrial scale (Eslamimanesh et al., 2012). The reader is referred to the works by Lee and Holder (2001), Koh et al. (2012) and Chong et al. (2015) for further detail on natural gas hydrates as an energy source.

2.5.3 Gas storage and transportation

An important feature of gas hydrates is their storage capacity. Potentially 180 volume units of gas at standard conditions (temperature of 273.15 K and a pressure of 0.1 MPa) can be packed into one volume unit gas hydrate crystals (Sloan 1998) making gas hydrate structures a possible storage media for various gases such as hydrogen, methane, and carbon dioxide. The use of gas hydrates as a means for storage and transportation of gas was first determined by Benesh (1942). A lower storage space requirement and the safety of the process are advantages of employing hydrate formation as a means

of storage and transportation of gases, compared to conventional storage methods such as liquefaction. Gas hydrate structures may also be used as storage media in air conditioning systems (Ogoshi and Takao, 2004; Wang et al., 2014). The reader is referred to Khokhar et al. (1998), Mimachi et al. (2014), Taheri et al. (2014), as well as the research performed by Hashemi (2015) within the Thermodynamics Research Unit for further details on this application.

2.5.4 Gas hydrates as a separation technique

The crystalline structure of a gas hydrate includes only water and the former. This distinctive property makes gas hydrate formation a promising separation technique that can be used in the separation of gas mixtures, concentration of food solutions, and the fractionation of gases and liquids.

Not all gases are able to form hydrates and those which are, are characterised by different formation conditions (Guo et al., 2004). Exploiting these different formation conditions, gas hydrate based separation processes can be used to recover carbon dioxide form flue gas as well as the separation and recovery of other greenhouse gases such as methane, hydrogen, nitrogen, hydrogen sulphide, sulphur hexafluoride, and Freons. Gas hydrate formation, with the aid of promoters, can prove to be a more economically viable option for gas separation over conventional methods such as amine absorption and membrane technology (Eslamimanesh et al., 2012).

The formation of gas hydrates occurs at temperatures above the freezing point of ice. It may therefore be more cost effective to concentrate dilute aqueous solutions with hydrate technology compared to crystallisation depending upon the pressure required. The concentration of proteins, lipids, carbohydrates, and various juices have been reported in literature (Eslamimanesh et al., 2012).

Eslamimanesh et al. (2012) reported that gas hydrate formation could be useful as an alternative method to conventional gas-liquid fractionation processes. This is due to the fact that the compositions of the hydrate-forming mixture and the hydrate phase differ. There are two major separation processes using hydrate formation proposed in literature. A low temperature extraction (LTX) process designed by Dorsett (1989) and the separation of oil and gas in a hydrate rig by Østergaard et al. (2000).

2.5.5 Desalination and industrial effluent treatment

Evaporation, freeze concentration, distillation, and membrane technology are among the many methods currently employed to treat industrial effluents and recover water (Englezos, 1993; Ngan and Englezos, 1996; Englezos, 1993)

Freeze concentration is a type of freeze crystallization that involves the fractional crystallization of water to ice and the subsequent removal of ice, leaving behind a more concentrated liquid (Englezos, 1994). Distillation, like freeze concentration, involves a phase change. Simply put, distillation is the process in which a liquid is vaporized, re-condensed and collected in a container. Multi-stage flash distillation (MSF) and multi-effect distillation (MED) are examples of distillation processes. Membrane based treatment technologies, such as reverse osmosis (RO) are single-phase processes involving a physical separation. Physical separations take advantage of already existing differences in unit weights, particle sizes, molecule sizes, and related properties.

The separation of salt from aqueous solutions, and subsequently the recovery of water, is carried out most frequently using thermal methods (such as distillation) over membrane technology. Despite these methods being generally more expensive, they produce pure water independent of the quality and salinity of the feed (Gryta, 2012). Impurities in the feed water make RO susceptible to fouling and scaling. A sophisticated pre-treatment is therefore often required. RO may however be employed for a preliminary concentration of saline wastewater thus reducing the cost of thermal methods. Effluents containing salts combined with several organic and inorganic substances, such as vinasse, are traditionally pre-treated by biological methods such as anaerobic digestion (section 1.1.4). Solutions containing large amounts of salts can be concentrated using membrane distillation (MD).

The primary difference between the processes mentioned above and hydrate-based treatment technology is the occurring phase change: vaporization versus fusion (physical process involves no phase change). A comparison of these methods is presented in Table 2-9.

Table 2-9: Characteristics of separation processes (Barron and Wrobel 1985).

Characteristic	Physical	Vaporization	Fusion
Number of applications	Many	Many	Many
Selectivity of making separations	Limited	Usually good	Usually good
Corrosion potential	Moderate	High	Low
Scaling potential	Moderate	High	Low
Ability to handle sensitive materials	Low	Low	High
Affected by viscosity	Yes	No	Yes
Complexity of equipment	Low	Moderate	Moderate
Base of retrofit	Easy	Easy	Easy
Commercial status	Yes	Yes	Beginning phase
Number of suppliers	Many	Many	Few
Product purity and value	Low	Moderate	High
Capital cost	Low	High	Low
Energy cost	Low to moderate	High	Low
Operations and maintenance cost	Moderate	High	Moderate

Hydrate-based desalination has been investigated extensively, with studies conducted on aqueous salt solutions and synthetic seawaters in order to generate precise hydrate phase equilibrium data which can be used to design efficient and economical hydrate-based wastewater treatment and desalination processes (McCormack and Andersen, 1995; Bradshaw et al., 2008; Park et al., 2011; Kang et al., 2014; Ngema et al., 2014). Hydrate-based desalination is of particular interest because at a specific temperature and pressure, only water and an appropriate former are able to form hydrates. The gas hydrates can then be dissociated, producing pure water. The released hydrate former may be recycled in for reuse.

In the 1960's and 1970's, several process configurations were developed and demonstrated at pilot scale but, due to the difficulty of separating the crystals from the concentrated brine solutions and the removal of dissolved hydrate former from the recovered water, was never realized at an industrial level (Khan, 1986; Park et al., 2011). In the 1990's, the Bureau of Reclamation commissioned work from the Thermal Energy Systems, Inc., to explore the feasibility of the technology and constructed pilot plants in Hawaii and San Diego (McCormack and Andersen, 1995; McCormack and Niblock, 2000). In the Thermal Energy Systems study, the hydrate former R141b, was pressurized in a tank of seawater at hydrate forming conditions of 100 psig and 5 ℃. Complex slurry of hydrates and brine was formed. The formed hydrates were small in size and dendritic in nature with a large amount of salt trapped within the *interstitial* spaces. Filtration was used to remove the hydrate crystals from the

concentrated brine and a wash column was used to remove the excess salt from the hydrate crystals. Even though this wash step produced hydrates with potable water quality as per total dissolved solids (TDS) requirements, it was the step that proved to be the largest detriment to overall process efficiency. This resulted in an estimated potable water cost of $0.46 - $0.52/m^3 (McCormack and Niblock, 2000).

More recently, Javanmardi and Moshfeghian (2003) estimated the energy required for the desalination of seawater based on a modified hydrate formation process (Figure 2-7), originally proposed by Knox et al. (1961). Seawater is pumped into the reactor where at specific conditions of temperature and pressure, a slurry of hydrate crystals is formed. The slurry is then filtered and washed in a separator and divided into two streams: brine and washed hydrate crystals. The washed hydrate crystals are transported to a decomposer, where potable water and gaseous hydrate former are produced. The potable water is then removed from the process. After passing through a throttling valve, liquid hydrate former is vaporized and recycled back to the reactor where it is reused in hydrate formation. In the reactor, the excess hydrate former provides the cooling duty required for hydrate formation. The detailed economic study which included the capital investment, operation, maintenance, and depreciation costs, demonstrated that, for the year 1990, the total cost of potable water production through hydrate formation, using propane as the former, was 2.8 US$ per ton when the yield was 30 % and 4.2 US$ per ton when the yield was 20 %. The results indicated that hydrate-based desalination could potentially be more economical than traditional methods with the use of an appropriate hydrate promoter.
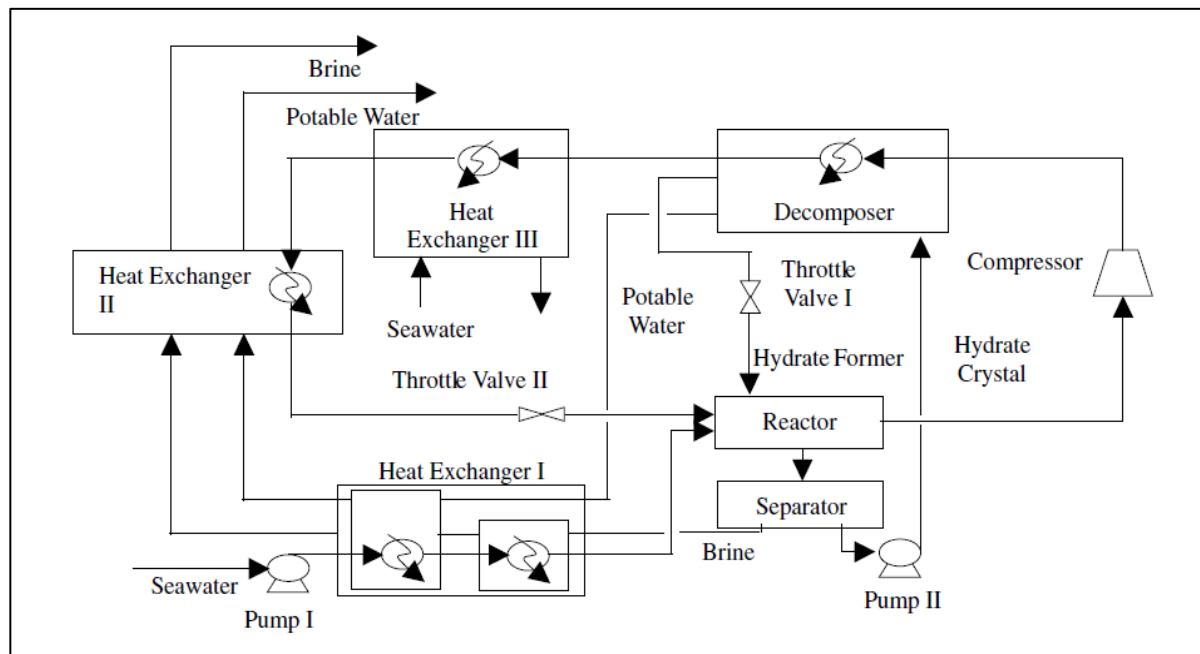
Figure 2-7: Proposed seawater desalination process (Javanmardi and Moshfeghian, 2003).

A similar hydrate desalination process (Figure 2-8) was proposed by Bradshaw et al. (2008). The primary steps required to produce potable water from seawater are: hydrate formation, separation of hydrates and brine, and dissociation of hydrates to produce water. Once hydrates have been formed and separated, the hydrate mixture is pumped as slurry to a separation chamber or a decomposer, which will be at suitable conditions of temperature and pressure in order to dissociate the hydrates. After dissociation, the hydrate former is recycled. In the study by Bradshaw et al. (2008), the problem of interstitial salt formation and the necessity of using wash columns was eliminated. The hydrate former R141b was used and resulted in hydrate formation significantly above the freezing point of water. Additives were utilized to inhibit dendritic growth and minimize interstitial salt entrapment. The rate of R141b hydrate formation in the presence of a heat exchange fluid depended on the degree of supercoiling, and the use of perfluorocarbon heat exchange fluid assisted separation of R141b hydrates from the concentrated brine (Bradshaw et al., 2008).

Figure 2-8: Hydrate-based desalination process proposed by Bradshaw et al. (2008).

Park et al. (2011) investigated the potential application of gas hydrates in the desalination process by studying the separation efficiencies of each dissolved cation from seawater samples. In addition the authors proposed a novel hydrate-based desalination apparatus to easily extract dehydrated high-density gas hydrates from a reactor containing hydrate slurries. Figure 2-9 shows a schematic of the

apparatus design, which continuously produces and pelletizes gas hydrates by a squeezing operation of a dual cylinder unit. The results of the study showed that a single stage hydrate-based desalination process was capable of producing a water product with between 72 and 80% reduction of each dissolved mineral present in the initial mixture. The dissolved minerals present in the seawater sample were removed in the following order: $K^+ > Na^+ > Mg^{2+} > B^{3+} > Ca^{2+}$. In addition, the results revealed that ion elimination by the hydrate process depends on the ionic size and charge. The results of the study conducted by Park et al. (2011) illustrated that the suggested method and apparatus may solve the separation difficulty between hydrate crystals and concentrated brine solutions and could potentially be applied for more effective desalination processes compared to membrane processes, which can increase operational costs owing to the fouling and scaling problems. The authors of the study recommended that the issue of ion rejection by the hydrate process was dependent on the ionic size and/or charge and should be clarified in order to gain an understanding into the ion rejection mechanism of dissolved minerals. Based on the work of Park et al. (2011) and using the same novel apparatus, Kang et al. (2014) investigated the effect of cations and anions, and their removal efficiencies in order to determine a more detailed ion rejection mechanism in the hydrate-based desalination process. Kang et al. (2014) concluded that ionic hydration due to ionic charge and size can be considered as key factors to understand the mechanism of ion removal in hydrate-based desalination. However due to the links with water molecules, the mechanism behind the ionic exclusion process is very complicated and the authors recommended that the correlation between ionic hydration and clathrate hydrate, and the property of ionic behaviour depending on its concentration, be investigated further. It should be noted that hydrates such as $NaOH \bullet 1H_2O$ precipitate at particular conditions as solids and their nature is different than clathrate hydrates.
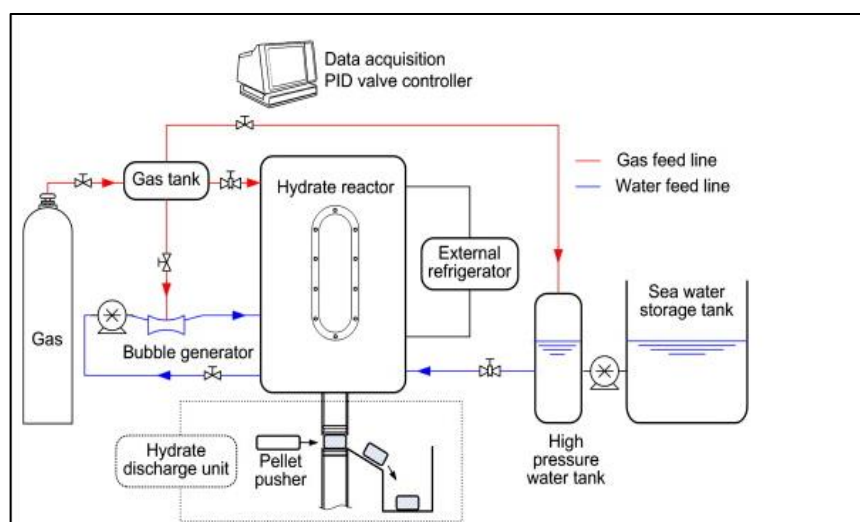
Figure 2-9: Experimental apparatus for hydrate-based desalination proposed by Park et al. (2011).

In additional to aqueous salt solutions and synthetic seawaters, the use of gas hydrate formation as a separation technology for the recovery and recycling of various pulp mill effluents has been investigated. Gaarder (1993), Ngan (1995) and Ngan and Englezos (1996) studied hydrate formation in various mechanical pulp mill effluents. It was found that gas hydrates of propane or carbon dioxide could be formed in these effluents. Ngan and Englezos (1996) also investigated the recovery of water from 2.5 wt. % NaCl solutions through propane hydrate formation. The results indicated that the total organic carbon was lowered by 23 % and the salt content was lowered by 26 % from the initial levels in the effluent. It was also found that the average reduction in the salt concentration of the recovered water, from the NaCl solution, was 31%. In addition to mechanical pulp mill effluent, deep mine reject water; waste from ammunition plants, metal-plating industry waste, and pharmaceutical waste streams are all possible areas of hydrate-based treatment technology (Englezos, 1993).

Hydrate-based desalination technology proves to be advantageous due to its lower energy requirement. The energy requirements of gas hydrate-based technology can be decreased compared to processes such as freeze concentration due to the ability of hydrates to form at temperatures several degrees above the freezing point of water. Freeze concentration of industrial effluents can therefore be more energy efficient if the crystallization step is replaced by the formation of gas hydrates (Englezos, 1993). Scaling, fouling, and corrosion are reduced due to lower operating temperatures compared to distillation and evaporation. A high heat transfer coefficient and surface area may also be achieved, as there is direct contact between the brine and the former.

$$3$$

CHAPTER THREE

PHASE EQUILIBRIUM AND THERMODYNAMIC MODELLING

For the successful design and operation of separation processes for systems containing mixtures, accurate and reliable phase equilibrium data is required. It is not possible to measure all phase equilibrium data for every system over an entire temperature and pressure range. Graphical methods, empirical correlations, thermodynamic and kinetic models are therefore used for the prediction of system properties such as temperature and pressure. In systems containing gas hydrates, the thermodynamic models used for predicating the equilibrium conditions are based on the solid solution theory of van der Waals and Platteeuw (Van der Waals and Platteeuw, 1959) and include the activity approach as well as the fugacity approach. The activity approach is established on the equality of water chemical potential in the liquid and hydrate phase (Holder et al., 1980). The fugacity approach is based on the equality of water fugacity in the liquid and hydrate phase (Avlonitis and Varotsis, 1996). These thermodynamic models have been shown to be most reliable and are thus used for the purpose of this study.

In this chapter, the phase equilibrium problem is formulated and the thermodynamic models required for the solution is presented. First the thermodynamic principles and fundamentals for phase equilibrium are outlined in section 3.1. Thereafter the selected equation of state (EOS) and mixing rule used to model the fluid phases are detailed in section 3.2. The thermodynamic model for the solid hydrate phase is presented in section 3.3. A brief overview of thermodynamic models for systems containing alcohols and salts, found in literature, is presented in section 3.4, and finally alternate methods for determining the hydrate phase is briefly presented in section 3.5.

3.1 Principles of thermodynamic modelling

When a system is in thermal, mechanical, and chemical equilibrium it is in thermodynamic equilibrium. For a system at constant temperature and pressure, the change in Gibbs free energy (G) is:

$$\overline{dG} = \left(\mu_i^\beta - \mu_i^\alpha\right) dn_i \tag{3-1}$$

where μ_i is the chemical potential of substance i in the α and β phase, and n_i is the number of moles of i.

At equilibrium, the Gibbs free energy of a system is at a minimum, therefore:

$$\left(\frac{\partial \overline{G}}{\partial n_i}\right)_{T,P,n_j} = 0 \tag{3-2}$$

As a result the chemical potential of substance i in each respective phase is equal:

$$\mu_i^\alpha = \mu_i^\beta \tag{3-3}$$

For multiphase-multicomponent equilibrium conditions, equation (3-3) can be extended to:

$$\mu_i^\alpha = \mu_i^\beta = \cdots = \mu_i^k, \text{for i} = 1,2,\dots,\text{N} \tag{3-4}$$

where k and N are the number of coexisting phases and the number of coexisting components respectively.

Based on the above equations, the equilibrium conditions may be calculated by direct minimization of the Gibbs energy or by using the principle of equality of chemical potentials (Walas, 1985).

The chemical potential of a system can be expressed in terms of the fugacity (f) by the following equation:

$$\mu = \mu^o + RTln\left(\frac{f(P)}{P^o}\right) \tag{3-5}$$

where μ^o is the reference state chemical potential, T is the temperature, R is the universal gas constant, P^o is the reference state pressure, and $f(P)$ is the fugacity as a function of pressure.

By combining equations (3-4) and (3-5), the equality of fugacities at thermodynamic equilibrium is represented as:

$$f_A^\alpha = f_A^\beta \ , f_B^a = f_B^\beta \qquad\qquad (3\text{-}6)$$

where f is the fugacity of component A or B in phase α or β.

As already stated, the hydrate phase equilibrium can be modelled using the approach of equal chemical potentials of water in the hydrate phase and in the fluid phases; or the approach of equal fugacities of water in the hydrate and fluid phases. In this study, the hydrate equilibrium conditions are modelled using the latter approach. Therefore, equilibrium amongst the gas (V), liquid (L) and hydrate (H) phases is represented by:

$$f_w^V(T,P) = f_w^L(T,P) = f_w^H(T,P) \qquad\qquad (3\text{-}7)$$

To solve these conditions, an EOS is used to calculate the fugacity in the fluid phase, and the solid solution theory of van der Waals and Platteeuw (1959) is used to calculate the fugacity of water in the hydrate phase. These are discussed in the sections that follow.

3.2 Thermodynamic model for the fluid phases

There are two well-known methods, which are based on the thermodynamic criteria for phase equilibrium, which are used for the computation of phase equilibrium data. The first is the combined, or gamma-phi $(\gamma - \varphi)$ method. In this method the activity coefficient γ and the fugacity coefficient φ are used to describe the liquid and vapour phase non-idealities respectively. An EOS is used to calculate the fugacity coefficient and an excess Gibbs energy model calculates the activity coefficient. The second method is the direct or the phi-phi $(\varphi - \varphi)$ method. In this method, the fugacity coefficient is used to describe both the liquid and vapour phase non-idealities. The fugacity coefficients for both phases are calculated using an EOS with an appropriate mixing rule. Both these methods have their limitations and have been reviewed extensively (Mühlbauer, 1990; Raal & Mühlbauer, 1997; Ramjugernath, 2000; Naidoo, 2004).

In this study, the direct method was chosen. The fugacity of water in solution in the vapour and the liquid phase, are calculated as follows:

$$f_w^V = \emptyset_w^V y_w P \tag{3-8}$$

$$f_w^L = \emptyset_w^L x_w P \tag{3-9}$$

It is difficult to select the most appropriate EOS, as there are several hundred available (Petticrew, 2011). Each EOS has its own shortcomings. In literature, three categories of EOS exist, these include: empirical, theoretical, and semi-empirical EOS. An empirical EOS is obtained by fitting experimental data to a function with numerous parameters. This EOS requires numerous experimental data and the use of a mixing rule for extension to mixtures. Theoretical EOS is determined from thermodynamic principles and is applicable to a wider range of systems, and semi-empirical EOS is a combination of empirical and theoretical EOS.

The van der Waals family of cubic EOSs are semi-empirical and are derived for pure liquids. They have been extended to mixtures by replacing the parameters with composition-dependent empirical mixing rules.

From literature, it was found that for systems containing H_2O (1) + former (2) and H_2O (1) + former (2) + inhibitors (3), the following EOS and mixing rules, presented in Table 3-1, are most commonly used:

Table 3-1: Commonly used EOS in hydrate modelling (adapted from Smith, 2015).

EOS	Reference	Mixing rule
Soave-Redlich-Kwong (1948)	Chun and Lee (1998)	Modified Huron-Vidal
	Kang et al. (1998)	Modified Huron-Vidal
	Sugahara et al. (2005)	van der Waals
	Delahaye et al. (2006)	Modified Huron-Vidal
Peng-Robinson (1976)	Ng and Robinson (1980)	Not stated
	Tohidi et al. (1995)	van der Waals
	Javanmardi et al. (2004)	Not stated
	Ngema et al. (2014)	van der Waals
Peng-Robinson-Stryjek-Vera (1986)	Klauda and Sandler (2000)	Not stated
	Sabil (2009)	Modified Huron-Vidal
Patel and Teja (1982)	Chen and Guo (1996)	Not stated
	Mei et al. (1996)	Not stated
	Ma et al. (2003)	Kurihara
Trebble-Bishnoi (1998)	Dholabhai et al. (1991)	Not stated
	Englezos (1992)	Quadratic
	Mahadev and Bishnoi (1999)	Not stated
Valderrama (1990)	Tohidi et al. (1995)	Non-density dependent
	Mohammadi et al. (2003)	Non-density dependant
	Masoudi et al. (2004b)	Non-density dependant
	Mohammadi et al. (2008b)	Non-density dependant

The Soave-Redlich-Kwong (SRK) EOS can be applied to non-polar or slightly polar fluids and the Peng-Robinson (PR) EOS requires little input information. The disadvantages of the PR EOS include low accuracy for liquid density prediction, inaccurate parameter prediction for non-hydrocarbons (particularly polar fluids), and inaccurate vapour predictions for pressures below 101.325 kPa (Naidoo, 2004).

At the expense of adding more parameters to the PR EOS, the Peng-Robinson-Stryjek-Vera (PRSV) EOS has improved vapour pressure predictions of non-polar and polar compounds. The Patel and Teja (PT) EOS is developed for non-polar systems only. The Valderamma EOS is a modification of the PT EOS. It is able to accurately predict equilibrium data for polar and non-polar compounds. Many articles have been reported recently which utilize the Valderamma EOS in conjunction with the non-density dependent (NDD) mixing rules. Mohammadi et al. (2008b) measured and modeled hydrate

dissociation data of methane, ethane, propane, and carbon dioxide in the presence of single NaCl, KCl, and CaCl$_2$ aqueous solutions.

In order to establish the effects of salts and thermodynamic inhibitors on the locus of incipient hydrate-liquid-water-vapour curve, Najibi et al. (2009) reported new experimental dissociation data for methane hydrates in the presence of alcohols (methanol and ethylene glycol) and electrolytes (NaCl, KCl, and CaCl$_2$). In both studies, the authors compared the experimental data with thermodynamic predictions that used the Valderrama EOS and NDD mixing rules to describe the fluid phase and the van der Waals and Platteeuw (1959) theory for describing the hydrate phase. Acceptable agreements were found between the experimental and predicted data of both studies. Deviations between the predicted and experimental results were not reported in either study. Belandria (2012) studied the hydrate phase equilibrium with gaseous mixtures of carbon dioxide and methane, and aqueous mixtures containing thermodynamic promoters. The author used the Valderrama EOS and the NDD mixing rule for modelling the fluid phases and the van der Waals and Platteeuw (1959) theory for modelling the hydrate phase. The author reported an absolute average relative deviation, on pressure measurements, of 9.7 %.

Englezos (1992) proposed a new theory for the computation of carbon dioxide hydrate formation conditions in aqueous electrolyte solutions. The author used the Trebble-Bishnoi EOS with quadratic mixing rule to describe the fluid phases. The results of the study showed a 7.2 % average deviation between the predicted and experimental pressure values. Klauda and Sandler (2000) proposed a fugacity model for gas hydrate phase equilibrium. The authors used the PRSV EOS and reported an overall average deviation based on pressure of 2.87 %. Sabil (2009) studied the phase behaviour, thermodynamics, and kinetics of gas hydrate systems of carbon dioxide in the presence of tetrahydrofuran and electrolytes. To describe the fluid phases, the author used the PRSV EOS with the Huron-Vidal-Orbey-Sandler (HVOS) mixing rule. For the system containing electrolytes, Sabil (2009) reported an average absolute deviation of 11.76 % between the predicted and experimental pressure values.

Based on the results from previous studies and the above-mentioned factors, the PR EOS as modified by Stryjek and Vera (PRSV EOS) (1986) in combination with the van der Waals classic mixing rule was selected for the phase equilibrium calculations of the fluid phases in this study.

3.2.1 The Peng-Robinson-Stryjek-Vera equation of state and classic mixing rule

The PR EOS modified by Stryjek and Vera (PRSV EOS) (1986) is defined as follows:

$$P = \frac{RT}{v - b} - \frac{a}{v(v + b) + b(v - b)} \tag{3-10}$$

where R is the universal gas constant, T is the temperature, P is the pressure, v is the molar volume, a is the attractive energy parameter, and b is the excluded volume parameter.

The parameters a and b may be calculated as follows:

$$a = 0.457235 \frac{(RT_c)^2}{P_c} \alpha \tag{3-11}$$

$$b = 0.077796 \frac{RT_c}{P_c} \tag{3-12}$$

In equation (3-11) and (3-12), T_c and P_c are the critical temperature and pressure, respectively, and α is the Stryjek-Vera temperature dependency, which is defined as:

$$\alpha = \left[1 + \kappa\left(1 + \sqrt{\frac{T}{T_c}}\right)\right]^2 \tag{3-13}$$

where κ is a function of temperature and is defined as:

$$\kappa = \kappa_0 + \kappa_1\left(1 + \sqrt{\frac{T}{T_c}}\right)\left(0.7 - \frac{T}{T_c}\right) \tag{3-14}$$

With

$$\kappa_0 = 0.378893 + 1.4897153\omega - 0.17131848\omega^2 + 0.0196554\omega^3 \tag{3-15}$$

In equation (3-15), ω is the acentric factor and κ_1 is an additional adjustable characteristic of each pure component.

The pure component parameters for the PRSV EOS (1986) used in this work are tabulated in Table 3-2.

Table 3-2: Properties of pure components for the PRSV EOS.

Component	P_C (MPa) [a]	T_C (K) [a]	ω [b]	κ_1 [b]
H_2O	22.064	647.14	0.3438	-0.06635
CO_2	7.3830	304.21	0.2250	0.04285

[a] Poling et al. (2001)

[b] Sabil (2009)

The compressibility of the liquid and vapour phases are found by obtaining the smallest and largest real roots respectively of the following cubic equation:

$$Z^3 - (1 - B)Z^2 + (A - 3B^2 - 2B)Z - (AB - B^2 - B^3) = 0 \qquad (3\text{-}16)$$

A and B are dimensionless forms of a and b respectively:

$$A = \frac{aP}{(RT)^2} \qquad (3\text{-}17)$$

$$B = \frac{bP}{RT} \qquad (3\text{-}18)$$

The classic mixing rule of van der Waals is used to extend the PRSV EOS to multicomponent systems. The a and b parameters are replaced with the following composition-dependent expressions:

$$a_{mix} = \sum_{i}^{n} \sum_{j}^{n} x_i x_j a_{ij} \qquad (3\text{-}19)$$

$$b_{mix} = \sum_{i}^{n} \sum_{j}^{n} x_i x_j b_{ij} \qquad (3\text{-}20)$$

a_{ij} and b_{ij} (i=j) are pure component (i) parameters while a_{ij} and b_{ij} (i≠j) are unlike-interaction parameters. The unlike-interaction parameters are related to pure-component parameters by:

$$a_{ij} = (1 - k_{ij})(a_{ii}a_{jj})^{0.5} \qquad (3\text{-}21)$$

$$b_{ij} = \frac{(b_{ii}b_{jj})}{2} \qquad (3\text{-}22)$$

where k_{ij} is a fitting parameter known as binary interaction coefficient. In this study, the binary interaction coefficient between water and CO_2 is taken as 0.1896 (Søreide and Whitson, 1992; Dhima et al., 1999; Smith, 2015).

The fugacity coefficient of component i in the liquid and vapour phase can then be calculated as follows (Smith et al., 2005):

$$\emptyset_i^{EOS} = \exp\left\{\frac{b_i}{b_{mix}}(Z-1) - \ln(Z-B) - \frac{A}{2\sqrt{2}B}\left(\frac{2\sum_j x_j a_{ij}}{a_{mix}} - \frac{b_i}{b_{mix}}\right) ln\left[\frac{Z+(1+\sqrt{2})B}{Z+(1-\sqrt{2})B}\right]\right\} \qquad (3\text{-}23)$$

3.2.2 The addition of an electrolyte component

Electrolytes are known to be excluded from the hydrate crystal lattice and the vapour phase (Englezos,1992). The addition of an electrolyte component to the system decreases the solubility of the guest molecule in the liquid phase. This is due to the fact that the interactions between the water molecules and the electrolytes are stronger compared to the interactions between the water and the dissolved guest molecules (the salting out effect). In the case of CO_2, even though the solubility decreases with the addition of electrolytes, it does not become negligible. The activity of water will therefore not only depend on the dissolved electrolytes but also on the CO_2. A model that accounts for the CO_2-water and electrolyte-water interactions is therefore required for the computation of the solubility of CO_2.

For systems containing electrolyte components, two approaches are used to predict the phase equilibrium. The first approach includes an EOS with mixing rules for the long and short range interactions. The second approach uses an EOS to describe the short-range interactions and an electrostatic term, such as Debye-Hückel, to describe the long-range interactions. The latter approach is used in this study. The reader is referred to Petticrew (2011) for further details on the various electrolyte models and the classifications of these models for the electrolyte component.

In 1991, Aasberg-Petersen developed a model to calculate the solubility of solutes like carbon dioxide in aqueous electrolyte solutions (Aasberg-Peterson et al., 1991). Englezos (1992) and Tohidi et al. (1995) both used this model for the determination of gas hydrate phase equilibrium conditions in systems containing electrolytes. Englezos (1992) compared the experimental data for the system CO_2 (1) + water (2) + 5.wt% NaCl (3) with the predicted data. The author reported an error, in terms of pressure, of 7.2 %. Tohidi et al. (1995) compared the experimental data for single and mixed salt

solutions for methane, ethane, propane, and carbon dioxide. The maximum deviation of the predicted hydrate formation temperature from the experimental values for these formers was ± 1 K.

In this study, the approach reported by Englezos (1992) and Tohidi et al. (1995) with the Aasberg-Peterson model (Aasberg-Peterson et al., 1991) for the electrolyte component was used. It is a generalized approach that can be simplified depending on the systems investigated. The Aasberg-Peterson model (Aasberg-Peterson et al., 1991) describes high-pressure solubility in aqueous electrolyte solutions and it is reasonably accurate for the determination of hydrate formation/dissociation conditions. In this model the liquid phase is treated as a salt-free mixture and the EOS approach as described in section 3.2.1 is used to describe it. However, the fugacity coefficient that is calculated by the EOS is corrected using the Debye-Hückel electrostatic term. This term depends on the ionic strength of the solution, the electrolyte concentration, and the type of electrolyte through an adjustable parameter that is independent of temperature and composition. It should be noted that non-temperature/non-composition dependent interaction parameter is only sufficient to describe the behaviour of systems at moderate temperatures and less concentrated conditions.

The fugacity in the aqueous liquid phase that contains the electrolytes are calculated from the following equation:

$$f_w^L = x_w \emptyset_w^{A-P} P \tag{3-24}$$

The fugacity coefficient, $\emptyset_w^{A-P}$, is determined from the Aasberg-Peterson model (Aasberg-Peterson et al., 1991) as follows:

$$ln\emptyset_w^{A-P} = ln\emptyset_w^{EoS} + ln\gamma_w^{EL} \tag{3-25}$$

The first term on the right hand side of equation (3-25) is determined from the EOS described in section 3.2.1. The second term accounts for the effect of the electrolytes and is given by Englezos (1992):

$$ln\gamma^{EL} = \frac{2Ah_{ws}M_mF(BI^{0.5})}{B^3} \tag{3-26}$$

where h_{ws} is the interaction coefficient between the dissolved salt and a non-electrolyte component and is calculated from (Tohidi, 1995):

$$h_{ws} = \frac{a + bT + cw_s + dw_s^2 + eTw_s}{1000} \tag{3-27}$$

where T is in K, w_s is the salt concentration in weight percent, and the constants $a, b, c, d,$ and e are fitting constants, or water-salt parameters, and presented in Table 3-3.

The fitting constants presented by Tohidi (1995) were determined by using vapour pressure depression data at 373.15 K and freezing point depression data of single salt solutions. These fitting constants can be used over a temperature range of 250 - 423 K as well as salt concentrations close to saturation (Tohidi, 1995).

In equation (3-26); M_m is the salt-free mixture molecular weight determined as a molar average, I is the ionic strength, and the parameters $A, B,$ and function F are given by the following equations:

$$A = 1.327757 \times 10^5 \frac{d_m^{0.5}}{(\varepsilon_m T)^{1.5}} \tag{3-28}$$

$$B = 6.359696 \times \frac{d_m^{0.5}}{(\varepsilon_m T)^{0.5}} \tag{3-29}$$

$$F(BI^{0.5}) = 1 + BI^{0.5} - \frac{1}{1 + BI^{0.5}} - 2\ln(1 + BI^{0.5}) \tag{3-30}$$

where ε_m is the salt-free mixture dielectric constant and is calculated from:

$$\varepsilon_m = x_N \varepsilon_N \tag{3-31}$$

In equation (3-31), x_N and ε_N are the salt-free mole fraction and dielectric constant of water respectively. The dielectric constant of water was obtained from the correlation developed by Zemaitis (1986) (where T is in K):

$$\varepsilon_N = 305.7 exp\left(-exp(-12.741 + 0.01875T) - \frac{T}{219}\right) \tag{3-32}$$

The equilibrium composition of the vapour (x_i) and liquid (y_i) phase components at the dissociation temperature and pressure conditions are required in the equations above. An Aspen Plus® flash calculation was conducted for each dissociation condition of the systems measured in this study. The reader is referred to Figure C-1 in Appendix C for the flow diagram of this calculation and Smith et al. (2005) for further information on flash calculations.

Table 3-3: Regressed constants for the interaction parameter, h_{ws}, in equation (3-27) (Tohidi et al., 1995).

Salt	a	b	c	d	e
NaCl	-11.91	1.037×10^{-2}	-6.043×10^{-2}	-5.814×10^{-3}	3.861×10^{-4}
KCl	-12.79	1.385×10^{-2}	5.184×10^{-2}	-2.152×10^{-3}	1.436×10^{-5}
CaCl$_2$	-5.672	8.037×10^{-3}	-3.330×10^{-1}	-1.771×10^{-3}	5.800×10^{-4}
Na$_2$SO$_4$	-5.495	7.476×10^{-3}	-1.769×10^{-2}	-8.905×10^{-4}	1.083×10^{-4}
NaF	-14.82	1.758×10^{-2}	-3.657×10^{-2}	-5.514×10^{-2}	1.258×10^{-3}
KBr	-14.04	1.705×10^{-2}	1.471×10^{-1}	-1.657×10^{-3}	-2.851×10^{-4}
MgCl$_2$	-6.420	1.066×10^{-2}	-6.186×10^{-1}	-4.556×10^{-3}	-1.312×10^{-3}
SrCl$_2$	-6.591	1.327×10^{-2}	-2.334×10^{-1}	9.035×10^{-4}	1.555×10^{-4}
BaCl$_2$	-5.905	8.248×10^{-3}	-9.799×10^{-2}	-2.780×10^{-4}	1.423×10^{-4}
MgCl$_2$	-6.420	1.066×10^{-2}	-6.186×10^{-1}	-4.556×10^{-3}	-1.312×10^{-3}
SrCl$_2$	-6.591	1.327×10^{-2}	-2.334×10^{-1}	9.035×10^{-4}	1.555×10^{-4}
BaCl$_2$	-5.905	8.248×10^{-3}	-9.799×10^{-2}	-2.780×10^{-4}	1.423×10^{-4}

The approach of Patwardhan and Kumar (1986) was employed to extend the above model to the mixed electrolyte solutions. In this model, an overall reduced ionic activity coefficient; related to the properties of single electrolyte solutions; was used to characterize the overall non-ideality of the aqueous mixed electrolyte solutions. This coefficient was calculated by the following equation (Tohidi, 1995):

$$\log a_w = \sum_i^{ns} S_i \log a_{w,i}^0 \tag{3-33}$$

where a_w is the activity of water in a solution of mixed electrolytes, $a_{w,i}^0$ represents the activity of water in a single electrolyte solution of the same ionic strength as that of a mixed electrolyte solution, i represents the electrolyte, and S_i represents the ionic strength fraction of electrolyte i.

Equation (3-33) does not contain any empirical constants and is valid over the entire concentration range encountered in this study (Patwardhan and Kumar, 1986).

The $a_{w,i}^0$ term in equation (3-33) was determined from the following:

$$a_w^0 = \frac{x_w \emptyset_w^{A-P}}{\emptyset_w^{EoS}} \tag{3-34}$$

Finally, the classical definition of activity was used to calculate the fugacity of the aqueous liquid phase that contained the mixed electrolytes:

$$f_w^L = a_w f_w^o \qquad\qquad (3\text{-}35)$$

where f_w^o is the fugacity of pure water at the specific dissociation temperature and pressure. The EOS outlined in section 3.2.1 was used to calculate the fugacity and fugacity coefficient in the liquid and vapour phases.

3.3 Thermodynamic model for the hydrate phase

The thermodynamic models for the representation of gas hydrate dissociation conditions are based on the solid solution theory of van der Waals and Platteeuw (1959). These authors derived the first equations, to calculate the hydrate dissociation conditions, by use of a simple model similar to the concept of the Langmuir gas adsorption.

The fundamental assumptions in the vdW-P theory are summarized as follows (Parrish and Prausnitz, 1972; Chen and Guo, 1998):

1) Each cavity in the hydrate lattice contains at most one molecule of hydrate former
2) The ideal gas partition function is applicable to the guest molecules
3) A pair potential function can describe the interaction between the guest and water molecules, and the cavity can be treated as perfectly spherical
4) Guest-guest molecule interactions can be neglected
5) No interaction occurs between the guest molecules in different cavities. The guest molecules interact only with the nearest neighbouring water molecules
6) The free energy contribution of the water molecules is independent of the modes of occupancy of dissolved guest molecules

The original van der Waals and Platteeuw (1959) model provided an approach that was sufficient for performing hydrate calculations, but was not adequate for accurate engineering calculations. Therefore, Parrish and Prausnitz (1972) extended the van der Waals and Platteeuw (1959) model.

These extensions included:

1) Non-ideal gas phase therefore accounting for higher pressures

2) Multicomponent gases in the gas phases. These included the hydrate formers and non-hydrate formers

3) London forces to account for the interactions between the gas and water molecules

4) Polar forces to account for bonding in the hydrate lattice

5) Kihara potential parameters used to determine the Langmuir parameters (refer to Parrish and Prausnitz (1972) for further details)

Numerous models have since been developed from the extension made by Parrish and Prausnitz (1972), each attempting to reduce the error between the experimental and modelled HLV equilibrium data, while maintaining the model simplicity for industrial purposes. These models are summarized and can be found in Appendix C.2, Table C-1.

According to the solid solution theory of van der Waals and Platteeuw (1959), at equilibrium conditions, the equality of fugacity of water in the liquid, vapour as well as the hydrate phases is applied as the criterion for hydrate dissociation conditions. Therefore:

$$f_w^L(T,P) = f_w^V(T,P) = f_w^H(T,P) \tag{3-36}$$

where f_w^L, f_w^V and f_w^H represent the fugacity of water in the liquid, vapour, and hydrate phases, respectively. The fugacity of water in the liquid and vapour phases can be determined using an EOS and an appropriate mixing rule (such as the PRSV EOS and classical mixing rule as used in this study).

The fugacity of water in the hydrate phase, f_w^H, is defined as (Klauda and Sandler, 2000):

$$f_w^H = f_w^{MT} \, exp\left(\frac{-\Delta\mu_w^{MT-H}}{RT}\right) \tag{3-37}$$

where, f_w^{MT} is the fugacity of water in the empty hydrate lattice and $-\Delta\mu_w^{MT-H}$ is the chemical potential difference of water between the empty hydrate lattice and the hydrate phase, and is determined using the following equation:

$$\Delta\mu_w^{MT-H} = \mu_w^{MT} - \mu_w^H = RT \sum_{m=1}^{NC} v_m \, ln\left(1 + \sum_{j=1}^{NH} C_{mj} f_j\right) \tag{3-38}$$

In equation (3-38), the superscripts NH and NC symbolize the number of hydrate formers and the number of cavity types in the hydrate lattice, respectively. Other symbols in the equation are explained as follow:

v_m is the number of cavities of type m per water molecule in a unit cell of a hydrate crystal lattice. These values are reported in Table 3-4. As stated previously (section 2.1), gas hydrate cavities are classified as either small or large.

f_j is the fugacity of the guest component in the vapour or liquid phase, which is calculated using an appropriate EOS.

C_{mj} is the Langmuir constant of the guest molecule j in the m cavity and it accounts for the gas-water interactions.

The Lennard-Jones-Devonshire theory (1938) is used to calculate the Langmuir constant $\left(C_{mj}\right)$ in equation (3-38) as follows (van der Waals and Platteeuw, 1959; Parrish and Prausnitz, 1972; Klauda and Sandler. 2000):

$$c_{mj} = \frac{4\pi}{kT} \int_{0}^{\infty} exp\left[\frac{-w(r)}{kT}\right] r^2 dr \tag{3-39}$$

where T is the absolute temperature, k is Boltzmann's constant, r is the radial distance from the centre of the cavity and $w(r)$ is the spherically symmetric cell potential and is defined as:

$$w(r) = 2z\varepsilon\left[\frac{\sigma^{12}}{\bar{R}^{11}r}\left(\delta^{10} + \frac{a}{R}\delta^{11}\right) - \frac{\sigma^6}{\bar{R}^5 r}\left(\delta^4 + \frac{a}{R}\delta^5\right)\right] \tag{3-40}$$

In equation (3-40), Z indicates the coordination number of each cavity (the number of molecules around the cavity) and $\bar{R}$ is the average radius of the cavity and the δ^N values are obtained from the following equation:

$$\delta^N = \left[\left(1 - \frac{r}{R} - \frac{a}{R}\right)^{-N} - \left(1 + \frac{r}{R} - \frac{a}{R}\right)^{-N}\right]/N \tag{3-41}$$

where N is an integer equal to 4,5,10 or 11 (Parrish and Prausnitz, 1972).

The reader is referred to the work of Parrish and Prausnitz (1972) for more information on equations (3-39) to (3-41).

For simplicity in calculations, Parrish and Prausnitz (1972) provided an emperical correlation for estimating the Langmuir constant (C_{mj}). For systems in the temeprature range 260 - 300 K, the Langmuir constants can be calculated with the following:

$$C_{mj} = \frac{A_{mj}}{T} exp\left(\frac{B_{mj}}{T}\right)$$ (3-42)

The values for A_{mj} and B_{mj} for different hydrate formers have been reported in open literature (Parrish and Prausnitz, 1972; Sloan and Koh, 2008). The values of A_{mj} and B_{mj} for calculating the Langmuir constants for the former (CO_2) used in this study as well as common hydrate formers are presented in Table 3-5.

Table 3-4: Ratio of the number of cavities to the number of water molecules present in the hydrate lattice (Van der Waals and Platteeuw, 1959).

Property	Structure 1	Structure 2
v_{small}	1/23	2/17
v_{large}	3/23	1/17

Table 3-5: Fitted parameters for calculating Langmuir constants for various gases, with an accuracy of ± 0.2% (Parrish and Prausnitz, 1972).

Former	Value (K)							
	Structure I				Structure II			
	Small		Large		Small		Large	
	A_{ml}	B_{ml}	A_{ml}	B_{ml}	A_{ml}	B_{ml}	A_{ml}	B_{ml}
	x 10^3	x 10^{-3}	x 10^2	x 10^{-3}	x 10^3	x 10^{-3}	x 10^2	x 10^{-3}
Methane	3.7237	2.7088	1.8372	2.7379	2.9560	2.6951	7.6068	2.2027
Ethane	0	0	0.6906	3.6316	0	0	4.0818	3.0384
Propane	0	0	0	0	0	0	1.2353	4.4061
Carbon dioxide	1.1978	2.8605	0.8507	3.2779	0.9091	2.6954	4.8262	2.5718

The fugacity of water in the empty hydrate lattice f_w^{MT} is calculated from the following equation (Englezos, 1992):

$$f_w^{MT} = f_w^L exp\left(\frac{\Delta\mu_w^{MT-L}}{RT}\right)$$ (3-43)

where f_w^L is the fugacity of liquid water and is calculated using an EOS, and $\Delta\mu_w^{MT-L} = \Delta\mu_w^{MT} - \Delta\mu_w^L$ and is the difference between the chemical potential of water in the empty hydrate lattice and pure liquid water. It is calculated from the equations proposed by Holder et al. (1980):

$$\frac{\Delta\mu_w^{MT-L}}{RT} = \frac{\Delta\mu_w^{\circ}}{RT_0} - \int_{T_0}^{T} \frac{\Delta h_w^{MT-L}}{RT^2} dT + \int_{P_0}^{P} \frac{\Delta V_w^{MT-L^{\circ}}}{RT} dP$$ (3-44)

where T_0 is the reference temperature (273.15 K), $\Delta\mu_w^{\circ}$ is a constant and represents the difference in the chemical potential of water in the empty hydrate lattice and the liquid water at the reference temperature, Δh_w^{MT-L} is the molecular enthalpy difference between the empty hydrate lattice and pure liquid water, and $\Delta V_w^{MT-L^{\circ}}$ is the molecular volume difference between the empty hydrate lattice and pure liquid water.

The variable Δh_w^{MT-L} is a function of temperature and is obtained from the following equation:

$$\Delta h_w^{MT-L} = \Delta h_w^{\circ} + \int_{T_o}^{T} \left(\Delta Cp_w^{\circ} + \beta(T - T^{\circ})\right) dT$$ (3-45)

where Δh_w° shows the enthalpy difference between the empty hydrate lattice and pure liquid water, and Cp_w° is heat capacity.

The parameters ($\Delta\mu_w^{\circ}, \Delta h_w^{\circ}, \Delta Cp_w^{\circ}, \Delta V_w^{MT-L^{\circ}}$ and β) needed to calulate the fugacity of water in the empty hydrate lattice have been reported in literature. A summary of these values is available in Englezos et al. (1991). In this work, the values reported by Parrish and Prausnitz (1972) were used and are shown in Table 3-6.

Table 3-6: Thermodynamic properties for sI and sII hydrates for liquid or ice and an empty hydrate lattice at 0 °C and zero pressure (Parrish and Prausnitz, 1972).

Property	Structure 1	Structure 2	Unit
$\Delta \mu_w^\circ$	1264	883	J/mol
Δh_w°	-4858	-5201	J/mol
$\Delta C p_w^\circ$	-38.13	-38.13	J/(mol.K)
β	0.141	0.141	J/(mol.K^2)
$\Delta V_w^{MT-L^\circ}$	4.6 x10^{-6}	5.0 x 10^{-6}	m^3/mol

3.4 A brief overview of thermodynamic models for systems containing alcohols and salts

Numerous studies have been conducted where thermodynamic models have been developed to predict hydrate equilibrium conditions for systems containing electrolytes and organic inhibitors. To the best of the author's knowledge, while there is an abundance of work on CO_2 and salt systems focused on desalination, there is limited data available in open literature on thermodynamic models for CO_2 gas hydrate systems containing alcohols and salts. As a result, gas hydrate systems with methane as the hydrate former have also been discussed below.

In a study conducted by Zuo et al. (2001), the authors developed a method to predict the hydrate forming conditions in a water-methanol-electrolyte solution. The authors extended the aqueous electrolyte EOS proposed by Fürst and Renon (1993) to water-methanol-electrolyte systems. The electrolytes studied were KCl, NaCl, and CaCl$_2$. By fitting vapour-liquid equilibrium (VLE) data for binary systems, the model parameters were determined. The predictions of VLE for the ternary water-methanol-electrolyte systems agreed well with the experimental data. The extended EOS was then combined with the Barkan and Sheinin (1993) model, which is based upon the statistical theory of gas hydrates, in pure water to develop a predictive method for the hydrate formation conditions. The method proposed by Zuo et al. (2001) was extensively tested in the study, for water-methanol-electrolyte systems with carbon dioxide as the hydrate former. The average deviation and the maximum deviation of the predicted pressures for the systems are presented in Table 3-7. The overall average absolute deviation of the predicted hydrate formation pressures was 4.3 %.

Table 3-7: Average and maximum deviations of the predicted pressures for aqueous-methanol-electrolyte systems asked on the model proposed by Zuo et al. (2001).

Electrolyte	Average deviation (%)	Maximum deviation (%)
KCl	3.0	11.7
NaCl	2.5	6.1
$CaCl_2$	4.9	12.9

Masoudi et al. (2005) extended an existing model (Valderrama EOS with the NDD mixing rules to describe the fluid phases and the van der Waals and Platteeuw (1959) theory to describe the hydrate phase) to include phase behaviour of aqueous solutions containing salts such as $CaCl_2$ and organic hydrate inhibitors such as ethylene glycol. The model was based on the equality of fugacities of salt in the salt phase and the aqueous phase, which was calculated from an EOS. The extended model treated the salts as pseudo components, which enabled the model to simultaneously predict gas hydrate formation and salt precipitation. The results of the study showed that the model was capable of predicting complex vapour-liquid-solid equilibrium (VLSE) for aqueous electrolytes and/or organic inhibitors over a wide range of pressure, temperature and salt concentrations. Methane and a methane-carbon dioxide gas mixture were used as the hydrate former in the study. No deviations between experimental and predicted results were reported. Hydrate dissociation data for a quaternary system, CH_4-H_2O-$CaCl_2$-ethylene glycol (EG), was measured at pressures up to 50 MPa. The predictive capabilities of the model for hydrate equilibrium were validated by the measured data. Good agreement between the model predictions and experimental data was observed. For more information on this model, the reader is referred to the work of Masoudi et al. (2005).

As already mentioned, Najibi et al. (2009) reported new experimental dissociation data for methane hydrates in the presence of alcohols (methanol and ethylene glycol) and electrolytes (NaCl, KCl and $CaCl_2$). The phase equilibrium was modelled using a thermodynamic approach that applied the Valderrama EOS with a modified Debye-Hückel electrostatic term to describe the fluid phases, and the theory of van der Waals and Platteeuw (1959) to describe the hydrate-forming phase. The authors of the study calculated the Langmuir constants using the Kihara potential model (Kihara, 1953). The freezing points of all the studied experimental aqueous solutions were measured in order to check the validity of a correlation developed previously by Najibi et al. (2006) for the prediction of hydrate equilibrium conditions in the presence of salts and alcohols. In the study methane was used as the

hydrate former and good agreement between measured data and predictions was observed. No deviations between experimental and predicted results were reported.

More recently Delavar and Haghtalab (2015) developed a thermodynamic model for the prediction of gas hydrate formation conditions in the presence of organic inhibitors, salts as well as their mixtures. The UNIQUAC model in combination with the Chen-Guo model (Chen and Guo, 1998) was used to describe the hydrate phase. The SRK EOS with the Huron-Vidal-Orbey-Sandler (HVOS) mixing rule, in conjunction with Henry's law was used to describe the fluid phase. Methanol, ethanol, monoethylene glycol, diethylene glycol, triethylene glycol, glycerol, NaCl, KCl, $CaCl_2$, and $MgCl_2$ were considered as hydrate inhibitors. The predictions in the study were performed in the presence of single inhibitors, mixed salts and a mixture of alcohol and salts. The formers investigated in the study were CH_4, C_2H_6, C_3H_8, CO_2, and H_2S. In their model, Delavar and Haghtalab (2015) obtained the binary interaction parameters of the UNIQUAC model through direct regression of hydrate experimental data. The salts were treated as single components (solvated salt molecules) in order to ignore the long-range interactions (electrostatic forces) resulting in a reduction of the interaction parameters. Despite the simplicity of the approach proposed by Delavar and Haghtalab (2015), the results of their study (predicted data) were in good agreement with experimental data. The reader is referred to the article by Delavar and Haghtalab (2015) for more information regarding the model as well as the detailed results of their study.

From the analysis performed on the literature data, it is evident that each model used by the various authors in the respective studies has its own set of limitations.

4

CHAPTER FOUR

A REVIEW OF EXPERIMENTAL METHODS AND EQUIPMENT

Since the discovery of gas hydrates, many apparatus and experimental methods have been used for the measurement of hydrate phase equilibrium. Presently, the most common experimental set-up comprises of a batch reactor cell, with a stirrer, and heating and cooling mechanisms. Gas sampling and visual observation systems are also common (Lee et al., 2005; Sloan and Koh, 2008). In this chapter, the various experimental methods developed for measurement of high-pressure hydrate phase equilibrium are presented. Thereafter a summary of the most common apparatus used for these measurements is presented. The experimental methods include isothermal, isobaric, and isochoric techniques. These methods can be further divided into direct and indirect procedures. Visual observation is the only way to determine hydrate phase equilibrium data directly. The visual isothermal method is an example of a direct procedure. The indirect procedure is based on the occurrence of an increase in pressure during hydrate dissociation. The non-visual isothermal method is an example of an indirect procedure. The visual method is only recommended for systems above the freezing point of water as it is difficult to distinguish between ice crystals and gas hydrates (Schroeter et al., 1983). In addition, the experimental data obtained visually on a microscopic and macroscopic level differ. Non-visual methods are more common and have a higher level of accuracy (Sloan and Koh, 2008).

During the discovery period of hydrates between 1810 and 1900, the apparatus used for the measurement of hydrate phase equilibrium were equipped with hand-blown glass and used at conditions of low pressure. This glass was expensive and fragile and did not have the ability to measure the conditions of gas hydrates at high pressures. Later, between 1888 and 1890, the glass

container was changed to a round metal container for the measurement of methane and ethane hydrate dissociation conditions at higher pressures (Villard, 1888; Villard, 1890). The apparatus currently used to measure hydrate phase equilibrium conditions include the quartz crystal microbalance, Cailletet, rocking cell, high-pressure differential scanning calorimetry, differential thermal analysis, and the high-pressure autoclave cell.

4.1 Available experimental methods

A variety of methods have been developed for high-pressure phase equilibrium measurements. The suitability of the method adopted depends on the experimental conditions, the application, the system under investigation, the properties to be measured, and the required accuracy (Belandria, 2012).

Different classifications of these experimental methods have been proposed. Richon (1996) based the classification of experimental methods on the method of equilibration between the phases in equilibrium. Two main categories may be distinguished in the classification by Richon (1996): dynamic (open circuit) and static (closed circuit) methods. Dynamic methods involve forced circulation of one or more phases and are usually associated with increased time and costs for maintenance and construction. In static methods, the equilibrium may be achieved with or without recirculation of the fluid phases, generally using an internal stirring mechanism to reduce the time required for reaching equilibrium (Raal and Mühlbauer, 1998). Dohrn et al. (2010) classified the different experimental measurements according to the manner in which the compositions of the equilibrium phases are determined (analytically or not), and whether or not the mixture under investigation has been synthesized with precisely known compositions, namely, analytical and synthetic methods respectively.

A further distinction among the experimental methods can be made between those based on visual and non-visual means of hydrate detection. At constant conditions of temperature or pressure, the experimental method adopted commonly requires visual observation of hydrate crystals. As previously mentioned, the visual experimental methods may only be used at temperatures above the freezing point of water in order to avoid any confusion with ice crystals (Schroeter et al., 1983). Over a wide range of pressures, hydrate phase equilibrium measurements may be performed in a constant volume cell without the need for visual observation.

Three experimental methods have thus been established for operating a hydrate formation apparatus: isothermal, isobaric, and isochoric (Sloan and Koh, 2008). The hydrate dissociation point is a repeatable thermodynamic equilibrium point (Tohidi et al., 2000) and is defined as the conditions of

temperature and pressure where the last hydrate crystal dissociates (Gjertsen and Fadnes, 2000). Therefore in all three procedures, the hydrate dissociation point is taken as the hydrate equilibrium conditions. The basic properties of each method are summarized in Table 4-1. For a detailed review on each experimental method the reader is referred to Appendix D.1 and the works by Sloan and Koh (2008), Petticrew (2011), Belandria (2012), and Smith (2015).

Table 4-1: Commonly used experimental methods for measuring hydrate dissociation conditions (Sloan and Koh, 2008).

Method	Principle	Hydrate formation	Hydrate dissociation
Isothermal - visual	Constant temperature	Visual observation	Visual observation
Isothermal - non visual	Constant temperature	Pressure decrease	Pressure increase
Isobaric	Constant pressure	Exchange of gas from external reservoir	Visual observation of hydrate disappearance
Isochoric	Constant volume	Pressure decrease	Intersection point of hydrate dissociation and cooling trace

4.2. Review of experimental equipment

The most common apparatus used for the measurement of hydrate phase equilibrium are: the quartz crystal microbalance (QCM), Cailletet, the high pressure rocking cell, high pressure differential scanning calorimetry, differential thermal analysis and high pressure autoclave. Table 4-2 below presents a summary of these apparatus. The operating principle, advantages and experimental difficulties typically encountered with their use are also presented.

For a detailed review on each apparatus the reader is referred to Appendix D and the works by Sloan and Koh (2008), Petticrew (2011), Belandria (2012), and Smith (2015). For a more detailed description on a specific apparatus, the reader is referred to the literature reference as indicated in Table 4-2.

Table 4-2: Summary of experimental apparatus used for the measurement of hydrate phase equilibrium.

Apparatus	Equipment description	Operating conditions a) Temperature b) Pressure	Advantages	Experimental difficulties	References
Quartz crystal microbalance (QCM)	The QCM consists of two electrodes, which are separated by a thin quartz disk. Passing an electric current through the electrodes will oscillate the crystal at a specific resonant frequency. A change in the resonant frequency will occur when a mass attaches itself to the surface of the crystal disk. Therefore hydrate formation (the mass) can be detected by the change in resonant frequency.	a) 273.8 - 284.6 K b) 13.56 - 45.36 MPa	1. Requires small experimental samples (~ drop of water). 2. Reduced time required for hydrate measurement (15 min per temperature step versus several hours for conventional methods.	1. Requires the hydrate to adhere to surface of quartz crystal. Failure to occur results in the unfeasibility of measurement.	Tohidi et al. (2002), Mohammadi et al. (2003) and Sloan and Koh (2008).
Cailletet	The Cailletet tube is essentially the equilibrium cell. The upper end of the tube is closed and the open end has a conical thickening enabling the tube to be mounted into an autoclave. By using mercury as a sealing and pressure-transmitting fluid, the experimental samples are confined in the top of the tube.	a) 250.2 - 450.2 K b) 0.35 - 15 MPa	1. High pressure apparatus.	1. Mercury is highly toxic. 2. Susceptible to mechanical degradation due to regular volume adjustments. 3. Requires visual observation.	Peters et al. (1986), Peters et al. (1993), Raeissi (2004), and Sabil (2009).

Table 4-2 (continued): Summary of experimental apparatus used for the measurement of hydrate phase equilibrium.

Apparatus	Equipment description	Operating conditions a) Temperature b) Pressure	Advantages	Experimental difficulties	References
High pressure rocking cell	High-pressure equilibrium cell mounted on a horizontal pivot for 180 ° pneumatic controlled rocking. The rocking of the cell, and consequent movement of the mixing balls within it, ensures adequate mixing of the cell fluids. The rocking rate of the cell is dependent on the degree of mixing required.	a) 243.2 - 325.2 K b) Up to 50.0 MPa	1. Allows data to be obtained continuously. 2. Automation of temperature control. 3. Allows for visual observation while using the isochoric experimental method.	1. Susceptible to mechanical deterioration due to the continuous rocking motion.	Najibi et al. (2009).

Table 4-2 (continued): Summary of experimental apparatus used for the measurement of hydrate phase equilibrium.

Apparatus	Equipment description	Operating conditions a) Temperature b) Pressure	Advantages	Experimental difficulties	References
High-pressure differential scanning calorimetry (DSC)	Equipped with two pressure-controlled cells: a sample cell and a reference cell. The sample cell contains the experimental solution and the reference cell remains empty. The sample cell is charged with the experimental system and placed in the furnace and connected to the gas feed line. The gas pressure is set to the desired value and kept constant for each experimental point.	a) 228.2 - 393.2 K b) Up to 40 bar.	1. Rapid and easy to operate. 2. May be used for thermodynamic and kinetic gas hydrate studies. 3. Requires small experimental samples (25 mg).	1. Method of data interpretation is complex. 2. Possibility of high measurement uncertainty.	Dalmazzone et al. (2002), Dalmazzone et al. (2003), Martinez et al. (2008), and Mayoufi et al. (2009).
Differential thermal analysis	Two symmetric transparent glass cells. One of the cells contains the experimental solution and the other cell contains an inert solution that is used as a reference. The setup is submerged in a temperature-controlled bath. The initial pressures in the cells are set by the injection of gas via an injection system.	a) 250.2 - 290.2 K b) Up to 40 bar.	1. Allows for high-pressure measurements.	1. Method of data interpretation is complex.	Fournaison et al. (2004)

Table 4-2 (continued): Summary of experimental apparatus used for the measurement of hydrate phase equilibrium.

Apparatus	Equipment description	Operating conditions a) Temperature b) Pressure	Advantages	Experimental difficulties	References
High pressure autoclave	The core of the apparatus is a high-pressure cylindrical cell that are constructed of either sapphire or 316 stainless steel. The cell can have a volume between 30 and 2000 cm^3. The autoclave cell may be visual or non-visual. For visual cells sapphire or Plexiglas windows are fitted into the cell for direct observation. A magnetic or mechanical stirrer generally achieves cell agitation. In cases where vortex formation is possible, baffles may be used to reduce the effect (Lee et al., 2005). The high-pressure cell is immersed in a thermostat bath for temperature control.	a) Extremely wide b) Extremely wide	1. Allows for simple construction and operation. 2. Capable of sampling cell contents if required. 3. Compatible with many chemicals. 4. Any experimental method may be used. 5. Fittings and o-rings are easily available for replacement.	1. Detecting a rectifying a pressure leak is time consuming.	Kang et al. (1998); Lee et al. (2005); Herri et al. (2011); Petticrew (2011); Smith (2015).

Extensive research has been conducted on gas hydrate phase equilibrium for pure water systems and aqueous solutions containing inhibitors, using high-pressure autoclaves. A summarized review on the various high-pressure autoclave apparatus used for gas hydrate equilibrium measurements on aqueous systems is presented in Table 4-3.

Table 4-3: Review of high-pressure autoclave apparatus.

Reference	Experimental method	Equilibrium cell a) MOC b) Volume c) Agitation (rpm)	Temperature a) Range b) Accuracy c) Measuring device	Pressure a) Range b) Accuracy c) Measuring device	Cooling/Heating mechanism	Additional studies conducted on the apparatus
Englezos and Bishnoi (1991)	Isothermal pressure search	a) Stainless steel with Plexiglas windows b) 293.6 - 221.2 cm^3 (variable volume - changed by floating piston) c) Magnetic stir bar coupled to a set of 10 magnets	a) 265.36 - 282.98 K b) ± 0.06 K c) Omega platinum resistance thermometers	a) 0.488 - 2.188 MPa b) ± 10 kPa c) Rosemount differential-pressure transducer and a Bourdon tube Heise Pressure gauge	Thermostatic bath with water/glycol mixture	Bishnoi and Dholabhai (1993), Dholabhai et al. (1993), and Dholabhai and Bishnoi (1994).
Dholabhai et al. (1991)	Isothermal pressure search	a) Stainless steel with Plexiglas windows b) 500 cm^3 c) Magnetic stir bar with external magnet	a) 264 - 284 K b) ± 0.05 K c) Two type T thermocouples	a) 2.5 - 9.7 MPa b) ± 25 kPa c) Rosemount differential-pressure transducer and a Bourdon tube Heise Pressure gauge	Insulated tank with continuously circulated water/glycol coolant	

Table 4-3 (continued): Review of high-pressure autoclave apparatus.

Reference	Experimental method	Equilibrium cell a) MOC b) Volume c) Agitation (rpm)	Temperature a) Range b) Accuracy c) Measuring device	Pressure a) Range b) Accuracy c) Measuring device	Cooling/Heating mechanism	Additional studies conducted on the apparatus
Englezos and Ngan (1993)	Isothermal pressure search	a) Stainless steel with Plexiglas windows b) Not stated c) Magnetic stir bar with external magnet	a) 261.9 - 278.3 K b) ± 0.10 K c) Two Omega copper – constantan thermocouples	a) 0.157 - 0.545 MPa b) ± 0.25 % of span c) Bourdon tube Heise Pressure gauge	Temperature controlled bath with 50/50 water/glycol mixture	Englezos and Hall (1994)
Chun et al. (1996)	Isochoric pressure search	a) Stainless steel with two sight glasses. b) 50 cm^3 c) Magnetic spin bar with an external magnet.	a) 276.3 - 286.2 K b) ± 0.10 K c) K - type thermocouple with a digital thermometer	a) 0.141 - 4.860 MPa b) ± 0.01 MPa c) Heise gauge for high-pressure measurements and a pressure gauge supplied by Ujin Instrument Co. for low-pressure measurements.	Thermostatic water bath	Chun et al. (2000)

Table 4-3 (continued): Review of high-pressure autoclave apparatus.

Reference	Experimental method	Equilibrium cell a) MOC b) Volume c) Agitation (rpm)	Temperature a) Range b) Accuracy c) Measuring device	Pressure a) Range b) Accuracy c) Measuring device	Cooling/Heating mechanism	Additional studies conducted on the apparatus
Dholabhai et al. (1996)	Isothermal pressure search	a) Sapphire b) Variable volume (volume changed by varying quantity of mercury in the reservoir). c) Stir bar coupled with external magnets.	a) 264.0 - 282.0 K b) 0.13 K c) Thermocouple	a) 1.500 - 10.40 MPa b) ± 5.4 kPa c) Heise gauge and gauge pressure transmitter	Thermostatic bath with water/glycol mixture	Dholabhai et al. (1997), Bishnoi and Dholabhai (1999), Mahadev and Bishnoi (1999)
Mei et al. (1996)	Isothermal pressure search	a) Transparent sapphire cell. b) 78 cm^3 (variable volume – adjusted by a floating piston). c) Magnetic stirrer with an external magnet.	a) 268.1 - 285.8 K b) ± 0.085 K c) Two platinum resistance thermometers	a) 2.050 - 12.68 b) ± 0.025 MPa c) Variable-span differential pressure transducer and a Heise pressure gauge.	Air bath	Mei et al. (1998), Fan and Guo (1999)

Table 4-3 (continued): Review of high-pressure autoclave apparatus.

Reference	Experimental method	Equilibrium cell a) MOC b) Volume c) Agitation (rpm)	Temperature a) Range b) Accuracy c) Measuring device	Pressure a) Range b) Accuracy c) Measuring device	Cooling/Heating mechanism	Additional studies conducted on the apparatus
Nixdorf and Oellrich (1997)	Isochoric pressure search	a) Acid and corrosion resistant stainless steel b) 500 cm^3 c) Permanent magnetic stirrer	a) 243.15 - 423.15 K b) ± 0.02 K c) Two platinum resistance thermometers	a) 0 - 25 MPa b) ± 0.06 MPa c) Pressure pick up capped with a transducer	Pressure less heating sleeve filled with circulating glycol/water mixture	
Ivanic et al. (2004)	Isochoric pressure search	a) Stainless steel b) 300 cm^3 c) Mechanical stirrer (400 rpm)	a) 274 - 300 K b) ± 0.05 K c) Omega thermistor probes	a) 0 - 35 MPa b) ± 5 % of span c) Sensotec pressure transducers	Emersion heaters and constant-flow portable cooling unit to warm and cool water bath respectively.	
Maekawa (2006)	Isothermal pressure search	a) Stainless steel b) 700 cm^3 c) Magnetic stirrer	a) 273.5 - 278.5 b) ± 0.1 K c) Two platinum resistance thermometers	a) 0 - 1 MPa b) ± 0.01 MPa c) Semi-conductor pressure transducer	Thermostatic bath with glycol/water mixture	Maekawa (2008), Maekawa (2010) and Maekawa (2013)

Table 4-3 (continued): Review of high-pressure autoclave apparatus.

Reference	Experimental method	Equilibrium cell a) MOC b) Volume c) Agitation (rpm)	Temperature a) Range b) Accuracy c) Measuring device	Pressure a) Range b) Accuracy c) Measuring device	Cooling/Heating mechanism	Additional studies conducted on the apparatus
Afzal et al. (2007)	Isochoric pressure search	a) Stainless steel with two sapphire windows b) 57.5 cm3 c) Magnetic stirrer	a) 264.7 - 282.6 K b) ± 0.02 K c) Two platinum resistance thermometers	a) 0.61 - 5.12 MPa b) ± 0.002 MPa c) Two pressure transducers: 0 - 0.6 MPa for low pressure and 0 - 8 MPa for high-pressure measurements.	Temperature controlled liquid bath	Mohammadi et al. (2008a), Mohammadi et al. (2008b) and (Mohammadi et al., 2009).
Ruffine et al. (2010)	Isobaric temperature search	a) Stainless steel with sapphire windows b) Variable volume (adjusted by displacement of a piston) c) N/S	a) 253 - 473 K b) ± 0.4 K c) K-type thermocouple	a) 0 - 60 MPa b) ± 0.01 MPa c) WIKA pressure transmitter	Welded metal jacket with circulating thermal fluid	

Table 4-3 (continued): Review of high-pressure autoclave apparatus.

Reference	Experimental method	Equilibrium cell a) MOC b) Volume c) Agitation (rpm)	Temperature a) Range b) Accuracy c) Measuring device	Pressure a) Range b) Accuracy c) Measuring device	Cooling/Heating mechanism	Additional studies conducted on the apparatus
He et al. (2011)	Isothermal pressure search	a) N/S b) N/S c) Mechanical stirrer (200 - 1400 rpm)	a) 276 K b) ± 0.1 K c) Thermocouple	a) 0 - 10 MPa b) ± 0.1 kPa c) Keller digital monometer	Temperature controlled water bath	
Herri et al. (2011)	Isochoric pressure search	a) Stainless steel b) 1 L c) Mechanical stirrer	a) 273 - 277 K b) ± 0.02 K c) Two platinum resistance thermometers	a) 0 - 10 MPa b) ± 0.05 MPa c) Keller pressure transducer	Double jacketed cell connected to an external cooler	
McNamee and Conrad (2011)	Isochoric pressure search	a) Stainless steel with sapphire windows b) 450 cm^3 c) Overhead and magnetic stirrer	a) 263.15 - 333.15 K b) ± 0.1 K c) Thermocouple	a) 20 MPa b) N/S c) Analogue pressure gauge and pressure transducer	Cooling jacket and chiller	

Table 4-3 (continued): Review of high-pressure autoclave apparatus.

Reference	Experimental method	Equilibrium cell a) MOC b) Volume c) Agitation (rpm)	Temperature a) Range b) Accuracy c) Measuring device	Pressure a) Range b) Accuracy c) Measuring device	Cooling/Heating mechanism	Additional studies conducted on the apparatus
Petticrew (2011) (modified from Tshibangu, 2010)	Isochoric pressure search	a) Stainless steel b) 60.0 cm^3 c) Impeller with embedded magnet (325 rpm)	a) 268.1 - 288.3 K b) ± 0.092 K c) Two platinum resistance thermometers	a) 86.0 - 645 kPa b) ± 0.640 kPa c) Two pressure transducers	Temperature controlled water bath with 80/20 glycol/water mixture	Ngema (2014), Ngema et al. (2014)
Javanmardi et al. (2012)	Isochoric pressure search	a) Stainless steel with sight glasses b) 75 cm^3 c) N/S	a) 256.4 - 282.0 K b) ± 0.1 K c) Platinum resistance probe	a) 1.97 - 6.96 MPa b) ± 0.01 MPa c) Pressure transducer	Thermostatic bath	
Ngema (2014)	Isochoric pressure search	a) Stainless steel b) 38.5 cm^3 (working volume). c) Magnetic stirring device coupled with an external magnet (600 rpm)	a) 272.6 - 291.8 K b) ± 0.09 K c) Platinum resistance probe	a) 0.098 - 1.345 MPa b) ± 0.005 MPa c) WIKA pressure transmitter	Temperature controlled water bath with 80/20 glycol/water mixture	Ngema et al. (2016a), Ngema et al. (2016b)

From the review conducted on high-pressure autoclave apparatus, it is evident that: the volume of the equilibrium cell has decreased, requiring smaller quantities of the experimental sample, the stirring speed had been reduced from 1400 rpm in some instances, to only 400 rpm; and the agitation device has been improved. These advances to the apparatus have improved the reliability of the equilibrium data obtained, reduced experimental uncertainties, and reduced the required time for the measurement of hydrate equilibrium data, allowing more data point to be obtained in a shorter time.

The high-pressure autoclave experimental set-up, combined with the isochoric pressure search method, was chosen for this study. The experimental set up, as well as the experimental method is discussed in detail in Chapter 5.

<div align="right">

5

</div>

<div align="right">

CHAPTER FIVE

</div>

DESCRIPTION OF EXPERIMENTAL APPARATUS AND PROCEDURE

Accurate gas hydrate equilibrium data is vital for the design of hydrate-based processes, such as desalination, and the development and testing of predictive thermodynamic models. In order to attain accurate hydrate equilibrium data, a reliable apparatus and a well-defined, reproducible experimental method is essential.

The static, non-visual isochoric pressure search method, discussed in Chapter 4, was selected to obtain the hydrate equilibrium data. This isochoric method is better than the isothermal and isobaric methods, as it is independent of visual observations, thus eliminating that source of uncertainty (Oellrich, 2004). The hydrate equilibrium data was measured in a static, high-pressure equilibrium apparatus. The advantages of this equipment-method combination include: higher levels of accuracy, stronger agitation, and an automated process, which made it possible to conduct measurements overnight.

This chapter describes the apparatus used in this study. The core of the experimental set-up is the static, high-pressure equilibrium cell that is placed inside a temperature-controlled bath. An agitator, temperature controllers, temperature and pressure sensors, vacuum pump, and a data acquisition system are additional devices used in the apparatus. The accuracy and limitation of the measuring devices are also presented. In addition, the materials used, their purities and supplies are described. Prior to conducting measurements, temperature and pressure calibrations, leak tests, cell preparation, and sample preparation is required. These are also explained.

5.1 Materials

The materials used in this study (for measurements and cell-preparation) as well as the purities and suppliers are reported in Table 5-1. Ultrapure Millipore water with a conductivity of 1.5 μS was used in all measurements. The Ultrapure Millipore water was supplied by the University of KwaZulu-Natal's analytical laboratory situated in the Chemical Engineering department.

Table 5-1: Purities and suppliers of gas, inorganic, and organic component used in this study.

Gas	Formula	Supplier	Purity[*] (vol %)
Carbon dioxide	CO_2	AFROX Ltd	99.999
Nitrogen	N_2	AFROX Ltd	99.999
Sodium chloride	NaCl	Merck (Pty) Ltd	> 99.0
Potassium chloride	KCl	Merck (Pty) Ltd	> 99.0
Anhydrous calcium chloride	$CaCl_2$	Merck (Pty) Ltd	> 98.0
Magnesium chloride hexahydrate	$MgCl2 \cdot H_2O$	Merck (Pty) Ltd	> 99.0
Anhydrous sodium sulphate	Na_2SO_4	Merck (Pty) Ltd	> 99.0
Ethanol	CH_3CH_2OH	Merck (Pty) Ltd	> 99.5
Acetic acid	$C_2H_4O_2$	Merck (Pty) Ltd	> 99.0
Propionic acid	$C_3H_6O_2$	Fluka Chemie AG	> 99.5

[*] Purity as stated by the Supplier

5.2 Experimental apparatus

A static, high-pressure equilibrium cell, originally commissioned by Ngema (Ngema, 2014), was used for the experimental hydrate measurements. A schematic of the apparatus is presented in Figure 5-1. The experimental set-up comprised of:

1. A static, high-pressure stainless steel equilibrium cell
2. A Heidolph RZR 2041 overhead stirring device
3. A liquid bath with viewing windows
4. A Grant TXF200 programmable temperature controller
5. A Pt-100 temperature probe
6. A WIKA pressure transducer, 0 - 10 MPa range
7. A Variac voltage regulator
8. A 349724A LXI Agilent data acquisition unit

9. A Polyscience® IP-35 cold finger

10. A mechanical jack

11. A RV3 Edwards vacuum pump

12. A Shinko ACS-13A controller
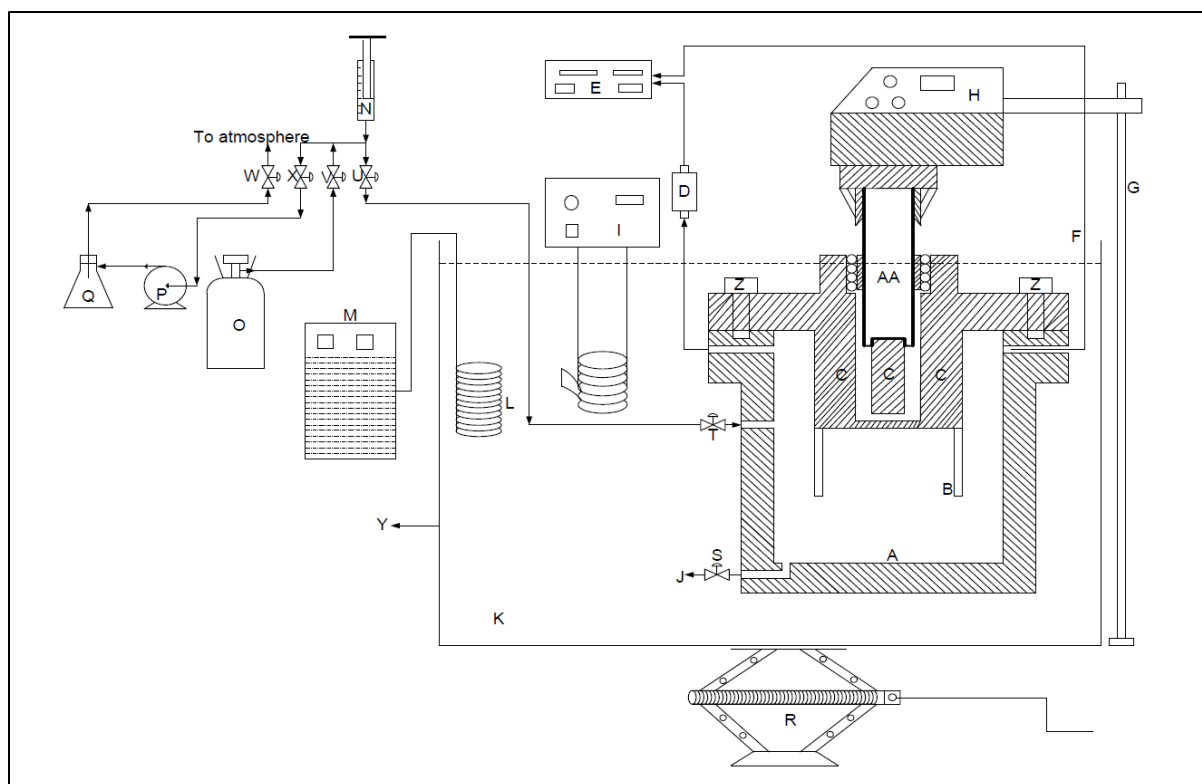
Figure 5-1: Schematic of the experimental setup. (A) Equilibrium cell; (B) Impeller; (C) Neodymium magnet; (D) Pressure transducer; (E) Data acquisition unit; (F) Pt-100; (G) Stainless steel stand; (H) Overhead mechanical stirrer; (I) Temperature programmable controller; (J) Drain line; (K) Thermosetting fluid; (L) Cooling coil; (M) Cold finger; (N) Liquid syringe with aqueous solution; (O) Caron dioxide gas cylinder; (P) Vacuum pump; (Q) Vacuum flask; (R) Mechanical jack; (S) Drain valve; (T) Inlet valve; (U) Loading valve; (V) Gas valve; (W) Vent valve to atmosphere; (X) Vacuum valve; (Y) Liquid bath and (Z) Stainless steel bolts (taken from Ngema, 2014).

5.2.1 The equilibrium cell

The static, high-pressure equilibrium cell is the core of the experimental set-up. The cell used in this study was constructed out of 316 stainless steel. This material is resistant to corrosion, has a long life span and excellent mechanical strength. The main advantage of stainless steel is that it performs well over a vast temperature range and can withstand the high pressures required for hydrate measurements. Figures 5-2 to 5-4 and Photograph 5-1 show schematics of the static, high-pressure equilibrium cell that was used in this study.
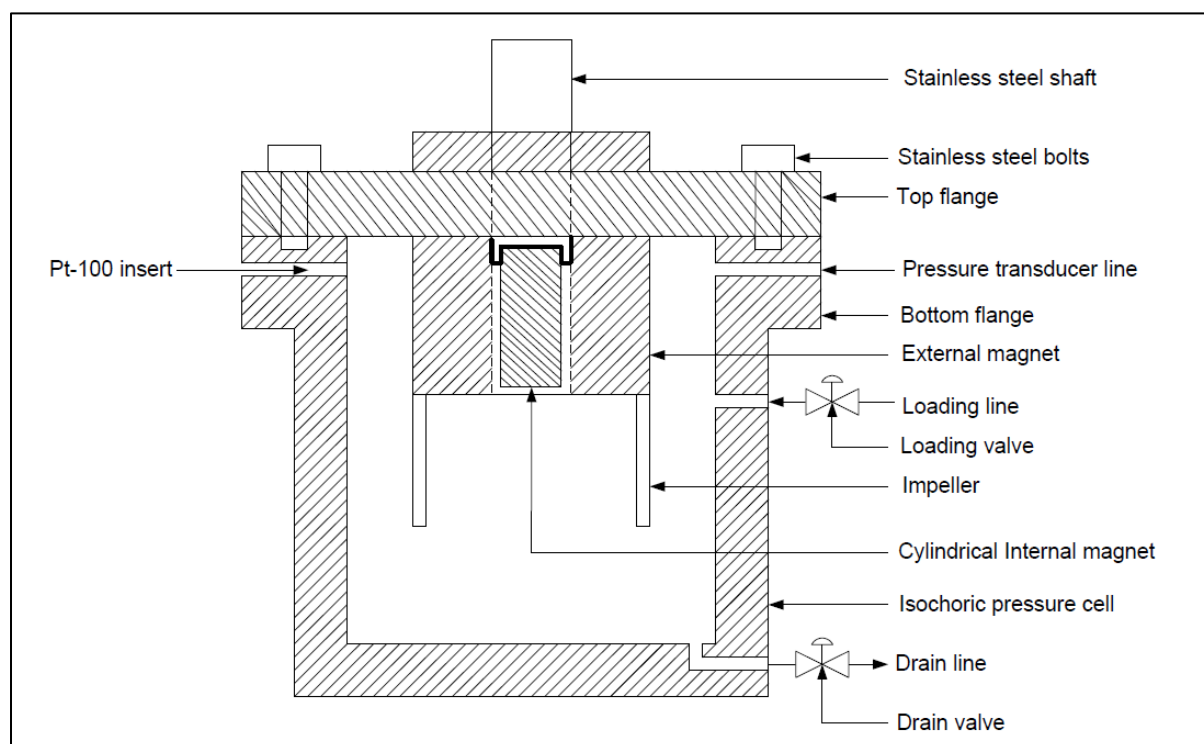
Figure 5-2: A schematic of the equilibrium cell (Ngema, 2014).

The cell had an internal height of 45 mm and an internal diameter of 40 mm. This resulted in an internal volume of approximately 56 cm^3. A magnetic stirring device (discussed in more detail in section 5.2.2) was placed inside the cell, resulting in a working volume of approximately 38.5 cm^3. A side view (exterior view) of the equilibrium cell indicating the cell dimensions is shown in Figure 5-3.

An O-ring was positioned into a groove in the bottom flange in order to ensure good sealing between the cell and top flange (see Photograph 5-1 and Figures 5-3 and 5-4). The groove for the O-ring was 2 mm in diameter and depth. The O-ring used must be compatible with all chemicals (cleaning solvents, components within the aqueous solution, and gases) used to carry out the measurements. For the purpose of this study, a Nitrile O-ring was used. The top flange was fixed to the top of the cell with 6

x 10 mm diameter stainless steel bolts. The top flange was 10 mm thick, with an outer diameter of 80 mm. The bottom flange was 15 mm thick also with an outer diameter of 80 mm.

Four holes, each with a diameter of 8 mm, were drilled into the equilibrium cell. The first hole, situated on the bottom flange was used to connect 1/16' inch 316 stainless steel tubing to the pressure transducer. The second hole, situated to the left of the first, housed a Class A Pt-100 temperature probe that measured the equilibrium cell temperature. The third hole situated on the opposite side of the pressure transducer line and below the bottom flange was used for filling, loading and evacuating the cell contents. The last hole, situated below the loading line was used for the discharge of cell contents. All stainless steel lines, fittings, compression valves, and ball valves were purchased from Swagelok.
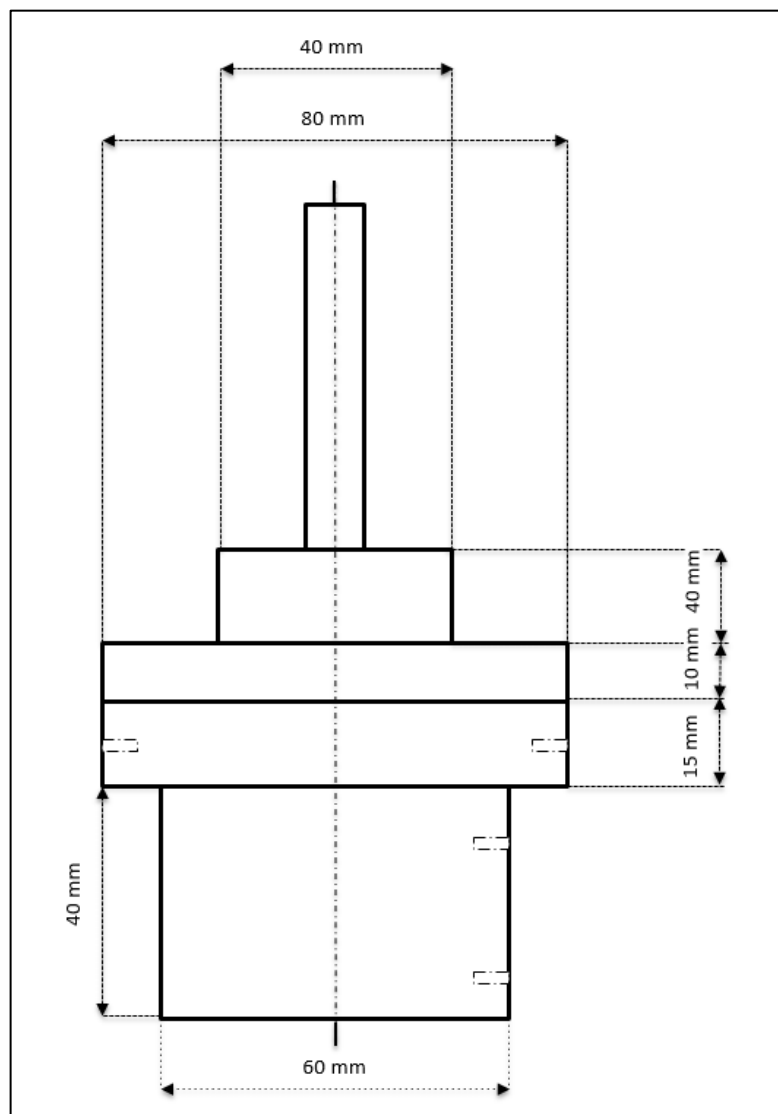
Figure 5-3: Exterior view of the equilibrium cell (sizes are in mm).
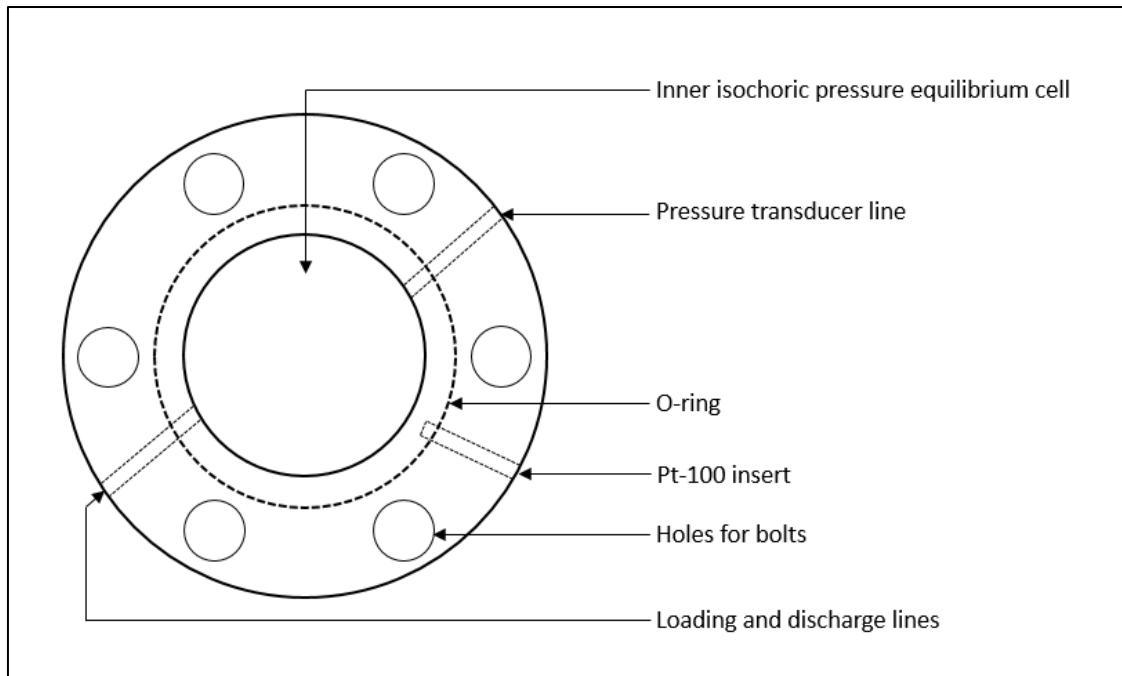
Figure 5-4: Top view of the equilibrium cell (Ngema, 2014).

Photograph 5-1: Side view of the equilibrium cell.

5.2.2 Agitation device

Agitation within the cell is required in order to reduce the gas hydrate metastability zone, to increase water transformation, and reduce the time in which equilibrium is achieved. The agitation system used in this study consisted of a Heidolph RZR 2041 overhead stirrer, a strong external cylindrical magnet that was placed outside the cell in a thimble-like cavity that was created in the top flange, and

a magnetic stirring device that was placed onto a stainless steel shaft within the equilibrium cell. The external cylindrical magnet and the magnet used in the stirring device were constructed of Neodymium. Neodymium magnets have an extremely strong magnetic field, high resistance to demagnetization, can operate up to a temperature of 353.15 K, and have a lower Curie temperature when compared to other types of permanent magnets (Gorman, 2009).

The Heidolph RZR 2041 overhead stirrer (Figure 5-5 and Photograph 5-2) drives a mechanical shaft that turns the cylindrical external magnet in the thimble-like cavity. This external magnet subsequently turns the magnetic stirring device within the equilibrium cell and mixes the contents. A rubber spacer was placed between the mechanical shaft and the external magnet in order to absorb any vibrations that might have occurred as a result of the stirring. The Heidolph RZR 2041 overhead stirrer consisted of two gear speeds, 40 - 400 rpm and 200 - 2000 rpm with an accuracy of 0.1 % of its final value. A speed of 400 rpm is suitable for complete agitation of the phases inside the equilibrium cell.

The magnetic stirring device consisted of an "external" ring magnet and two removable impeller blades. The longest length of these blades was 12 mm; the width was 5 mm and the thickness 1 mm. The two blades are attached to the "external" ring magnet, which has an external diameter of 30 mm, an internal diameter of 17 mm and a height of 10 mm. This "external" ring magnet was coated with a copper-gold coating in order to protect the magnet from any corrosive liquids. Polytetrafluoroethylene (PTFE) was used to line the inner of the magnetic stirring device (Photograph 5-3). This was done in order to prevent friction between the stainless steel shaft and the neodymium magnet. The magnetic stirring device with blades was removable from the stainless steel shaft. The placement of the magnetic stirring device on the stainless steel shaft allows for effective magnetic coupling between the stirring device and the cylindrical magnet within the thimble-like cavity (Photograph 5-4).

This agitation system is extremely effective in mixing the gas, liquid, and hydrate phase within the cell allowing the aqueous solution to reach equilibrium faster. Additional associated advantages of this stirring system includes (Ngema, 2014):

1. Reduction in the time required for gas hydrate formation and dissociation through fast homogenization
2. Superior stirring power and efficiency compared to a magnetic stirrer bar
3. Direct agitation within the cell promoting homogenous aqueous solution
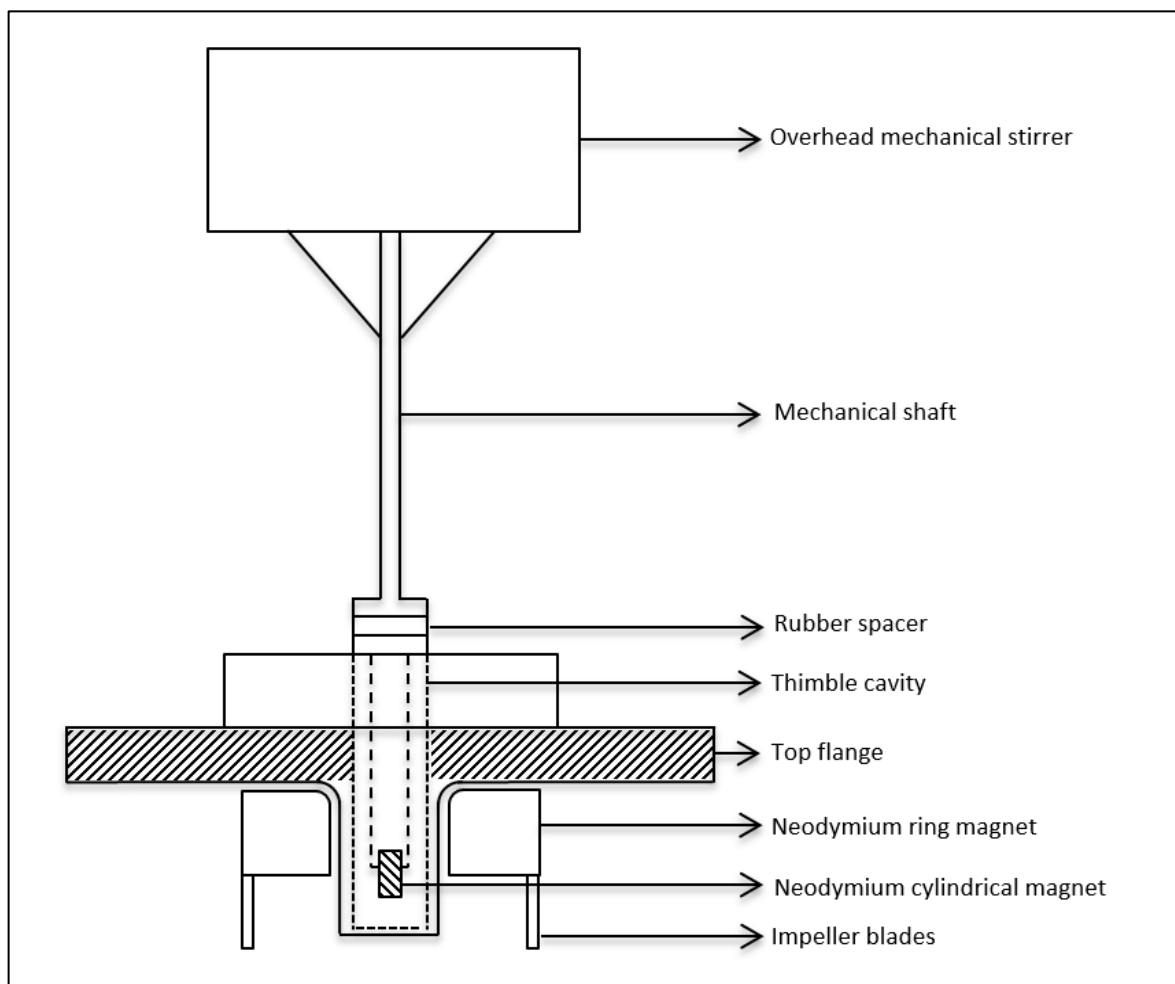
Figure 5-5: A schematic diagram of the stirring mechanism.

Photograph 5-2: Overhead-stirring mechanism

Photograph 5-3: The magnetic stirring device
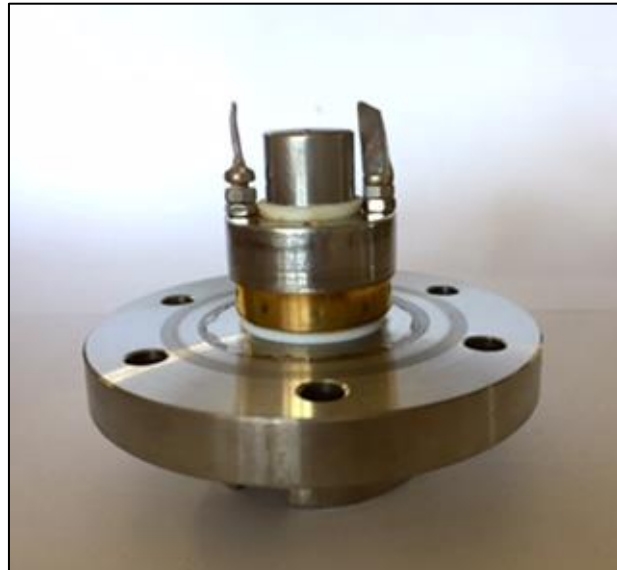
Photograph 5-4: Magnetic stirring device placed on shaft

5.2.3 Temperature and pressure sensors

Temperature

One platinum resistance thermometer (Pt-100) supplied by WIKA was used to measure the temperature within the equilibrium cell. The Pt-100 is capable of sensing temperatures between 73.15 K and 1073.15 K with an accuracy of $\pm$ 0.03 K. The probe was fixed on the side of the equilibrium cell. The probe was connected to the 34972A LXI Agilent data acquisition unit where the temperature readings were displayed electronically with respect to time and logged at three-second intervals.

Pressure

One WIKA pressure transducer was used to measure the cell pressure. The pressure transducer was situated on the side of the equilibrium cell and was able to measure pressures in the range of 0 - 10 MPa, with a stated accuracy of 0.05 % (full span). The total pressure exerted on the cell was the sum of the 0 - 10 MPa pressure transducer and the atmospheric pressure. The atmospheric pressure was taken as 101.325 kPa for all measurements. The transducer was connected to the 34972A LXI Agilent data acquisition unit where the pressure readings were electronically displayed with respect to time and logged at three-second intervals.

5.2.4 Liquid bath

The equilibrium cell was kept at isothermal conditions by immersing it in a galvanized steel liquid temperature bath. The bath consisted of two metal sheets: an internal case and an external case. A polycarbonate sheet of thickness 25 mm was inserted between the two sheets as insulating material. The bath had internal dimensions of 440 mm x 350 mm x 260 mm. The dimensions resulted in an internal volume of 40 L. The bath had 2 Perspex® viewing windows with dimensions 115 mm x 80 mm on the front and back. An iron framework supported the bath. This framework also supported the equilibrium cell and its housing. A mechanical jack was used to facilitate the movement of the bath up and down to submerge the equilibrium cell in the bath fluid. The bath fluid used depends on the temperature range required for the systems to be measured. The bath fluid used in this work was a mixture of 80/20 wt % ethylene glycol and water. This allowed for operation in the temperature range of 228 K (melting point at atmospheric pressure) and 397 K (boiling point at atmospheric pressure). The top surface of the bath was covered with polystyrene foam pellets in order to prevent heat loss or gain from the surroundings.

5.2.5 Temperature controllers

The temperature of the bath was controlled using a Grant® Model TXF200 programmable controller. The temperature range of the controller for a water-glycol solution was 243.15 K to 343.15 K. It contained an immersion circulator pump with an internal temperature probe. The programmable temperature controller cooled or heated the water-glycol solution in the bath, which in turn cooled or heated the contents of the equilibrium cell. In order to ensure that adequate separation between the hydrate crystals and salt solution was achieved, the temperature of the equilibrium cell contents was controlled at a specified rate. The controller was connected to the computer set-up (PC). Software supplied by Labwise® was used to program the cooling and heating steps during hydrate formation

and dissociation. The bath contents were cooled by an immersion cooler, or cold finger, supplied by Polyscience® (IP-35 model). It operated at temperatures as low as 173.15 K.

The pressure transducer was housed in a 75 x 58 x 78 mm aluminium block. Two heating cartridges, each with an outer diameter and length of 8 mm and 40 mm respectively, were inserted into the top of the aluminium block in order to supply heat energy. The heating cartridges were connected to a variac voltage regulator TDGC2 model that was controlled by a Shinko ACS-13A controller, used to supply uniform heat to the aluminium block. This ensured the pressure transducer was maintained at a constant temperature due to its sensitivity to temperature fluctuations. The transducer was maintained at 313.15 K, which was the maximum temperature the experimental apparatus was expected to reach. The line connecting the pressure transducer to the equilibrium cell was heated with nichrome wire. This prevented condensation in the lines leading to the pressure transducer.

5.3 Preparation of experimental set-up prior to measurements

Prior to conducting experimental measurements, the equipment set-up must be prepared. The preparation consists of cleaning the equilibrium cell, leak testing the equilibrium cell and the adjoining lines and valves, and calibrating the temperature and pressure sensors.

5.3.1 Cleaning the equilibrium cell

Before undertaking any experimental measurements, the equilibrium cell and all connecting lines were cleaned. This was done to reduce contamination of the cell contents. All components of the unassembled cell were washed with industrial grade soap and warm water. Thereafter, the components of the cell were rinsed with distilled water and Millipore water, followed by acetone (except the O-ring) and dried with compressed air. The cell was then reassembled and all lines connected. Once connected, the cell was flushed three times with high-pressure nitrogen to ensure that the cell was clean and dry. The Edwards vacuum pump was then used to evacuate the cell to a pressure of 0.0002 kPa for 120 minutes to remove any air or volatile matter that might be present in the cell.

Cleaning the cell between measurements required just as an intensive procedure as all systems contained various salts at different concentrations as well as ethanol, acetic acid and lactic acid. The cell contents were first drained using the drain line. Due to the set-up of the apparatus, gravitational draining was not possible. The pressure of the gas present in the cell was therefore used as the driving force to flush out the contents. Once all the contents had been released from the cell, the pressure

transducer and temperature probe were disconnected. The top flange was removed and the cleaning procedure stated above was performed. The O-ring was also inspected and changed if required

5.3.2 Leak testing

Leak testing was conducted on the equilibrium cell in order to reduce errors that could occur as a result of a pressure loss. Leak testing was done before calibrations and hydrate measurements as well as after a line had been disconnected or a fitting replaced. For a leak test, the cell was filled with nitrogen to a pressure of 9 MPa and all valves leading to the cell were closed. A leak detecting fluid (SNOOP®) was applied to all fittings and connections. A leak was detected at a fitting or a connection by observing the occurrence of foam or bubbles as a result of the gas exiting from the specific connection point. All fittings and connections where a leak was observed were tightened, wrapped with thread tape or replaced. Thereafter, the equilibrium cell was immersed in the liquid bath. The temperature of the bath was kept constant at 298.15 K to eliminate temperature and pressure fluctuations. In order to ensure that no significant pressure loss occurred, the experimental set-up was left at these conditions (9.0 MPa and 298.15 K) for 24 hours; the same time period as the experiment. Once no leaks were detected, the calibrations were conducted.

5.3.3 Calibrations

5.3.3.1 Temperature calibration

The Pt-100 temperature probe used in this study was calibrated against a CTH 6500 temperature standard, supplied by WIKA. For a temperature range between 73.15 K and 473.15 K, the standard probe had a stated full-scale uncertainty of $\pm$ 0.02 K. The temperature probe, together with the standard probe, was immersed into a liquid silicon oil bath. In order to reduce any temperature gradients that may occur, the probes were held together using a thin copper wire. At the specified, stabilized temperatures, readings from the temperature probe and standard probe were recorded. Initially, the liquid bath temperature was set to 313.15 K. Thereafter; increments of 5 K were used to reach a final temperature of 263.15 K. In order to account for hysteresis, the same procedure was used to increase the temperature to 313.15 K, followed by decreasing the temperature back to 263.15 K. Two additional readings were taken at 274.15 K and 272.15 K. This was done to ensure the accuracy of the temperature readings in the lower ranges. For each point, once the temperature had stabilized, the temperature readings were logged every 2 seconds over a 5 minute period and averaged. The temperature of the standard probe was plotted against the temperature reading of the Pt-100

temperature probe and a first order polynomial was fitted to the data points, which is shown in Figure 5-6. Deviations from the standard temperature due to the first order relation are plotted in Figure 5-7. As can be observed from Figure 5-7, the maximum temperature deviation from the standard temperature probe is $\pm$ 0.024 K.
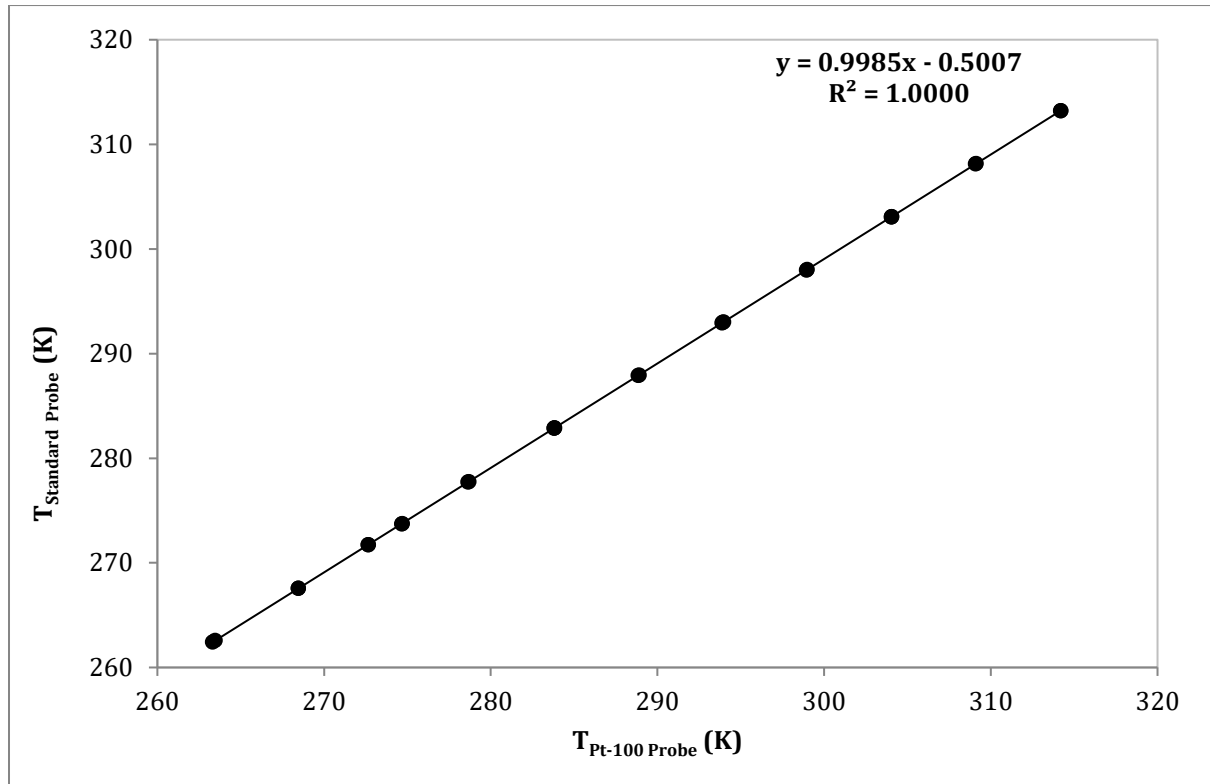
Figure 5-6: Calibration of the Pt-100 temperature probe used in this study. A first order relation between the standard probe and Pt-100 probe was achieved. The calibration was performed in June 2016 and confirmed in December 2016.
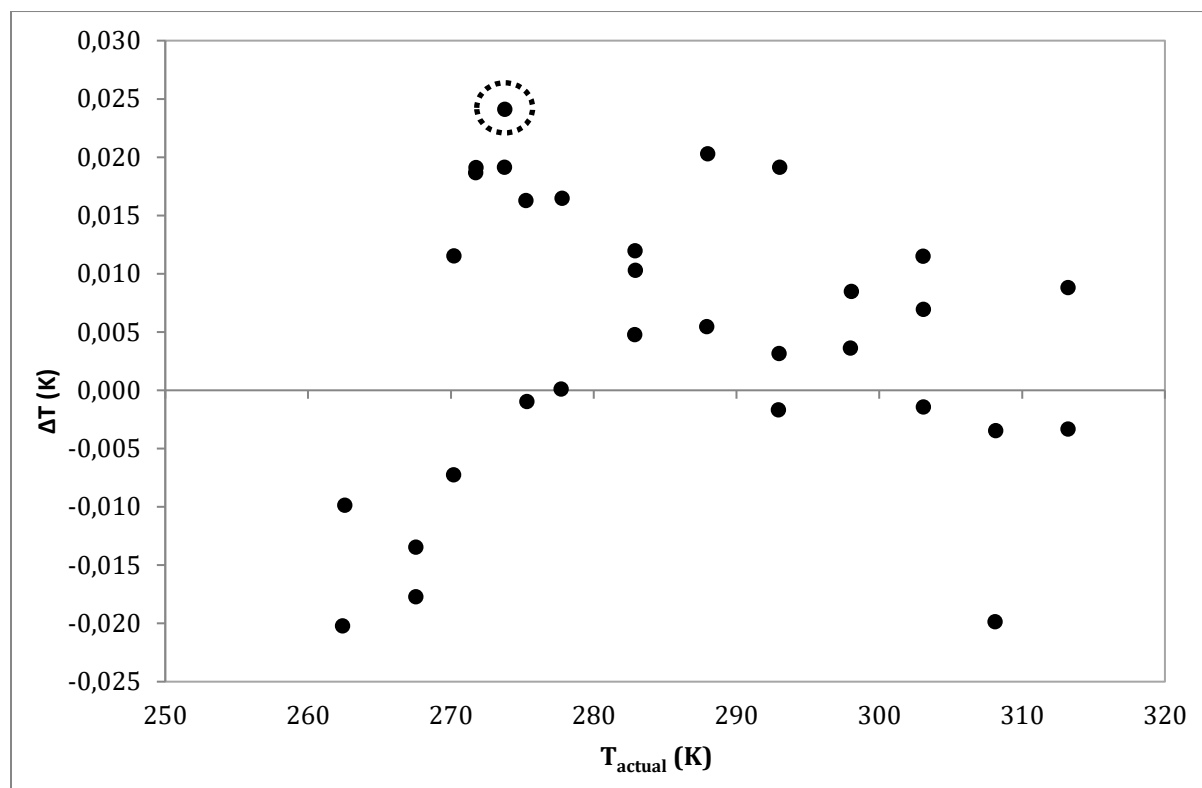
Figure 5-7: Deviations from the standard temperature probe due to the first order relation, with maximum deviation of $\pm$ 0.024 K.

5.3.3.2 Pressure calibration

The WIKA pressure transducer used in this study was calibrated internally against a Mensor CPC 8000 high-end pressure controller, supplied by WIKA. The Mensor pressure controller was fitted with a standard 0 - 250 bar transducer with a stated full-scale accuracy of $\pm$ 0.010 % (full span). As previously mentioned, the pressure transducer was maintained at a temperature of 313.15 K to eliminate any effect of environmental temperature fluctuations on the pressure readings. Throughout the pressure calibration, the temperature of the cell was maintained at 298.15 K. The pressure transducer was connected to a common pressure manifold together with the standard. At specified stabilized pressures, the readings from the pressure transducer and the standard transducer were recorded. Initially, the equilibrium cell was loaded with nitrogen gas until a pressure 0.5 MPa was achieved. Thereafter, increments of 0.5 MPa were used to reach a final pressure of 5.5 MPa. In order to account for the effect of hysteresis, the same procedure was used to decrease the pressure to 0.5 MPa followed by increasing the pressure back up to 5.5 MPa. For each point, once the pressure had stabilized, the pressure readings were logged every 2 seconds over a 5 minute period and averaged. The measurements from the pressure transducer were plotted against the standard pressure

measurements and a first order polynomial was fitted to the data points. The first order relation between the pressure transducer and the standard is presented in Figure 5-8. A deviation of the transducer from the standard transducer is plotted in Figure 5-9. As observed from Figure 5-9, the maximum pressure deviation from the standard is ± 0.0006 MPa.

The temperature and pressure calibration was performed in June 2016. These calibrations were confirmed once the experimental work had been completed, in December 2016. The confirmation of these calibrations can be seen in Figures E-1 and E-2, of Appendix E.
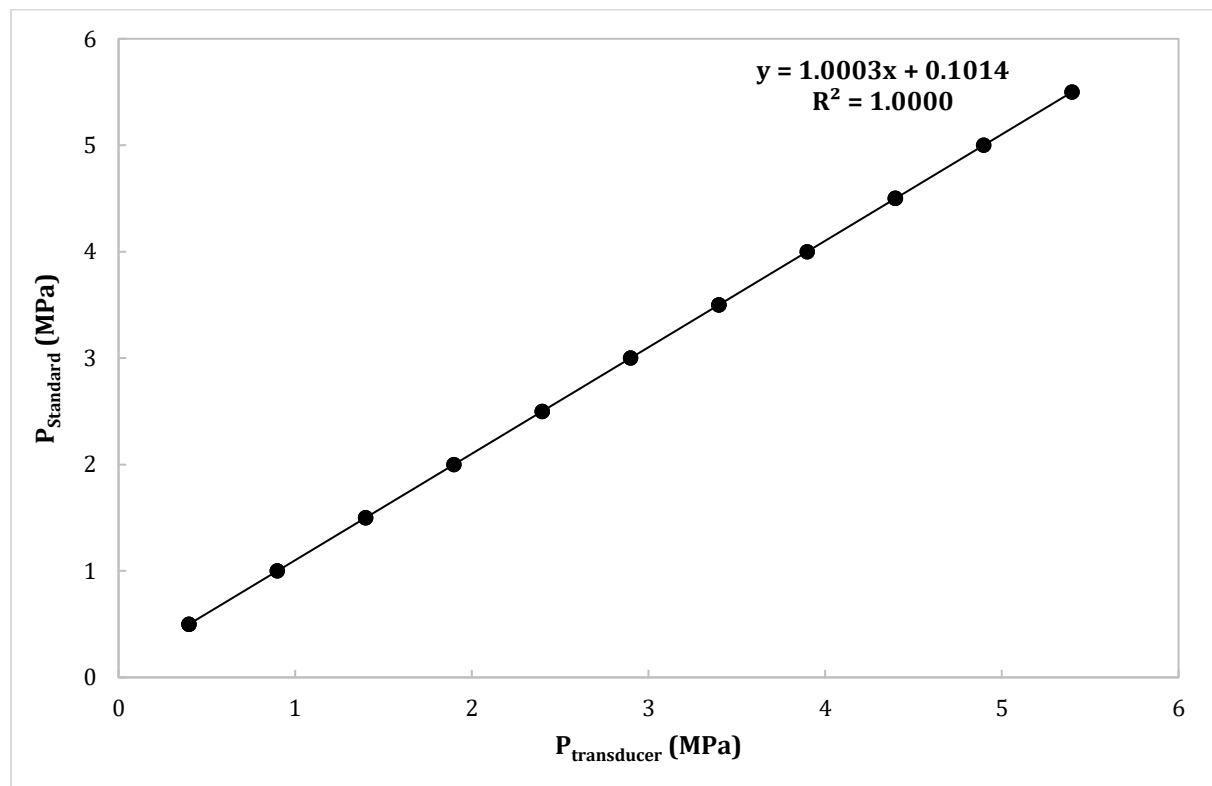
Figure 5-8: Calibration of the 1-10 MPa WIKA pressure transducer used in this study. A first order relation between the standard and the transducer was achieved. The calibration was performed in June 2016 and verified in December 2016.
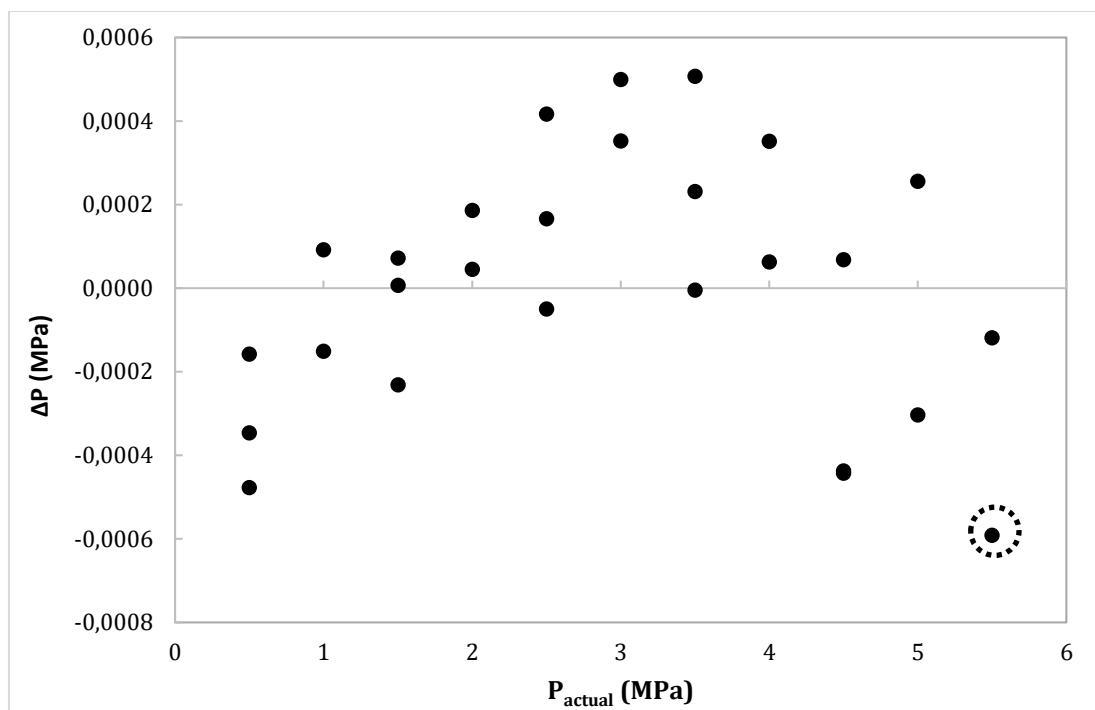
Figure 5-9: Deviations from the standard pressure due to the first order relation, with maximum deviation of ± 0.0006 MPa.

5.3.4 Sample preparation

All aqueous solutions were prepared on a weight/weight basis using the gravimetric method. The solutions were prepared in a 100 ml beaker using an OHAUS AV 114 digital mass balance. The mass balance had a full-scale uncertainty of ± 0.0001 g. The required mass of inorganic components, organic components and water for each desired system was determined. Initially the mass of the empty beaker was recorded. Thereafter the mass of the required components was measured. The amount of water required to obtain the final solution weight percent was then slowly added with a syringe. The solution was then heated and stirred at 298 K for 20 min. This was to ensure that the solutes were properly incorporated with the solvent. This allowed for easy injection of the solution into the equilibrium cell, eliminating changes in the initial concentration of the solution, and preventing any precipitation within the cell.

5.4 Experimental procedure for gas hydrate measurements

The measurements of the hydrate dissociation points are conducted using the isochoric pressure search method. With the isochoric method, the hydrate dissociation points are established through temperature and pressure measurements. No complicated calculations or visual observations are required, allowing for reliable determination of hydrate equilibrium data. This experimental method is also suitable over the entire range of temperature and pressure required for hydrate formation. No volume changes are required in this method. In addition, the method is suited to automated control of experiments (Smith, 2015). The isochoric method is therefore considered advantageous, compared to the isobaric and isothermal approaches, to investigate the phase behaviour of multicomponent systems. For the reasons stated, the isochoric method combined with stepwise heating and efficient mixing was applied in this study.

5.4.1 Experimental procedure for hydrate measurements

After the cell had been cleaned, leak testing performed and calibrations conducted, the apparatus was deemed ready for hydrate measurements. The cell as well as the line connecting the gas cylinder to the cell was evacuated, to a pressure of 0.0002 kPa for a period of 30 minutes, using the Edwards vacuum pump. This was done to remove any air trapped either in the cell or in the line that could cause the composition of the prepared solution to change. The inlet value to the cell was then closed in order to maintain the cell under vacuum and the Edwards pump switched off. A 20 ml sample of the prepared experimental solution of interest was drawn into a 50 ml plastic syringe. Tapping the syringe lightly removed any air bubbles that were present in the syringe. The filled syringe was connected to the inlet valve of the cell. The solution was fed into the equilibrium cell by slowly opening the inlet valve. The inlet valve was then closed and the syringe removed. The system temperature was then set. Once the temperature had stabilized, the cell was pressurized with the selected former (carbon dioxide) to the desired pressure. For systems that had been measured previously in literature, the system temperature was set to a valve outside the expected hydrate stability region and the system pressure was set to the expected dissociation value. For systems that had not been previously measured, the system temperature was set to 298.15 K and the pressure was set to a value below the hydrate phase boundary at 298.15 K.

Once the initial conditions of temperature and pressure had been set, the magnetic stirrer was switched on and set to 400 rpm. Once the gas had been completely adsorbed into the solution and the system pressure stabilized, the programmable temperature controller was set to 10 K below the anticipated hydrate dissociation temperature. If the set temperature was above 273.15 K, the hydrate

phase was in equilibrium with the water phase. If the set temperature was below 273.15 K, the hydrate phase was in equilibrium with ice. The temperature was decreased at a rate of 1 K/h. This was done to ensure adequate hydrate formation and good separation between the hydrate and salt. This process generated the cooling curve. Two distinct gradients are observed on the cooling curve. The first gradient is characterized by a small decrease in pressure and indicates the occurrence of the nucleation process. This small pressure change was predominantly a function of the change in temperature. This cooling curve is represented by the vapour-liquid (V-L) isochoric curve in Figure 5-10. A significant decrease in pressure indicated that hydrate growth had occurred and hydrates had formed (refer to Figure 5-10). If no pressure drop was observed, the temperature was decreased further. Once hydrates had formed and the system temperature and pressure had stabilized, the temperature was increased in a stepwise manner. This heating process generated the heating curve. At each temperature increase, the system was given 1 hour to stabilize. Initially temperature increments of 1 K/h were used. As the system approached the dissociation point, temperature increments of 0.1 K were used. Two distinct gradients were observed on the heating curve. The first gradient is characterized by significant increases in pressure, which is a result of the hydrates dissociation and releasing the guest molecule into the vapour space (refer to Figure 5-10). The point at which the gradient changed was the hydrate dissociation point. After the dissociation point (the second gradient), the pressure change was primarily a function of temperature. This is represented by the vapour-liquid (V-L) isochor in Figure 5-10.

In order to verify the measured results of new systems, three methods were used. The first method used was to scatter the order of the pressures at which the measurements were conducted. For instance if measurements were to be conducted at 4.0, 3.5, 3,0 and 2.5 MPa, the measurement at 2.5 MPa was conducted first followed by the measurement at 3.5, 3.0 and finally 4.0 MPa. This was done in order to reduce the effect of hysteresis on the system. The second method was to repeat a dissociation point in order to show reliability and reproducibility in the experimental technique. The third method used was to linearly regress the hydrate dissociation points. The obtained results were in good agreement as they presented a highly linear relationship when plotted on an lnP versus 1/T scale.
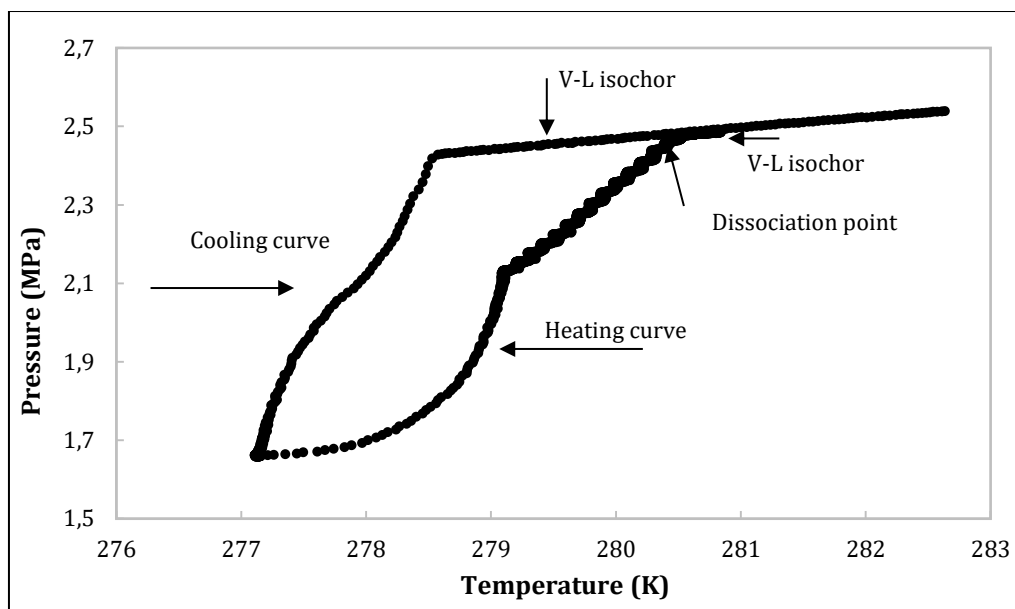
5-10: Heating and cooling curve for the CO_2 (1) + water (2) system at 2.5 MPa.

5.4.2 Shutdown procedure

Once hydrate measurements on the particular aqueous system was complete, the data logger was stopped and shutdown. The overhead mechanical stirrer, cold finger, and programmable temperature controller were switched off. The liquid bath was lowered and the drain valve opened to empty the contents of the cell and release the gas. The cleaning procedure mentioned in section 5.3.1 was then followed before undertaking the next set of measurements.

5.5 Experimental accuracy and uncertainty for HLV equilibrium data

The ability of measuring devices and the experimenter undertaking measurements are restricted by systematic and random errors. These errors affect the uncertainty of measured data. The uncertainty of measured data is described as an interval around a data set or point such that if the measurement were to be repeated at the same conditions, the result would lie within the stated interval. Presenting the uncertainties of experimental measurements allows for easy comparison of results from different researchers and laboratories in the same area of study. This allows a person of interest to analyse the accuracies of experimental data and select those with a higher level of accuracy. The calculation of uncertainty is performed according to the guidelines outlined by the National Institute of Standards and Technology (NIST).

Before presentation of the original measured data, all non-negligible possible sources of uncertainty must be accounted for and reported on. The combined standard uncertainty (u_c) and the combined expanded uncertainty (U_c) are the most inclusive expressions for uncertainty. According to the NIST guidelines, the combined standard uncertainty is descried by the following equation (refer to Taylor and Kuyatt (1994) for more details):

$$u_c(x) = \pm \sqrt{\sum_i u_i(x)^2}$$

(5-1)

where $u_i(x)$ is the standard uncertainty for a value x; such as manufacturers uncertainty on instruments and uncertainty arising from calibration standards.

During calculation of $u_c(x)$, two categories of uncertainty arise, namely, Type A or Type B. These categories of uncertainty are based on the method used to estimate their numerical value. Type A uncertainties are evaluated by statistical methods. These uncertainties have a larger tendency to lie around the mean and may be calculated from:

$$u_i(x) = \frac{\sigma}{\sqrt{N}}$$

(5-2)

where σ is the standard deviation of the data and N is the number of data points.

Type B uncertainties are evaluated by all other means and available information related to the measurements. These uncertainties are likely to fall anywhere between the upper and lower limit of the distribution. Such distributions are termed rectangular and are estimated by the following equation:

$$u_i(x) = \frac{b}{\sqrt{3}}$$

(5-3)

where b is half the width of the interval. The rectangular distribution model is always the default model in the absence of any other information (Nelson, 2012).

When all uncertainty components, whether determined by Type A or Type B methods, have been accounted for and the combined standard uncertainty has been determined, it is necessary to expand the combined standard uncertainty with a coverage factor, k, to produce combined expanded uncertainty $U(x)$.

The combined expanded uncertainty is therefore defined as:

$$U(x) = ku_c(x) \tag{5-4}$$

The combined expanded uncertainty provides a greater interval for the experimental measurement opposed to the combined standard uncertainty. Typically a coverage factor of 2 is used to define an interval, with a level of confidence of approximately 95 % (Nelson, 2012).

5.5.1 Temperature and pressure uncertainty

In this study only two parameters were measured: temperature and pressure. The type A uncertainties for temperature and pressure are a result of the numerous transducer readings taken at steady state. Type B uncertainties for temperature and pressure are a result of the polynomials fitted to the calibrations as well as any manufactures' specification.

Based on equation (5-1) and considering all sources of uncertainty in the measurement of temperature, the combined standard uncertainty for temperature is:

$$u_c(T) = \pm\sqrt{u_{calib}(T)^2 + u_{rep}(T)^2 + u_{inst}(T)^2} \tag{5-5}$$

where $u_{rep}(T)$ is the standard uncertainty due to repeatability of a measurement (Type A), $u_{inst}(T)$ is the uncertainty of the Pt-100 temperature probe, and $u_{calib}(T)$ is the uncertainty produced by the temperature calibration and can be determined by:

$$u_{calib}(T) = \pm\sqrt{u_{corr}(T)^2 + u_{std}(T)^2} \tag{5-6}$$

where $u_{corr}(T)$ is the standard uncertainty due to the temperature calibration correlation (Type B) and $u_{std}(T)$ is the standard uncertainty of the temperature probe (Type B).

The uncertainty from the temperature calibration is determined from the calibration first order polynomial, and is illustrated in Figure 5-7. From Figure 5-7, the maximum deviation or the quantity b in equation (5-3) is ± 0.024 K. The manufacturer supplied the accuracy of the Pt-100 temperature probe as ± 0.03 K and the standard temperature probe used in the calibrations as ± 0.02 K

During an experiment, temperature fluctuations could occur as a result of inefficient liquid circulation in the bath, heat loss or gain to or from the environment, and any error from the instrument manufacture. The repeatability uncertainty was therefore calculated using the following equations:

$$u_{rep}(T) = \left(\frac{1}{n(n-1)} \sum_{k=1}^{n} (T_{i,k} - \bar{T}_i)^2 \right)^{0.5} \tag{5-7}$$

Where

$$\bar{T}_i = \frac{1}{n} \sum_{k=1}^{n} T_{i,k} \tag{5-8}$$

Similarly, the combined uncertainty for pressure is:

$$u_c(P) = \pm \sqrt{u_{corr}(P)^2 + u_{std}(P)^2 + u_{rep}(P)^2 + u_{inst}(P)^2} \tag{5-9}$$

where $u_{corr}(P)$ is the standard uncertainty due to the pressure calibration correlation (Type B), $u_{std}(P)$ is the standard uncertainty of the pressure transducer (Type B), and $u_{rep}(P)$ is the standard uncertainty due to the repeatability of the pressure measurement (Type A).

The maximum deviation or the quantity b in equation (5-3) for the pressure calibration is ± 0.0006 MPa (Figure 5-9). The manufacturer supplied the accuracy of the 0 - 10 WIKA pressure transducer as 0.05% (full span). The accuracy of the Mensor CPC 8000 high-end pressure controller was reported as $\pm 0.010 \%$ (full span).

The combined standard uncertainties (U) are both multiplied by a coverage factor of 2 in order to obtain the combined expanded uncertainty. A summary of the instrument accuracy as reported by the manufacturers and the maximum deviation of the calibration's first order polynomial used to determine the accuracies in this study, is presented in Table 5-2. The calculated uncertainties are discussed in more detail in Chapter 6.

Table 5-2: Temperature and pressure uncertainties in this study.

Temperature (K)	
Pt-100 temperature probe accuracy	0.030
Standard temperature probe accuracy	0.020
Calibration uncertainty	0.024
Pressure (MPa)	
WIKA 0 - 10 MPa transducer accuracy	0.005
Mensor CPC 8000 high-end pressure controller	0.003
Calibration uncertainty	0.001

6

CHAPTER SIX

RESULTS AND DISCUSSION

The aim of this chapter is to provide the results, and a discussion, of the research carried out in this study,followed by the plant design and economic evaluation.. This chapter is divided into two parts. Part 1 contains the results and discussion of the experimental measurements and thermodynamic modelling. In the experimental section, the experimental apparatus and procedure are discussed. The characterisation of vinasse performed in this study, of which determined the experimental work plan, is also discussed. The measured hydrate dissociation data for CO_2 + aqueous solutions are reported. The aqueous solutions include: single salts, mixed salts, and a solution, representative of vinasse, containing both organic and inorganic components. In the thermodynamic modelling section, hydrate phase equilibria for all measured systems were predicted using the aforementioned methods outlined in Chapter 3.

Part 2 contains the industrial application section. Here the hydrate separation technology is presented with a proposed process. An economic evaluation for the proposed process is also presented, and compared to traditional desalination technologies.

PART 1: Results and Discussion of experimental data and modelling

6.1 Experimental apparatus

Ngema (Ngema, 2014) originally commissioned the apparatus that was used in this study. The apparatus of Ngema (2014) is very similar to the high-pressure autoclave cell of Smith (2015) (section 4.2.1.1). The most significant difference between the setup of Ngema (2014) and Smith (2015) is the working volume of the equilibrium cells, which were 38.5 cm^3 and 53 cm^3 respectively. In addition, the autoclave cell of Smith (2015) utilized two Pt-100 temperature probes whereas the autoclave cell of Ngema (2014) utilized only one Pt-100 temperature probe to measure the temperature of the equilibrium cell.

Slight modifications were made to the initial design of the experimental set-up of Ngema (2014). The most important modification was made to the size of the bath. The original bath had internal dimensions of 510 mm x 400 mm x 320 mm (volume of 65 L). The resulting large volume of thermosetting fluid present in the bath required extensive heating and cooling which often resulted in an increase in the time required for a hydrate measurement. The new bath had internal dimensions of 440 mm x 350 mm x 260 mm, which resulted in a volume of 40 L (25 L volume difference). The new bath required a new steel framework to support the change in size. As a result the valves had to be repositioned on the steel framework. The manner in which the cell was held in position was also modified. Despite these 'cosmetic changes', no changes were made to the original operating principle of the equilibrium cell such as a change in dimensions, change in the feed and discharge lines, or the pressure transducer and temperature probe lines. The new bath no longer required the Polyscience® Model IP-80 cold finger that was used in the study of Ngema (2014), which had a temperature control fixed at -80 ℃. A lower duty Polyscience® cold finger, Model IP-35, with a temperature control fixed at -35 ℃, was used. In the original set up by Ngema (2014), it was only possible to input a temperature program, to obtain the heating or cooling curve, on the Polyscience® Model 7312 temperature controller unit. This was time consuming and it increased the possibility of human error. The temperature controller was replaced by the Grant® Model TXF200 temperature controller. In conjunction with Labwise®, the controller was programmable from the PC. With these slight modifications, the time required for one hydrate measurement was improved from approximately 20 - 24 hours to approximately 16 - 20 hours.

The two main contributions to temperature and pressure uncertainty during hydrate measurements are heat gain and loss from the environment and fluctuating temperatures within the environment. Covering the top surface of the liquid bath with polystyrene foam pellets reduced temperature

gain/loss from/to the environment. Fluctuating environmental temperatures were prevented by the use of a heating block on the pressure transducer. The heating block maintained the pressure transducer at a constant temperature of 313.15 K, which was the maximum temperature at which the measured systems were expected to reach. The pressure transducer was maintained at this temperature during calibrations as well. The maximum rating on the pressure transducer was 333.15 K, well above the temperature at which it was maintained.

During hydrate measurements, in order for the process of nucleation to occur (section 2.2.1), the liquid phase requires supersaturation with the hydrate former. In the absence of agitation, the nucleation process requires a significant amount of time. With vigorous agitation, needle-like hydrates form (Petticrew, 2011). Needle-like crystals are not desirable in a hydrate-based desalination/separation process, as they are difficult to separate from the concentrate brine (Petticrew, 2011). An agitation speed of 400 rpm was selected, based on the extensive research by the Thermodynamic Research Unit at the University of KwaZulu-Natal using similar stirrers and cells.

6.2 Measurement uncertainties

The measurement uncertainties relating to temperature and pressure were discussed in Chapter 5.5. In summary the uncertainties included the instrument error, calibration, and repeatability. An additional uncertainty was the composition of the water used in the preparation of experimental solutions. In order to reduce this uncertainty, millipore water was used. The use of millipore water minimized the amount of ions present in the water. Ions have an inhibiting effect on hydrate formation and can affect the formation of hydrates in systems containing no other inhibitors, such as the pure water system. The millipore water used for the each system measured had a conductivity of 1.5 μS. This eliminated the effect of the initial water composition on the gas hydrate measurements.

Table 6-1 provides a summary of the uncertainty of the measurements undertaken in this study. All uncertainties were calculated using equations (5-1) to (5-9) in Chapter 5.5. From Table 6-1 it can be seen that the error on repeatability was calculated to be zero. It therefore did not contribute to the combined expanded uncertainty and was not considered. The combined expanded uncertainty reported in Table 6-1 is applicable to all measurements conducted in this study.

Table 6-1: Measurement uncertainties related to this study.

Uncertainty source	Temperature (K)	Pressure (MPa)
Instrument error	± 0.03	± 0.005
Standard instrument error	± 0.02	± 0.003
Calibration	± 0.02	± 0.001
Repeatability	± 0.00	± 0.000
Combined standard uncertainty, $u_c(x)$	± 0.03	± 0.003
Combined expanded uncertainty, $U(x)$	± 0.1	± 0.01

From here onwards, temperature and pressure (and their corresponding uncertainties) are reported to one and two decimal places respectively.

6.3 Experimental procedure

The equilibrium stainless steel cell was cleaned rigorously according to the procedure outlined in section 5.3 before a new system was measured. This was done to prevent system contamination. In addition, any foreign matter present in the cell may have prevented the formation of gas hydrates. During the measurement of new systems, if the particular system was discharged from the cell and additional points were required to be measured in order to complete the particular system, the cell was cleaned in the same manner. This was to ensure that the conditions when measuring new systems were kept as constant at possible. To reduce uncertainty, after the cell had been cleaned it was flushed with high-pressure nitrogen. This was to remove any remaining fluid or foreign matter that might still have been present. Thereafter the cell was placed under vacuum at a pressure of 0.0002 kPa for a minimum of 120 minutes. Very good results were obtained for the test systems (section 6.5) verifying that little or no contaminants were present in the cell.

Hydrate dissociation was conducted using the isochoric method (section D.1.3 and described visually in Figure D-1). The isochoric method requires no visual observations of hydrate phenomena and no volume change of experimental solutions. For systems that had been measured previously in literature (test systems), the system temperature was set to a value outside the expected hydrate stability region and the system pressure was set to the expected dissociation value. For systems that had not been previously measured (new systems), the system temperature was set to 298.15 K and the pressure was set to a value in the hydrate instability region.

During hydrate dissociation, the heating curve was obtained in a stepwise manner. The temperature was increased in a particular increment and the system pressure was allowed to stabilize at each temperature step for a period of 1 hour. According to literature, the hydrate dissociation point is taken at the intersection of the hydrate dissociation trace with the initial cooling trace. In some cases where the solubility of the former gas is significant, such as the case with CO_2, the hydrate dissociation trace does not always intersect with the initial cooling trace. Second order polynomials are then fitted to the two gradients observed on the heating curve. Solver (program in Excel®) was then used to calculate the intersection of the two polynomials, and thus the temperature and pressure. The calculated temperature and pressure was then taken as the hydrate dissociation point.

During hydrate measurements, the first data point for a particular system took approximately 30 hours to measure. Hydrate crystals form immediately after the nucleation process (section 2.1.1). The induction time is defined as the time between the creation of the supersaturated solution and the appearance of the first hydrate crystals (He et al., 2011) and is therefore dependent on the time required for the nucleation process to occur. As a result of the memory effect, the induction time is reduced for systems in which hydrates have previously formed. Therefore after the first data point had been measured, subsequent measurements in the particular system took approximately 16 - 20 hours.

6.4 Systems measured

The basis of systems measured in this study was dependent on the constituents present in vinasse. From the extensive literature review conducted and presented in (section 1.1.2), it was seen that the characteristics of vinasse are extremely variable and dependent on several factors such as the specific industrial process used in the production of bioethanol, the type of sugarcane harvested and the soil characteristics. The constituents of vinasse are comprised of both inorganic components, present in the form of ions, and organic components. The main inorganic components present in vinasse are K^+ and SO_4^{2-}, with K^+ being present in the highest concentration. Based on the literature review conducted, K^+ and SO_4^{2-} have a range of 0.470 - 4.695 wt % and 0.890 - 3.567 wt %, respectively. The additional significant inorganic components, in no particular order, present in vinasse are Ca^{2+} (0.088 - 1.013 wt %), Mg^{2+} (0.127 - 0.608 wt %), Na^+ (0.009 - 0.164 wt %), PO_4^{3-} (0.001 - 0.030 wt %), NO_3^- (0.001 - 0.004 wt %), and Cl^- (0.003 - 1.398 wt %). These ranges are presented in Table 6-2. The significant organic components present in vinasse are ethanol, acetic acid, and propionic acid with a concentration of 2.101 wt %, 0.224 wt %, and 0.430 wt %, respectively (Table 6-2).

Table 6-2: Main inorganic constituents present in vinasse according to literature (Ortegón et al., 2016).

	Cations (wt.%)				Anions (wt.%)			
	K^+	Ca^{2+}	Mg^{2+}	Na^+	PO_4^{3-}	NO_3^-	Cl^-	SO_4^{2-}
Min	0.470	0.088	0.127	0.009	0.001	0.001	0.003	0.890
Max	4.695	1.013	0.608	0.167	0.030	0.004	1.398	3.567

Table 6-3: Main organic constituents present in vinasse according to literature (España-Gamboa et al., 2012).

Organic constituent	wt.%
Ethanol	2.101
Acetic acid	0.224
Propionic acid	0.430

Due to the fact that the characteristics of vinasse are so variable, and in order to account for a wide concentration range of the constituents, the maximum concentration for each constituents found in literature was selected as the basis for the measurements. Due to the numerous constituents present in vinasse, only the constituents that had significant and quantifiable levels were selected for investigation. For the inorganic constituents, these were the K^+, Ca^{2+}, Mg^{2+}, Na^+, Cl^-, and SO_4^{2-} ions. For the organic constituents these were ethanol, acetic acid, and propionic acid.

Phosphate is present in vinasse at low concentration levels. In addition some phosphates, such as magnesium phosphate and calcium phosphate, are very slightly soluble in water. It is expected that any solids and insoluble components would be removed prior to processing via gas hydrate technology. Phosphate was therefore not selected for investigation. In addition, nitrate was not considered as it had unquantifiable concentration levels. For a more detailed and extensive characterisation of vinasse derived from sugar cane molasses, the reader is referred to Appendix A, Table A-1.

Based on the literature data and the assumptions stated above, a series of systems on which to perform hydrate measurements was formulated. The Sugar Milling Research Institute supplied a characterisation of molasses derived vinasse (SMRI, 2016) (Tables 6-4 and 6-5). The values of the constituents supplied by SMRI (2016) lay within the concentration range found in literature. This ensured that the hydrate-based treatment method for South African vinasse derived from sugarcane

molasses could be based on the hydrate phase equilibrium data obtained from the measurements conducted in this study as the "typical concentration values" estimated from the analysis fell within the concentration range found in literature.

Table 6-4: Main cations present in the vinasse sample supplied by SMRI (SMRI, 2016).

	Cation (wt.%)							
	Ca^{2+}	Mg^{2+}	Mn^{2+}	Sr	Fe^{2+}	Si^{4+}	Na^+	K^+
Min	0.210	0.189	0.002	0.000	0.006	0.031	0.320	2.018
Max	0.301	0.254	0.003	0.001	0.009	0.068	0.444	3.001
Average	0.258	0.215	0.003	0.001	0.007	0.040	0.365	2.469

Table 6-5: Main anions present in the vinasse sample supplied by SMRI (SMRI, 2016).

	Anion (wt.%)		
	Cl^-	PO_4^{3-}	SO_4^{2-}
Min	0.811	0.023	0.497
Max	1.170	0.060	0.593
Average	0.998	0.030	0.538

From the literature studied, the characterisation of sugarcane vinasse by Ortegón et al. (2016) provided the maximum concentration for the inorganic constituents and the characterisation provided by España-Gamboa et al. (2012) provided the maximum concentration for the organic components.

The series of systems selected for measurement were (test systems and new systems):

- Test system: CO_2 (1) + water (2)
- Test system: CO_2 (1) + water (2) + 5 wt % NaCl (3)
- Test system: CO_2 (1) + water (2) + 5 wt % KCl (3)
- New system: CO_2 (1) + water (2) + 5 wt % Na_2SO_4 (3)
- Test system: CO_2 (1) + water (2) + 5 wt % NaCl (3) + 5 wt % KCl (4)
- New system: CO_2 (1) + water (2) + 5 wt % KCl (3) + 5 wt % Na_2SO_4 (4)
- New system: CO_2 (1) + water (2) + mixed salts A (3)
- New system: CO_2 (1) + water (2) + mixed salts B (3)
- New system: CO_2 (1) + water (2) + synthesised Vinasse (3)

Where: **Mixed salts A** = 3 wt % KCl + 1 wt % Na_2SO_4 + 0.5 wt % $MgCl_2$ + 0.5 wt % $CaCl_2$

Mixed salts B = 5 wt % KCl + 1 wt % Na_2SO_4 + 0.5 wt % $MgCl_2$ + 0.5 wt % $CaCl_2$

Synthesized vinasse = 5 wt % KCl + 1 wt % Na_2SO_4 + 0.5 wt % $MgCl_2$ + 0.5 wt % $CaCl_2$ +
2.2 wt % ethanol + 0.5 wt % propionic acid + 0.3 wt % acetic acid

These systems are discussed in more detail in sections 6.5 (test systems) and 6.6 (new systems).

6.5 Test systems

In order to test the reliability of the experimental apparatus and procedure used in this study, hydrate measurements on known systems were conducted. Since vinasse contains a number of both inorganic (in the form of ions) and organic constituents, measurements needed to be conducted on various combinations of salts solutions as well as a synthesized vinasse solution. Therefore in order to verify the sample preparation of the solutions, the test systems measured included pure water, single salt and binary salt systems. These systems were listed above in section 6.4.

As mentioned before, the main constituent present in vinasse is potassium. According to literature data, it is present in concentrations up to 4.695 % (Ortegón et al., 2016). The CO_2 (1) + water (2) + 5 wt % KCl (3) was therefore an important system to study for the development of a hydrate-based treatment method. According to literature, the CO_2 (1) + water (2) + 5 wt % KCl (3) system had only been measured once, by Dholabhai et al. (1993). It was therefore decided to measure this system not only as a test system but also as a means of confirming the hydrate equilibrium data in the literature.

In order to ensure that the hydrate instability region was not reached, measurements conducted on the test systems were performed between the upper and lower quadruple points of the system in question. The measured temperature and pressure ranges of the test systems investigated in this study are presented in Table 6-6 and the hydrate dissociation data points measured are presented in Table 6-7.

The difference occurring between the measured and literature data may be reported in terms of either temperature or pressure. Since the isochoric pressure search method was used in this study, the difference in data was reported in terms of pressure.

Table 6-6: Temperature and pressure ranges of the test systems measured for HLV equilibrium.

System	Temperature (K)	Pressure (MPa)
CO_2 (1) + water (2)	273.5 - 281.4	1.24 - 3.48
CO_2 (1) + water (2) + 5 wt % NaCl (3)	271.4 - 279.4	1.31 - 3.59
CO_2 (1) + water (2) + 5 wt % KCl (3)	274.1 - 281.2	1.69 - 4.20
CO_2 (1) + water (2) + 5 wt % NaCl (3) + 5 wt % KCl (4)	270.5 - 278.8	1.46 – 4.02

Combined expanded uncertainty (U) on measurements: U(T) = 0.1 K and U(P) = 0.01 MPa

Table 6-7: Measured hydrate dissociation data for the test systems examined in this study.

System	T (K)	P (MPa)
CO_2 (1) + water (2)	281.4	3.48
	280.5	3.04
	279.1	2.57
	276.9	1.93
	275.3	1.59
	273.5	1.24
CO_2 (1) + water (2)+ 5 wt % NaCl (3)	279.4	3.59
	275.2	2.09
	274.7	1.94
	274.0	1.78
	271.4	1.31
CO_2 (1) + water (2)+ 5 wt % KCl (3)	281.2	4.20
	280.0	3.54
	278.7	2.99
	276.7	2.34
	274.1	1.69
CO_2 (1) + water (2)+ 5 wt % NaCl (3) + 5 wt % KCl (4)	278.8	4.02
	277.6	3.47
	276.3	2.94
	275.7	2.72
	273.6	2.10
	270.5	1.46

Combined expanded uncertainty (U) on measurements: U(T) = 0.1 K and U(P) = 0.01 MPa

The measured data for the CO_2 (1) + water (2) system was compared to the literature data of Deaton and Frost (1946), Englezos and Hall (1994), and Mohammadi et al. (2005) and is plotted in Figures 6-1 and 6-2. In Figure 6-1, the data is plotted on an Ln P versus 1/T scale in order to demonstrate the liner relationship between the measured results and literature data. In Figure 6-2, the data is plotted, on a P versus T scale, with ± 0.05 MPa error bars. The reported pressure uncertainty in this study (± 0.01 MPa) was not visible on Figure 6-2 hence the reason for using the stated error bars of ± 0.05 MPa. All remaining figures in this section have been plotted on either an Ln P versus 1/T scale or a P versus T scale, with ± 0.05 MPa error bars. The same reasoning for Figures 6-1 and 6-2 applies to the figures below. The literature data for all tests systems used in this study is available in Table B-14 of Appendix B.9.
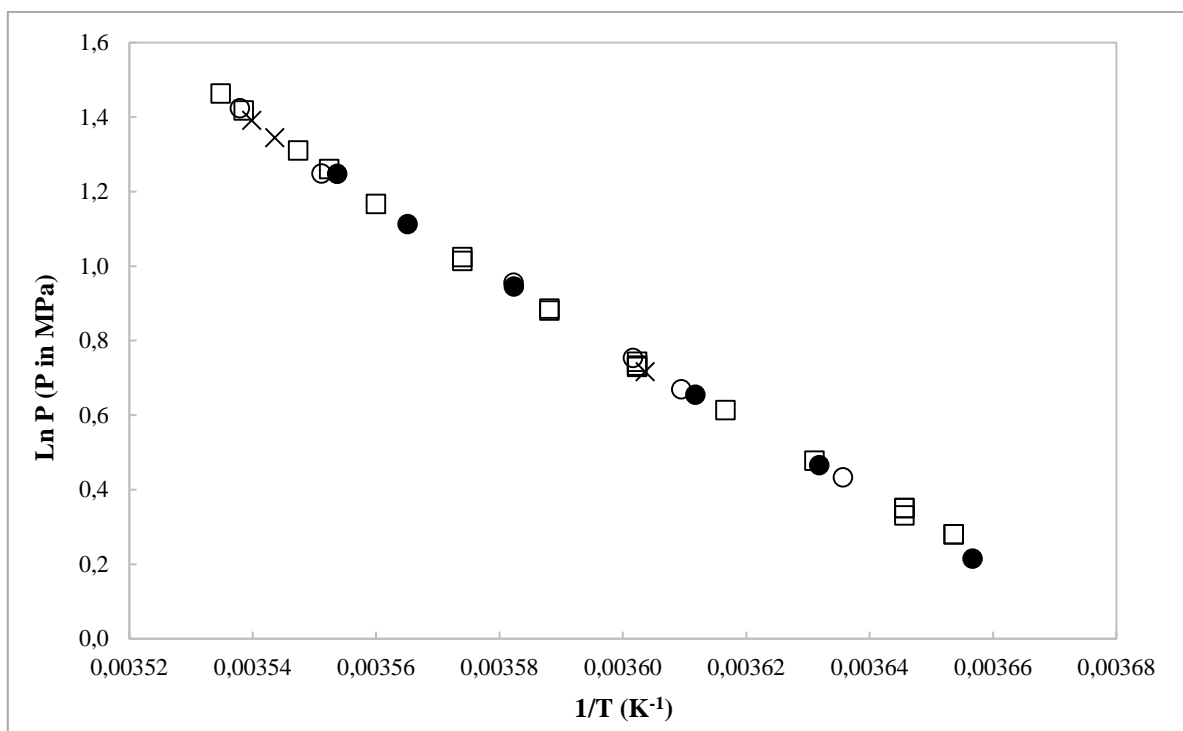
Figure 6-1: Ln P versus 1/T plot of the hydrate dissociation conditions for the CO_2 (1) + water (2) system: (●) Exp, This study; (□) Deaton and Frost (1946); (o) Englezos and Hall (1994); (x) Mohammadi et al. (2005).
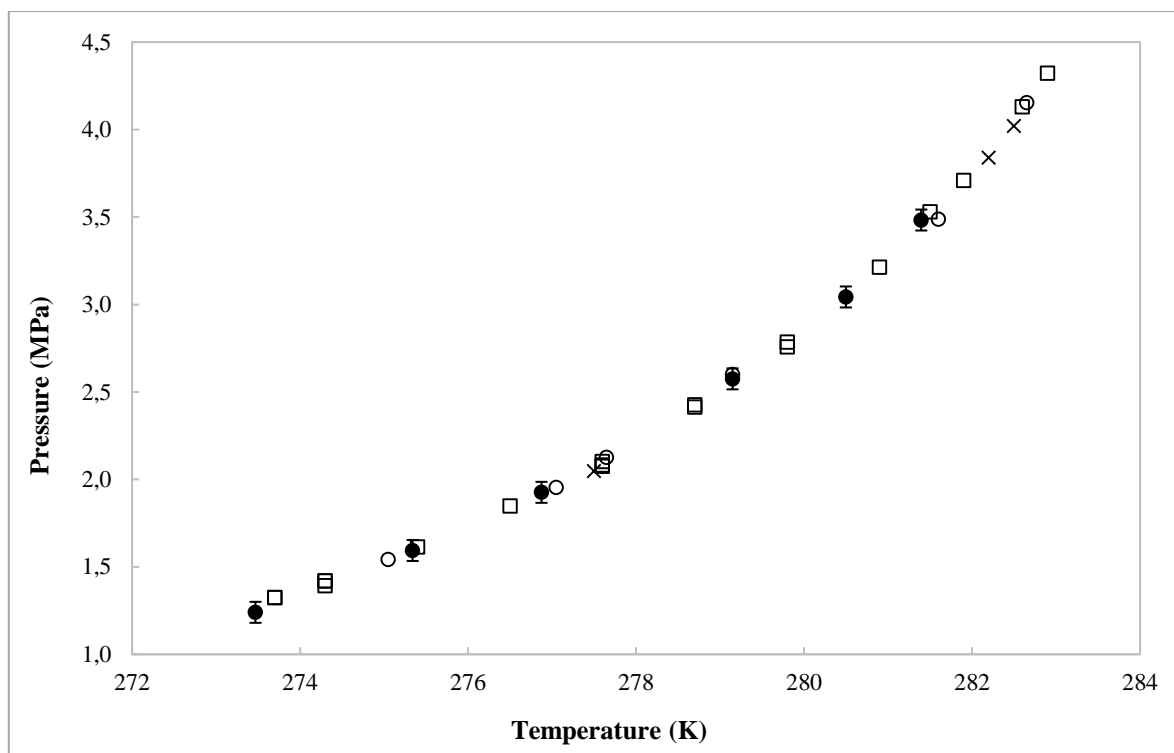
Figure 6-2: Hydrate dissociation conditions for the CO_2 (1) + water (2) system: (●) Exp, This study with ± 0.05 MPa error bars; (□) Deaton and Frost (1946); (o) Englezos and Hall (1994); (x) Mohammadi et al. (2005).

As mention in section 6.4, the expanded uncertainty (U) on hydrate measurements was found to be ± 0.1 K and ± 0.01 MPa. These uncertainties were acceptable when compared to the uncertainties of ± 0.1 K and ± 0.007 MPa reported by Mohammadi et al. (2005). The measurements in the work of Mohammadi et al. (2005) were conducted using the isochoric pressure search technique in a 75 cm^3 (maximum pressure of 41 MPa) equilibrium cell. No uncertainties were reported by Deaton and Frost (1946) or Englezos and Hall (1994). From Figure 6-1 it can be seen that there is reasonable agreement between the data obtained from this study and literature data.

For the hydrate dissociation temperatures measured in this work, the pressure deviation between the experimental data and literature data were determined by fitting a cubic spline curve in Excel® to the literature data of Deaton and Frost (1946), Englezos and Hall (1994), and Mohammadi et al. (2005). The pressure deviations, for the measured temperatures, between the experimental and literature data are presented in Table 6-8. A maximum pressure deviation of ± 51.63 kPa occurred at a temperature of 280.5 K, between the measured data and the literature data of Englezos and Hall (1994). A maximum pressure deviation of ± 56.30 kPa, at a temperature of 273.5 K, occurred between the literature data of Deaton and Frost (1946) and Mohammadi et al. (2005). Due to the fact that the maximum deviation observed between measured data and literature data was smaller than the

maximum deviation between literature data, the data measured in this study for the CO_2 (1) + water (2) system was found to be in good agreement with literature data.

Table 6-8: Difference in pressure, at certain temperatures, between measured and literature data for the CO_2 (1) + water (2) system.

This work		Ref 1	Ref 2	Ref 3
T (K)	P (MPa)	ΔP (kPa)	ΔP (kPa)	ΔP (kPa)
281.4	3.48	± 44.78	± 6.51	± 6.51
280.5	3.04	± 23.63	± 51.63	± 37.75
279.1	2.57	± 6.12	± 9.36	± 20.14
276.9	1.93	± 12.85	± 15.13	± 28.04
275.3	1.59	± 14.24	± 10.55	± 36.84
273.5	1.24	± 14.69	± 6.79	± 41.61

Combined expanded uncertainty (U) on measurements: U(T) = 0.1 K and U(P) = 0.01 MPa

$\Delta P = |P_{Literature} - P_{Exp, This study}|$

Ref 1: Deaton and Frost (1946)

Ref 2: Englezos and Hall (1994)

Ref 3: Mohammadi et al. (2005)

The measured data of the CO_2 (1) + water (2) + 5 wt % NaCl (3) system was compared to the literature data of Dholabhai et al. (1993) and Mohammadi et al. (2008b) and is plotted in Figures 6-3 and 6-4.
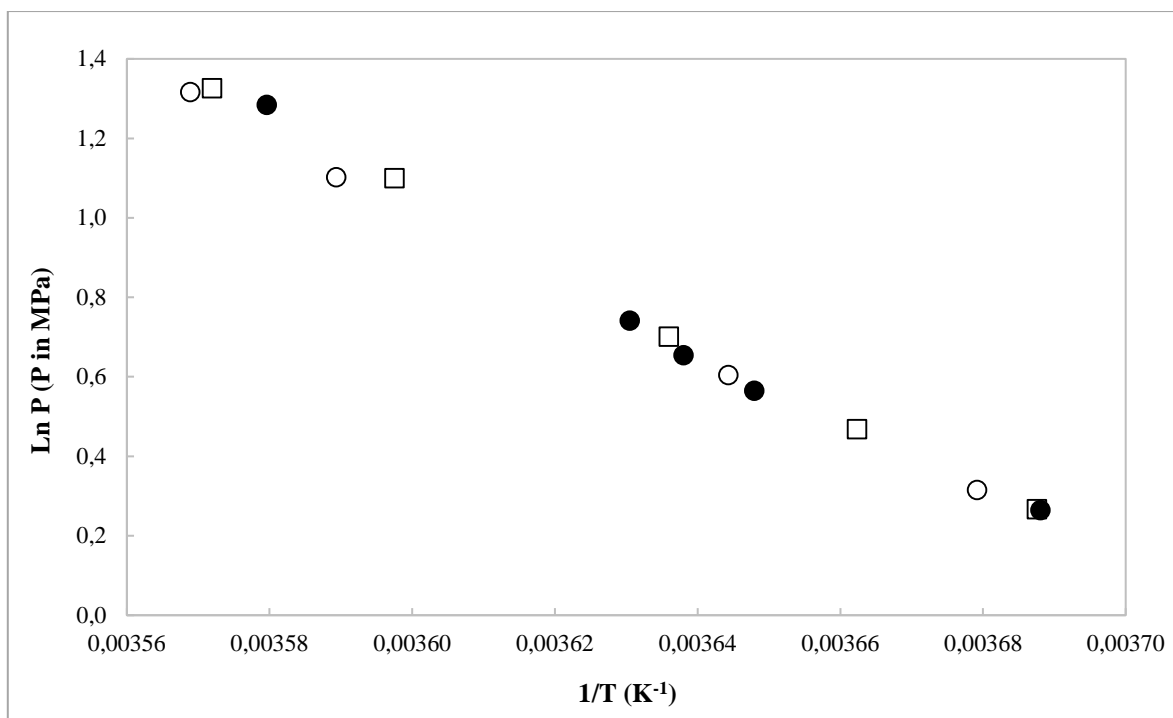
Figure 6-3: Ln P versus 1/T plot of the hydrate dissociation conditions for the CO_2 (1) + water (2) + 5 wt % NaCl (3) system: (●) Exp, This study; (□) Dholabhai et al. (1993); (o) Mohammadi et al. (2008b).
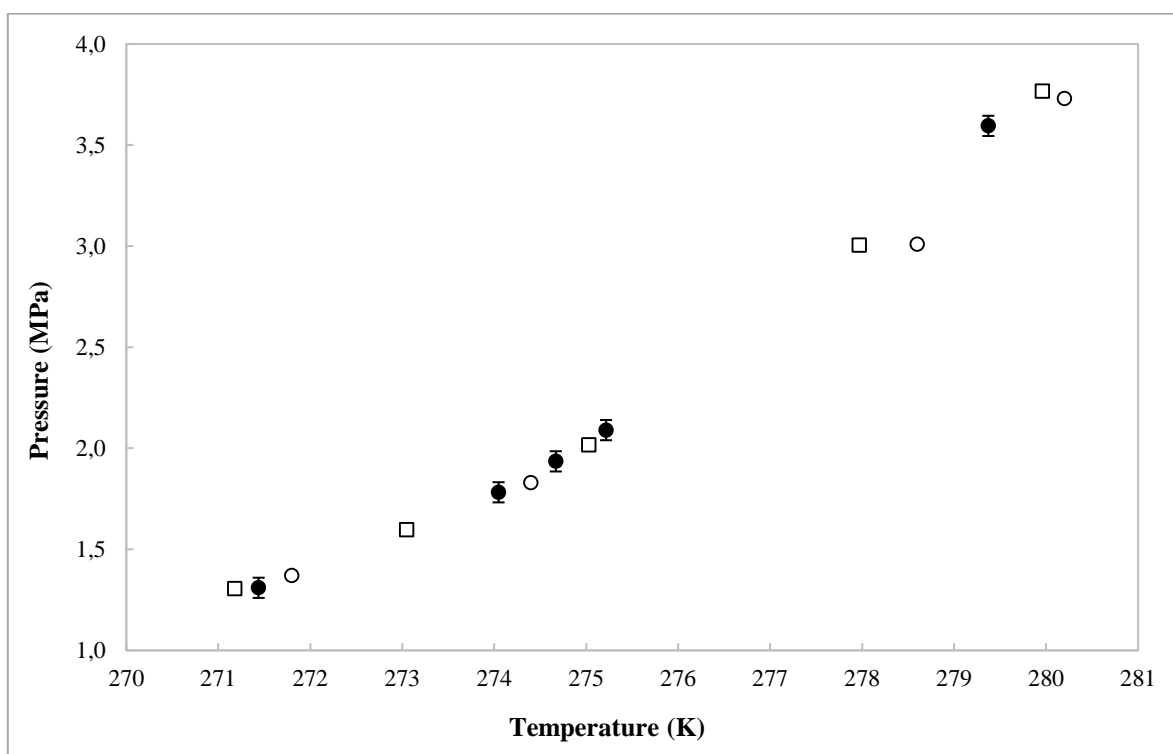
Figure 6-4: Hydrate dissociation conditions for the CO_2 (1) + water (2) + 5 wt % NaCl (3) system: (●) Exp, This study with ± 0.05 MPa error bars; (□) Dholabhai et al. (1993); (o) Mohammadi et al. (2008b)Mohammadi et al. (2008b) reported temperature and pressure uncertainties of ± 0.1 K and ±

0.005 MPa respectively. No uncertainties were reported by Dholabhai et al. (1993). Again, the measurement uncertainties reported in this study were acceptable when compared to uncertainties reported in literature. The measurements in the work of Dholabhai et al. (1993) were conducted using the isothermal experimental method in a 221.2 - 293.6 cm^3 variable volume equilibrium cell and the measurements in the work of Mohammadi et al. (2008b) were conducted using the isochoric experimental method in a 57.5 $\pm$ 0.5 cm^3 equilibrium cell.

From Figures 6-3 and 6-4, it can be seen that at low pressures, the data measured in this study compares well to the literature data. However, at high pressures (P > 3.00 MPa), there is significant discrepancy between the literature and measured data. As with the CO_2 (1) + water (2) system, the pressure deviations between the literature and measured data were determined by fitting a cubic spline curve to the literature data in Excel$^®$. The pressure deviation, for the measured temperatures, between the experimental and literature data is presented in Table 6-9.

Table 6-9: Difference in pressure, at certain temperatures, between measured and literature data for the CO_2 (1) + water (2) + 5 wt % NaCl (3) system.

This work		Ref 1	Ref 2
T (K)	P (MPa)	ΔP (kPa)	ΔP (kPa)
279.4	3.59	$\pm$ 112.61	$\pm$ 314.66
275.2	2.09	$\pm$ 65.07	$\pm$ 28.54
274.7	1.94	$\pm$ 92.69	$\pm$ 10.66
274.0	1.78	$\pm$ 60.86	$\pm$ 10.29
271.4	1.31	$\pm$ 25.68	$\pm$ 50.29

Combined expanded uncertainty (U) on measurements: U(T) = 0.1 K and U(P) = 0.01 MPa

ΔP = $|P_{Literature} - P_{Exp, \ This \ study}|$

Ref 1: Dholabhai et al. (1993)

Ref 2: of Mohammadi et al. (2008b)

A maximum pressure deviation of $\pm$ 314.66 kPa occurred at a temperature of 279.4 K, between the measured data and the literature data of Mohammadi et al. (2008b). The purity of the carbon dioxide and NaCl used in this study and reported in the literature was the same. The experimental technique used in this study and the study of Mohammadi et al. (2008b) was the isothermal method, and the isothermal experimental technique was used in the study of Dholabhai et al. (1993). As a result both the experimental technique and chemical purities cannot be assured contributing factors to the deviation in experimental data at high pressures. The difference in cell volume and auxiliary

equipment, such as pressure transducers, as well as differences in experimenters' techniques, could be contributing factors to the deviation at high pressures. In addition, faulty temperature and pressure sensors, faulty pressure transducers or temperature controllers, incorrect temperature and pressure readings, or human error in the preparation of the experimental solution could be contributing factors to the difference in literature and experimental data at the higher pressures.

Considering the remaining four measured data points (T = 275.4, 274.9, 274.1 and 274.1 K), a maximum pressure deviation of $\pm$ 92.69 kPa, at a temperature of 274.9 K, between the measured data and the literature data of Dholabhai et al. (1993). This maximum deviation is lower than the maximum pressure deviation of $\pm$ 93.61 kPa (at a temperature of 275.4 K) between the literature data of Dholabhai et al. (1993) and Mohammadi et al. (2008b). Apart from the high pressure point, the maximum deviation observed between measured data and literature data was smaller than the maximum deviation between literature data and as a result, the data measured in this study for the CO_2 (1) + water (2) + 5 wt % NaCl (3) system was found to be in good agreement with literature data. The measured data of the CO_2 (1) + water (2) + 5 wt % KCl (3) system and the CO_2 (1) + water (2) + 5 wt % NaCl (3) + 5 wt % KCl (4) system was compared to the literature data of Dholabhai et al. (1993). The CO_2 (1) + water (2) + 5 wt % KCl (3) data is plotted in Figures 6-5 and 6-6 and the CO_2 (1) + water (2) + 5 wt % NaCl (3) + 5 wt % KCl (4) data is plotted in Figures 6-7 and 6-8. The pressure deviations, for the measured temperatures, between the experimental and literature data are presented in Table 6-10 (5 wt % KCl) and Table 6-11 (5 wt % NaCl + 5 wt % KCl). It appears that the hydrate dissociation conditions for these two systems have only been measured by Dholabhai et al. (1993). As a result, the measured data for the CO_2 (1) + water (2) + 5 wt % KCl (3) system and the CO_2 (1) + water (2) + 5 wt % NaCl (3) + 5 wt % KCl (4) system has only been compared to one set of literature data.
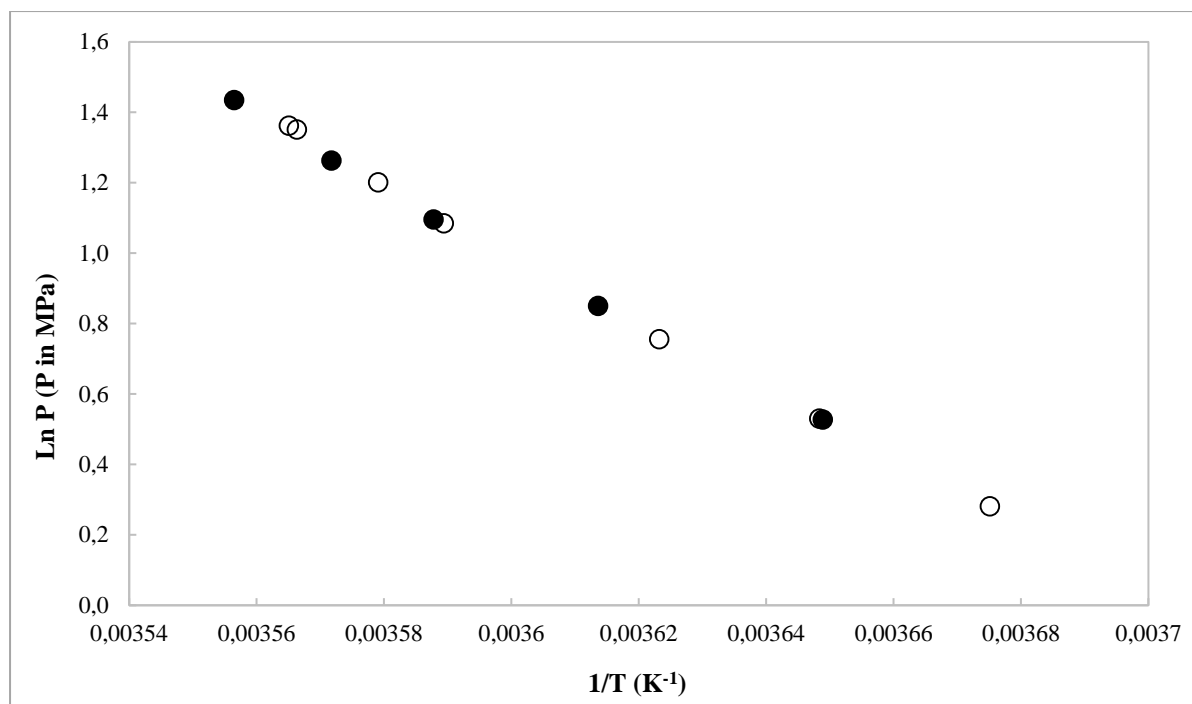
Figure 6-5: Ln P versus 1/T plot of the hydrate dissociation conditions for the CO_2 (1) + water (2) + 5 wt % KCl (3) system: (●) Exp, This study; (□) Dholabhai et al. (1993).
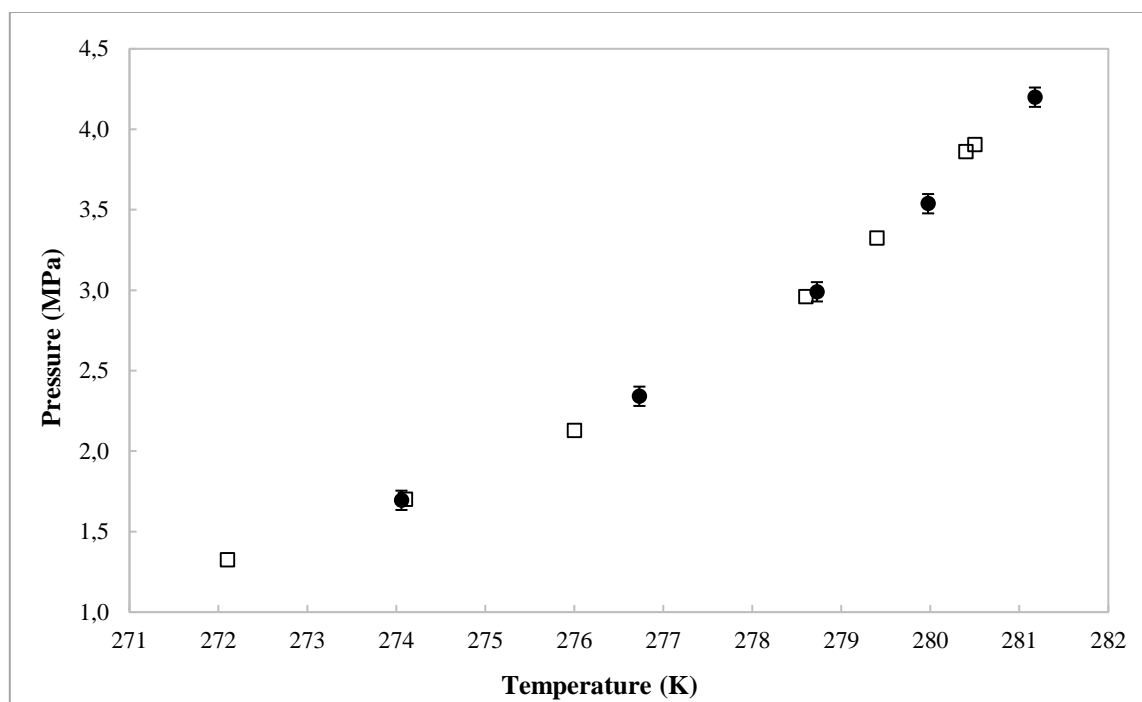
Figure 6-6: Hydrate dissociation conditions for the CO_2 (1) + water (2) + 5 wt % KCl (3) system: (●) Exp, This study with ± 0.05 MPa error bars; (□) Dholabhai et al. (1993).

Table 6-10: Difference in pressure, at certain temperatures, between measured and literature data for the CO_2 (1) + water (2) + 5 wt % KCl (3) system.

	This work	Ref 1
T (K)	P (MPa)	ΔP (kPa)
279.4	3.61	± 12.44
275.4	2.10	± 50.95
274.9	1.92	± 66.56
274.1	1.76	± 24.92
271.1	1.30	± 16.21

Combined expanded uncertainty (U) on measurements: U(T) = 0.1 K and U(P) = 0.01 MPa

ΔP = $|P_{Literature} - P_{Exp,This\ study}|$

Ref 1: Dholabhai et al. (1993)

The maximum pressure deviation for the CO_2 (1) + water (2) + 5 wt % KCl (3) system, between the literature and the measured data, was ± 66.56 kPa. This maximum pressure deviation is comparable to the maximum pressure deviations of the CO_2 (1) + water (2) system and the CO_2 (1) + water (2) + 5 wt % NaCl (3) systems.
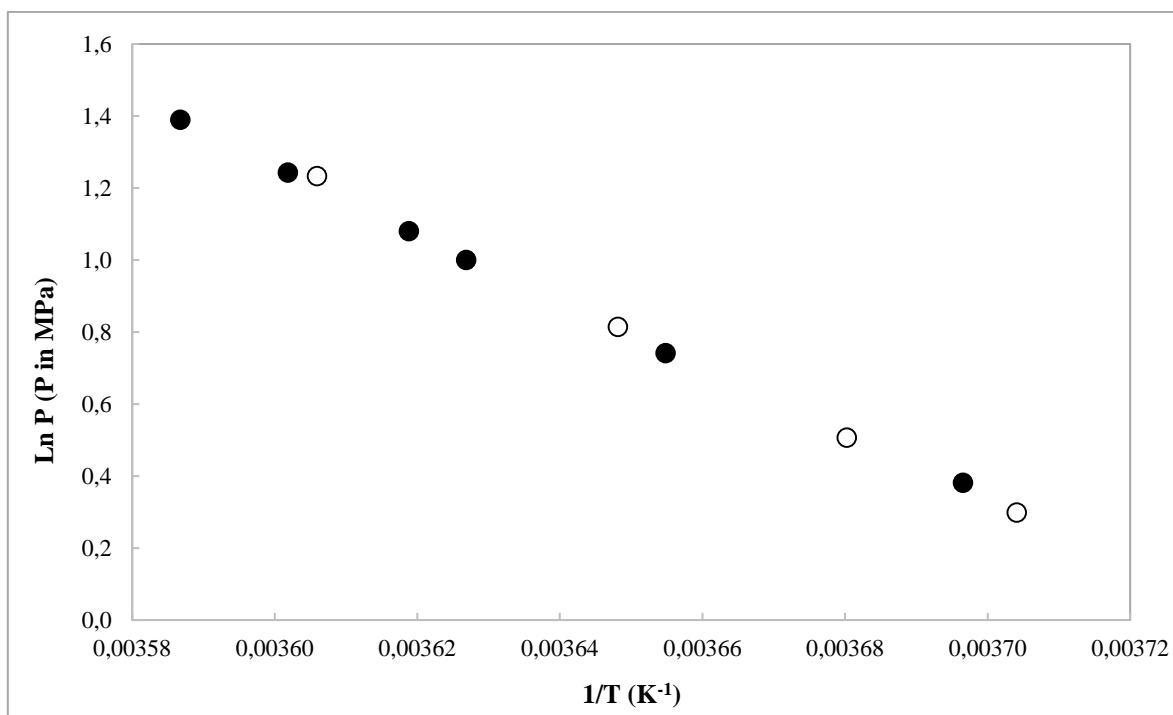
Figure 6-7: Ln P versus 1/T plot of the hydrate dissociation conditions for the CO_2 (1) + water (2) + 5 wt % NaCl (3) + 5 wt % KCl (4) system: (●) Exp, This study; (□) Dholabhai et al. (1993).
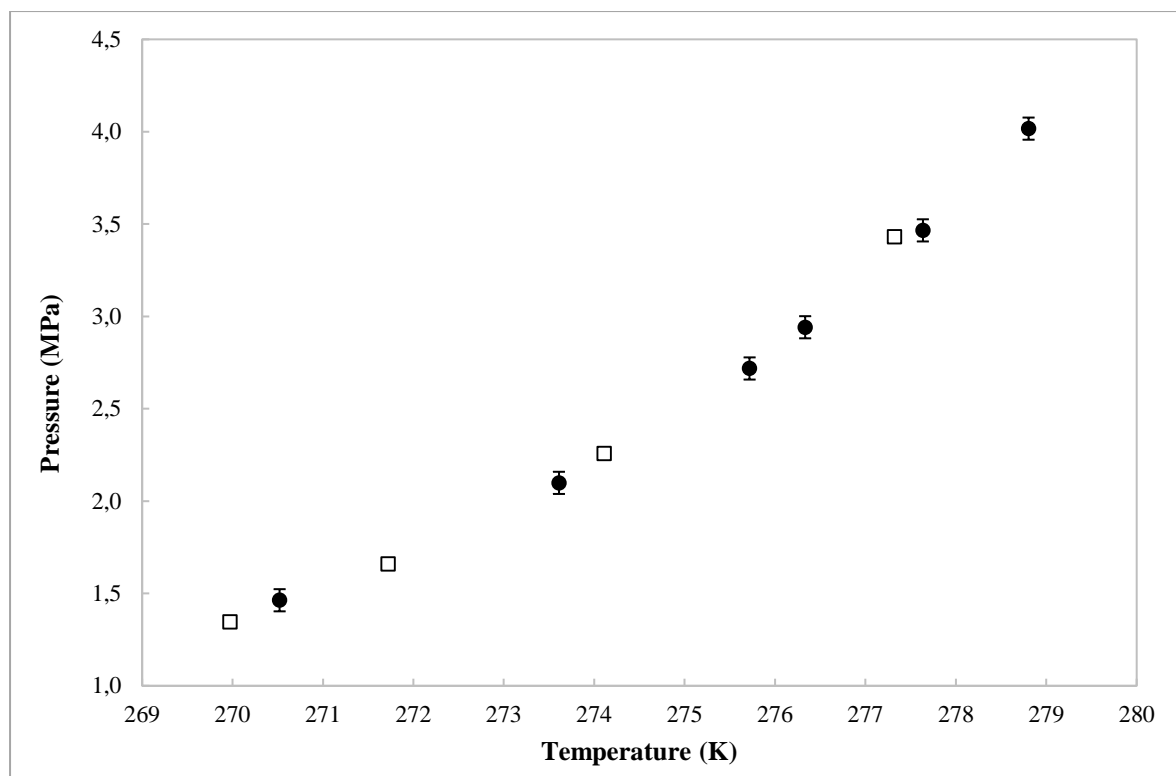
Figure 6-8: Hydrate dissociation conditions for the CO_2 (1) + water (2) + 5 wt % NaCl (3) + 5 wt % KCl (4) system: (●) Exp, This study with ± 0.05 MPa error bars; (□) Dholabhai et al. (1993).

Table 6-11: Difference in pressure, at certain temperatures, between measured and literature data for the CO_2 (1) + water (2) + 5 wt % NaCl (3) + 5 wt % KCl (4) system.

This work		Ref 1
T (K)	P (MPa)	ΔP (kPa)
278.8	4.01	± 98.72
277.6	3.47	± 92.32
276.3	2.95	± 88.48
275.7	2.72	± 86.62
273.6	2.10	± 43.74
270.5	1.46	± 16.21

Combined expanded uncertainty (U) on measurements: U(T) = 0.1 K and U(P) = 0.01 MPa

$\Delta P = |P_{Literature} - P_{Exp,This\ study}|$

Ref 1: Dholabhai et al. (1993)

The maximum pressure deviation for the CO_2 (1) + water (2) + 5 wt % NaCl (3) + 5 wt % KCl (4) system, between the literature and the measured data, was ± 98.72 kPa. This maximum pressure

deviation is comparable to the maximum pressure deviations of the CO_2 (1) + water (2), the CO_2 (1) + water (2) + 5 wt % NaCl (3), and the CO_2 (1) + water (2) + 5 wt % KCl (3) systems.

From the analysis performed on the test systems, it can be concluded that the measured hydrate dissociation data for the test systems compared well in comparison to the data reported in literature, confirming the reliability of the experimental apparatus and method used.

6.6 New systems

The temperature and pressure ranges of the new systems investigated in this study are presented in Table 6-12.

The freezing point of water is depressed in the presence of salts (section 2.4.2) and other solutes such as ethanol and acetic acid. For the measurements, the lowest temperature measurement value was dependent on the freezing point data of the system in question. Gas hydrate based desalination of industrial wastewater was not intended for operation below 273.15 K due to the high-energy consumption. As a result, few measurements were conducted below this temperature.

Table 6-12: New HLV equilibrium data measured in this study.

System	T (K)	P (MPa)
CO_2 (1) + water (2) + 5 wt % Na_2SO_4 (3)	272.2 - 281.3	1.22 - 3.82
CO_2 (1) + water (2) + 5 wt % KCl (3) + 5 wt % Na_2SO_4 (4)	270.9 - 280.2	1.37 - 4.12
CO_2 (1) + water (2) + mixed salts A (3)	272.5 - 280.9	1.46 - 3.99
CO_2 (1) + water (2) + mixed salts B (3)	271.2 - 280.4	1.33 - 4.01
CO_2 (1) + water (2) + synthesized vinasse (3)	271.5 - 279.3	1.54 - 4.23

Combined expanded uncertainty (U) on measurements: U(T) = 0.1 K and U(P) = 0.01 MPa

Where: Mixed salts A = 3 wt % KCl + 1 wt % Na_2SO_4 + 0.5 wt % $MgCl_2$ + 0.5 wt % $CaCl_2$

Mixed salts B = 5 wt % KCl + 1 wt % Na_2SO_4 + 0.5 wt % $MgCl_2$ + 0.5 wt % $CaCl_2$

Synthesized vinasse = 5 wt % KCl + 1 wt % Na_2SO_4 + 0.5 wt % $MgCl_2$ + 0.5 wt % $CaCl_2$ + 2.2 wt % Ethanol + 0.5 wt % Propionic Acid + 0.3 wt % Acetic acid

The measured results of the new systems were verified by three different methods. Firstly, the order of measurements within the pressure ranges was varied, such that any effect of hysteresis on the system was reduced. Secondly, in each measured system, at least one dissociation point was repeated. This showed reliability of the experimental technique and repeatability of the hydrate dissociation data. Thirdly, a linear regression was conducted on the hydrate dissociation data points. The results

obtained were in good agreement as they presented a highly linear relationship when plotted on an LnP versus 1/T scale (Figure 6-10).

The measured data points for the new systems investigated are presented in Table 6-13. The results are plotted in Figures 6-9 (P versus T) and Figure 6-10 (Ln P versus 1/T). The CO_2 and pure water system is also plotted in these figures for visual observation of the equilibrium shift for systems containing inhibitors (inorganic and organic).

Table 6-13: Hydrate dissociation points for the new systems measured in this study (CO_2 (1) + water (2) + inhibitors (3)).

System: CO_2 (1) + water (2) + inhibitor/s (3)	Temperature (K)	Pressure (MPa)
5 wt % Na_2SO_4	281.3	3.82
	280.7	3.52
	280.2	3.29
	279.2	2.86
	277.6	2.33
	275.2	1.74
	274.4	1.60
	272.2	1.22
5 wt % KCl + 5 wt % Na_2SO_4	280.2	4.12
	278.6	3.36
	278.5	3.35
	278.1	3.19
	277.8	3.04
	277.7	3.02
	276.6	2.66
	276.5	2.60
	274.7	2.09
	270.9	1.37
Mixed salt A	280.9	3.99
	280.1	3.60
	279.4	3.25
	278.1	2.78
	276.2	2.20
	272.5	1.46
Mixed salt B	280.4	4.01
	278.8	3.26
	276.5	2.45
	273.6	1.72
	271.2	1.33

Combined expanded uncertainty (U) on measurements: U(T) = 0.1 K and U(P) = 0.01 MPa

Table 6-13 (continued): Hydrate dissociation points for the new systems measured in this study (CO_2 (1) + water (2) + inhibitors (3)).

System: CO_2 (1) + water (2) + inhibitors (3)	Temperature (K)	Pressure (MPa)
Synthesized vinasse	279.2	4.21
	278.1	3.47
	277.2	3.07
	277.1	3.00
	275.4	2.44
	271.5	1.54

Combined expanded uncertainty (U) on measurements: U(T) = 0.1 K and U(P) = 0.01 MPa
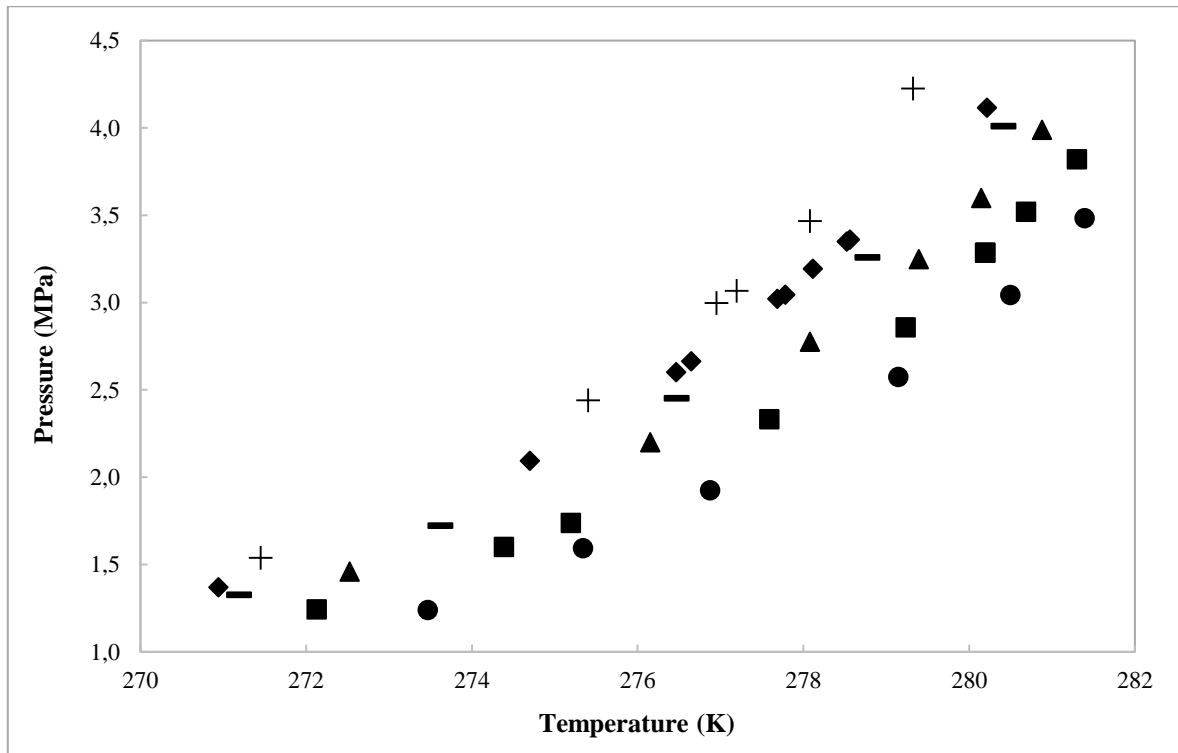
Figure 6-9: Hydrate dissociation conditions for the systems containing CO_2 (1) + water (2) + inhibitors (3). (●) Pure water; (■) 5 wt % Na_2SO_4; (♦) 5 wt % KCl + 5 wt % Na_2SO_4; (▲) mixed salts A; (─) mixed salts B; (+) synthesized vinasse.
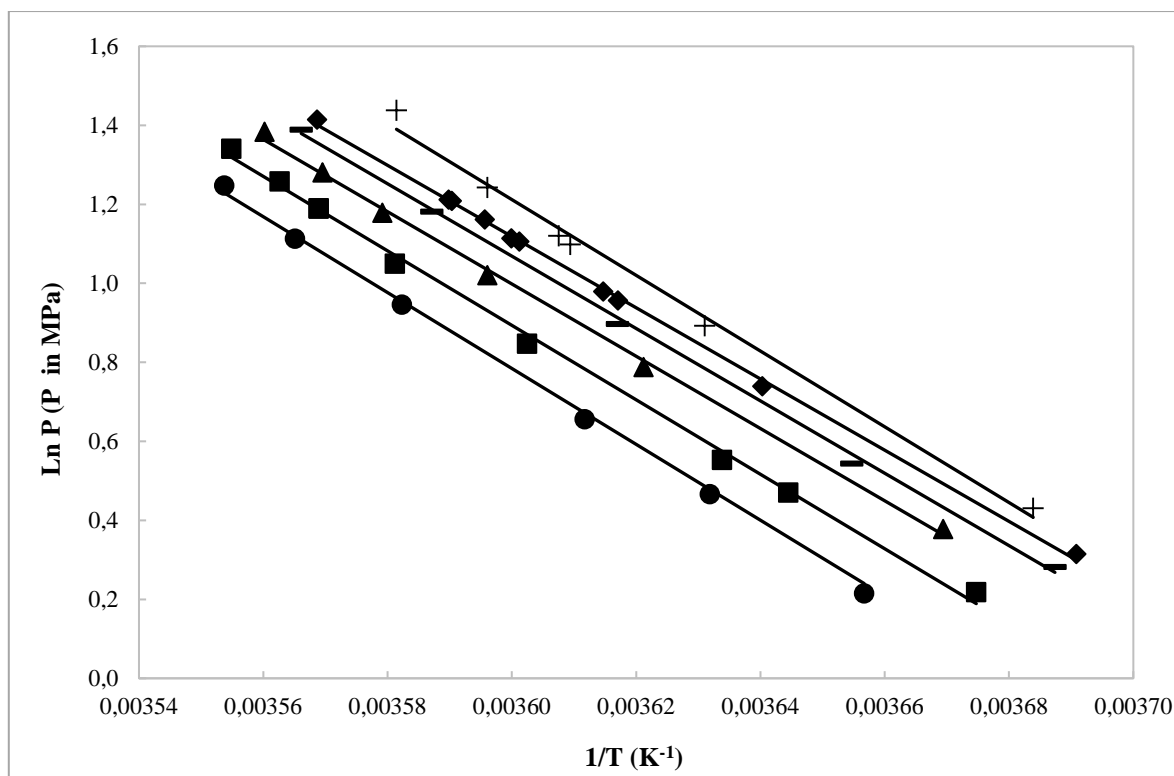
Figure 6-10: Ln P versus 1/T plot for the systems containing CO_2 (1) + water (2) + inhibitors (3). (●) Pure water; (■) 5 wt % Na_2SO_4; (♦) 5 wt % KCl + 5 wt % Na_2SO_4; (▲) mixed salts A; (─) mixed salts B; (+) synthesized vinasse. The straight lines represent the liner regression performed on each system's results.

The addition of inhibitors to a system reduces the temperature at which a hydrate forms, resulting in a temperature shift. This is evident from Figure 6-9 and Figure 6-10. The average shift in temperature between the system containing no inhibitors (CO_2 (1) + water (2)) and the systems containing inhibitors (CO_2 (1) + water (2) + inhibitor (3)) is reported in Table 6-14.

Table 6-14: Average temperature shift between systems containing inhibitors and pure water.

System	Average temperature shift (K)
5 wt % Na_2SO_4	- 0.9
5 wt % KCl + 5 wt % Na_2SO_4	- 2.9
Mixed salt A (5 wt % inhibitors)	- 1.9
Mixed salt B (7 wt % inhibitors)	- 2.4
Synthesized vinasse (10 wt % inhibitors)	- 3.4

From Table 6-14 and Figure 6-9, it can be seen that an increase in the concentration of an inhibitor results in a larger temperature shift from the CO_2 (1) + water (2) system. Even though the synthesized vinasse system and the system containing 5 wt % KCl + 5 wt % Na_2SO_4 both have a 10 wt % inhibitor concentration, the highest average temperature shift is exhibited by the synthesized vinasse system. The average temperature shift for the synthesized vinasse system is 0.5 K greater than the average temperature shift for the 5 wt % KCl + 5 wt % Na_2SO_4. Since both systems contain 5 wt % KCl, it can be concluded that the organic inhibitors combined with NaCl, $MgCl_2$ and $CaCl_2$ have a greater inhibition effect compared to Na_2SO_4.

The hydrate dissociation conditions for all systems measured in this study (test and new systems) are plotted in Figure 6-11. From the figure it can be seen that the system that exhibits the greatest temperature and pressure shift is the CO_2 (1) + water (2) + 5 wt % NaCl (3) + 5 wt % KCl (4) test system. The average temperature shift for this system from the pure water and carbon dioxide system is - 4.1 K, compared to - 3.4 K for the synthesized vinasse system.
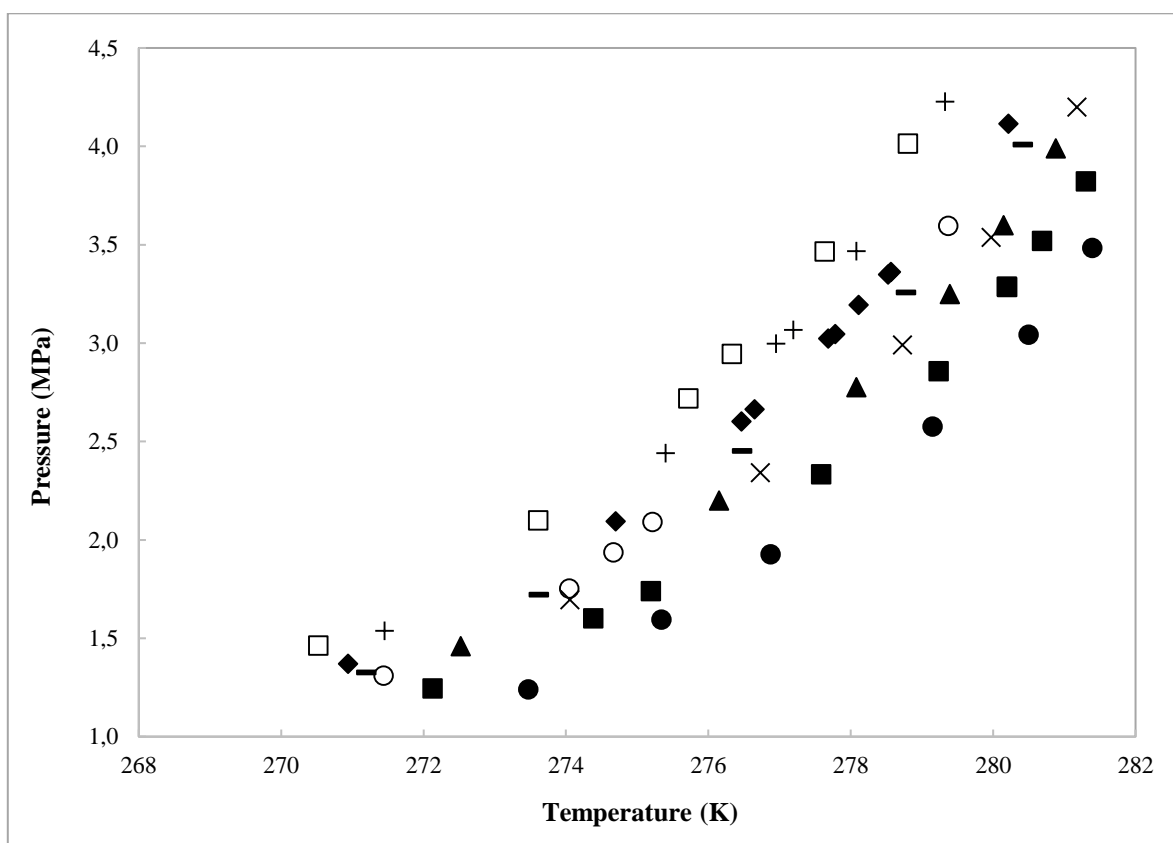
Figure 6-11: Hydrate dissociation conditions for all systems measured in this study. (●) Pure water; (■) 5 wt % Na_2SO_4; (▲) mixed salts A; (×) 5 wt % KCl; (─) mixed salts B; (o) 5 wt % NaCl; (♦) 5 wt % Na_2SO_4 + 5 wt % KCl; (+) synthesized vinasse and (□) 5 wt % NaCl + 5 wt % KCl.

6.7 Data modelling

In this study the fugacity approach was used to model the measured data. This approach is based on the equality of fugacity in the liquid, vapour, and hydrate phases, and is the most suitable approach for the representation of phase equilibrium for systems containing water in equilibrium with gases that have significant water solubility, such as CO_2. The direct $(\varphi - \varphi)$ method was used in which the fugacity coefficient described both the liquid and vapour phase non-idealities. The PRSV EOS in conjunction with the van der Waals classical mixing rule was used to determine these fugacity coefficients and describe the fluid phases. Aspen Plus® flash calculations were conducted to obtain the equilibrium composition of the vapour and liquid phase components at the dissociation conditions. The PRSV EOS accounted for the solubility of the hydrate former. The model developed by Aasberg-Petersen et al. (1991) was used to account for the salts present in the system as well as for the solubility of CO_2 in aqueous electrolyte solutions (Englezos, 1992). The aqueous phase is first treated as a salt-free mixture and the PRSV EOS is used to determine the fugacity coefficient. The calculated fugacity coefficient is than corrected with the Debye-Hückel electrostatic term. The water-salt interaction coefficients were accounted for using the parameters reported by Tohidi et al. (1995) and can be found in Table 3-3. The solid phase was modelling according to the statistical thermodynamic model of Parrish and Prausnitz (1972). The literature data used to model the solid phase was that reported in Parrish and Prausnitz (1972) and can be found in Tables 3-4 to 3-6. Carbon dioxide forms both small and large hydrates of sI. The predictive model was programmed using Matlab®. In this section, the results of the predictive models are presented and discussed. The percent average absolute deviation (%AAD) between the experimental and predicted values are also presented. For the purpose of this study, the percent average absolute deviation is reported in terms of pressure (%AADp), according to the following equation:

$$\%AAD_P = \frac{1}{n}\sum_n \frac{|P_{exp} - P_{calc}|}{P_{calc}} \times 100 \qquad (6\text{-}1)$$

where, P_{exp} and P_{calc} present the measured experimental and predicted pressure respectively, and n represents the number of data points.

Due to the complexity of the systems measured, the focus of the study was on testing the feasibility of the hydrate-based treatment technology rather than the development of a thermodynamic model. Therefore, in this study, only predictive models were used to compare the measured data and data regression was not performed. The synthesized vinasse system contained 7 inhibitors in total, which were organic and inorganic in nature. As a result, a predictive model was not developed to compare

the measured data. Another study within the Thermodynamics Research Unit, focused on developing such a predictive model, and the results for the system measured are presented below.

6.7.1 Results from the predictive modelling

The flow diagrams presenting the approach used to predict the dissociation pressures for the measured temperatures are given in Figures 6-12 to 6-14 for the CO_2 (1) + water (2), CO_2 (1) + water (2) + single salt (3) and CO_2 (1) + water (2) + mixed salt (3) systems respectively. The results of the predictive models as well as the experimental data are displayed in Figures 6-15 to 6-20. The predicted pressures compared to the experimental pressures and the corresponding %AADp for the pure water system and the systems containing single and mixed salts are reported in Table 6-15, Table 6-16 and Table 6-17 respectively.
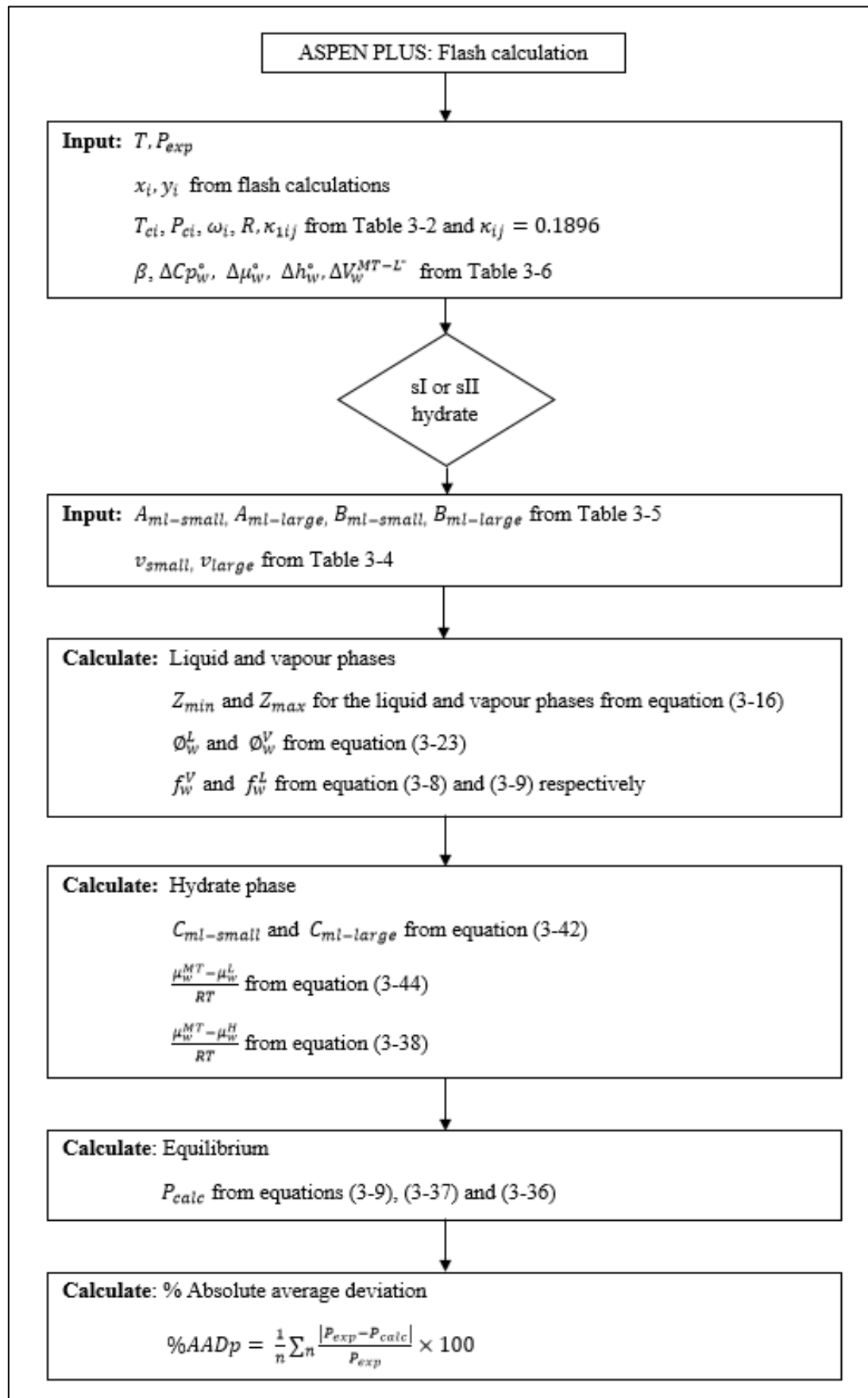
Figure 6-12: Computation flow chart for the predictive model for the CO_2 (1) + water (2) system.
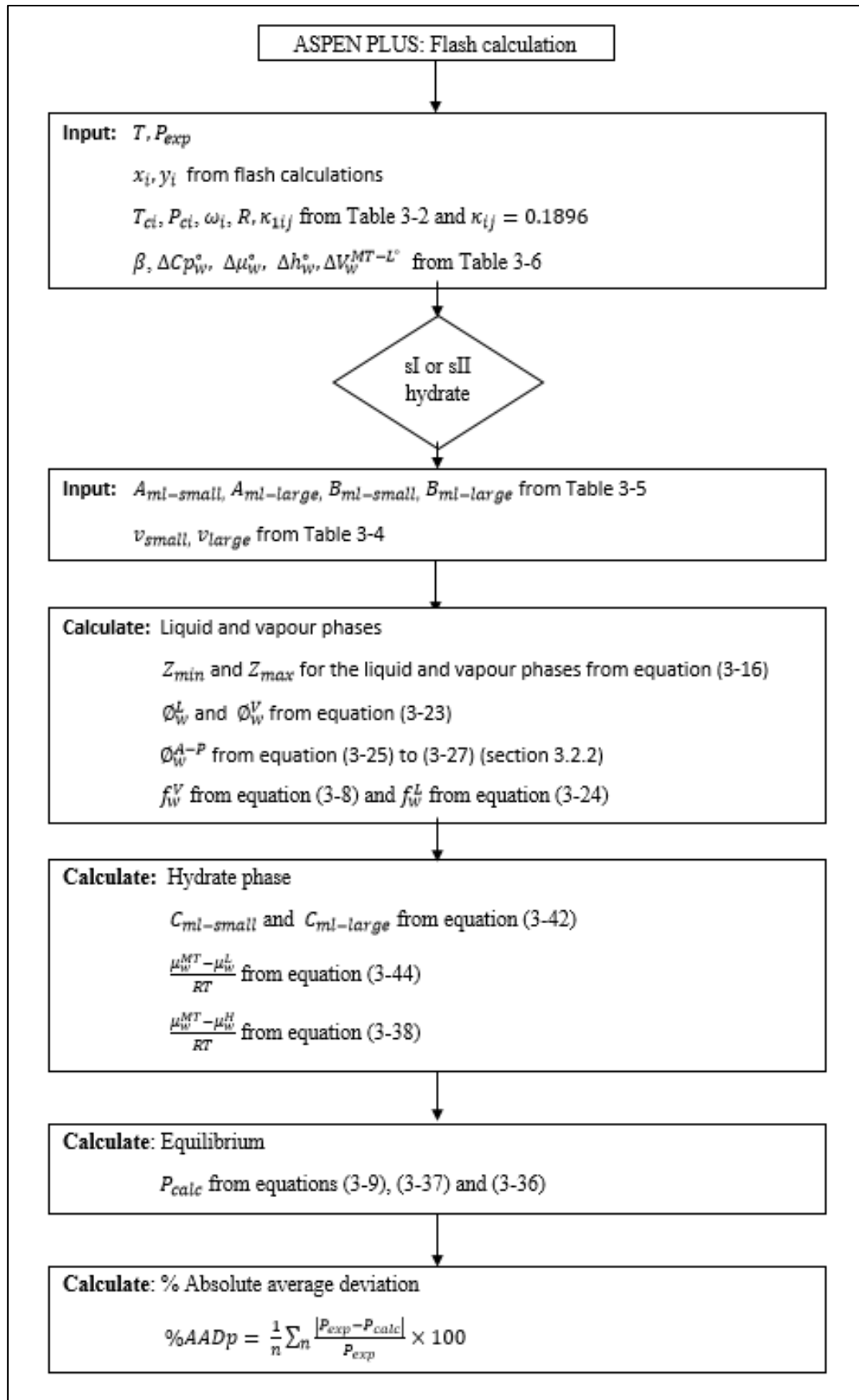
Figure 6-13: Computation flow chart for the predictive model for the CO_2 (1) + water (2) + single salt (3) system.
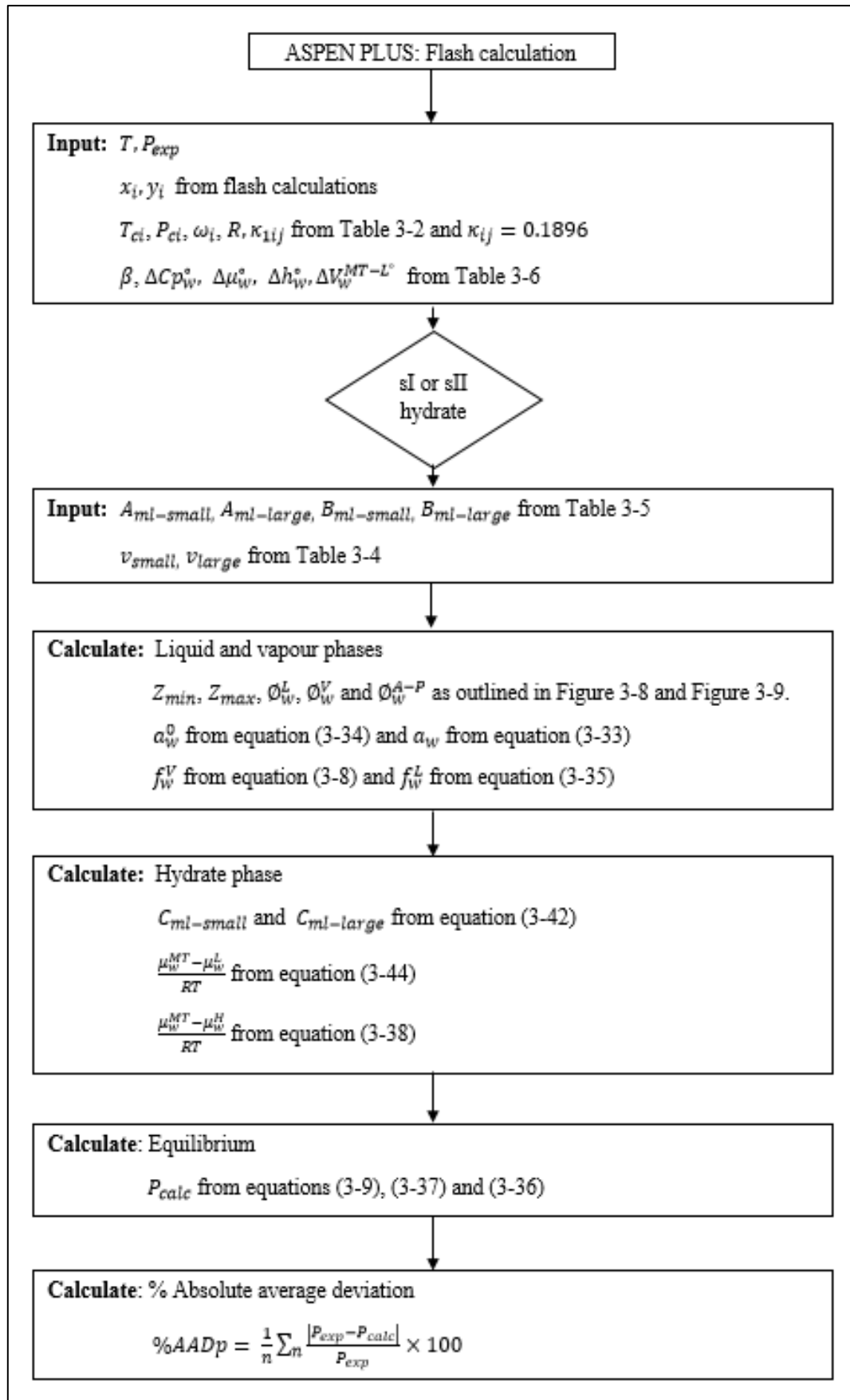
Figure 6-14: Computation flow chart for the predictive model for the CO_2 (1) + water (2) + mixed salts (3) system.
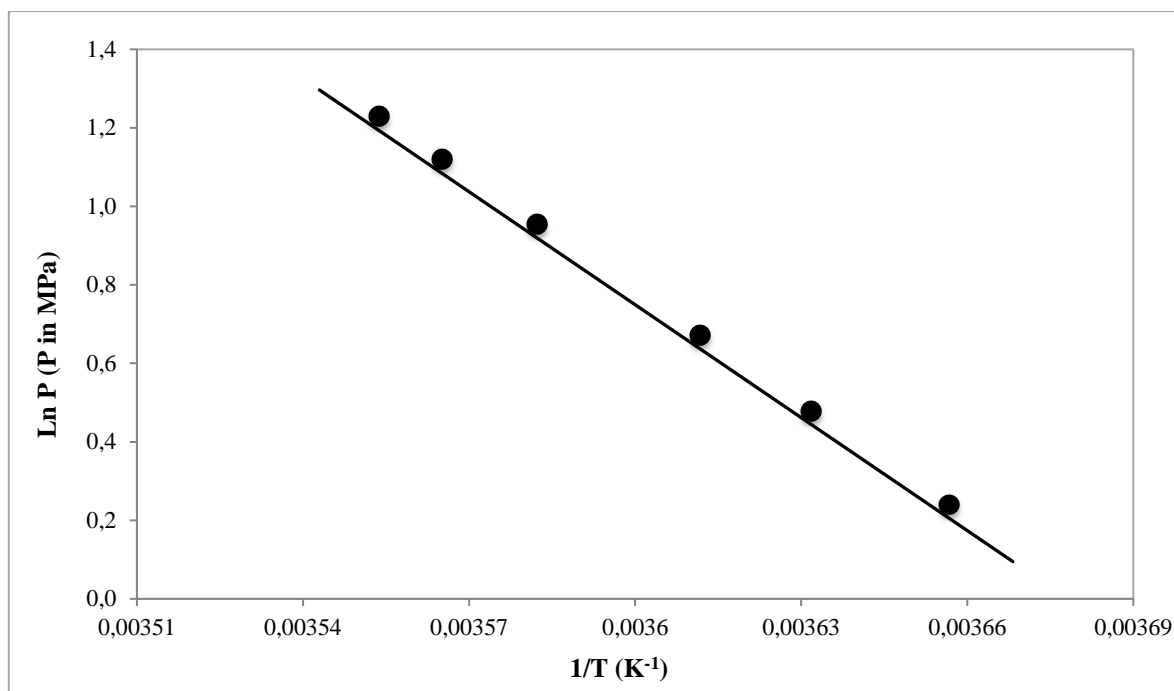
Figure 6-15: Measured and predicted HLV equilibrium data for the CO_2 (1) + water (2) system. (●) Exp, This study; (—) predictive model used in this study.

From Figure 6-15, it can be seen that for the CO_2 (1) + water (2) system, the predictive model used in this study under-predicted the hydrate dissociation pressures. The predicted dissociation pressures are however comparable to the measured dissociation pressures. This can be seen in Table 6-15. The difference between the predicted and measured hydrate dissociation pressure was more evident at higher pressures (P > 2.50 MPa). The average difference between the two pressures was 0.07 MPa. The largest difference between the two pressures was 0.14 MPa, which occurred at a measured pressure of 3.48 MPa (and temperature of 281.4 K). The predictive model used in this study therefore described the solubility of the system at lower temperatures and pressures well, but deviated from measured data as the temperatures and pressures increased. This is not unexpected as at high temperatures and pressures, the significance of phase non-idealities becomes increasingly apparent and the PRSV EOS with the van der Waals mixing rules was not adequate in defining the liquid phase density and accounting for the solubility of the CO_2.

The %AADp for the pure water system was calculated to be 2.53 %. Petticrew (2011) and Smith (2015) conducted gas hydrate research on salt and sucrose aqueous solutions respectively within the Thermodynamics Research Unit. In their research, the authors both used the PR EOS with the classical mixing rule to describe the fluid phases and the van der Waals and Platteeuw theory (Van der Waals and Platteeuw, 1959) to describe the hydrate phase. The authors reported a %AADp of 3.20 and 3.00 % respectively for the CO_2 (1) + water (2) system. The improved %AADP achieved in this

study is attributed to the use of the PRSV EOS. The PRSV EOS, compared to the PR EOS, is superior in predicting VLE for pure components.

When developing their fugacity model for gas hydrate phase equilibrium, Klauda and Sandler (2000) compared the results of their model to the results of other models: the models of Parrish and Prausnitz (1972), Chen and Guo (1998), and Sloan (1998). For the CO_2 (1) + water (2) system, Klauda and Sandler (2000) reported a %AADp of 12.75 % when the model of Parrish and Prausnitz (1972) was used; 8.01 % when the model of Chen and Guo (1998) was used; 9.32 % when the model of Sloan (1998) was used and a %AADp of 2.87 % when their model was used. Klauda and Sandler (2000) did not report which of the many available equations of states and mixing rules was used to describe the fluid phase when they used the models of Parrish and Prausnitz (1972), Gen and Guo (1998), and Sloan (1998), however it was reported that the PRSV EOS was used in the development of their model. No mixing rule was reported.

Table 6-15: Experimental versus predicted pressure encountered in this study for the CO_2 (1) + water (2) system.

Experimental P (MPa)	Predicted P (MPa)	Δ P (MPa)	%AADp
3.48	3.34	0.14	2.53
3.04	2.94	0.11	
2.57	2.50	0.07	
1.93	1.89	0.03	
1.59	1.57	0.03	
1.24	1.23	0.01	

Combined expanded uncertainty (U) on measurements: U(P) = 0.01 MPa

$\Delta P = |P_{Experimental} - P_{Predicted}|$

$$\%AAD_P = \frac{1}{n}\sum_n \frac{|P_{exp} - P_{calc}|}{P_{calc}} \times 100$$

Figure 6-16 shows the results of the predictive model and the experimental data for the single salt systems investigated in this study. In Figure 6-16, the literature data of Mohammadi et al. (2008b) and the results from the predictive model used in this study, for the CO_2 (1) + water (2) + 10 wt % KCl (3) system has been plotted. This was done to demostrate that the data measured and predicted in this study follows trends from literature. From Figure 6-16 it can be seen that, as with the pure water system, the predicted dissociation pressures are comparable to the measured dissociation pressures. The average pressure difference between the measured and predicted data was 0.06 MPa, 0.09 MPa, and 0.11 MPa and the largest pressure difference between the two pressures was 0.12 MPa, 0.16 MPa, and 0.20 MPa for the 5 wt % NaCl, 5 wt % KCl, and 5 wt % Na_2SO_4 systems respectively. These

pressure differences, and the corresponding pressures at which they occurred can be seen in Table 6-16. From these results it can be seen that the model was least accurate for the CO_2 (1) + water (2) + 5 wt % Na_2SO_4 (3) system.
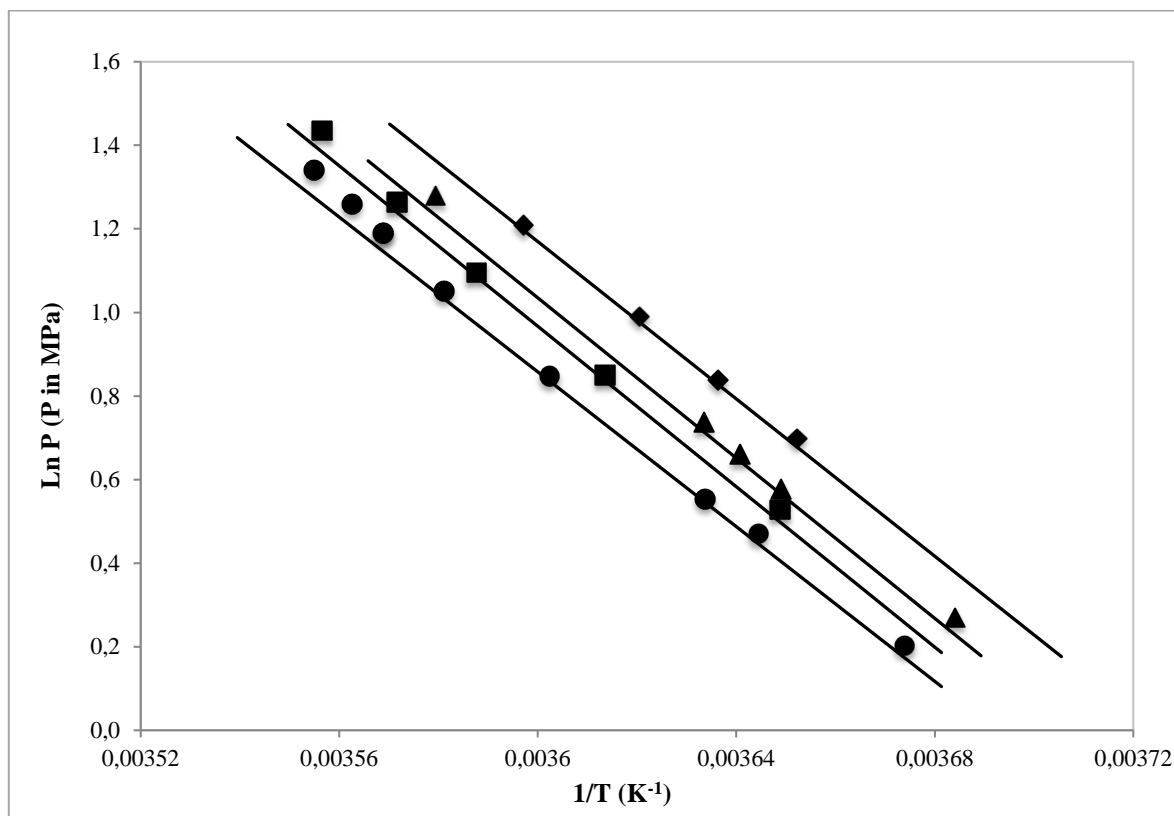
Figure 6-16: Measured and predicted HLV equilibrium data for the CO_2 (1) + water (2) + single salt (3) system. (●) Exp, This study: 5 wt % Na_2SO_4; (■) Exp, This study: 5 wt % KCl; (▲) Exp, This study, 5 wt % NaCl; (♦) Literature data: 10 wt % KCl (Mohammadi et al., 2008b); (—) predictive model used in this study.

Figures 6-17 to 6-20 shows the results of the predictive model and the experimental data for the mixed salt systems investigated in this study. Literature data of Dholabhai et al. (1993) and the predicted pressures from the model used in this study are plotted in these figures in order to demonstrate that the measured and predicted data in this study follow similar trends. From these figures, it can be seen that the pressures predicted in this study for the mixed salt systems deviated to a greater extent from the measured pressures compared to the pure water and single salt systems. The difference in these pressures (predicted and measured) can be found in Table 6-17. The average pressure difference was 0.20 MPa for the CO_2 (1) + water (2) + 5 wt % NaCl (3) + 5 wt % KCl (4) system, 0.15 for the CO_2 (1) + water (2) + 5 wt % KCl (3) + 5 wt % Na_2SO_4 (4) system, 0.13 MPa for the CO_2 (1) + water (2) +

mixed salts A (3), and 0.13 MPa for the CO_2 (1) + water (2) + mixed salts B (3) system. The largest pressure difference for these systems was 0.29 MPa, 0.25 MPa, 0.21 MPa, and 0.23 MPa respectively.

Table 6-16: Experimental versus predicted pressure encountered in this study for the CO_2 (1) + water (2) + single salt (3) systems.

System: CO_2 (1) + water (2) + single salt (3)	Experimental P (MPa)	Predicted P (MPa)	Δ P (MPa)
5 wt % NaCl	3.59	3.47	0.12
	2.09	2.05	0.04
	1.94	1.87	0.07
	1.78	1.72	0.06
	1.31	1.28	0.03
5 wt % KCl	4.20	4.04	0.16
	3.54	3.42	0.12
	2.99	2.90	0.09
	2.34	2.28	0.06
	1.69	1.66	0.03
5 wt % Na_2SO_4	3.82	3.63	0.20
	3.52	3.35	0.17
	3.29	3.14	0.15
	2.86	2.74	0.15
	2.33	2.25	0.11
	1.74	1.69	0.09
	1.60	1.55	0.05
	1.22	1.21	0.05

Combined expanded uncertainty (U) on measurements: U(P) = 0.01 MPa

$\Delta P = |P_{Experimental} - P_{Predicted}|$
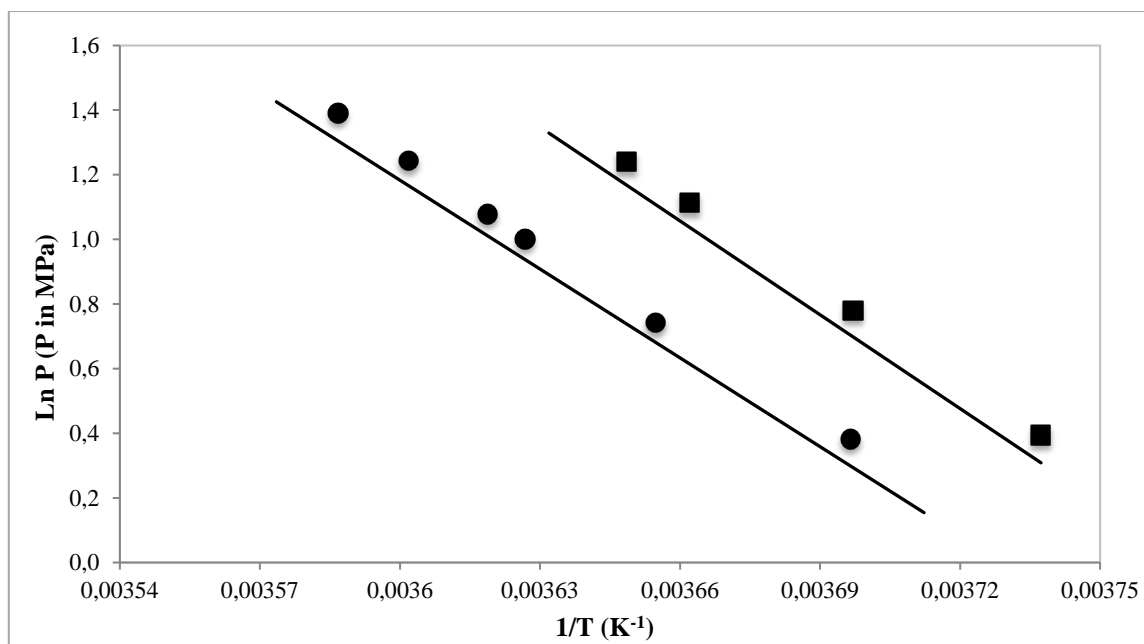
Figure 6-17: Measured and predicted HLV equilibrium data for the CO_2 (1) + water (2) + 5 wt % NaCl (3) + 5 wt % KCl (4) system. (●) Exp, This study; (■) Literature data: 7 wt % NaCl + 10 wt % KCl (Dholabhai et al., 1993); (—) predictive model used in this study.
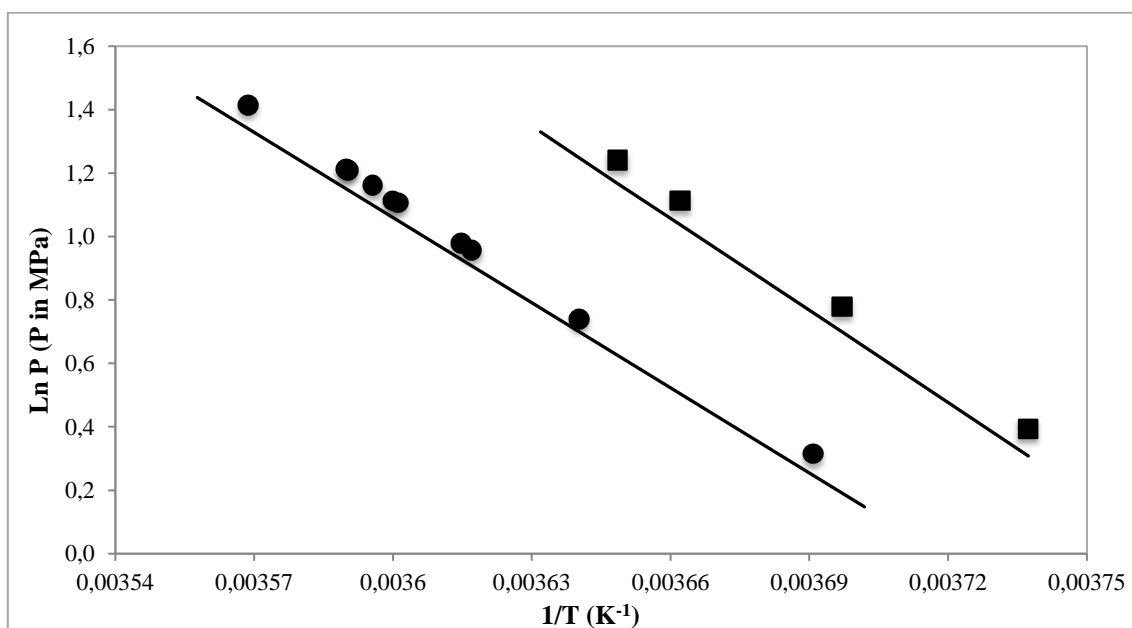
Figure 6-18: Measured and predicted HLV equilibrium data for the CO_2 (1) + water (2) + 5 wt % KCl (3) + 5 wt % Na_2SO_4 (4) system. (●) Exp, This study; (■) Literature data: 7 wt % NaCl + 10 wt % KCl (Dholabhai et al., 1993); (—) predictive model used in this study.
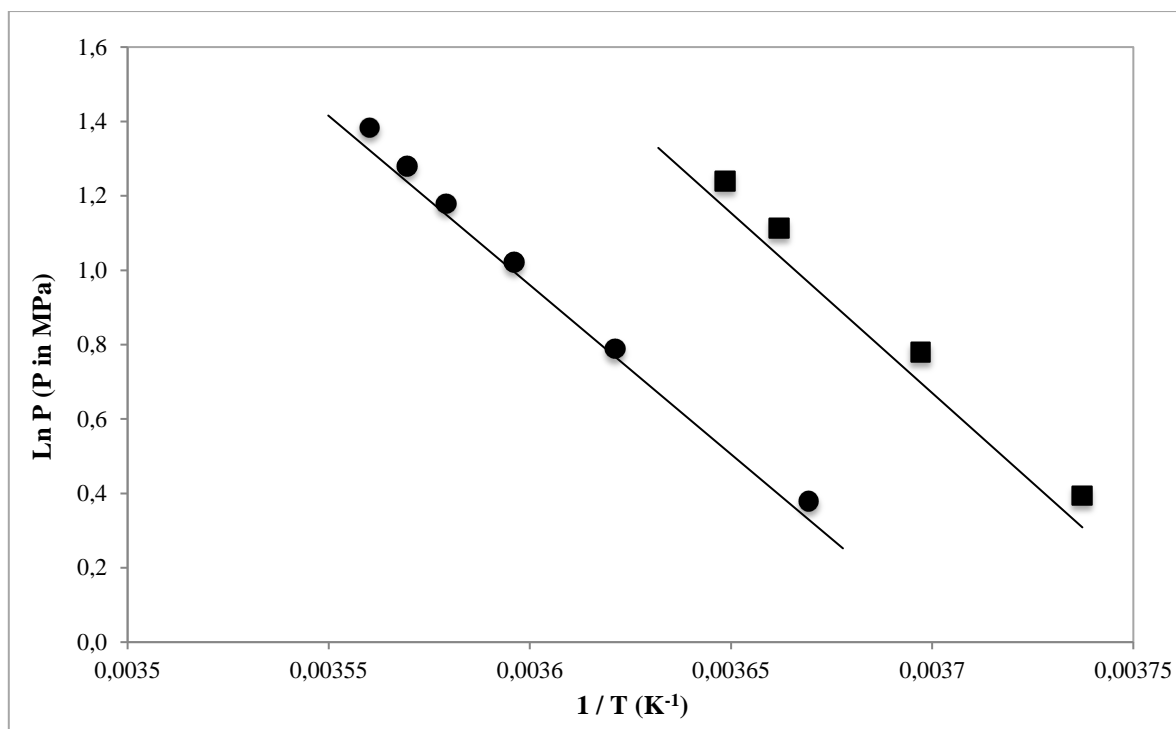
Figure 6-19: Measured and predicted HLV equilibrium data for the CO_2 (1) + water (2) + mixed salts A (3) system. (●) Exp. This study; (■) Literature data: 7 wt % NaCl + 10 wt % KCl (Dholabhai et al., 1993); (—) predictive model used in this study.
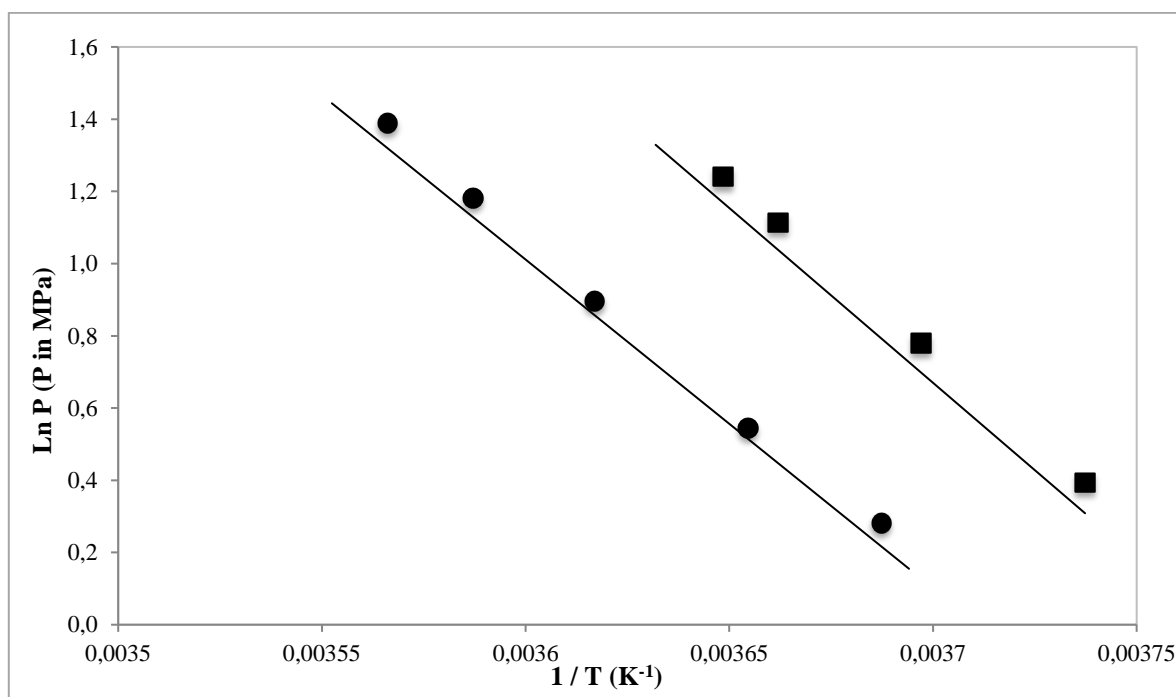
Figure 6-20: Measured and predicted HLV equilibrium data for the CO_2 (1) + water (2) + mixed salts B (3) system. (●) Exp. This study; (■) Literature data: 7 wt % NaCl + 10 wt % KCl (Dholabhai et al., 1993); (—) predictive model used in this study.

Table 6-17: Experimental versus predicted pressure encountered in this study for the CO_2 (1) + water (2) + mixed salt (3) systems.

System: CO_2 (1) + water (2) + mixed salts (3)	Experimental P (MPa)	Predicted P (MPa)	Δ P (MPa)
5 wt % NaCl + 5 wt % KCl	4.02	3.72	0.29
	3.47	3.22	0.25
	2.94	2.73	0.21
	2.72	2.53	0.19
	2.10	1.96	0.14
	1.46	1.36	0.10
5 wt % KCl + 5 wt % Na_2SO_4	4.12	3.87	0.25
	3.36	3.17	0.20
	3.35	3.15	0.19
	3.19	3.01	0.18
	3.04	2.87	0.17
	3.02	2.85	0.17
	2.66	2.52	0.15
	2.60	2.46	0.14
	2.09	1.99	0.11
	1.37	1.30	0.07
Mixed salts A	3.99	3.78	0.21
	3.60	3.42	0.18
	3.25	3.10	0.15
	2.78	2.65	0.12
	2.20	2.11	0.09
	1.46	1.40	0.05
Mixed salts B	4.01	3.78	0.23
	3.26	3.08	0.17
	2.45	2.33	0.12
	1.72	1.65	0.07
	1.33	1.27	0.06

Combined expanded uncertainty (U) on measurements: U(P) = 0.01 MPa

$\Delta P = |P_{Experimental} - P_{Predicted}|$

From the results reported in Figures 6-16 to 6-20 and Tables 6-16 and 6-17, it can be seen that pressures predicted for salt systems, by the model used in this study, deviated from the measured data. At lower temperatures and pressures the deviation between the two pressures was to a lesser extent compared to the deviation at higher temperatures and pressures. As already stated, this is not unexpected as at high temperatures and pressures, the significance of phase non-idealities becomes increasingly apparent and the PRSV EOS with the van der Waals mixing rules was not adequate in defining the liquid phase density. The deviation between the pressure predicted by the model and the measured data increased as the concentration of the salts present in the system increased. In addition, the model predicted pressures more accurately for single salt systems compared to mixed salt systems. This result is due to the intrinsic limitation of the used model at the high concentration range of electrolytes and the large solubility of carbon dioxide in aqueous solutions. When developing the numerical model capable of predicting hydrate phase equilibrium for electrolyte solutions, Tohidi et al. (1995) ignored the gas solubility as well as the change of gas solubility in the presence of salts. Carbon dioxide is extremely water-soluble. In addition, the solubility of carbon dioxide increases with an increase in pressure, and, with the addition of an electrolyte (and subsequently an increase in the concentration of the electrolyte), decreases. The difference between the predicted and measured pressures could be attributed to the reasons stated above.

The %AADp for the systems investigated in this study are reported in Table 6-18.

Table 6-18: The percent average absolute pressure deviation (%AADp) for the systems investigated in this study.

System	%AADp
Pure water	2.53
5 wt % NaCl	2.92
5 wt % KCl	2.89
5 wt % Na_2SO_4	3.78
5 wt % NaCl + 5 wt % KCl	7.01
5 wt % KCl + 5 wt % Na_2SO_4	5.63
Mixed salts A	4.46
Mixed salts B	5.06

$$\%AAD_P = \frac{1}{n}\sum_n \frac{|P_{exp} - P_{calc}|}{P_{calc}} \times 100$$

As mentioned in section 3.4, Delavar and Haghtalab (2015) developed a thermodynamic model for predicting conditions of gas hydrate formation in the presence of organic inhibitors, salts, and their mixtures using the UNIQUAC model in combination with the Chen-Guo model (Chen and Guo, 1998) to describe the hydrate phase. In their research they compared the %AAD (in terms of pressure) of their model result to that of Hsieh et al. (2012) and Chin et al. (2013). In the work of Hsieh et al. (2012), the authors presented a predictive method for the change in equilibrium conditions of gas hydrates with the addition of organic inhibitors and electrolytes. The authors used the PRSV EOS with the COSMO-SAC activity coefficient liquid model through the modified Huron-Vidal mixing rule to describe the fluid phases and the van der Waals and Platteeuw (1959) model to describe the hydrate phase. COSMO-SAC (Conductor like screening model-segment activity coefficients) is a quantum mechanical method. The COSMO models are able to predict phase equilibrium without the requirement for experimental data (Wang et al., 2009). Chin et al. (2013) developed a new approach for predicting the melting curves of gas hydrates with single or multiple additives, including organic inhibitors and electrolytes, by using an explicit pressure-dependent Langmuir adsorption constant in the van der Waals and Platteeuw (1959) model for the hydrate phase. As in the work of Hsieh et al. (2012), the authors used the PRSV EOS with the COSMO-SAC activity coefficient liquid model through the modified Huron-Vidal mixing rule to describe the fluid phases. The results of the research conducted by Delavar and Haghtalab (2015) and the comparison of data, for systems where CO_2 was used as the former, is reported in Tables 6-19 and 6-20. Where applicable, the results of this study are also presented for comparison purposes.

The %AADp for the CO_2 (1) + water (2) + 5 wt % NaCl (3) system and the CO_2 (1) + water (2) + 5 wt % KCl (3) system in this study was calculated to be 2.92 % and 2.89 % respectively. These deviations are much lower than the deviations reported by Hsieh et al. (2012), Chin et al. (2013) and Delavar and Haghtalab (2015) for the same systems. The salt concentration and the temperature and pressure ranges for the NaCl and KCl single salt systems studied in this research fall in the ranges reported by Hsieh et al. (2012), Chin et al. (2013) and Delavar and Haghtalab (2015) (Table 6-19).

According to the author's knowledge, the CO_2 (1) + water (2) + 5 wt % Na_2SO_4 (3) system has to date not been reported in literature. In addition, the author could not find predictive model results presented in open literature, for the system. The %AADp for the CO_2 (1) + water (2) + 5 wt % Na_2SO_4 (3) was calculated to be 3.78 %. Excluding the 3.71 %AADp reported by Chin et al. (2013) for $MgCl_2$, the calculated %AADp for the 5 wt % Na_2SO_4 salt system is lower than the % AADp reported for the single salt systems in Table 6-19. Again, the salt concentration and the temperature and pressure range studied in this research for Na_2SO_4 fall within the ranges reported by Hsieh et al. (2012), Chin et al. (2013), and Delavar and Haghtalab (2015) (Table 6-19).

The %AADp for the CO_2 (1) + water (2) + 5 wt % NaCl (3) + 5 wt % KCl (4) was calculated to be 7.01 %. This is less than the %AADp reported by Delavar and Haghtalab (2015) and higher than the %AADp reported by Hsieh et al. (2012) and Chin et al. (2013) (Table 6-20). The difference in these values could be attributed to the difference between the mixing rules and the predictive models used in this study and literature. The %AADp for the CO_2 (1) + water (2) + 5 wt % KCl (3) + 5 wt % Na_2SO_4 (4) system, the CO_2 (1) + water (2) + Mixed Salt A (3) system and the CO_2 (1) + water (2) + Mixed Salt B (3) system was calculated to be 5.63 %, 4.46 % and 5.06 % respectively.

From these results and the analysis performed on the literature data for similar gas hydrate forming systems it can be concluded that the predictive model outlined in Chapter 3 and used in this study to predict the dissociation pressures is satisfactory and acceptable.

Table 6-19: The percent average absolute deviation (%AADp) between measured and predicted pressures for CO_2 hydrate forming systems in the presence of single salts as reported in literature (reported by Delavar and Haghtalab, 2015).

Salt	Salt mass fraction	T (K)	P (MPa)	%AADp			
				Hsieh et al. (2012)	Chin et al. (2013)	Delavar and Haghtalab (2015)	This work
NaCl	0.03 - 0.20	265.40 - 280.90	1.162 - 4.227	6.73	7.70	5.26	2.92
KCl	0.03 - 0.15	269.00 - 281.10	1.130 - 3.905	8.73	3.83	8.73	2.89
$CaCl_2$	0.03 - 0.20	259.20 - 280.90	0.960 - 3.824	5.42	6.25	9.80	-
$MgCl_2$	0.03 - 0.10	272.50 - 281.00	1.540 - 3.950	10.83	3.71	4.36	-

$$\%AAD_P = \frac{1}{n}\sum_n \frac{|P_{exp} - P_{calc}|}{P_{calc}} \times 100$$

Table 6-20: The percent average absolute deviation (%AADp) between measured and predicted pressures for CO_2 hydrate forming systems in the presence of mixed salts as reported in literature (reported by Delavar and Haghtalab, 2015).

Salt mass fraction			T (K)	P (MPa)	%AADp			
NaCl	KCl	$CaCl_2$			Hsieh et al. (2012)	Chin et al. (2013)	Delavar and Haghtalab (2015)	This work
0.03-0.15	0.03-0.05	-	262.90 - 279.90	1.218 - 3.976	6.26	4.55	7.47	7.01
0.02-0.15	-	0.02-0.147	259.00 - 279.20	0.909 - 3.697	6.34	2.64	11.98	-

$$\%AAD_P = \frac{1}{n}\sum_n \frac{|P_{exp} - P_{calc}|}{P_{calc}} \times 100$$

Dr. Saeideh Babaee, a post-doctoral scholar within the Thermodynamics Research Unit at the University of KwaZulu-Natal has been developing a thermodynamic model to predict the dissociation conditions for systems containing salts and organic inhibitors. This predictive model by Babaee (2017) (work in progress) uses the approach of equal fugacity to predict the hydrate phase conditions. The solid solution theory of van der Waals and Platteeuw (1959) is used to model the gas hydrate phase. The Valderrama modification of the Patel and Teja equation of state (VPT EOS) (Valderrama, 1990) is used to estimate the fugacity of the CO_2 gas molecule.

Figures 6-21 and 6-22 show the preliminary results of the predictive model developed by Babaee (2017) compared to the experimental data measured in this study.
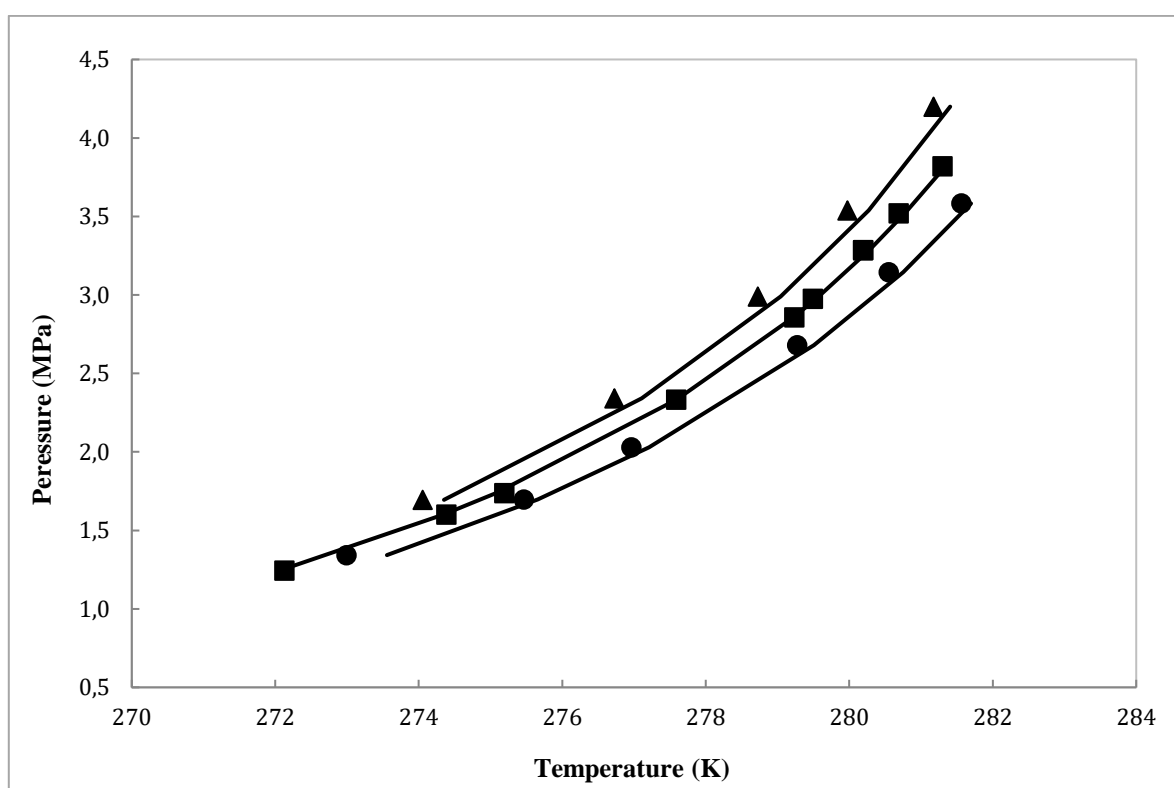
Figure 6-21: Carbon dioxide hydrate dissociation conditions in the presence of pure aqueous solutions (experimental and thermodynamic modeling) (●) Pure water experimental data, this study; (■) 5 wt % Na₂SO₄ experimental data, this study; (▲) 5 wt % KCl experimental data, this study; (—) predictive model developed by Babaee (2017).
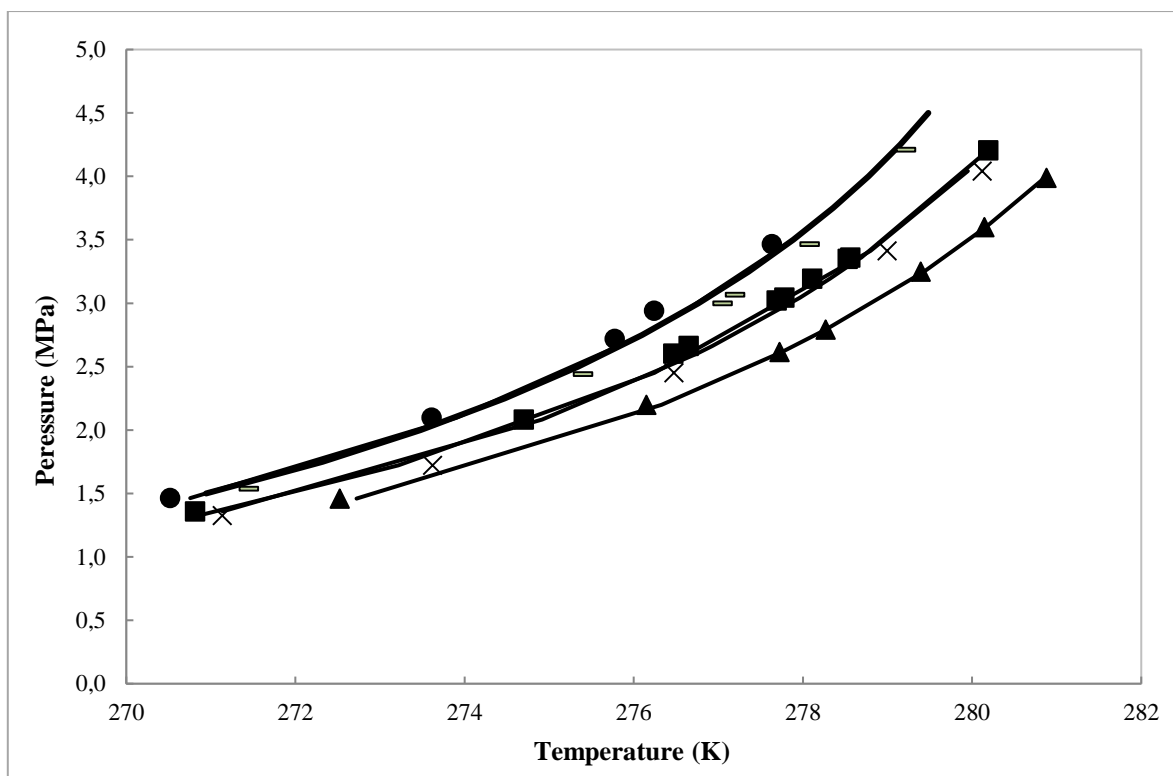
Figure 6-22: Carbon dioxide hydrate dissociation conditions in the presence of mixed salt and alcohol aqueous solutions (experimental and thermodynamic modeling) (●) 5 wt % NaCl + 5 wt % KCl experimental data, this study; (■) 5 wt % KCl + 5 wt % Na$_2$SO$_4$ experimental data, this study; (▲) Mixed salt A experimental data, this study; (x) Mixed salt B experimental data, this study; (-) Synthesised vinasse experimental data, this study; (—) predictive model developed by Babaee (2017).

From Figures 6-21 and 6-22 it can be seen that compared to the measured data the model predicts dissociation conditions well. From Figure 6-22 it can also be seen that as the concentration of the inhibitors increase, the model deviates from the experimental data.

The preliminary results of the predictive model being developed by Babaee (2017) demonstrate that once the model has been complete, it will be able to accurately predict the dissociation conditions for systems containing salts and organic inhibitors, such as vinasse.

PART 2: Gas Hydrate Separation Technology: Plant design and economic evaluation

6.8 Plant design

During the formation of gas hydrates, it is assumed that only water and the former take part in the solid ice like structure. The fundamental operating principle of a process for removing water from an aqueous solution, such as desalination of industrial wastewater, is therefore the formation of gas hydrates followed by the separation of the solid particles from the concentrate. The unit operations that comprise a hydrate-based separation technology are reviewed below.

6.8.1 Basic unit operations

A basic hydrate separation process consists of four main stages. The first stage involves hydrate nucleation and growth, which leads to the formation of gas hydrates. Depending on the hydrate former selected for use, this reaction may either be a homogenous crystallization from a miscible former, or a multiphase reaction involving the aqueous solution, solid hydrate, and one or more hydrate former phases. The second stage involves the separation of the concentrated fluid from the solid hydrate phase. Due to poor crystal growth, in both size and geometry, this stage is considered the bottleneck of hydrate-based separation processes (Werezak, 1969). Various separation techniques such as filtration and centrifugation are available for use in this stage. Filtration cannot successfully remove the major portion of hydrate crystals, which results in the requirement of extensive washing. Centrifugation appears to be the most promising separation method, however a small amount of crystal washing may be necessary (Huang et al., 1965; Werezak, 1969). With regards to the washing process, small crystal sizes require larger quantities of fresh water, which result in a lower yield for the desalination process, while larger crystal sizes require less fresh water and produce higher yields. The ideal crystal size is in excess of 400 μm in diameter (McCormack and Andersen, 1995). Circone et al. (2003) reported a CO_2 hydrate crystal size of 50 - 300 μm and Klapp et al. (2010) reported that the crystallite sizes of natural gas hydrates are in the range of 200 - 400 μm. In the third stage, the hydrate crystals are dissociated to produce a water-former mixture. Either increasing the temperature or reducing the pressure achieves this. The final stage involves the recycling of the hydrate former. Despite the recycle of the former gas, a small amount of make-up gas may be required. The major unit operations of a hydrate separation process are therefore: a reactor or hydrator, a separator, a decomposer, and a recycle system. This is shown in block form in Figure 6-23.
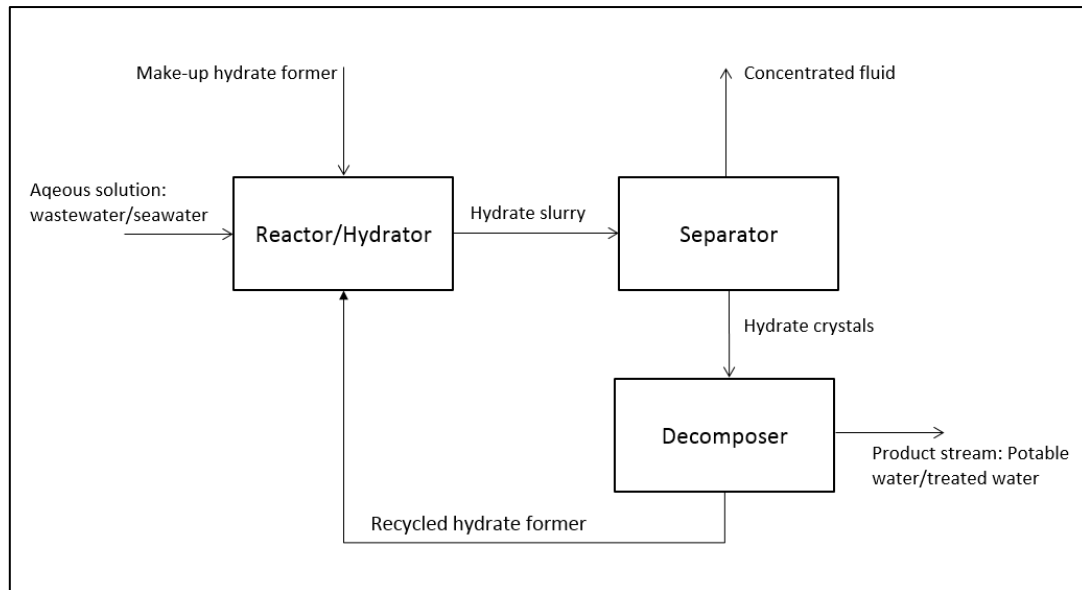
Figure 6-23: Hydrate separation process diagram (adapted from Werezak, 1969 and Bradshaw et al., 2008).

6.8.2 The proposed process for the treatment of vinasse

Based on the available scientific information on hydrate technology for desalination of industrial wastewater/seawater in literature (McCormack and Andersen, 1995; Javanmardi and Moshfeghian, 2003; Bradshaw et al., 2008; Park et al., 2011; Kang et al., 2014) the author proposes a process for the treatment of vinasse through hydrate technology as shown in Figure 6-24. The separation scheme is based on the proposal by Javanmardi and Moshfeghian (2003) for the desalination of seawater, which was first proposed by Knox et al. (1961). The process includes the 4 main stages as outlined in section 6.8.1.

Since the characteristics of vinasse are so complex and require extensive treatment, it was assumed that the vinasse being treated and concentrated by hydrate technology would first undergo several pre-treatment steps. These steps would include: filtration to remove any suspended solids, anaerobic treatment for the reduction of BOD and COD,aerobic treatment for further reduction of COD, reduction of the characteristic dark brown colour, and finally, hydrate-based separation for the removal of salts and other dissolved impurities. As already stated, it is assumed that only pure water and the former gas take part in the formation of hydrate crystals. The final products of the hydrate-based desalination step are therefore a concentrated brine stream with the majority of the dissolved salts present and a potable water stream.

The potable water produced can be used in various areas of the overall sugar production process. Based on the final composition of the potable water, it could potentially be used for irrigation purposes or disposed of safely in the ocean. Treating and/or disposing of the concentrated brine also needs to be considered. One option would be to combine it with pressmud in a predetermined ratio for the production of biomanure for use in the agriculture section. Pressmud is a by-product of the sugar production process. The reader is referred to the work of Smith (2015) for an overview of the South African sugar milling process. Nandy et al. (2002) reported the application of wastewater management techniques adopted in a combined distillery and sugar mill plant that involved the recovery of bio resource. The authors presented data for the full-scale implementation of a system, which uses biomethanation to recover biogas. The waste management options involved the use of plant nutrient rich pressmud with the anaerobically treated vinasse in a ratio of 2:1 (2 m^3 of concentrated post-anaerobic vinasse and 1 tonne of pressmud) for the production of biomanure. This waste management option contributed to the combined distillery and sugar mill plant achieving very low effluent discharges (no final figure was reported). Since the vinasse in this study has undergone an additional treatment (gas hydrate based) the composition of the concentrated brine would differ from the anaerobically treated vinasse and an investigation into the acceptable concentrated brine to pressmud ratio would be required. An important aspect to consider with the production of biomanure is that sugarcane manufacturing is a seasonal operation and pressmud availability is often a constraint. Alternative materials can however be considered such as rice husk, wood chips and bagasse (Satyawali and Balakrishnan, 2008).

Various researches have reported that irrigation with distillery effluent increased crop yield, dry matter, leaf area, and total chlorophyll (Pathak et al., 1999; Ramana et al., 2002; Mahimairaja, 2004). Anaerobically treated vinasse still contains considerable plant nutrients in terms of potassium, sulphur, nitrogen, and phosphorus, and large amounts of micronutrients such as calcium, copper, magnesium, and zinc. Since only water and the former take part in the formation of hydrates, the produced brine from gas hydrate treatment would still contain these elements but in more concentrated levels. Therefore, post gas hydrate treated vinasse could be used for irrigation purposes as a liquid fertilizer in controlled doses.

Even though the disposal of potable water and the further treatment of the concentrated brine was studied, only the hydrate-based desalination treatment step, was further investigated in this study.

As shown in Figure 6-24, the treated vinasse, free from suspended solids, BOD, and COD is cooled in heat exchanger I and II by exchanging heat with the cooler concentrated brine and potable water streams before it is sent to the hydrate reactor. Under suitable conditions of temperature and pressure, and with the addition of the selected hydrate former (CO_2), hydrate crystals are formed. The hydrate

slurry that was produced in the reactor, which consists of approximately 25 % by weight ice crystals and 75 % brine water of increased salinity, is sent to a separator where it is filtered and divided into two streams: the concentrated brine (75 %) and hydrate crystals (25 %). The concentrated brine stream, after exchanging heat with the vinasse in heat exchanger I, and potable water in heat exchanger III, is removed from the process. The hydrate crystals are transported to the decomposer where they are dissociated to produce potable water and CO_2. The produced CO_2 is recycled back to the reactor for reuse in the formation of hydrate crystals. The potable water is removed from the process in the same manner as the concentrated brine after exchanging heat in heat exchanger II and III. Excess CO_2 is continuously circulated and used as a refrigerant to provide the cooling duty required for hydrate formation in the hydrate reactor. Thereafter the excess CO_2 is compressed, which raises its temperature. The CO_2 is then sent to the decomposer where it dissociates the hydrate crystals. This CO_2 is circulated back to the hydrate reactor. In the proposed process, the hydrate former therefore has two roles: to take part in the hydrate structure and to act as a direct heat exchange agent. A conceptual design of the proposed process was performed using the process-simulation and modelling tool Aspen Plus®. The design is discussed in detail in the next section.
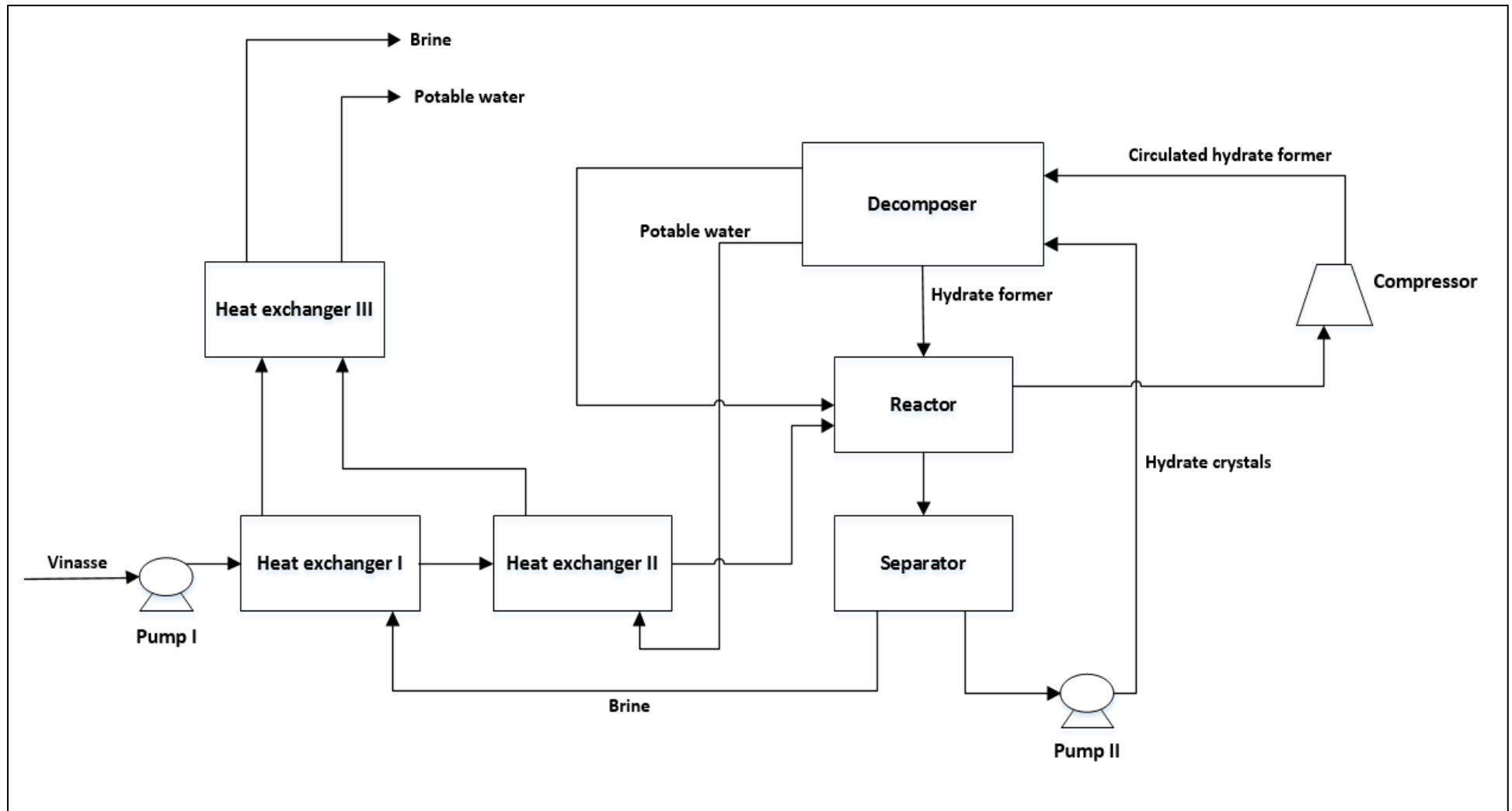
Figure 6-24: Flow sheet for the proposed desalination process for the treatment of vinasse (based on the process proposed by Knox et al., 1961 and Javanmardi and Moshfeghian, 2003).

6.8.3 The conceptual design

From the systems investigated in this study, it can be seen that the system that exhibits the greatest temperature shift from the CO_2 (1) + water (2) system is CO_2 (1) + water (2) + 5 wt % NaCl (3) + 5 wt % KCl (4) (Figure 6-11). The conceptual design was therefore based on the conditions of this system. This ensured that the design accounted for the worst-case scenario. The conceptual design was performed using the process modelling tool Aspen Plus® in conjunction with a mass balance performed over the proposed process. In the work of Javanmardi and Moshfeghian (2003), two cases were investigated. In both cases, propane was used as the hydrate former, however, in *Case A* it was a assumed that a yield of 20 % was achieved and the feed to the system was seawater that contained only NaCl with a molality equal to 1.2 (gmol/1000g solvent). In *Case B*, a 30 % yield was assumed and the feed to the system was seawater that contained only NaCl and $CaCl_2$ with molalities equal to 1 and 0.5 respectively (gmol/1000g solvent). In their study, Javanmardi and Moshfeghian (2003) prepared a computer program for the simulation of the proposed process.

6.8.3.1 Mass balance

A basis of 1000 tons of potable water produced per day was chosen for the design. This was chosen for better comparison of the results for the process proposed in this study to the hydrate-based desalination process proposed by Javanmardi and Moshfeghian (2003), who also selected a basis of 1000 ton/day. In addition Park et al. (1997) conducted an economic analysis of various desalination plants which made use of established desalination processes such as MSF, MED and RO. The selected 1000 ton basis allowed for direct comparison of the results obtained in this study to the results presented by Park et al. (1997).

The removal efficiency of a hydrate-based desalination plant depends on the ionic radius and strength of the positive ionic charge of the minerals present in the feed: the stronger the charge of the ion present in the feed, the lower the removal efficiency; similarly, the greater the radius of the ion present in the feed, the greater the removal efficiency (Park et al., 2011). Park et al. (2011) found that in a single-stage hydrate process, between 72 and 80 % of each dissolved mineral present in the feed stream ended up in the concentrated brine product. Based on an iterative process and the findings by Park et al. (2011), it was assumed that 80 % of the salts present in the vinasse would end up in the brine. No removal efficiency was reported in the work of Javanmardi and Moshfeghian (2003).

Javanmardi and Moshfeghian (2003) defined yield as the quantity (mass or moles) of potable water produced per quantity of vinasse fed to the process. Javanmardi and Moshfeghian (2003) investigated

the effect of yield on economic parameters. Their results indicated that increasing the yield would decrease the total energy consumption and the total product cost. Their calculations covered a yield range from 5 to 35 %. When performing the analysis for the desalination costs, Javanmardi and Moshfeghian (2003) selected a yield of 30 %. As a result, the same 30 % yield was selected for the design of the proposed process in this study.

McCormack and Andersen (1995) presented a report on the preliminary research, design, and cost estimates for a hydrate-based desalination plant. The hydrate formers considered in their study was CO_2 and R141b. Based on the molecular weights of the CO_2 hydrate and pure CO_2, the authors found that 0.264 kg's CO_2 was required per litre of potable water produced. The same ratio was used in this study to determine the amount of CO_2 required to produce the chosen amount of potable water. Due to the design of the proposed process, a continuous recycle of excess CO_2 is required in addition to the amount of CO_2 required for hydrate formation. In order to ensure that the required amount of CO_2 for hydrate formation was always available, an excess amount of 200 % was selected. In most cases, the optimum amount of excess to use involves an economic trade-off between some beneficial effect and the cost of recovering and recycling the excess. According to Douglas (1988), there are unfortunately no suitable rules of thumb available to make a reasonable guess of the optimum amount of excess, and the economic analysis should be carried out in terms of this additional design variable. Carbon dioxide is a by-product from the production of bioethanol. It was therefore assumed that CO_2 would be readily available and, as a result, its cost was taken to be zero. The value of 200 % excess was obtained through a trial-and-error process during the simulation in Aspen Plus® of the proposed process.

Based on the above assumptions, the mass balance was performed. A detailed calculation procedure of the mass balance is presented in Appendix F.1. A summary of the design parameters discussed above is presented in Table 6-21.

Table 6-21: Operational conditions and design parameters used in performing the mass balance for the proposed process.

Composition of "*vinasse*"	5 wt % NaCl; 5 wt % KCl; 90 wt % H_2O
Potable water produced [a]	1000 tons/day
Percentage of salts originally in feed present in brine [b]	80%
Yield [a]	30%
CO_2 required / litre of potable water [c]	0.264 kg/litre of potable water

[a] based on the results of the research conducted by Javanmardi and Moshfeghian (2003)

[b] based on the results of the research conducted by Park et al. (2011)

[c] based on the results of the research conducted by McCormack and Andersen (1995)

6.8.3.2 Aspen Plus® simulation

The design parameters and operating conditions used in the Aspen Plus® simulation of the proposed process are presented in Table 6-22 and discussed in detail below.

Table 6-22: Operational conditions and design parameters used in the simulation of the proposed process.

Conditions of vinasse feed	298.15 K and 1 atm.
Reactor temperature	276.15 K
Reactor Pressure	3 MPa
Decomposer discharge pressure	4.5 MPa
Compressor efficiency	80 % (isentropic)

The upper quadruple point of a particular former, i.e. the intersection of the hydrate formation and the condensation curves, is the highest temperature at which a pure gaseous hydrate former can form hydrates. Therefore in order to operate at the highest possible temperature, thus minimizing the energy consumption, the most feasible conditions for the hydrate reactor and the decomposer is near the quadruple point. The quadruple point of CO_2 is 283.05 K and 4.757 MPa (Sloan and Koh, 2008). In addition the reactor must operate on the left-hand side of the hydrate equilibrium curve and the decomposer must operate on the right-hand side of the hydrate equilibrium curve. The typical phase diagram of a gaseous hydrate former such as CO_2 and the hydrate and condensation curves for CO_2 is shown in Figure 6-25 and Figure 6-26 respectively. Based on the above-mentioned statements and the measured hydrate dissociation conditions for the CO_2 (1) + water (2) + 5 wt % NaCl (3) + 5 wt % KCl (4) system, the selected hydrate reactor operating conditions were 276.15 K and 3 MPa. The decomposer pressure was selected to be 4.5 MPa. Based on the differences in quadruple point pressures for propane and carbon dioxide (562.07 kPa and 4757.06 kPa respectively), Javanmardi and Moshfeghian (2003) selected a reactor and decomposer pressure of 0.45 MPa and 0.65 MPa respectively for propane.

The kinetic data/information is required when simulating a reactor on Aspen Plus®. The kinetics of gas hydrate forming systems is not readily available in the open literature. A mixer, a cooler, and a separator were therefore used to simulate the reactor in Aspen Plus®. The cooled vinasse stream and a stream containing the total CO_2 (required and excess) were mixed and cooled to the desired temperature of 276.15 K (at the required pressure). Thereafter, the hydrate slurry was separated from the unreacted CO_2 (continuously circulated CO_2) and sent to the separator shown in Figure 6-24. The details of the simulation of the reactor was not discussed in the article of Javanmardi and Moshfeghian (2003).
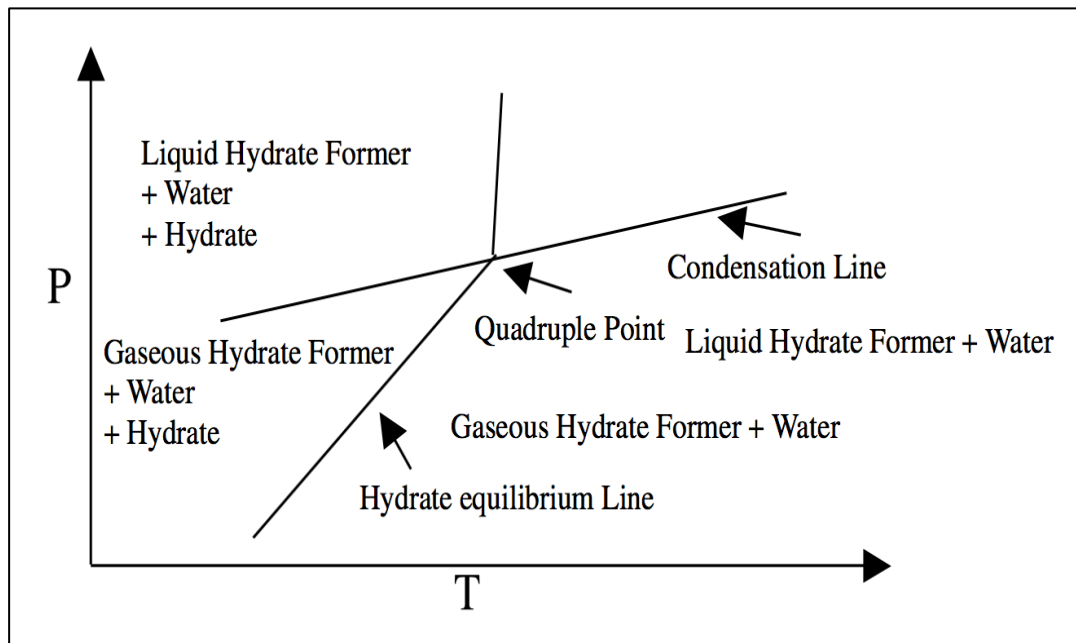
Figure 6-25: Typical phase diagram of a gaseous hydrate former (Javanmardi and Moshfeghian, 2003).
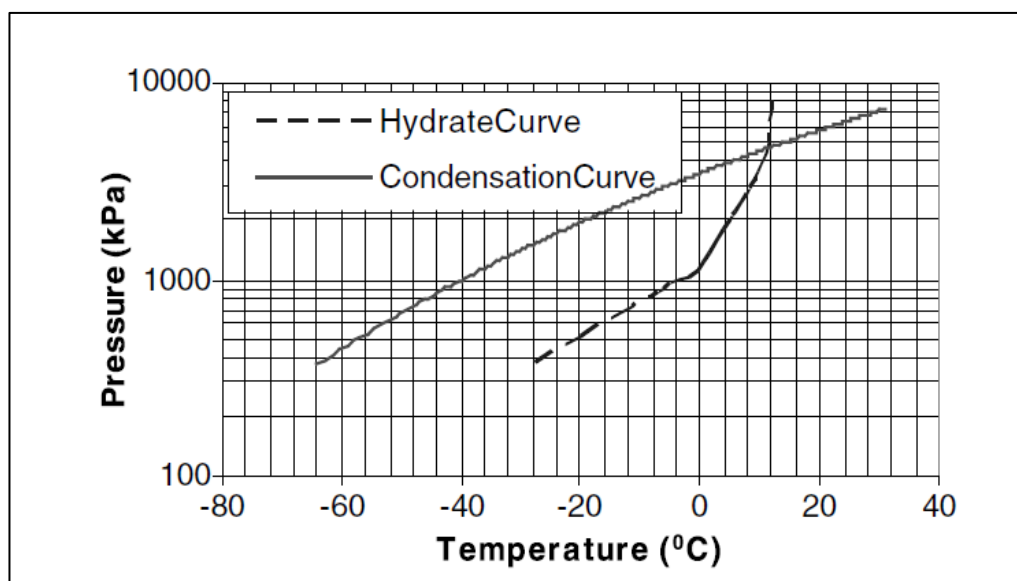
Figure 6-26: Hydrate and condensation curves for CO_2 (Javanmardi and Moshfeghian, 2003).

Since the design of the proposed process required a continuous circulation of CO_2, a dynamic compressor was selected for use opposed to a positive displacement compressor. There are two classifications of dynamic compressors: axial flow and centrifugal. Axial flow compressors are used mainly as compressors for gas turbines. Due to the nature of the proposed industrial process a centrifugal compressor was selected. In order to simulate the compressor in the conceptual design of the process, an isentropic efficiency of 80 % was selected. Typical isentropic efficiencies range from

70 - 90 %. A centrifugal compressor with an efficiency of 80 % was also used by Javanmardi and Moshfeghian (2003).

Due to the temperature sensitive nature of gas hydrates, it was assumed that the temperature of the hydrate slurry from the reactor, the separator, and the exit streams from the separator were all maintained at the temperature and pressure conditions of the reactor (276.15 K and 3 MPa). This was to ensure that premature dissociation of the hydrate crystals does not occur.

Gas hydrates can dissociate through an increase in temperature or a decrease in pressure. In this proposed study, as in the process proposed by Javanmardi and Moshfeghian (2003), the hydrates are dissociated via an increase in temperature. The continuously circulated CO_2 provides the heat in which to do so. The decomposer therefore, in essence, behaves like a heat exchanger and was designed as one in Aspen Plus®. In the simulation on Aspen Plus®, a splitter was placed after the decomposer on the dissociated hydrate stream in order to separate the potable water from the hydrate former. As in the work of Javanmardi and Moshfeghian (2003), all heat exchangers were designed as counter-current shell and tube exchangers with a maximum hot/cold approach temperature of 6 ℃.
The assumptions made in this study were, for the large part, based on the assumptions put forward by Javanmardi and Moshfeghian (2003). This was to ensure reliable comparison between the results of the two studies. The details of the computer program used by Javanmardi and Moshfeghian (2003) for the simulation of their proposed process was not discussed in detail in their article. Therefore, further assumptions for the simulation of the reactor and the placement of various supplementary units, such as splitters, had to be made. In the proposed process by Javanmardi and Moshfeghian (2003) (Figure 2-7), a heat exchanger was placed after the decomposer. The benefits of placing a heat exchanger after the decomposer in the simulation of the proposed process in this study were negligible and thus omitted. For simplicity, Heat Exchanger I (Figure 2-7) in the process proposed by Javanmardi and Moshfeghian (2003) was simulated on Aspen Plus® as two heat exchangers.
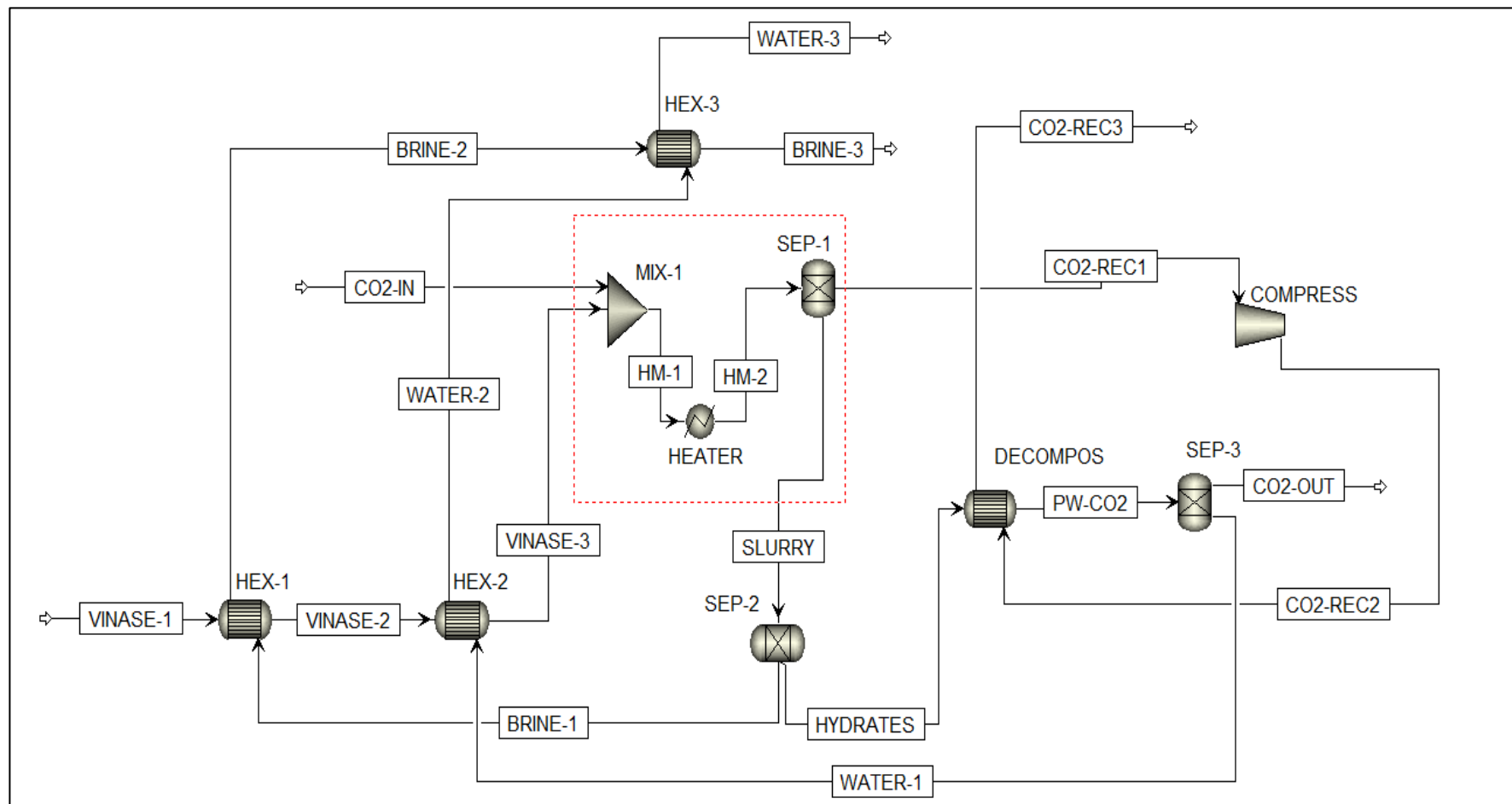
Figure 6-27: Flow diagram from the Aspen Plus® simulation performed in this study, for the proposed process. The - - - - square around MIX-1, SEP-1, and HEATER units represent the units that were used to model the reactor.

Table 6-23: Key for Figure 6-27

Stream name	Stream description	Unit name	Unit description
VINASE-1	Feed stream	HEX-1	Heat exchanger 1
VINASE-2	Cooled vinasse from heat exchanger 1	HEX-2	Heat exchanger 2
VINASE-3	Cooled vinasse from heat exchanger 2	HEX-3	Heat exchanger 3
CO2-IN	Inlet CO_2	SEP-1	Separator 1
HM-1	Vinasse and CO_2 mixed stream to reactor	SEP-2	Separator 2
HM-2	Vinasse and CO_2 mixed stream from reactor	SEP-3	Separator 3
SLURRY	Hydrate slurry consisting of hydrate crystals and brine	DECOMPOS	Decomposer
BRINE-1	Concentrated brine separated from hydrate slurry	COMPRESS	Compressor
BRINE-2	Heated concentrated brine from heat exchanger 1	MIX-1	Mixer
BRINE-3	Final brine product	HEATER	Heater
HYDRATES	Hydrate crystals that were separated from hydrate slurry	Dashed box	The dashed box around MIX-1, SEP-1, and
PW-CO2	Decomposed hydrate crystals		HEATER represents the hydrate reactor
CO2-OUT	Recovered CO_2 after dissociation gas hydrates		
CO2-REC1	Recycled CO_2		
CO2-REC2	Recycled CO_2		
CO2-REC3	Recycled CO_2		
WATER-1	Recovered potable water		
WATER-2	Heated potable water from heat exchanger 2		
WATER-3	Final potable water stream		

The results of the design were used in performing the economic evaluation, which is discussed in the following section. The results of the Aspen Plus® simulation (including mass balance), together with the Aspen Plus® flow diagram of the proposed process are reported in Appendix F.2.

6.9 Economic evaluation

There are numerous costs required to build and operate an industrial plant. Some of the costs associated add to the capital investment, whereas others add to the operating expenses. Fortunately, most of the costs can be related directly to the installed equipment costs through the use of various factors. Peters and Timmerhaus (1968) prepared a concise summary of the costs involved. Douglas (1988) presented a modified version of their summary for the total capital investment.

The shortcut method put forward by Douglas (1988) was used to perform the economic evaluation of the proposed process. The shortcut method involves determining the total installed cost of equipment in order to estimate the total investment. The total installed cost of equipment is determined by using correlations proposed by Guthrie (1969), which are based on information of the purchase cost and the installed cost of various pieces of process equipment. These correlations provide much more information than other cost correlations such as the correlations of Happel and Jordan (1975), despite them being as simple to use as other procedures. One of the advantages of using the correlations of Guthrie (1969) is that if a breakdown of the total cost for piping or instrumentation for all process units in the proposed process for this study is required, the information could be developed on a consistent basis. The shortcut method of Douglas (1988) with the correlations of Guthrie (1969) is used for a preliminary estimate of the total capital costs with an error of 15-25 %.

This method is the same method that was used by Javanmardi and Moshfeghian (2003) to perform the economic evaluation of their proposed hydrate-based seawater desalination process. This method was used later by Javanmardi et al. (2005) to perform an economic evaluation of using natural gas hydrates as a natural gas transportation alternative. For a natural gas hydrate (NGH) production process, Javanmardi et al. (2005) reported a total capital investment of 236 MM$ (million) would be required for a plant capacity of 2.83 x 10^6 Std m³/day. The authors compared this to a literature value; for the same process, plant capacity, and operating parameters, of 217 MM$ which had been reported by Chang (2001). This result showed that the calculated capital investment was in good agreement with literature data. In addition, it could be concluded that the calculation method used to perform the economic evaluation of the process proposed by Javanmardi et al. (2005) for the production of natural gas hydrate was acceptable. For this reason, the short cut method put forward by Douglas (1988) in

combination with the correlations proposed by Guthrie (1696) was concluded to be acceptable for use in this study. In addition, for accurate comparison of the cost for the process proposed in this study (where CO_2 was used as the hydrate former) to the cost of the hydrate-based seawater desalination process proposed by Javanmardi and Moshfeghian (2003) (in which propane was used as the former) the same method for the economic evaluation needed to be followed.

There are very few researchers who have conducted an economic evaluation of hydrate-based seawater desalination plants in a benchmark or even a full-scale capacity. In fact, apart from the economic evaluation performed by Javanmardi and Moshfeghian (2003), the only cost analysis for a desalination plant was performed in the work of McCormack and Andersen (1995) in which they presented a report on the preliminary research, design, and cost estimates for a hydrate-based desalination plant. The work of McCormack and Andersen (1995) has already been introduced to the reader in section 2.5.5. The design of the plant was configured such that the hydrate former was injected through an inner pipe of a submerged pipeline to a predetermined ocean depth at which the ocean temperature is less than the hydrate forming temperatures. The hydrate former than combines with seawater within the annulus of the outer pipe to form slurry of hydrate crystals and brine that is pumped to the surface. The hydrate crystals are separated from the brine, washed, and melted; and the remaining water is separated from the hydrate former. In their cost analysis, McCormack and Andersen (1995) priced each equipment item for the 13600 M^3/Day commercial plant, as well as the freight and installation cost for each equipment item, through vendor quotes and educated estimates. Due to the size of the plant, the differences in plant configuration and the fact that the hydrate crystals were formed at ocean depth, the author of this research decided against using the cost analysis procedure used by McCormack and Andersen (1995).

The cost of equipment and utilities could have been obtained from the Aspen Plus® simulation, however the manner in which the reactor was simulated and the placement of a splitter after the decomposer would have added to the overall cost, giving inconsistent results. The procedure for the economic evaluation is discussed in detail in the following sections.

6.9.1 Total capital investment

According to Douglas (1988), the total capital investment (Tot. Inv.) is obtained from the following expression:

$$Tot.Inv. = 2.36\,(Onsite) \qquad (6\text{-}2)$$

The onsite costs correspond to the total sum of the installed equipment costs for the heat exchangers, compressor, decomposer, and reactor shown in Figure 6-24. These onsite costs can be estimated directly from Guthrie's correlations (Guthrie, 1969).

The installed cost of the gas compressor was estimated by the following Guthrie correlation (Guthrie, 1969):

$$Installed\ cost, \$ = \left(\frac{M\&S}{280}\right)(517.5)(bhp)^{0.82}(2.11 + F_c) \qquad (6\text{-}3)$$

In the above equation, $M\&S$ is the Marshall and Swift cost index, which is used for updating the cost correlation. The author used a value of 1501.35 for 2012. This was the most recent value the author could find in open literature. The variable bhp is the brake horsepower. The parameter F_c depends on the compressor design type. If the bhp is between 30 and 10000 kW then $F_c = F_d$

The installed cost of the heat exchangers was estimated by the following Guthrie correlation (Guthrie, 1969):

$$Installed\ cost, \$ = \left(\frac{M\&S}{280}\right)(101.3)(A)^{0.65}\left(2.29 + \left((F_d + F_p)F_m\right)\right) \qquad (6\text{-}4)$$

In this equation, A, is the heat exchanger area in ft^2. The parameter F_d depends on the heat exchanger design type, F_p depends on the design pressure, and F_m depends on the material of construction of the heat exchangers.

The heat of formation should be removed in the hydrate reactor (Javanmardi et al., 2005). The reactor therefore behaves as a heat exchanger. In addition, an increase in temperature is used to decompose the hydrate crystals. The decomposer therefore also behaves like a heat exchanger. Equation (6-4) is therefore used to estimate the installed costs of the hydrate reactor and the decomposer.

6.9.2 Operation and maintenance cost

In order to estimate the operational and maintenance (O&M) costs, the following equation proposed by Douglas (1988) was used:

$$O\&M = 1.031(Raw\ matl. + Util.) + 0.186(Onsite) + 2.13(Operating\ labour) \quad (6\text{-}5)$$
$$+ 0.0256(Revenue)$$

In the above equation, *Raw matl.*, is the cost of raw materials and *Util.* is the cost of utilities. Since the proposed process in this study is for the treatment of industrial wastewater and due to the fact that the former proposed for this study is available as a by-product from the production of bioethanol, the cost of raw materials was taken to be zero. It was assumed that the hydrate-based treatment of vinasse would occur on the same site as a combined sugar mill and bioethanol distillery. Since burning bagasse provides for all the fuel requirements on a sugar mill, the utility component was also taken to equal zero. The onsite costs are given in the previous section. The required "man-hour/day-processing step" can be estimated from the following equation (Peters and Timmerhaus, 1968):

$$Operating\ labour = \exp(2.791 + 0.234\ln(capacity)) \quad (6\text{-}6)$$

In equation (6-6) the capacity is in tons of feed (vinasse) to the reactor per day.

It is assumed that for the suggested process shown in Figure 6-24, one processing step is required (Wessel, 1952). Based on four operational shifts per day and eight hours operation per day for each shift, dividing equation (6-6) by six yields the required number of employees per day (Javanmardi and Moshfeghian, 2003). Since the proposed process is for a treatment facility, the revenue for potable water was taken as zero. No revenue assumptions were stated by Javanmardi and Moshfeghian (2003).

Substituting the above parameters in equation (6-5), yield the O&M cost in US dollars ($) per day. The onsite costs obtained previously must be divided by the plant useful life before substituting into equation (6-5) (Javanmardi and Moshfeghian, 2003).

The reader is referred to Appendix F.3 for a list of assumptions made by Douglas (1988) in deriving equation (6-2) and equation (6-5).

6.9.3 Amortized total capital investment

Assuming a plant useful life of 20 years and a continuous discount rate, *i,* equal to 8 %, the amortized total capital investment is obtained by:

$$Amortized\ tot.inv. = \frac{\left(\frac{\exp(0.08 \times 20)}{\sum_{i=0}^{19} \exp(0.08 \times i)}\right)}{365 \times capacity} \times Tot.inv. \tag{6-7}$$

The above parameter is in $ per ton. The plant useful life of 20 years has been chosen by many investigators such as Park et al. (1997) for MSF, MED and RO processes and by Javanmardi and Moshfeghian (2003) for hydrate-based desalination. Better comparison of the economic parameters of the proposed process in this study is attained when using the same economic life and discount rate. Capacity is in tons of feed (vinasse) to the reactor per day.

6.9.4 Amortized O&M costs

Since the O&M costs obtained in the previous section is in $ per day, the amortized O&M costs are obtained in $ per ton by using the following equation:

$$Amortized\ O\&M = \frac{O\&M}{Capacity} \tag{6-8}$$

As in equation (6-8), capacity is the tons of feed (vinasse) to the reactor per day.

6.9.5 Total product cost

The total cost, based on the amount of feed to the reactor, to produce a ton of potable water is the summation of the amortized costs:

$$Total\ product\ cost = Amortized\ tot.inv. + Amortized\ O\&M \tag{6-9}$$

The reader is referred to Appendix F.4 for the parameters used in equations (6-3) and (6-4) and Appendix F.5 for the detailed calculation procedure for the proposed process.

6.9.6 The hydrate separation process cost analysis

As stated above, the economic evaluation of the proposed process was based on a potable water production rate of 1000 ton/day. This value was chosen, as it would allow for cost comparison to other desalination processes, including a hydrate-based process. The results for the economic evaluation preformed in this study are shown in Table 6-24, along with the results from the economic analysis of traditional desalination processes performed by Park et al. (1997) and the results of the economic evaluation of the hydrate-based desalination processes proposed by Javanmardi and Moshfeghian (2003). For accurate comparison, all costs must be evaluated based on the same year. For this purpose, the economic indicators for 2012 were selected, as this was the same year of the M&S index used to assess the economic evaluation for the proposed process in this study. All costs were converted using the following relationship:

$$Present\ cost = original\ cost \left(\frac{index\ value\ for\ present\ year}{index\ value\ at\ time\ original\ cost\ was\ obtained}\right) \quad\quad (6\text{-}10)$$

The cost data, shown in Table 6-24, for each plant includes the total capital investment, the O&M cost, the amortized capital investment, the amortized or unit O&M cost, the total product cost for the year in which the particular study was conducted, as well as the present day (2012) total product cost. Park et al. (1997) reported the results based on 1990 prices. Javanmardi and Moshfeghian (2003) did not report what year the results of the study was based on. However, since Javanmardi and Moshfeghian (2003) compared the results of their study to the results of the study conducted by Park et al. (1997), it was assumed that they also based their evaluation on 1990 prices. As a result, the results reported by Park et al. (1997) and Javanmardi and Moshfeghian (2003) were converted from 1990 prices to 2012 prices using equation (6-10). The 2012 total product cost for the process proposed in this study was calculated to be $ 6.09/ton. This total product cost was compared to other processes and discussed below.

Table 6-24: Results of economic evaluation and cost comparison performed in this study.

Process	Total cap.inv. (M$)	O&M (M$)	Amortized tot.cap. Inv. ($/ton)	Amortized O&M ($/ton)	1990 Total product cost ($/ton)	2012 Total product cost ($/ton)
MSF [a]	2.67	0.66	0.75	1.81	2.56	5.17
MSF [a]	2.33	6.16	0.65	1.72	2.37	4.78
MSF [a]	2.93	7.15	0.82	2.00	2.82	5.69
MED [a]	2.26	6.28	0.63	1.75	2.38	4.80
MED [a]	2.62	7.78	0.73	2.17	2.90	5.85
RO [a]	2.30	1.18	0.64	3.23	3.87	7.81
RO [a]	2.31	0.53	0.65	0.19	0.84	1.70
RO [a]	1.97	0.51	0.55	0.19	0.74	1.49
Gas hydrates – Case A [b]	7.18	NR	2.05	2.17	4.23	7.35
Gas hydrates – Case B [b]	5.46	NR	1.56	1.20	2.76	4.80
This study [c]	4.71	0.02	0.40	5.64		**6.09**

Ref: [a] Park et al. (1997), [b] Javanmardi and Moshfeghian (2003), [c] based on cost in year 2102.

NR: not reported

Case A: Propane former, 20 % yield, feed contained only NaCl with molality equal to 1.2 (gmol/1000g solvent)

Case B: Propane former, 30 % yield, feed contained NaCl and $CaCl_2$ with molality equal to 1.0 and 0.5 respectively (gmol/1000g solvent).

Cost comparison to process proposed by Javanmardi and Moshfeghian (2003):

The total product cost obtained in this study was lower than Case A (propane former and 20 % yield) and higher than Case B (propane former and 30 % yield) for the process proposed by Javanmardi and Moshfeghian (2003).

In order to minimize the energy consumption of a hydrate-based process, the hydrate former should have condensation and hydrate equilibrium curves with the following specification:

- The upper quadruple point should be characterised by low pressure or high temperature.
- A considerable heat of vaporization near the quadruple point i.e. the quadruple point of the desired hydrate former must be as far as possible from its critical point.

The quadruple and critical point pressures for propane are: 562.07 kPa and 4247.36 kPa, respectively. The corresponding values for CO_2 are: 4757.06 kPa and 7371.47 kPa, respectively (Javanmardi and Moshfeghian, 2003). As is evident from these values, the critical point pressure of propane is further from its corresponding quadruple point pressure compared to CO_2. Propane also forms hydrates at significantly lower pressure and higher temperature compared to CO_2. As a result, operating conditions of the reactor and decomposer are at more favourable conditions when propane is used as a hydrate former, which results in lower total capital investment and O&M costs, and, therefore a lower total product cost. As stated in section 6.8.3.1, Javanmardi and Moshfeghian (2003) investigated the effect of yield on economic parameters. Their results indicated that a higher yield would decrease the total energy consumption and the total product cost. This relationship can be seen from Figure 6-28. A yield of 30 % was used in this study and in Case B of the study conducted by Javanmardi and Moshfeghian (2003). Case A assumed a 20 % yield.
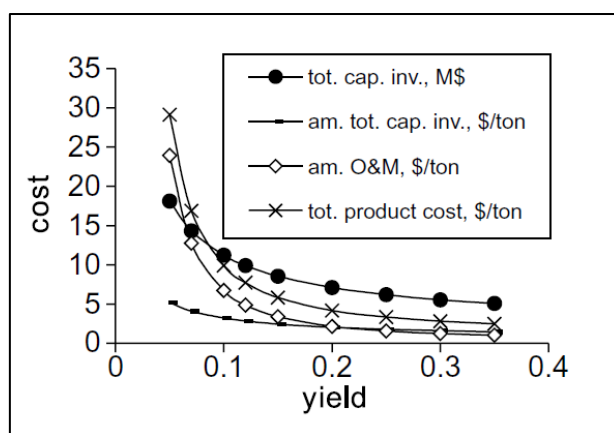
Figure 6-28: Effect of yield on economic parameters (Javanmardi and Moshfeghian, 2003).

The calculated total product cost is affected by the design method, operating conditions of the process, the utility requirements, and the revenue assumptions made. The difference in the total product cost of Case A compared to the process proposed in this study can be attributed to these factors. For the purpose of this process, it was assumed that all the utility requirements would be obtained from the plant itself (burning of bagasse) where Javanmardi and Moshfeghian (2003) assumed the electricity cost was approximately $0.04/kWh. In addition, based on the different operating conditions (summarized in Table 6-25) and method in which the design was conducted, the required power of the compressor and the area of the heat exchangers would differ. This would affect the total capital investment of the process and therefore the total product cost. The areas of the reactor, decomposer, and heat exchangers nor the bhp of the compressor was reported by Javanmardi and Moshfeghian (2003). However, based on the difference in operating conditions of the reactor, decomposer and compressor as well as the difference in yields between Case A, Case B, and this study, the lower product cost of the process proposed in this study compared to Case A (and therefore the higher product cost of Case B) is reasonable.

Table 6-25: Summary of operating conditions used in this study compared to those used by Javanmardi and Moshfeghian (2003).

Conditions	Case A and B	This study
Reactor pressure (MPa)	0.45	3.0
Decomposer pressure (MPa)	0.65	4.5
Discharge pressure of the compressor (MPa)	1.40	5.0

Cost comparison to traditional desalination processes – MSF, MED and RO:

The 2012 total product cost for this process is higher than the total product cost for MSF, MED and RO processes, except for one instance where the 2012 total product cost for a RO process was $ 7.81/ton. The biggest cost associated with the proposed process is the cost of the reactor, which affects the O&M cost. The cost is based on the correlation for a heat exchanger, which is directly dependent on the area of the heat exchanger. The large heat duty required as well as the high flow rates entering and leaving the "heat exchanger" resulted in a reactor area requirement of approximately 942 m^2 and a total reactor cost of $ 1 143 354,54. It should be noted that the total product cost of the processes reported in the article of Park et al. (1997) are for plants that are in operation and therefore the economic parameters, especially amortized O&M costs, have been optimized from the initial design. This, along with the shortcomings of the selected economic

evaluation procedure, describes the difference in cost between the proposed hydrate-based process and the traditional desalination technologies.

The proposed process is not economical under normal operating conditions, and is unable to compete with established and operational traditional desalination technologies. However, by using a suitable hydrate-forming promoter, the produced potable water total cost can drop significantly making the proposed process attractive. As already stated, a promoter increases the temperature at which a hydrate will form which would result in an increase in the required reactor temperature. A higher required reactor temperature would result in the requirement of less energy intense heat exchanger I and II (Figure 6-24). In addition, it would save the energy consumption of the compressor. Simply, the more the promoting effect of the promoter, the less the total cost of the process. Javanmardi and Moshfeghian (2003) investigated the effect of a promoter on economic parameters. In their investigation Javanmardi and Moshfeghian (2003) considered two cases. The first case assumed that the promoter increased only the reactor temperature and the second case assumed that the promoter takes part in the hydrate lattice and increases the decomposer temperature as well. For the first assumed case (promoter increased only the reactor temperature) and using the processing conditions of Case B (Table 6-23), Javanmardi and Moshfeghian (2003) found that with a 6 degree elevation in temperature, the potable water cost dropped from 2.76 $/ton to approximately 2.4 $/ton. This can be seen in Figure 6-29.

The proposed process could also be made more economical by using an alternate hydrate former. This can be seen from comparing the results of the economic evaluation performed by Javanmardi and Moshfeghian (2003), in which propane was used as the hydrate former, to the economic evaluation performed in this study. It has been shown that the hydrate dissociation temperatures for the fluorinated former R410a and water system are close to ambient temperatures. Again, this would increase the required reactor temperature and reduce the energy requirements of the proposed process.
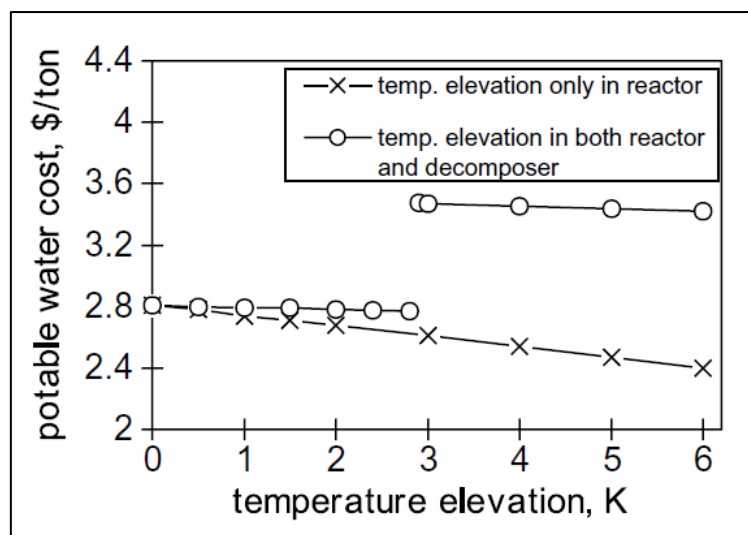
Figure 6-29: Effect of the hydrate formation temperature elevation in the presence of promoters, on economic parameters (Javanmardi and Moshfeghian, 2003).

Accurate kinetics is required for the successful design and costing of a reactor. The kinetics of hydrate forming systems is not readily available in open or closed literature. Investigating the kinetics and using the results in an efficient reactor design would improve the accuracy of the cost estimate and could potentially reduce the total capital investment, making the proposed process more attractive in comparison to traditional desalination technologies. In addition, mixing was not considered in the design of the proposed process nor the economic evaluation. Adequate mixing assists in the formation of gas hydrates. Mixing enhances the mass and heat transfer between the phases thus reducing the time required for hydrate formation. A reduction in the hydrate formation time would result in a more efficient and economical process. In a more detailed design of the proposed process different mixing configurations, such as a sparger or paddle mixer, should be investigated.

It is already known that a higher yield positively impacts the economic parameters associated with the proposed process (Figure 6-28). Innovative ways in which a higher yield can be obtained would significantly reduce the cost of the process, making it more attractive compared to traditional desalination technologies. In addition, further research into this technology, such as forming stable hydrates, must be fully investigated before accurate costing exercises may be covered in detail. The Thermodynamics Research Unit at the University of KwaZulu-Natal is already performing research of this nature in an alternate study, on a large-scale reactor.

The design and economic evaluation performed in this research was done on a conceptual level, which included many ideal assumptions. A detailed design and economic evaluation should be performed on the proposed process in order to obtain an accurate process cost.

7

CHAPTER SEVEN

CONCLUSIONS

The main objective of this study was to determine the possibility of using gas hydrate technology for the treatment of vinasse. Vinasse is the aqueous by-product generated during the production of bioethanol. Various feedstocks can be used for the production of bioethanol. This study concentrated on the vinasse derived from using sugarcane molasses to produce bioethanol.

An extensive literature review was conducted on vinasse, which included the generation of vinasse, the characteristics of vinasse, and the various contributing factors affecting these characteristics. The current treatment methods were also researched. The systems measured in this study were based on the results of the literature review conducted on the characteristics of vinasse.

Reliable gas hydrate equilibrium experimental data plays a crucial role in the successful design of a hydrate-based process. Hydrate-liquid-vapour experiments were performed to measure hydrate dissociation data with acceptable accuracy using a stainless steel equilibrium cell that had a working volume of 38.5 cm^3. A Pt-100 temperature sensor and a 0 - 10 MPa WIKA pressure transducer was used to measure the temperature and pressure within the equilibrium cell respectively. Mixing of the cell contents was achieved with a Heidolph RZR 2041 overhead stirrer coupled with an internal magnetic stirring device.

In order to reduce measurement uncertainty, a number of procedures were undertaken. This included preventing heat loss/gain to/from the surrounding environment by using insulation, and preventing heat fluctuations by using heating blocks. In addition, a temperature calibration for the Pt-100 temperature sensor and a pressure calibration for the 0 - 10 MPa pressure transducer were conducted.

The expanded uncertainties (which included calibration and manufacturer uncertainty) were calculated to be $\pm$ 0.1 K and $\pm$ 0.01 MPa for temperature and pressure respectively.

The experimental method and calibrations were verified through the measurement of known test systems: CO_2 (1) + water (2), CO_2 (1) + water (2) + 5 wt % NaCl, CO_2 (1) + water (2) + 5 wt % KCl (3) and CO_2 (1) + water (2) + 5 wt % NaCl (3) + 5 wt % KCl (4). The measured data compared well to that of literature.

The new systems measured included CO_2 (1) + water (2) + 5 wt % Na_2SO_4 (3), CO_2 (1) + water (2) + 5 wt % KCl (3) + 5 wt % Na_2SO_4, (4), CO_2 (1) + water (2) + mixed salts A (3), CO_2 (1) + water (2) + mixed salts B, and CO_2 (1) + water (2) + synthesised vinasse (3). The mixed salt A and mixed salt B samples contained [3/5] wt % KCl + 1 wt % Na_2SO_4 + 0.5 wt % $MgCl_2$ + 0.5 wt % $CaCl_2$ and the synthesized vinasse sample contained 5 wt % KCl + 1 wt % Na_2SO_4 + 0.5 wt % $MgCl_2$ + 0.5 wt % $CaCl_2$ + 2.2 wt % ethanol + 0.5 wt % propionic acid + 0.3 wt % acetic acid.

The results obtained from the measured hydrate dissociation data exhibited that the presence of salts and organic constituents (hydrate inhibitors) has an inhibition effect on gas hydrate phase equilibrium. In addition, the results showed that a higher concentration of inhibitors in the system resulted in a greater inhibition effect on the gas hydrate phase equilibrium. This is marked by the shift of the HLV equilibrium phase boundary, from the pure water system, to lower temperatures.

The greatest inhibition effect was displayed by the CO_2 (1) + water (2) + 5 wt % NaCl (3) + 5 wt % KCl (4) system, which was measured as a test system. The temperature shift, from pure water, for this system was - 4.1 K. The average temperature shifts for the new systems measured were: -0.9 K for the 5 wt % Na_2SO_4 system, -2.9 K for the 5 wt % KCl + 5 wt % Na_2SO_4 system, -1.9 K for the mixed salt A system, -2.4 K for the mixed salt B system, and -3.4 K for the synthesized vinasse system.

The thermodynamic model used to predict the hydrate dissociation pressures is based on the direct $(\varphi - \varphi)$ method; the fugacity coefficient is used to describe both the liquid and vapour phase non-idealities. The van der Waals and Platteeuw (1959) solid solution theory was used to model the hydrate phase. The Peng-Robinson-Stryjek-Vera (1986) EOS with the classical mixing rules was used to describe the fluid phases. The model developed by Aasberg-Petersen et al. (1991) was used to account for the salts present in the system as well as for the solubility of CO_2 in aqueous electrolyte solutions. The calculated fugacity coefficient was corrected with the Debye-Hückel electrostatic term. The water-salt interaction coefficients were accounted for using the parameters reported by Tohidi et al. (1995). The predictive model was programmed using Matlab®. The predicted results were acceptable in comparison to the experimental results. The model predicted more accurately for the CO_2 (1) + water (2) system. In addition, the model predicted more accurately at lower pressures and

lower concentrations of the salt systems. As the pressure, number of salts, and concentration of salts increased, there was some discrepancy between the predicted dissociation pressure and measured dissociation pressure.

The lowest and highest %AADp was calculated to be 2.53 % and 7.01 % for the CO_2 (1) + water (2) system and CO_2 (1) + water (2) + 5 wt % NaCl (3) + 5 wt % KCl (4) system respectively (both test systems). The %AADp for the new systems measured were: 3.78 % for the 5 wt % Na_2SO_4 system, 5.63 % for the 5 wt % KCl + 5 wt % Na_2SO_4 system, 4.46 % for the mixed salt A system, and 5.06 % for the mixed salt B system.

Due to the complexity of the synthesized vinasse system (inorganic and organic inhibitors) a predictive model was not developed to predict the dissociation conditions in this study however a predictive model was developed by Babaee (2017). There is good comparison between the results of this newly developed model of Babaee (2017) and the experimental data measured in this work.

A conceptual design for the treatment of vinasse is proposed, based on the process of Javanmardi and Moshfeghian (2003). A simple mass balance and energy balance was performed over the proposed process, which was simulated in Aspen Plus®. The results of which were used in the economic evaluation.

The final products of hydrate-based desalination are concentrated brine and potable water. The produced potable water can be used at various areas of the sugar production processing plant, for irrigation, or disposed safely in the ocean. The concentrated brine can be used in the production of biomanure.

The results of the economic analysis indicated, on a 2012 basis, a total product cost of $ 6.09/ton for the proposed process. The total product cost was comparable to the $ 7.35/ton (2012 basis) obtained for the hydrate-based process proposed by Javanmardi and Moshfeghian (2003) for the desalination of seawater. Compared to traditional desalination technologies such as MSF, MED, and RO, the cost of the proposed process as presented in this study is more expensive and recommendations are proposed in order to reduce the cost.

Even though gas hydrates show promise for desalination, and the production cost is believed to be similar to that of commercially available desalination technologies, the process is yet to be operated on a completely functional level. There are no continuously operating hydrate-based desalination facilities, even on pilot scale. In order to commercialise the hydrate-based desalination concept, industrial research needs to be conducted and key technologies need to be developed in order to improve upon the challenges that face hydrate-based desalination and to optimize the process. These

challenges relate to the control of hydrate nucleation, hydrate size and morphology, agglomeration, amount of entrapped salt, and the efficient separation of hydrate crystals from concentrated brine.

8

CHAPTER EIGHT

RECOMMENDATIONS

Treatment and purification of effluents is an important aspect of any industry. Gas hydrate technology is not a new processing technique, however, the desalination of industrial effluent through the formation of gas hydrates has yet to be implemented on an industrial scale. Currently, the technology is not feasible compared to established, traditional desalination technologies.

The results of measured systems in this study have shown that the presence of inhibitors, such as salts and alcohols, shift hydrate phase equilibrium to lower temperatures. Further measurements should be conducted with CO_2 as the hydrate former, on synthesized vinasse containing a wider range of constituents. It is also recommended that further hydrate measurements on systems representative of industrial vinasse with fluorinated formers such as R134a, R410a and R507 be conducted. Furthermore, it is recommended that the addition of a promoter, such as cyclopentane, to the systems measured in this study and the recommended systems be investigated, in order to determine whether ambient operating conditions could be reached.

It is recommended that a detailed kinetic study on measured and recommended systems be conducted in order to determine how long it will take for hydrate formation to occur. This would be extremely beneficial in the design of a hydrate-based desalination plant for the treatment of vinasse.

It is recommended that measurements be conducted on a cell equipped with observation windows in order to observe the formation of gas hydrates. During kinetic measurements, nucleation can occur, in some cases, instantaneously. Observation windows would therefore be beneficial during kinetic

measurements on hydrate forming systems. On the equipment used in this study, it took approximately 16 - 20 hours to measure one dissociation data point. Any power outage would result in a significant amount of experimental data being lost. It is therefore recommended that the equipment be connected to an uninterrupted power supply.

In order for hydrate-based treatment technologies to be implemented into industry, crystal size and quality of the gas hydrates need to be determined. In addition, feasible techniques to determine the concentration of the final solution need to be established. Molecular and mesoscopic experimental methods are possible solutions to overcome these limitations that can be investigated. Solid-state NMR Spectroscopy, Raman Spectroscopy and X-Ray diffraction are molecular level experimental methods for studying hydrate properties. Hydrate properties such as structure identification and changes in hydrate structure during formation and decomposition can be obtained by use of these molecular level experimental methods. On a mesoscopic level, Laser Scattering and Particle Video Microscope can be used to determine hydrate crystal size during formation and decomposition.

Two methods have been presented in literature by Huang et al. (1965) to determine the extent of separation and thus the concentration of the final solution. These methods include direct and indirect methods. The direct method involves the use of a centrifuge and the indirect method involves filtration and titration. Investigation into these methods is recommended in order to acquire an accurate and repeatable method to determine the solids content of the final concentrated solution.

The equilibrium cell could not be opened during hydrate formation due to the temperature and pressure sensitivity. Therefore, the concentration of the solution after hydrate formation, and thus the degree of separation, could not be determined. However, the equilibrium cell can be equipped with a sampler to determine the compositions of the liquid and vapour phases in equilibrium with the gas hydrate.

Since the PRSV EOS with the classical mixing rules did not account for the non-ideal liquid and vapour phases at high temperatures and pressures accurately, other EOS and mixing rules such as the Patel and Teja (1982), Trebble and Bishnoi (1988), or Valderrama (1990) EOS with the quadratic or non-density-dependent mixing rules as well as models such as the Mixed-solvent electrolyte model (Wang et al., 2002; Wang et al., 2004; Wang et al., 2006) should be investigated. In addition, the development of a new model to account for the inhibition effect of all components present in vinasse would be valuable for the prediction of hydrate dissociation pressures in vinasse streams. It is therefore recommended that additional HLV measurements be performed on aqueous solutions containing the various constituents in order for a more accurate model to be developed. Finally,

investigations into industrially supplied vinasse samples must be performed. Such investigations would deliver better understanding into a gas hydrate based treatment facility.

The focus of this study was to determine the capability and feasibility of using gas hydrate technology in the treatment of vinasse. Only a preliminary study was conducted and therefore the use of promoters was not considered. Future measurements on vinasse systems using promoters are recommended.

An in-depth, detailed design including energy integration and mass and heat transfer considerations should be undertaken. In addition an economic evaluation should be done on the new design in order to determine a detailed investment and operating cost. Finally, investigations into industrially supplied vinasse samples must be performed. Such investigations would provide a better understanding into the hydrate formation conditions, which would aid in the successful design and costing of gas hydrate based desalination plant for the treatment of vinasse.

REFERENCES

Aasberg-Petersen, K., Stenby, E. & Fredenslund, A. 1991. Prediction of high-pressure gas solubilities in aqueous mixtures of electrolytes. *Industrial & Engineering Chemistry Research,* 30**,** 2180-2185.

Acharya, B. K., Mohana, S. & Madamwar, D. 2008. Anaerobic treatment of distillery spent wash – a study on upflow anaerobic fixed film bioreactor. *Bioresource Technology,* 99**,** 4621-4626.

Afzal, W., Mohammadi, A. H. & Richon, D. 2007. Experimental measurements and predictions of dissociation conditions for carbon dioxide and methane hydrates in the presence of triethylene glycol aqueous solutions. *Journal of Chemical & Engineering Data,* 52**,** 2053-2055.

Ahmed, O., Sulieman, A. M. E. & Elhardallou, S. B. 2013. Physicochemical, chemical and microbiological characteristics of vinasse, a by-product from ethanol industry. *American Journal of Biochemistry,* 3**,** 80-83.

Angayarkanni, J., Palaniswamy, M. & Swaminathan, K. 2003. Biotreatment of distillery effluent using aspergillus niveus. *Bulletin of Environmental Contamination and Toxicology,* 70**,** 0268-0277.

Atilhan, M., Deniz, E., Benyahia, F. & Aparicio, S. 2012. Natural gas hydrates. *Advances in Natural Gas Technology.*

Avlonitis, D. & Varotsis, N. 1996. Modelling gas hydrate thermodynamic behaviour: theoretical basis and computational methods. *Fluid Phase Equilibria,* 123**,** 107-130.

Babaee, S. 2017. A thermodynamic model to predict the dissociation conditions for systems containing salts and organic inhibitors. University of Kwazulu-Natal.

Barkan, E.S & Sheinin, D.A. 1993. A general technique for the calculation of formation conditions for natural gas hydrates. *Fluid Phase Equilibria,* 86, 111-136.

Belandria, V. 2012. Hydrate phase equilibria study of CO_2 containing gases in thermodynamic promoter aqueous mixtures. Ecole Nationale Supérieure Des Mines De Paris.

Benesh, M. B. 1942. The use of gas hydrates in improving the load factor of gas supply systems. Google Patents.

Benitez, F. J., Real, F. J., Acero, J. L., Garcia, J. & Sanchez, M. 2003. Kinetics of the ozonation and aerobic biodegradation of wine vinasses in discontinuous and continuous processes. *Journal of Hazardous Materials,* 101**,** 203-218.

Benito, G. G., Miranda, M. P. & De Los Santos, D. R. 1997. Decolorization of wastewater from an alcoholic fermentation process with trametes versicolor. *Bioresource Technology,* 61**,** 33-37.

Bernhardt, H. 1998. Centrifugal clarification of molasses. *Proc S Afv Sug Technol Ass,* 72**,** 278-284.

Bhandari, H. C., Mitra, A. K. & Kumar, S. Crest's integrated system: Reduction and recycling of effluents in distilleries. Tewari, P.K. (Ed.), Liquid Asset, Proceedings of indo-eu workshop on promoting efficient water use in agro-based industries, 2004. New Delhi, India: Teri Press, 167-169.

Bishnoi, P. & Dholabhai, P. 1993. Experimental study on propane hydrate equilibrium conditions in aqueous electrolyte solutions. *Fluid Phase Equilibria,* 83**,** 455-462.

Bishnoi, P. & Dholabhai, P. D. 1999. Equilibrium conditions for hydrate formation for a ternary mixture of methane, propane and carbon dioxide, and a natural gas mixture in the presence of electrolytes and methanol. *Fluid Phase Equilibria,* 158**,** 821-827.

Bishnoi, P. R. & Natarajan, V. 1996. Formation and decomposition of gas hydrates. *Fluid Phase Equilibria,* 117**,** 168-177.

Bories, A., Raynal, J. & Bazile, F. 1988. Anaerobic digestion of high-strength distillery wastewater (cane molasses stillage) in a fixed-film reactor. *Biological Wastes,* 23**,** 251-267.

Bouchemoua, A., Brantuas, P. & Herri, J.-M. Equilibrium data of CO_2-based semi-clathrates from quaternary ammonium solutions. 7th International conference on gas hydrates (ICGH 2011), 2011. 439.

Bradshaw, R. W., J.A, G., Cygan, R. T., Simmons, B. A., Dedrick, D. E. & Majzoub, E. H. 2008. Desalination utilizing clathrate hydrates (LDRD Final Report). Washington, D.C.; Oak Ridge, Tenn.: United States. Dept. Of Energy ; Distributed By The Office Of Scientific And Technical Information, U.S. Dept. Of Energy.

Breland, E. & Englezos, P. 1996. Equilibrium hydrate formation data for carbon dioxide in aqueous glycerol solutions. *Journal Of Chemical & Engineering Data,* 41**,** 11-13.

Carroll, J. 2014. *Natural gas hydrates: A guide for engineers*, Gulf Professional Publishing.

Chandra, R. & Singh, H. 1999. Chemical decolorization of anaerobically treated distillery effluent. *Indian Journal Of Environmental Protection,* 19**,** 833-837.

Chang, I.-S., Choo, K.-H., Lee, C.-H., Pek, U.-H., Koh, U.-C., Kim, S.-W. & Koh, J.-H. 1994. Application of ceramic membrane as a pretreatment in anaerobic digestion of alcohol-distillery wastes. *Journal Of Membrane Science,* 90**,** 131-139.

Chang, S. Comparing exploitation and transportation technologies for monetisation of offshore stranded gas. Spe Asia Pacific oil and gas conference and exhibition, 2001. Society of Petroleum Engineers.

Chapoy, A., Mazloum, S., Burgass, R., Haghighi, H. & Tohidi, B. 2012. Clathrate hydrate equilibria in mixed monoethylene glycol and electrolyte aqueous solutions. *The Journal Of Chemical Thermodynamics,* 48**,** 7-12.

Chatti, I., Delahaye, A., Fournaison, L. & Petitet, J.-P. 2005. Benefits and drawbacks of clathrate hydrates: a review of their areas of interest. *Energy Conversion And Management,* 46**,** 1333-1343.

Chaturvedi, S., Chandra, R. & Rai, V. 2006. Isolation and characterization of phragmites australis (l.) rhizosphere bacteria from contaminated site for bioremediation of colored distillery effluent. *Ecological Engineering,* 27**,** 202-207.

Chaudhari, P. K., Mishra, I. & Chand, S. 2008. Effluent treatment for alcohol distillery: catalytic thermal pretreatment (catalytic thermolysis) with energy recovery. *Chemical Engineering Journal,* 136**,** 14-24.

Chaudhari, P. K., Mishra, I. M. & Chand, S. 2007. Decolourization and removal of chemical oxygen demand (cod) with energy recovery: treatment of biodigester effluent of a molasses-based alcohol distillery using inorganic coagulants. *Colloids And Surfaces A: Physicochemical And Engineering Aspects,* 296**,** 238-247.

Chaudhary, A., K., S. A. & Singh, B. 2013. Study of physio-chemical characteristics and biological treatment of molasses-based distillery effluent. *2013,* 2**,** 4.

Chen, G.-J. & Guo, T.-M. 1996. Thermodynamic modeling of hydrate formation based on new concepts. *Fluid Phase Equilibria,* 122**,** 43-65.

Chen, G.-J. & Guo, T.-M. 1998. A new approach to gas hydrate modelling. *Chemical Engineering Journal,* 71**,** 145-151.

Chin, H.-Y., Hsieh, M.-K., Chen, Y.-P., Chen, P.-C., Lin, S.-T. & Chen, L.-J. 2013. Prediction of phase equilibrium for gas hydrate in the presence of organic inhibitors and electrolytes by using an explicit pressure-dependent langmuir adsorption constant in the van der Waals–Platteeuw model. *The Journal Of Chemical Thermodynamics,* 66**,** 34-43.

Chong, Z. R., Yang, S. H. B., Babu, P., Linga, P. & Li, X.-S. 2015. Review of natural gas hydrates as an energy resource: prospects and challenges. *Applied Energy*.

Chopra, P., Singh, D., Verma, V. & Puniya, A. K. 2004. Bioremediation of melanoidins containing digested spent wash from cane-molasses distillery with white rot fungus, coriolus versicolour. *Indian Journal Of Microbiology,* 44**,** 197-200.

Christofoletti, C. A., Escher, J. P., Correia, J. E., Marinho, J. F. U. & Fontanetti, C. S. 2013. Sugarcane vinasse: environmental implications of its use. *Waste Management,* 33**,** 2752-2761.

Chun, M.-K. & Lee, H. 1998. Phase equilibria of R22 ($CHClF_2$) hydrate system in the presence of sucrose, glucose and lactic acid. *Fluid Phase Equilibria,* 150–151**,** 361-370.

Chun, M.-K., Lee, H. & Ryu, B.-J. 2000. Phase equilibria of R22 ($CHClF_2$) hydrate systems in the presence of NaCl, Kcl, and $MgCl_2$. *Journal Of Chemical & Engineering Data,* 45**,** 1150-1153.

Chun, M.-K., Yoon, J.-H. & Lee, H. 1996. Clathrate phase equilibria for the water + deuterium oxide + carbon dioxide and water + deuterium oxide + chlorodifluoromethane (R22) systems. *Journal Of Chemical & Engineering Data,* 41**,** 1114-1116.

Circone, S., Stern, L. A., Kirby, S. H., Durham, W. B., Chakoumakos, B. C., Rawn, C. J., Rondinone, A. J. & Ishii, Y. 2003. CO_2 hydrate: synthesis, composition, structure, dissociation behavior,

and a comparison to structure I CH$_4$ hydrate. *The Journal Of Physical Chemistry B,* 107**,** 5529-5539.

Cortez, L. & Brossard PéRez, L. 1997. Experiences on vinasse disposal: Part III: Combustion of vinasse # 6 Fuel oil emulsions. *Brazilian Journal Of Chemical Engineering,* 14.

Dahiya, J., Singh, D. & Nigam, P. 2001. Decolourisation of synthetic and spentwash melanoidins using the white-rot fungus phanerochaete chrysosporium Jag-40. *Bioresource Technology,* 78**,** 95-98.

Dalmazzone, C., Herzhaft, B., Rousseau, L., Le Parlouer, P. & Dalmazzone, D. Prediction of gas hydrates formation with dsc technique. Spe Annual Technical Conference And Exhibition, 2003. Society Of Petroleum Engineers.

Dalmazzone, D., Kharrat, M., Lachet, V., Fouconnier, B. & Clausse, D. 2002. DSC and PVT Measurements: methane and trichlorofluoromethane hydrate dissociation equilibria. *Journal Of Thermal Analysis And Calorimetry,* 70**,** 493-505.

De Roo, J., Peters, C., Lichtenthaler, R. & Diepen, G. 1983. Occurrence of methane hydrate in saturated and unsaturated solutions of sodium chloride and water in dependence of temperature and pressure. *AIChE Journal,* 29**,** 651-657.

Deaton, W. M. & Frost, E. M. 1946. Gas hydrates and their relation to the operation of natural-gas pipe lines. *Oil Gas J,* 45**,** 170-178.

Delahaye, A., Fournaison, L., Marinhas, S., Chatti, I., Petitet, J.-P., Dalmazzone, D. & Fürst, W. 2006. Effect of THF on equilibrium pressure and dissociation enthalpy of CO$_2$ hydrates applied to secondary refrigeration. *Industrial & Engineering Chemistry Research,* 45**,** 391-397.

Delavar, H. & Haghtalab, A. 2015. Thermodynamic modeling of gas hydrate formation conditions in the presence of organic inhibitors, salts and their mixtures using uniquac model. *Fluid Phase Equilibria,* 394**,** 101-117.

Dhima, A., De Hemptinne, J.-C. & Jose, J. 1999. Solubility of hydrocarbons and co2 mixtures in water under high pressure. *Industrial & Engineering Chemistry Research,* 38**,** 3144-3161.

Dholabhai, P., Englezos, P., Kalogerakis, N. & Bishnoi, P. 1991. Equilibrium conditions for methane hydrate formation in aqueous mixed electrolyte solutions. *The Canadian Journal of Chemical Engineering,* 69**,** 800-805.

Dholabhai, P. D. & Bishnoi, P. R. 1994. Hydrate equilibrium conditions in aqueous electrolyte solutions: mixtures of methane and carbon dioxide. *Journal of Chemical and Engineering Data,* 39**,** 191-194.

Dholabhai, P. D., Kalogerakis, N. & Bishnoi, P. R. 1993. Equilibrium conditions for carbon dioxide hydrate formation in aqueous electrolyte solutions. *Journal of Chemical and Engineering Data,* 38**,** 650-654.

Dholabhai, P. D., Parent, J. S. & Bishnoi, P. R. 1996. Carbon dioxide hydrate equilibrium conditions in aqueous solutions containing electrolytes and methanol using a new apparatus. *Industrial & Engineering Chemistry Research,* 35**,** 819-823.

Dholabhai, P. D., Parent, J. S. & Bishnoi, P. R. 1997. Equilibrium conditions for hydrate formation from binary mixtures of methane and carbon dioxide in the presence of electrolytes, methanol and ethylene glycol. *Fluid Phase Equilibria,* 141**,** 235-246.

Dohrn, R., Peper, S. & Fonseca, J. M. 2010. High-pressure fluid-phase equilibria: experimental methods and systems investigated (2000–2004). *Fluid Phase Equilibria,* 288**,** 1-54.

Dorsett, L. Ltx: Realization of proven technology. Spe Gas Technology Symposium, 1989. Society Of Petroleum Engineers, 239-246.

Douglas, J. M. 1988. *Conceptual Design Of Chemical Processes*, Mcgraw-Hill.

Driessen, W., Tielbaard, M. & Vereijken, T. 1994. Experience on anaerobic treatment of distillery effluent with the uasb process. *Water Science and Technology,* 30**,** 193-201.

Duc, N. H., Chauvy, F. & Herri, J.-M. 2007. CO_2 capture by hydrate crystallization – A potential solution for gas emission of steelmaking industry. *Energy Conversion And Management,* 48**,** 1313-1322.

Englezos, P. 1992. Computation of the incipient equilibrium carbon dioxide hydrate formation conditions in aqueous electrolyte solutions. *Industrial & Engineering Chemistry Research,* 31**,** 2232-2237.

Englezos, P. 1993. Clathrate hydrates. *Industrial & Engineering Chemistry Research,* 32**,** 1251-1274.

Englezos, P. 1994. The freeze concentration process and its applications. *Developments In Chemical Engineering And Mineral Processing,* 2**,** 3-15.

Englezos, P. & Bishnoi, P. 1991. Experimental study on the equilibrium ethane hydrate formation conditions in aqueous electrolyte solutions. *Industrial & Engineering Chemistry Research,* 30**,** 1655-1659.

Englezos, P. & Hall, S. 1994. Phase equilibrium data on carbon dioxide hydrate in the presence of electrolytes, water soluble polymers and montmorillonite. *The Canadian Journal of Chemical Engineering,* 72**,** 887-893.

Englezos, P., Kalogerakis, N., Dholabhai, P. & Bishnoi, P. 1987. Kinetics of formation of methane and ethane gas hydrates. *Chemical Engineering Science,* 42**,** 2647-2658.

Englezos, P. & Ngan, Y. T. 1993. Incipient equilibrium data for propane hydrate formation in aqueous solutions of sodium chloride, potassium chloride and calcium chloride. *Journal of Chemical and Engineering Data,* 38**,** 250-253.

Englezos, P. & Ngan, Y. T. 1994. Effect of polyethylene oxide on gas hydrate phase equilibria. *Fluid Phase Equilibria,* 92**,** 271-288.

Eslamimanesh, A., Mohammadi, A. H., Richon, D., Naidoo, P. & Ramjugernath, D. 2012. Application of gas hydrate formation in separation processes: a review of experimental studies. *The Journal of Chemical Thermodynamics,* 46**,** 62-71.

España-Gamboa, E., Mijangos-Cortes, J., Barahona-Perez, L., Dominguez-Maldonado, J., Hernández-Zarate, G. & Alzate-Gaviria, L. 2011. Vinasses: characterization and treatments. *Waste Management & Research,* 29**,** 1235-1250.

España-Gamboa, E. I., Mijangos-Cortés, J. O., Hernández-Zárate, G., Maldonado, J. A. D. & Alzate-Gaviria, L. M. 2012. Methane production by treating vinasses from hydrous ethanol using a modified uasb reactor. *Biotechnology for Biofuels,* 5**,** 1.

Espinosa, A., Rosas, L., Ilangovan, K. & Noyola, A. 1995. Effect of trace metals on the anaerobic degradation of volatile fatty acids in molasses stillage. *Water Science and Technology,* 32**,** 121-129.

Fahy, V., Fitzgibbon, F., Mcmullan, G., Singh, D. & Marchant, R. 1997. Decolourisation of molasses spent wash by phanerochaete chrysosporium. *Biotechnology Letters,* 19**,** 97-99.

Fan, S.-S. & Guo, T.-M. 1999. Hydrate oormation of CO_2-rich binary and quaternary gas mixtures in aqueous sodium chloride solutions. *Journal of Chemical & Engineering Data,* 44**,** 829-832.

Fernández, N., Montalvo, S., Borja, R., Guerrero, L., Sánchez, E., Cortes, I., Colmenarejo, M., Travieso, L. & Raposo, F. 2008. Performance evaluation of an anaerobic fluidized bed reactor with natural zeolite as support material when treating high-strength distillery wastewater. *Renewable Energy,* 33**,** 2458-2466.

Fournaison, L., Delahaye, A., Chatti, I. & Petitet, J.-P. 2004. CO_2 hydrates in refrigeration processes. *Industrial & Engineering Chemistry Research,* 43**,** 6521-6526.

Friedrich, J. 2004. Bioconversion of distillery waste. *Fungal Biotechnology and Agricultural, Food, and Environmental Applications.* Crc Press Boca Raton, Usa.

Fujita, M., Era, A., Ike, M., Soda, S., Miyata, N. & Hirao, T. 2000. Decolorization of heat-treatment liquor of waste sludge by a bioreactor using polyurethane foam-immobilized white rot fungus equipped with an ultramembrane filtration unit. *Journal of Bioscience and Bioengineering,* 90**,** 387-394.

Fürst, W. & Renon, H. 1993. Representation of excess properties of electrolyte solutions using a new equation of state. *AIChE Journal,* 39**,** 335-343.

Gaarder, C. 1993. *Crystallization of mechanical pulp mill effluents through hydrate formation for the recovery of water.* Doctoral Dissertation, University Of British Columbia.

Ghosh, M., Ganguli, A. & Tripathi, A. 2002. Treatment of anaerobically digested distillery spentwash in a two-stage bioreactor using pseudomonas putida and aeromonas sp. *Process Biochemistry,* 37**,** 857-862.

Gjertsen, L. H. & Fadnes, F. H. 2000. Measurements and predictions of hydrate equilibrium conditions. *Annals of the New York Academy of Sciences,* 912**,** 722-734.

González, T., Terrón, M. C., Yagüe, S., Zapico, E., Galletti, G. C. & González, A. E. 2000. Pyrolysis/gas chromatography/mass spectrometry monitoring of fungal‑biotreated distillery wastewater using trametes sp. I-62 (Cect 20197). *Rapid Communications in Mass Spectrometry,* 14**,** 1417-1424.

Goyal, S., Seth, R. & Handa, B. 1996. Diphasic fixed-film biomethanation of distillery spentwash. *Bioresource Technology,* 56**,** 239-244.

Gryta, M. 2012. *Desalination of industrial effluents using integrated membrane processes*, Intech Open Access Publisher.

Guimarães, C., Porto, P., Oliveira, R. & Mota, M. 2005. Continuous decolourization of a sugar refinery wastewater in a modified rotating biological contactor with phanerochaete chrysosporium immobilized on polyurethane foam disks. *Process Biochemistry,* 40**,** 535-540.

Guo, T.-M., Wu, B.-H., Zhu, Y.-H., Fan, S.-S. & Chen, G.-J. 2004. A review on the gas hydrate research in china. *Journal of Petroleum Science and Engineering,* 41**,** 11-20.

Guthrie, K. M. 1969. Capital cost estimating. *Chem. Eng.,* 76.

Hammerschmidt, E. 1934. Formation of gas hydrates in natural gas transmission lines. *Industrial & Engineering Chemistry,* 26**,** 851-855.

Happel, J. & Jordan, D. G. 1975. *Chemical Process Economics*, M. Dekker.

Harada, H., Uemura, S., Chen, A.-C. & Jayadevan, J. 1996. Anaerobic treatment of a recalcitrant distillery wastewater by a thermophilic UASB reactor. *Bioresource Technology,* 55**,** 215-221.

Harmens, A. & Sloan, E. D. 1990. The phase behaviour of the propane-water system: a review. *The Canadian Journal of Chemical Engineering,* 68**,** 151-158.

Hashemi, H. 2015. *Application of gas hydrates in cold storage technology: experimental study and thermodynamic modeling.* Ph.D., University Of Kwa-Zulu Natal.

He, Y., Rudolph, E. S. J., Zitha, P. L. & Golombok, M. 2011. Kinetics of CO_2 and methane hydrate formation: an experimental analysis in the bulk phase. *Fuel,* 90**,** 272-279.

Herri, J.-M., Bouchemoua, A., Kwaterski, M., Fezoua, A., Ouabbas, Y. & Cameirao, A. 2011. Gas hydrate equilibria for CO_2–N_2 and CO_2–CH_4 gas mixtures - experimental studies and thermodynamic modelling. *Fluid Phase Equilibria,* 301**,** 171-190.

Holder, G., Corbin, G. & Papadopoulos, K. 1980. Thermodynamic and molecular properties of gas hydrates from mixtures containing methane, argon, and krypton. *Industrial & Engineering Chemistry Fundamentals,* 19**,** 282-286.

Holder, G. & Hand, J. 1982. Multiple‑phase equilibria in hydrates from methane, ethane, propane and water mixtures. *AIChE Journal,* 28**,** 440-447.

Hsieh, M.-K., Yeh, Y.-T., Chen, Y.-P., Chen, P.-C., Lin, S.-T. & Chen, L.-J. 2012. Predictive method for the change in equilibrium conditions of gas hydrates with addition of inhibitors and electrolytes. *Industrial & Engineering Chemistry Research,* 51**,** 2456-2469.

Huang, C., Fennema, O. & Powrie, W. 1965. Gas hydrates in aqueous-organic systems: i. preliminary studies. *Cryobiology,* 2**,** 109-115.

Huo, Z., Hester, K., Sloan, E. D. & Miller, K. T. 2003. Methane hydrate nonstoichiometry and phase diagram. *AIChE Journal,* 49**,** 1300-1306.

Ivanic, J., Huo, Z. & Sloan, E. 2004. Improved hydrate equilibrium measurements in ternary gas and black oil systems. *Fluid Phase Equilibria,* 222**,** 303-310.

Jain, N., Minocha, A. & Verma, C. 2002. Degradation of predigested distillery effluent by isolated bacterial strains. *Indian Journal of Experimental Biology,* 40**,** 101-105.

Javanmardi, J., Ayatollahi, S., Motealleh, R. & Moshfeghian, M. 2004. Experimental measurement and modeling of R22 (CHClF$_2$) hydrates in mixtures of acetone + water. *Journal Of Chemical & Engineering Data,* 49**,** 886-889.

Javanmardi, J., Babaee, S., Eslamimanesh, A. & Mohammadi, A. H. 2012. Experimental measurements and predictions of gas hydrate dissociation conditions in the presence of methanol and ethane-1, 2-diol aqueous solutions. *Journal of Chemical & Engineering Data,* 57**,** 1474-1479.

Javanmardi, J. & Moshfeghian, M. 2003. Energy consumption and economic evaluation of water desalination by hydrate phenomenon. *Applied Thermal Engineering,* 23**,** 845-857.

Javanmardi, J., Nasrifar, K., Najibi, S. & Moshfeghian, M. 2005. Economic evaluation of natural gas hydrate as an alternative for natural gas transportation. *Applied Thermal Engineering,* 25**,** 1708-1723.

Jeffrey, G. 1984. Hydrate inclusion compounds. *Journal Of Inclusion Phenomena,* 1**,** 211-222.

Jensen, L., Thomsen, K. & Von Solms, N. 2008. Propane hydrate nucleation: experimental investigation and correlation. *Chemical Engineering Science,* 63**,** 3069-3080.

Jiranuntipon, S., Chareonpornwattana, S., Damronglerd, S., Albasi, C. & Delia, M.-L. 2008. Decolorization of synthetic melanoidins-containing wastewater by a bacterial consortium. *Journal of Industrial Microbiology & Biotechnology,* 35**,** 1313-1321.

Kahraman, S. & Yeşilada, O. 2003. Decolorization and bioremediation of molasses wastewater by white-rot fungi in a semi-solid-state condition. *Folia Microbiologica,* 48**,** 525-528.

Kalavathi, D. F., Uma, L. & Subramanian, G. 2001. Degradation and metabolization of the pigment—melanoidin in distillery effluent by the marine cyanobacterium oscillatoria boryana Bdu 92181. *Enzyme and Microbial Technology,* 29**,** 246-251.

Kamath, V., Holder, G. & Angert, P. 1984. Three phase interfacial heat transfer during the dissociation of propane hydrates. *Chemical Engineering Science,* 39**,** 1435-1442.

Kang, K. C., Linga, P., Park, K.-N., Choi, S.-J. & Lee, J. D. 2014. Seawater desalination by gas hydrate process and removal characteristics of dissolved ions (Na$^+$, K$^+$, Mg^{2+}, Ca^{2+}, B^{3+}, Cl$^-$, SO$_4^{2-}$). *Desalination,* 353**,** 84-90.

Kang, S.-P., Chun, M.-K. & Lee, H. 1998. Phase equilibria of methane and carbon dioxide hydrates in the aqueous $MgCl_2$ solutions. *Fluid Phase Equilibria,* 147**,** 229-238.

Kannan, A. & Upreti, R. K. 2008. Influence of distillery effluent on germination and growth of mung bean (vigna radiata) seeds. *Journal of Hazardous Materials,* 153**,** 609-615.

Karaaslan, U. & Parlaktuna, M. 2002. PEO, a new hydrate inhibitor polymer. *Energy & Fuels,* 16**,** 1387-1391.

Katz, D. L., Cornell, D., Kobayashi, R., Poettmann, F. H., Vary, J. A., Elenbaas, J. R. & Weinaug, C. F. 1959. *Handbook Of Natural Gas Engineering,* New York, Mcgraw-Hill.

Katz, D.L. 1945. Predictions of conditions for hydrate formation in natural gases. *Transactions of the Aime*, 160, 140-149.

Khan, A. H. 1986. Freezing. *Desalination Processes And Multistage Flash Distillation Practice.* Amsterdam U.A.: Elsevier.

Khokhar, A., Gudmundsson, J. & Sloan, E. 1998. Gas storage in structure H hydrates. *Fluid Phase Equilibria,* 150**,** 383-392.

Kihara, T. 1953. Virial coefficients and models of molecules in gases. *Reviews of Modern Physics,* 25**,** 831.

Kim, S. J. & Shoda, M. 1999. Batch decolorization of molasses by suspended and immobilized fungus of geotrichum candidum Dec 1. *Journal of Bioscience and Bioengineering,* 88**,** 586-589.

Klapp, S. A., Hemes, S., Klein, H., Bohrmann, G., Macdonald, I. & Kuhs, W. F. 2010. Grain size measurements of natural gas hydrates. *Marine Geology,* 274**,** 85-94.

Klauda, J. B. & Sandler, S. I. 2000. A fugacity model for gas hydrate phase equilibria. *Industrial & Engineering Chemistry Research,* 39**,** 3377-3386.

Knapp, J. S., Vantoch-Wood, E. J., Zhang, F. & 2001. Use of wood-rotting fungi for the decolorization of dyes and industrial effluents. *Fungi in Bioremediation.* Cambridge University Press.

Knox, W. G., Hess, M., Jones, G. E. & Smith, H. B. 1961. The hydrate process. *Chem. Eng. Prog,* 57**,** 66-71.

Koh, C. A., Sloan, E. D., Sum, A. K. & Wu, D. T. 2011. Fundamentals and applications of gas hydrates. *Annual Review of Chemical and Biomolecular Engineering,* 2**,** 237-257.

Koh, C. A., Sum, A. K. & Sloan, E. D. 2012. State of the art: natural gas hydrates as a natural resource. *Journal of Natural Gas Science And Engineering,* 8**,** 132-138.

Kubota, H., Shimizu, K., Tanaka, Y. & Makita, T. 1984. Thermodynamic properties of R13 ($CCIF_3$), R23 (CHF_3), R152a ($C_2H_4F_2$), and propane hydrates for desalination of sea water. *Journal of Chemical Engineering of Japan,* 17**,** 423-429.

Kumar, V., Wati, L., Fitzgibbon, F., Nigam, P., Banat, I., Singh, D. & Marchant, R. 1997. Bioremediation and decolorization of anaerobically digested distillery spent wash. *Biotechnology Letters,* 19**,** 311-314.

Kumar, V., Wati, L., Nigam, P., Banat, I. M., Yadav, B. S., Singh, D. & Marchant, R. 1998. Decolorization and biodegradation of anaerobically digested sugarcane molasses spent wash effluent from biomethanation plants by white-rot fungi. *Process Biochemistry,* 33**,** 83-88.

Kumari, K. & Phogat, V. 2010. Characterization of spent wash from different distilleries operating in haryana and its utilization as a source of liquid manure in agriculture. *Journal of The Indian Society of Soil Science,* 58**,** 347.

Kuo, P.-C., Chen, L.-J., Lin, S.-T., Chen, Y.-P., 2010. Measurement for the dissociation conditions of methane hydrate in the presence of 2-methyl-2-propanol. *J. Chem. Eng. Data,* 55**,** 5036-5039.

Lalov, I. G., Guerginov, I. I., Krysteva, M. A. & Fartsov, K. 2000. Treatment Of waste water from distilleries with chitosan. *Water Research,* 34**,** 1503-1506.

Lata, K., Kansal, A., Balakrishnan, M., Rajeshwari, K. V. & Kishore, V. V. N. 2002. Assessment of biomethanation potential of selected industrial organic effluents in india. *Resources, Conservation and Recycling,* 35**,** 147-161.

Le Parlouër, P., Dalmazzone, C., Herzhaft, B., Rousseau, L. & Mathonat, C. 2004. Characterisation of gas hydrates formation using a new high pressure micro-DSC. *Journal of Thermal Analysis and Calorimetry,* 78**,** 165-172.

Lee, B. R., Sa, J.-H., Park, D.-H., Cho, S., Lee, J., Kim, H.-J., Oh, E., Jeon, S., Lee, J. D. & Lee, K.-H. 2012. "Continuous" method for the fast screening of thermodynamic promoters of gas hydrates using a quartz crystal microbalance. *Energy & Fuels,* 26**,** 767-772.

Lee, J. D., Susilo, R. & Englezos, P. 2005. Kinetics of structure H gas hydrate. *Energy & Fuels,* 19**,** 1008-1015.

Lee, S.-Y. & Holder, G. D. 2001. Methane hydrates potential as a future energy source. *Fuel Processing Technology,* 71**,** 181-186.

Lee, S., Liang, L., Riestenberg, D., West, O. R., Tsouris, C. & Adams, E. 2003. CO_2 Hydrate composite for ocean carbon sequestration. *Environmental Science & Technology,* 37**,** 3701-3708.

Li, S., Shen, Y., Liu, D., Fan, L. & Tan, Z. 2015. Concentrating orange juice through CO_2 clathrate hydrate technology. *Chemical Engineering Research And Design,* 93**,** 773-778.

Ma, C. F., Chen, G. J., Wang, F., Sun, C. Y. & Guo, T. M. 2001. Hydrate formation of ($CH_4 + C_2H_4$) and ($CH_4 + C_3H_6$) gas mixtures. *Fluid Phase Equilibria,* 191**,** 41-47.

Ma, Q.-L., Chen, G.-J. & Guo, T.-M. 2003. Modelling the gas hydrate formation of inhibitor containing systems. *Fluid Phase Equilibria,* 205**,** 291-302.

Maekawa, T. 2001. Equilibrium conditions for gas hydrates of methane and ethane mixtures in pure water and sodium chloride solution. *Geochemical Journal,* 35**,** 59-66.

Maekawa, T. 2006. Phase equilibria for hydrate formation from binary mixtures of ethane, propane and noble gases. *Fluid Phase Equilibria,* 243**,** 115-120.

Maekawa, T. 2008. Equilibrium conditions of propane hydrates in aqueous solutions of alcohols, glycols, and glycerol. *Journal of Chemical & Engineering Data,* 53**,** 2838-2843.

Maekawa, T. 2010. Equilibrium conditions of clathrate hydrates formed from propane and aqueous solutions of propanone and sodium chloride. *Journal of Chemical & Engineering Data,* 55**,** 3645-3648.

Maekawa, T. 2013. Equilibrium conditions of clathrate hydrates formed from xenon and aqueous solutions of acetone, 1,4-dioxane and 1,3-dioxolane. *Fluid Phase Equilibria,* 339**,** 15-19.

Mahadev, K. N. & Bishnoi, P. R. 1999. Equilibrium conditions for the hydrogen sulfide hydrate formation in the presence of electrolytes and methanol. *The Canadian Journal of Chemical Engineering,* 77**,** 718-722.

Mahimairaja, S. 2004. Problems and prospects of agricultural use of distillery spentwash in India. *Magnesium,* 1715**,** 2100.

Makogon, T. Y., Mehta, A. P. & Sloan, E. D. 1996. Structure H and structure I Hydrate equilibrium data for 2,2-dimethylbutane with methane and xenon. *Journal of Chemical & Engineering Data,* 41**,** 315-318.

Makogon, T. Y. & Sloan, E. D. J. 1994. Phase equilibrium for methane hydrate from 190 to 262 K. *Journal of Chemical and Engineering Data,* 39**,** 351-353.

Makogon, Y. F. 1965. Gazov. *Promst.,* 5, 14.

Mandal, A. & Laik, S. 2008. Effect of the promoter on gas hydrate formation and dissociation. *Energy & Fuels,* 22**,** 2527-2532.

Mane, J. D., Modi, S., Nagawade, S., Phadnis, S. P. & Bhandari, V. M. 2006. Treatment of spentwash using chemically modified bagasse and colour removal studies. *Bioresource Technology,* 97**,** 1752-1755.

Martinez, M., Dalmazzone, D., Fürst, W., Delahaye, A. & Fournaison, L. 2008. Thermodynamic properties of THF + CO_2 hydrates in relation with refrigeration applications. *AIChE Journal,* 54**,** 1088-1095.

Martins, S. I. & Van Boekel, M. A. 2005. A kinetic model for the glucose/glycine maillard reaction pathways. *Food Chemistry,* 90**,** 257-269.

Masoudi, R., Tohidi, B., Anderson, R., Burgass, R. W. & Yang, J. 2004a. Experimental measurement and thermodynamic modelling of clathrate hydrate equilibria and salt solubility in aqueous ethylene glycol and electrolyte solutions. *Fluid Phase Equilibria,* 219**,** 157-163.

Masoudi, R., Tohidi, B., Danesh, A. & Todd, A. C. 2004b. A new approach in modelling phase equilibria and gas solubility in electrolyte solutions and its applications to gas hydrates. *Fluid Phase Equilibria,* 215**,** 163-174.

Masoudi, R., Tohidi, B., Danesh, A., Todd, A. C., Anderson, R., Burgass, R. W. & Yang, J. 2005. Measurement and prediction of gas hydrate and hydrated salt equilibria in aqueous ethylene glycol and electrolyte solutions. *Chemical Engineering Science,* 60**,** 4213-4224.

Mayoufi, N., Dalmazzone, D., FüRst, W., Delahaye, A. & Fournaison, L. 2009. CO_2 enclathration in hydrates of peralkyl-(ammonium/phosphonium) salts: stability conditions and dissociation enthalpies. *Journal of Chemical & Engineering Data,* 55**,** 1271-1275.

Mccormack, R. A. & Andersen, R. K. 1995. Clathrate desalination plant preliminary research study.

Mccormack, R. A. & Niblock, G. A. 2000. *Investigation of high freezing temperature, zero ozone, and zero global warming potential, clathrate formers for desalination*, U.S. Department of The Interior, Bureau of Reclamation, Technical Service Center, Water Treatment Engineering And Research Group.

Mcnamee, K. & Conrad, P. The effect of autoclave design and test protocol on hydrate test results. Proceedings of the 7th International Conference on Gas Hydrates (ICGH 2011), Edinburgh, 17-21 July, 2011.

Mei, D.-H., Liao, J., Yang, J.-T. & Guo, T.-M. 1996. Experimental and modeling studies on the hydrate formation of a methane + nitrogen gas mixture in the presence of aqueous electrolyte solutions. *Industrial & Engineering Chemistry Research,* 35**,** 4342-4347.

Mei, D.-H., Liao, J., Yang, J.-T. & Guo, T.-M. 1998. Hydrate formation of a synthetic natural gas mixture in aqueous solutions containing electrolyte, methanol, and (electrolyte + methanol). *Journal of Chemical & Engineering Data,* 43**,** 178-182.

Meyer, J.H., Van Antwerpen, R. & McElligott D.M. Site-specific guidelines for vinasse and CMS disposal on irrigated sugarcane lands in Southern Africa. *Proceedings of the Annual Congress - South African Sugar Technologists' Association,* Durban, South Africa, 16-18 August, 2016, 89**,** 186-201.

Migo, V. P., Matsumura, M., Del Rosario, E. J. & Kataoka, H. 1993. Decolorization Of molasses wastewater using an inorganic flocculant. *Journal of Fermentation and Bioengineering,* 75**,** 438-442.

Mimachi, H., Takeya, S., Yoneyama, A., Hyodo, K., Takeda, T., Gotoh, Y. & Murayama, T. 2014. Natural gas storage and transportation within gas hydrate of smaller particle: size dependence of self-preservation phenomenon of natural gas hydrate. *Chemical Engineering Science,* 118**,** 208-213.

Miranda, M. P., Benito, G. G., Cristobal, N. S. & Nieto, C. H. 1996. Color elimination from molasses wastewater by aspergillus niger. *Bioresource Technology,* 57**,** 229-235.

Miyata, N., Mori, T., Iwahori, K. & Fujita, M. 2000. Microbial decolorization of melanoidin-containing wastewaters: combined use of activated sludge and the fungus coriolus hirsutus. *Journal of Bioscience and Bioengineering,* 89**,** 145-150.

Mohammadi, A. H., Afzal, W. & Richon, D. 2007. Experimental data and predictions of dissociation conditions for ethane and propane simple hydrates in the presence of distilled water and methane, ethane, propane, and carbon dioxide simple hydrates in the presence of ethanol aqueous solutions. *Journal of Chemical & Engineering Data,* 53**,** 73-76.

Mohammadi, A. H., Afzal, W. & Richon, D. 2008a. Experimental data and predictions of dissociation conditions for ethane and propane simple hydrates in the presence of methanol, ethylene glycol, and triethylene glycol aqueous solutions. *Journal of Chemical & Engineering Data,* 53**,** 683-686.

Mohammadi, A. H., Afzal, W. & Richon, D. 2008b. Gas hydrates of methane, ethane, propane, and carbon dioxide in the presence of single nacl, kcl, and cacl$_2$ aqueous solutions: experimental measurements and predictions of dissociation conditions. *The Journal of Chemical Thermodynamics,* 40**,** 1693-1697.

Mohammadi, A. H., Anderson, R. & Tohidi, B. 2005. Carbon monoxide clathrate hydrates: equilibrium data and thermodynamic modeling. *AIChE Journal,* 51**,** 2825-2833.

Mohammadi, A. H., Kraouti, I. & Richon, D. 2009. Methane hydrate phase equilibrium in the presence of NaBr, KBr, CaBr$_2$, K$_2$CO$_3$, and MgCl$_2$ aqueous solutions: experimental measurements and predictions of dissociation conditions. *The Journal of Chemical Thermodynamics,* 41**,** 779-782.

Mohammadi, A. H. & Richon, D. 2009a. Equilibrium data of nitrous oxide and carbon dioxide clathrate hydrates. *Journal of Chemical & Engineering Data,* 54**,** 279-281.

Mohammadi, A. H. & Richon, D. 2009b. Methane hydrate phase equilibrium in the presence of salt (NaCl, KCl, or CaCl$_2$)+ ethylene glycol or salt (NaCl, KCl, or CaCl$_2$) + methanol aqueous solution: experimental determination of dissociation condition. *The Journal of Chemical Thermodynamics,* 41**,** 1374-1377.

Mohammadi, A. H. & Richon, D. 2009c. Phase equilibria of hydrogen sulfide clathrate hydrates in the presence of methanol, ethanol, NaCl, KCl, or CaCl$_2$ aqueous solutions. *Industrial & Engineering Chemistry Research,* 48**,** 7847-7851.

Mohammadi, A. H. & Richon, D. 2010a. Gas hydrate phase equilibrium in the presence of ethylene glycol or methanol aqueous solution. *Industrial & Engineering Chemistry Research,* 49**,** 8865-8869.

Mohammadi, A. H. & Richon, D. 2010b. Ice−clathrate hydrate−gas phase equilibria for air, oxygen, nitrogen, carbon monoxide, methane, or ethane+ water system. *Industrial & Engineering Chemistry Research,* 49**,** 3976-3979.

Mohammadi, A. H. & Richon, D. 2012a. Phase equilibria of hydrogen sulfide and carbon dioxide simple hydrates in the presence of methanol, (Methanol + NaCl) and (Ethylene Glycol + Nacl) aqueous solutions. *The Journal of Chemical Thermodynamics,* 44**,** 26-30.

Mohammadi, A. H. & Richon, D. 2012b. Phase equilibria of hydrogen sulphide clathrate hydrates in the presence of single or mixed salt aqueous solution. *The Journal of Chemical Thermodynamics,* 53**,** 82-85.

Mohammadi, A. H., Tohidi, B. & Burgass, R. W. 2003. Equilibrium data and thermodynamic modeling of nitrogen, oxygen, and air clathrate hydrates. *Journal of Chemical & Engineering Data,* 48**,** 612-616.

Mohana, S., Acharya, B. K. & Madamwar, D. 2009. Distillery spent wash: treatment technologies and potential applications. *Journal of Hazardous Materials,* 163**,** 12-25.

Mohana, S., Desai, C. & Madamwar, D. 2007. Biodegradation and decolourization of anaerobically treated distillery spent wash by a novel bacterial consortium. *Bioresource Technology,* 98**,** 333-339.

Mooijer-Van Den Heuvel, M. M. 2004. *Phase behaviour and structural aspects of ternary clathrate hydrate systems, the role of additives.* Tu Delft, Delft University Of Technology.

Mooijer-Van Den Heuvel, M. M., Peters, C .J., 2002a. The Influence of additives components on gas hydrate equilibria H-L_w-V and H-L_w-L_{HC}: change of the hydrate structure versus mutual solubility effects. *Proceeding Of The Fourth International Conference On Gas Hydrates, Yokohama*.

Naeiji, P., Mottahedin, M. & Varaminian, F. 2014. Separation of methane–ethane gas mixtures via gas hydrate formation. *Separation and Purification Technology,* 123**,** 139-144.

Najibi, H., Chapoy, A., Haghighi, H. & Tohidi, B. 2009. Experimental determination and prediction of methane hydrate stability in alcohols and electrolyte solutions. *Fluid Phase Equilibria,* 275**,** 127-131.

Najibi, H., Mohammadi, A. H. & Tohidi, B. 2006. Estimating the hydrate safety margin in the presence of salt and/or organic inhibitor using freezing point depression data of aqueous solutions. *Industrial & Engineering Chemistry Research,* 45**,** 4441-4446.

Naidoo, P. 2004. *High-Pressure Vapour-Liquid Equilibrium Studies* Phd, University Of Kwa-Zulu Natal.

Nakajima-Kambe, T., Shimomura, M., Nomura, N., Chanpornpong, T. & Nakahara, T. 1999. Decolorization of molasses wastewater by bacillus sp. under thermophilic and anaerobic conditions. *Journal of Bioscience and Bioengineering,* 87**,** 119-121.

Nakamura, T., Makino, T., Sugahara, T. & Ohgaki, K. 2003. Stability boundaries of gas hydrates helped by methane structure H hydrates of methylcyclohexane and cis-1, 2-dimethylcyclohexane. *Chemical Engineering Science,* 58**,** 269-273.

Nandy, T., Shastry, S. & Kaul, S. 2002. Wastewater management in a cane molasses distillery involving bioresource recovery. *Journal of Environmental Management,* 65**,** 25-38.

Nataraj, S. K., Hosamani, K. M. & Aminabhavi, T. M. 2006. Distillery wastewater treatment by the membrane-based nanofiltration and reverse osmosis processes. *Water Research,* 40**,** 2349-2356.

Natarajan, V., Bishnoi, P. & Kalogerakis, N. 1994. Induction phenomena in gas hydrate nucleation. *Chemical Engineering Science,* 49**,** 2075-2087.

Nelson, W. M. 2012. *Separation of trichlorosilane: measurment, modeling and simulation.* Doctor Of Philosophy, University Of Kwazulu-Natal.

Neytzell-De Wilde, F. 1987. Demineralization of a molassess distillery waste water. *Desalination,* 67**,** 481-493.

Ng, H.-J. & Robinson, D. B. 1980. A method for predicting the equilibrium gas phase water content in gas-hydrate equilibrium. *Industrial & Engineering Chemistry Fundamentals,* 19**,** 33-36.

Ng, H.-J. & Robinson, D. B. 1985. Hydrate formation in systems containing methane, ethane, propane, carbon dioxide or hydrogen sulfide in the presence of methanol. *Fluid Phase Equilibria,* 21**,** 145-155.

Ng, H. J. & Robinson, D. B. First international conference on natural gas hydrates 1994.

Ngan, Y. T. 1995. *Concentration of bleached-chemi-thermo-mechanical pulp effluent by propane hydrate formation.* Master of Applied Science, University of British Columbia.

Ngan, Y. T. & Englezos, P. 1996. Concentration of mechanical pulp mill effluents and nacl solutions through propane hydrate formation. *Industrial & Engineering Chemistry Research,* 35**,** 1894-1900.

Ngema, P. T. 2014. *The use of fluorinated refrigerants in the application of gas hydrates for deslaination.* Master of Science in Engineering, University of Kwazulu-Natal.

Ngema, P. T., Naidoo, P., Mohammadi, A. H., Richon, D. & Ramjugernath, D. 2016a. Experimental clathrate hydrate dissociation data for systems comprising refrigerant + $CaCl_2$ aqueous solutions. *Journal of Chemical & Engineering Data,* 61**,** 827-836.

Ngema, P. T., Naidoo, P., Mohammadi, A. H., Richon, D. & Ramjugernath, D. 2016b. Thermodynamic stability conditions of clathrate hydrates for refrigerant (R134a or R410a or R507) with $MgCl_2$ aqueous solution. *Fluid Phase Equilibria,* 413**,** 92-98.

Ngema, P. T., Petticrew, C., Naidoo, P., Mohammadi, A. H. & Ramjugernath, D. 2014. Experimental measurements and thermodynamic modeling of the dissociation conditions of clathrate hydrates for (refrigerant + Nacl + water) systems. *J. Chem. Eng. Data Journal of Chemical & Engineering Data,* 59**,** 466-475.

Nixdorf, J. & Oellrich, L. R. 1997. Experimental determination of hydrate equilibrium conditions for pure gases, binary and ternary mixtures and natural gases. *Fluid Phase Equilibria,* 139**,** 325-333.

Oellrich, L. Natural gas hydrates and their potential for future energy supply. XVII National and VI ISHMT/ASME heat and mass transfer conference, 2004.

Ogoshi, H. & Takao, S. 2004. Air-conditioning system using clathrate hydrate slurry. *JFE Tech. Rep,* 3**,** 1-5.

Ohmomo, S., Aoshima, I., Tozawa, Y., Sakurada, N. & Ueda, K. 1985. Purification and some properties of melanoidin decolorizing enzymes, P-III and P-IV, from mycelia of coriolus versicolor Ps4a. *Agricultural and Biological Chemistry,* 49**,** 2047-2053.

Ohmomo, S., Daengsubha, W., Yoshikawa, H., Yui, M., Nozaki, K., Nakajima, T. & Nakamura, I. 1988. Screening of anaerobic bacteria with the ability to decolorize molasses melanoidin. *Agricultural and Biological Chemistry,* 52**,** 2429-2435.

Ortegón, G. P., Arboleda, F. M., Candela, L., Tamoh, K. & Valdes-Abellan, J. 2016. Vinasse application to sugar cane fields. effect on the unsaturated zone and groundwater at Valle Del Cauca (Colombia). *Science of the Total Environment,* 539**,** 410-419.

Østergaard, K., Tohidi, B., Danesh, A., Burgass, R., Todd, A. & Baxter, T. 2000. A novel approach for oil and gas separation by using gas hydrate technology. *Annals of the New York Academy of Sciences,* 912**,** 832-842.

Pala, A. & Erden, G. 2005. Decolorization of a baker's yeast industry effluent by fenton oxidation. *Journal of Hazardous Materials,* 127**,** 141-148.

Pandey, R., Malhotra, S., Tankhiwale, A., Pande, S., Pathe, P. & Kaul, S. 2003. Treatment of biologically treated distillery effluent - A case study. *International Journal of Environmental Studies,* 60**,** 263-275.

Pant, D. & Adholeya, A. 2007. Biological approaches for treatment of distillery wastewater: A review. *Bioresource Technology,* 98**,** 2321-2334.

Park, K.-N., Hong, S. Y., Lee, J. W., Kang, K. C., Lee, Y. C., Ha, M.-G. & Lee, J. D. 2011. A new apparatus for seawater desalination by gas hydrate process and removal characteristics of dissolved minerals (Na^+, Mg^{2+}, Ca^{2+}, K^+, B^{3+}). *Desalination,* 274**,** 91-96.

Park, M.-H., Park, N.-S., Park, H., Shin, H.-S. & Kim, B.-D. 1997. An economic analysis of desalination for potential application in Korea. *Desalination,* 114**,** 209-221.

Parker, D. 2009. *How SA could liberate power and fuel from its sugar cane fields* [Online]. Available: Http://Www.Engineeringnews.Co.Za/Article/How-Sa-Could-Liberate-Power-And-Fuel-From-Its-Sugar-Cane-Fields-2009-08-07 [Accessed 17 April 2016].

Parrish, W. R. & Prausnitz, J. M. 1972. Dissociation pressures of gas hydrates formed by gas mixtures. *Industrial & Engineering Chemistry Process Design And Development,* 11**,** 26-35.

Patel, A., Pawar, P., Mishra, S. & Tewari, A. 2001. Exploitation of marine cyanobacteria for removal of color from distillery effluent. *Indian Journal of Environmental Protection,* 21**,** 1118-1121.

Pathak, H., Joshi, H., Chaudhary, A., Chaudhary, R., Kalra, N. & Dwiwedi, M. 1999. Soil amendment with distillery effluent for wheat and rice cultivation. *Water, Air, and Soil Pollution,* 113**,** 133-140.

Patil, P., Kapadnis, B. & Dhamankar, V. 2003. Decolorisation of synthetic melanoidin and biogas effluent by immobilised fungal isolate of aspergillus niger UM2. *International Sugar Journal,* 105**,** 8, 10-13.

Patwardhan, V.S & Kumar, A. 1986. A unified approach for prediction of thermodynamic properties of aqueous mixed-electrolyte solutions. *Vapour Pressure and Heat of Vapourization, AIChE J*, 32, 1419.

Pena, M., Coca, M., Gonzalez, G., Rioja, R. & Garcıa, M. 2003. Chemical oxidation of wastewater from molasses fermentation with ozone. *Chemosphere,* 51**,** 893-900.

Peters, C., De Roo, J. & De Swaan Arons, J. 1993. Phase equilibria in binary mixtures of propane and hexacontane. *Fluid Phase Equilibria,* 85**,** 301-312.

Peters, C., Lichtenthaler, R. & De Swaan Arons, J. 1986. Three phase equilibria in binary mixtures of ethane and higher n-alkanes. *Fluid Phase Equilibria,* 29**,** 495-504.

Peters, M. S. & Timmerhaus, K. D. 1968. Plant design and economics for chemical engineers. New-York: Mcgraw-Hill.

Petticrew, C. 2011. *An investigation into the use of fluorinated hydrating agents in the desalination of industrial wastewater.* MSc Engineering, University Of Kwazulu-Natal.

Phillips, L. 2011. *Can South Africa run on sugar power?* [Online]. Available: Http://Www.Farmersweekly.Co.Za/Article.Aspx?Id=10940&H=Can-South-Africa-Run-On-Sugar-Power [Accessed 20 April 2016].

Poling, B. E., Prausnitz, J. M. & O'connell, J. P. 2001. *The properties of gases and liquids,* New York, Mcgraw-Hill.

Prasad, R. K. & Srivastava, S. 2009. Electrochemical degradation of distillery spent wash using catalytic anode: factorial design of experiments. *Chemical Engineering Journal,* 146**,** 22-29.

Prasad, S., Singh, A. & Joshi, H. 2007. Ethanol As an alternative fuel from agricultural, industrial and urban residues. *Resources, Conservation and Recycling,* 50**,** 1-39.

Raal, J. D. & Mühlbauer, A. L. 1998. *Phase equilibria : Measurement and computation,* Washington, D.C., Taylor & Francis.

Raeissi, S. 2004. *On the phenomenon of double retrograde vaporization: within a study on supercritical deterpenation of orange oils with ethane*, Tu Delft, Delft University of Technology.

Raghukumar, C., Mohandass, C., Kamat, S. & Shailaja, M. S. 2004. Simultaneous detoxification and decolorization of molasses spent wash by the immobilized white-rot fungus flavodon flavus isolated from a marine habitat. *Enzyme and Microbial Technology,* 35**,** 197-202.

Rais, M. & Sheoran, A. 2015. Treatment of sugarcane industry effluents: science & technology issues. *International Journal of Engineering Research and Applications,* 5**,** 11-19.

Rajeshwari, K. V., Balakrishnan, M., Kansal, A., Lata, K. & Kishore, V. V. N. 2000. State-of-the-art of anaerobic digestion technology for industrial wastewater treatment. *Renewable and Sustainable Energy Reviews,* 4**,** 135-156.

Ramana, S., Biswas, A., Singh, A. & Yadava, R. 2002. Relative efficacy of different distillery effluents on growth, nitrogen fixation and yield of groundnut. *Bioresource Technology,* 81**,** 117-121.

Reddy, W. 2013. *Desalination of industrial waste water using gas hydrates and promoters.* Msc. Eng (Chemical Engineering), University of Kwazulu-Natal.

Richon, D. 1996. New experimental developments for phase equilibrium measurements. *Fluid Phase Equilibria,* 116**,** 421-428.

Robinson, D. & Metha, B. 1971. Hydrates in the propane-carbon dioxide-water system. *Journal of Canadian Petroleum Technology,* 10**,** 33-35.

Robinson, D. B. & Ng, H. J. 1986. Hydrate formation and inhibition in gas or gas condensate streams. *Journal of Canadian Petroleum Technology,* 25**,** 26-30.

Ruffine, L., Donval, J.-P., Charlou, J.-L., Cremière, A. & Zehnder, B. 2010. Experimental study of gas hydrate formation and destabilisation using a novel high-pressure apparatus. *Marine and Petroleum Geology,* 27**,** 1157-1165.

Sabil, K. B. M. 2009. *Phase behaviour, thermodynamics and kinetics of clathrate hydrate systems of carbon dioxide in presence of tetrahydrofuran and electrolytes.* Master of Science in Chemical Engineering, Universiti Sains Malaysia, Malaysia.

Salomon, K. R. & Lora, E. E. S. 2009. Estimate of the electric energy generating potential for different sources of biogas in Brazil. *Biomass and Bioenergy,* 33**,** 1101-1107.

Sanchez Riera, F., Cordoba, P. & Siñeriz, F. 1985. Use of the UASB reactor for the anaerobic treatment of stillage from sugar cane molasses. *Biotechnology and Bioengineering,* 27**,** 1710-1716.

Sangave, P. C., Gogate, P. R. & Pandit, A. B. 2007. Combination of ozonation with conventional aerobic oxidation for distillery wastewater treatment. *Chemosphere,* 68**,** 32-41.

Satyawali, Y. & Balakrishnan, M. 2007. Removal of color from biomethanated distillery spentwash by treatment with activated carbons. *Bioresource Technology,* 98**,** 2629-2635.

Satyawali, Y. & Balakrishnan, M. 2008. Wastewater treatment in molasses-based alcohol distilleries for cod and color removal: A review. *Journal of Environmental Management,* 86**,** 481-497.

Schroeter, J., Kobayashi, R. & Hildebrand, M. 1983. Hydrate decomposition conditions in the system hydrogen sulfide-methane-propane. *Industrial & Engineering Chemistry Fundamentals,* 22**,** 361-364.

Seth, R.,Goyal, S. & Handa, B. 1995. Fixed film biomethanation of distillery spentwash using low cost porous media. *Resources, Conservation and Recycling,* 14**,** 79-89.

Shahnazar, S. & Hasan, N. 2014. Gas hydrate formation condition: review on experimental and modeling approaches. *Fluid Phase Equilibria,* 379**,** 72-85.

Shayegan, J., Pazouki, M. & Afshari, A. 2005. Continuous decolorization of anaerobically digested distillery wastewater. *Process Biochemistry,* 40**,** 1323-1329.

Sirianuntapiboon, S., Phothilangka, P. & Ohmomo, S. 2004a. Decolorization of molasses wastewater by a strain No. BP103 of acetogenic bacteria. *Bioresource Technology,* 92**,** 31-39.

Sirianuntapiboon, S., Sihanonth, P., Somchai, P., Atthasampunna, P. & Hayashida, S. 1995. An absorption mechanism for the decolorization of melanoidin by rhizoctonia Sp. D-90. *Bioscience, Biotechnology, and Biochemistry,* 59**,** 1185-1189.

Sirianuntapiboon, S., Somchai, P., Sihanonth, P., Atthasampunna, P. & Ohmomo, S. 1988. Microbial decolorization of molasses waste water by mycelia sterilia D90. *Agricultural and Biological Chemistry,* 52**,** 393-398.

Sirianuntapiboon, S., Zohsalam, P. & Ohmomo, S. 2004b. Decolorization of molasses wastewater by citeromyces Sp. WR-43-6. *Process Biochemistry,* 39**,** 917-924.

Sloan , E. D. 1998. *Clathrate Hydrates of Natural Gases,* New York, Marcel Decker.

Sloan, E. D. 2000. Clathrate Hydrates: The other common solid water phase. *Industrial & Engineering Chemistry Research,* 39**,** 3123-3129.

Sloan, E. D. 2004. Introductory overview: Hydrate knowledge development. *American Mineralogist,* 89**,** 1155-1161.

Sloan, E. D., Khoury, F. M. & Kobayashi, R. 1976. Water content of methane gas in equilibrium with hydrates. *Ind. Eng. Chem. Fund. Industrial & Engineering Chemistry Fundamentals,* 15**,** 318-323.

Sloan, E. D. & Koh, C. 2008. *Clathrate Hydrates of Natural Gases,* New York, CRC Press.

Sloan, E. D., Sparks, K. A. & Johnson, J. J. 1987. Two-phase liquid hydrocarbon-hydrate equilibrium for ethane and propane. *Industrial & Engineering Chemistry Research,* 26**,** 1173-1179.

Smith, A. 2015. *Phase equilibria of refrigerant gas hydrate systems in the presence of sucrose.* MSc Engineering, University Of Kwazulu-Natal.

Smith, J., Van Ness, H. & Abbott, M. 2005. *Introduction to chemical engineering thermodynamics. Seventh Edition*, Mcgraw-Hill.

SMRI 2014. Call for research and development funding proposals. *In:* Institue, S.M.R.& Technology, D.O.S.A. (Eds.).

SMRI. 2016. *Personal communication.*

Søreide, I. & Whitson, C. H. 1992. Peng-Robinson predictions for hydrocarbons, CO_2, N_2, And H_2S with pure water and NaCl brine. *Fluid Phase Equilibria,* 77**,** 217-240.

Sreethawong, T. & Chavadej, S. 2008. Color removal of distillery wastewater by ozonation in the absence and presence of immobilized iron oxide catalyst. *Journal of Hazardous Materials,* 155**,** 486-493.

Sugahara, T., Murayama, S., Hashimoto, S. & Ohgaki, K. 2005. Phase equilibria for $H_2 + CO_2 + H_2O$ system containing gas hydrates. *Fluid Phase Equilibria,* 233**,** 190-193.

Syutsubo, K., Harada, H., Ohashi, A. & Suzuki, H. 1997. An effective start-up of thermophilic uasb reactor by seeding mesophilically-grown granular sludge. *Water Science and Technology,* 36**,** 391-398.

Taheri, Z., Shabani, M. R., Nazari, K. & Mehdizaheh, A. 2014. Natural gas transportation and storage by hydrate technology: Iran case study. *Journal of Natural Gas Science and Engineering,* 21**,** 846-849.

Tajima, H., Yamasaki, A. & Kiyono, F. 2004. Energy consumption estimation for greenhouse gas separation processes by clathrate hydrate formation. *Energy,* 29**,** 1713-1729.

Taylor, B. N. & Kuyatt, C. E. 1994. *Guidelines for evaluating and expressing the uncertainty of nist measurement results*, UD Department of Commerce, Technology Administration, National Institute of Standards and Technology Gaithersburg, Md.

Tohidi, B., Burgass, R., Danesh, A., Østergaard, K. & Todd, A. 2000. Improving the accuracy of gas hydrate dissociation point measurements. *Annals of The New York Academy of Sciences,* 912**,** 924-931.

Tohidi, B., Burgass, R. W., Danesh, A. & Todd, A. C. Application of quartz crystal microbalance to gas hydrate stability zone measurements. 4th International conference on gas hydrates, 2002 Yokohama. 380-383.

Tohidi, B., Danesh, A. & Todd, A. 1995. Modelling single and mixed electrolyte solutions and its applications to gas hydrates. *Chemical Engineering Research & Design,* 73**,** 464-472.

Tohidi, B., Danesh, A., Todd, A. & Burgass, R. 1997. Hydrate-free zone for synthetic and real reservoir fluids in the presence of saline water. *Chemical Engineering Science,* 52**,** 3257-3263.

Tondee, T., Sirianuntapiboon, S. & Ohmomo, S. 2008. Decolorization of molasses wastewater by yeast strain, issatchenkia orientalis No. SF9-246. *Bioresource Technology,* 99**,** 5511-5519.

Tshibangu, M. M. 2010. *Measurements of HP-VLE data for fluorinated systems.* Msc Thesis, University Of Kwa-Zulu Natal.

Vadivel, R., Minhas, P. S., Kumar, S., Singh, Y., Dvk, N. R. & Nirmale, A. 2014. Significance of vinasses waste management in agriculture and environmental quality - review. *African Journal of Agricultural Research,* 9**,** 2862-2873.

Vahabzadeh, F., Mehranian, M. & Saatari, A. 2004. Color removal ability of phanerochaete chrysosporium in relation to lignin peroxidase and manganese peroxidase produced in molasses wastewater. *World Journal of Microbiology and Biotechnology,* 20**,** 859-864.

Valderrama, J. O. 1990. A Generalized patel-teja equation of state for polar and nonpolar fluids and their mixtures. *Journal of Chemical Engineering of Japan,* 23**,** 87-91.

Valderrama, L. T., Del Campo, C. M., Rodriguez, C. M., De-Bashan, L. E. & Bashan, Y. 2002. Treatment of recalcitrant wastewater from ethanol and citric acid production using the microalga chlorella vulgaris and the macrophyte lemna minuscula. *Water Research,* 36**,** 4185-4192.

Van Der Waals, J. & Platteeuw, J. 1959. Clathrate solutions. *Advances In Chemical Physics,* 2**,** 1-57.

Villard, P. 1888. Sur Quelques Nouveaux Hydrates De Gaz. Compt. Rend., 106, 1602-1603.

Villard, P. 1890. Sm Quelques Noiiveaux Hydrates De Gaz. Compt. Rend, 111, 302.

Wang, P., Anderko, A., Springer, R.D. and Young, R.D. 2006. Modeling phase equilibria and speciation in mixed-solvent electrolyte systems: II. Liquid–liquid equilibria and properties of associating electrolyte solutions. *Journal of Molecular Liquids*, *125*(1), pp.37-44.

Wang, P., Anderko, A. and Young, R.D. 2002. A speciation-based model for mixed-solvent electrolyte systems. *Fluid Phase Equilibria*, *203*(1-2), pp.141-176.

Wang, P., Springer, R.D., Anderko, A. and Young, R.D. 2004. Modeling phase equilibria and speciation in mixed-solvent electrolyte systems. *Fluid Phase Equilibria*, *222*, pp.11-17.

Wang, X., Dennis, M. & Hou, L. 2014. Clathrate hydrate technology for cold storage in air conditioning systems. *Renewable and Sustainable Energy Reviews,* 36**,** 34-51.

Werezak, G. N. 1969. Aqueous solution concentration by a clathrate hydrate type of gas hydrate formation. *Chemical Engineering Progress Symposium Series: Unusal Methods of Separation,* 65**,** 6-18.

Wessel, H. 1952. New graph correlates operating laor for chemical process. *Chem. Eng.,* 57**,** 209-210.

Wierzchowski, S. & Monson, P. 2006. Calculating the phase behavior of gas-hydrate-forming systems from molecular models. *Industrial & Engineering Chemistry Research,* 45**,** 424-431.

Wilcox, W. I., Carson, D. B. & Katz, D. L. 1941. Natural gas hydrates. *Industrial & Engineering Chemistry,* 33**,** 662-671.

Wilkie, A. C., Riedesel, K. J. & Owens, J. M. 2000. Stillage characterization and anaerobic treatment of ethanol stillage from conventional and cellulosic feedstocks. *Biomass And Bioenergy,* 19**,** 63-102.

Yang, S., Cho, S., Lee, H. & Lee, C. 2001. Measurement and prediction of phase equilibria for water + methane in hydrate forming conditions. *Fluid Phase Equilibria,* 185**,** 53-63.

Yeoh, B. 1997. Two-phase anaerobic treatment of cane-molasses alcohol stillage. *Water Science And Technology,* 36**,** 441-448.

Zemaitis, J.F., Clark, D.M., Rafal, M. & Scrivner, N.D., 1986. Handbook of aqueous electrolyte thermodynamics: theory & application. John Wiley & Sons.

Zhang, J., Lee, S. & Lee, J. W. 2007. Kinetics of methane hydrate formation from sds solution. *Industrial & Engineering Chemistry Research,* 46**,** 6353-6359.

Zulu, I. 27 September 2016. *Personal communication.*

Zuo, J. Y., Zhang, D. & Stenby, E. H. 2001. A thermodynamic model for gas hydrates in the presence of salts and methanol. *Chemical Engineering Communications,* 184**,** 175-192.

VINASSE CHARACTERISTICS AND TREATMENT METHODS

A.1 Vinasse Characterization

A detailed literature survey was conducted on the characteristics of molasses-derived vinasse. The results of the literature survey are shown in Table A-1 below.

Table A-1: Characteristics of molasses-derived vinasse from different literature sources.

Reference	1	1	1	1	1	2	3	4	5	6	7
pH	4.8			4.3	4.5	4.5	4.2 - 4.3	3.0 - 4.5	4	4.5	3.5 - 4
TSS							2000 - 2200	13000 - 15000	16357	4578	350
Dissolved solids							89000 - 91000	90000 -150000	68182	16866	80000
Total solids			91750	69322				110000 - 190000		214444	30000 -100000
BOD						50000	52000 - 58000	50000 - 60000	48000	7752	30000 - 70000
COD						95000	92000 - 100000	110000 - 190000	108400	13824	65000 - 130000
Chlorides							5800 - 7600	8000 - 8500	6500	1300	
Sulphide							600 - 700				
Sulphates						1500	2100 - 2300	7500 - 9000	4940	120	2000 - 6000
Nitrates											
Nitrogen	408	3160	1835	1019	153	1000		5000 - 7000		604.8	1000 - 2000
Sodium											
Phosphorus	102	20	12	5097	1	40	300 - 400	2500 - 2700	220	2	800 - 1200
Potassium	4893	8767	10704	4078	9073	11000	8700 - 9700		7650		8000 - 12000
Calcium	714	1121	2039		143		750000 - 820000		2200		
Magnesium	204	1529	1325		61						
Manganese											
Iron							15500 - 18000		28		
Copper									26	1.71	

Table A-1 (continued): Characteristics of molasses-derived vinasse from different literature sources.

Reference	1	1	1	1	1	2	3	4	5	6	7
Phenols								8000 - 10000		34	
Ethanol											
Acetic Acid											
Propionic Acid											

All values are expressed in mg/L except pH, TSS: total suspended solids, REF: (1) Cortez and Brossard Pérez (1997); (2) Pathak et al. (1999); (3) Nandy et al. (2002); (4) Acharya et al. (2008);

(5) Chaudhari et al. (2008); (6) Kannan and Upreti (2008); (7) Satyawali and Balakrishnan (2008)

Table A-1 (continued): Characteristics of molasses-derived vinasse from different literature sources.

Reference	8	9	9	9	9	9	9	10	11	12	13	14
Parameter												
pH	4.2-5.0	4.1	4	3.7	3.9	4	3.7	4	4.31	3.9	3.1-4.7	3.98 - 5.1
TSS								20273			2500 - 5000	
Dissolved solids		87000	103000	85000	69000	88000	106000	45543	10500		9000 - 21000	117416 - 599400
Total solids	81500	117000	125000	119000	99000	121000	129000				70000 - 95000	
BOD	25000	50000	43000	49000	52000	40000	50000		36666.67	5046	42000 - 51000	
COD	65000	96000	105000	90000	86000	91000	89000	121000	117000		85000 - 100000	
Chlorides												271 - 13980
Sulphide								168				
Sulphates								5336	820	710	4500 - 7200	8901 - 35670
Nitrates									600			
Nitrogen	450 - 1600	1338	1289	1064	980	1127	1305	1341			800 - 1200	
Sodium										50.2		90.7 - 1671
Phosphorus	100 - 290	34	33	30	23	29	38	141	78	190	180 - 350	8.7 - 297
Potassium	3740 - 7830	7875	12187	7375	8375	9168	7656	7262		2056	6000 - 12000	4698 - 46950
Calcium	450 - 5180								1734.67	719		879 - 10133
Magnesium	420 - 1520									237		1272 - 6080
Manganese		0.42	0.28	0.33	0.34	0.22	0.26		14			23 - 6410

Table A-1 (continued): Characteristics of molasses-derived vinasse from different literature sources.

Reference	8	9	9	9	9	9	9	10	11	12	13	14
Iron		12.7	9.7	8.8	6.1	7.7	9.6		17			0.5 - 21125
Copper		0.27	0.22	0.43	0.17	0.21	0.16		86	0.35		
Phenols												4.8
Ethanol								21007				
Acetic Acid								2237				
Propionic Acid								4304				

All values are expressed in mg/L except pH, TSS: total suspended solids, REF: (8) Salomon and Lora (2009); (9) Kumari and Phogat (2010); (10) España-Gamboa et al. (2012); (11) Ahmed et al. (2013); (12) Christofoletti et al. (2013); (13) Chaudhary et al. (2013), (14) Ortegón et al. (2016)

A.2 Current vinasse treatment methods

A.2.1 Anaerobic treatment

The high organic content of vinasse brands anaerobic treatment more appealing compared to aerobic treatment; and it is widely accepted as the important, first step in the treatment of vinasse (Pant and Adholeya, 2007; Satyawali and Balakrishnan, 2008).

Aerobic treatment is not recommended as the first stage of treatment due to the high energy consumption for aeration and cooling. In addition, 50% of the COD is converted to sludge (España-Gamboa et al., 2011). In contrast anaerobic digestion produces less sludge (10% of the sludge yield of aerobic treatment), requires less energy, can be successfully operated at high organic loading rates, and requires less nutrients (Wilkie et al., 2000; Mohana et al., 2009). More importantly, anaerobic digestion is capable of converting a significant portion of the effluents COD (>50%) into biogas (Wilkie et al., 2000; España-Gamboa et al., 2011).

Vinasse, with a COD of over 100 g/L, has been found to inhibit stable digestion. This may be overcome by dilution of the vinasse to a COD level of approximately 50 g/L, using other waste streams at the plant. Despite its advantages, the high potassium, heavy metal, sulphate, and phenolic compound levels present in vinasse, comprise a deficiency of anaerobic treatment (Wilkie et al., 2000). The main colour component present in vinasse, the melanoidins, are difficult to degrade via anaerobic treatments, so aerobic and physico-chemical treatments are needed as refining treatments (Wilkie et al., 2000).

Anaerobic systems may be operated as either a single-phase or two-phase system. In single-phase systems, only one reactor is used for the organic matter to be digested by the microorganisms, whereas in two-phase systems, the acidogenic and methanogenic organisms are separated into two separate reactors. However, the simplest option for the anaerobic treatment of vinasse is anaerobic lagoons. Large land area requirements, odour generation, and the possibility of ground water contamination (as the lagoons are generally unlined) restrict their use (Satyawali and Balakrishnan, 2008). Even though anaerobic lagoons are still employed in some distilleries, high rate anaerobic reactors are more popular (Lata et al., 2002). The advantage of high rate reactors is that hydraulic retention time can be separated from the solids retention time, allowing slow growing anaerobic microorganisms to remain in the reactor independent of the vinasse flow.

A fixed film, upflow anaerobic sludge blanket (UASB), and a fluidized bed reactor (Figures A-1 to A-3), are the most common types of reactors used in the treatment of vinasse. These reactors are

analysed and compared in Table A-2, and their performance in the treatment of molasses-derived vinasse, in both lab studies and pilot/commercial scale operations, is summarized in Table A-3.
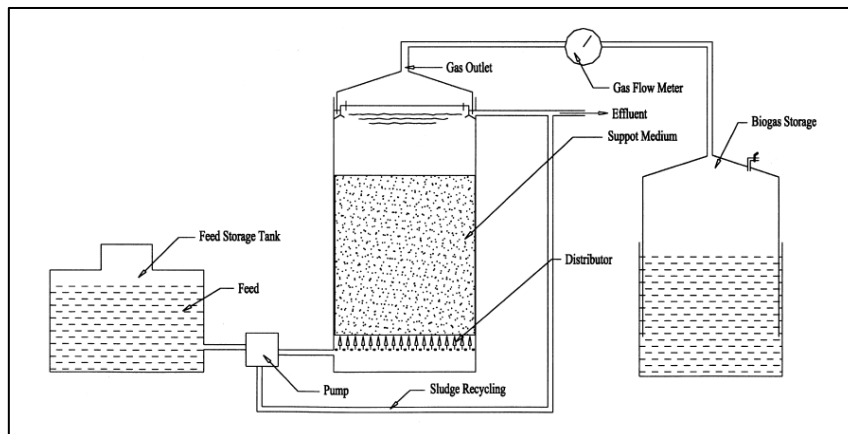
Figure A-1: Fixed film reactor (Rajeshwari et al., 2000).
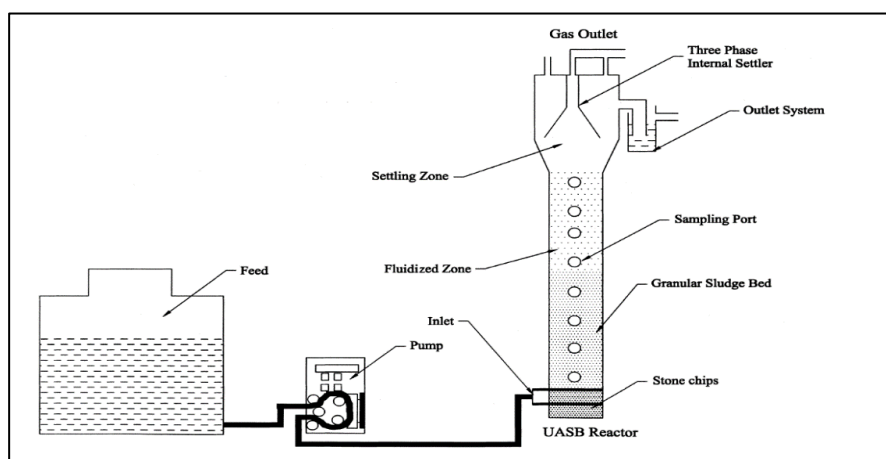
Figure A-2: Up flow anaerobic sludge blanket reactor (UASB) (Rajeshwari et al., 2000).
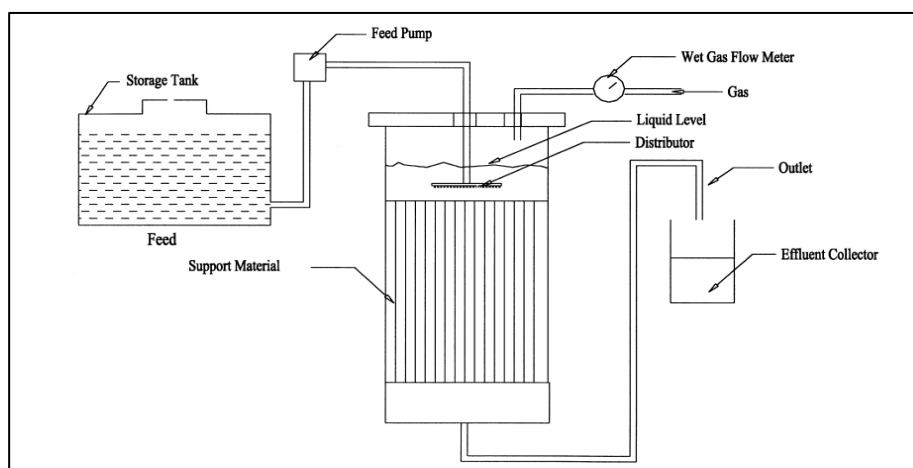
Figure A-3: Anaerobic fluidized bed reactor (Rajeshwari et al., 2000).

Table A-2: Comparison of commonly used high rate reactors for anaerobic treatment of vinasse.

Configuration	Fixed Film	UASB	Fluidized Bed
Description	The reactor has an inert support structure (media) for biomass immobolization e.g activated carbon, glass beads or sand. The vinasse is distributed from either above or below the media. The microorganisms attach themselves to one another creating a thin biofilm.	The most utilized high rate reactor for the treatment of industrial wastewaters such as vinasse. A UASB is only suitable for the treatment of vinasse when the process has a successful start-up and stable operation. The reactor may be operated under mesophilic or thermophilic conditions.	Small particle sized inorganic media such as sand, gravel, activated carbon, anionic and cationic exchange resin is used for the bacterial attachment and growth. The drag forces exerted by the vinasse maintains the fluidized state. A large surface area for biofilm formation and growth is provided by each media under the fluidized state. The reactors may be operated in either upflow or downflow modes.
Advantages	- Simplicity of construction, elimination of mechanical mixing, better stability at higher loading rates. - Able to withstand toxic shock loads - Quick recovery after periods of starvation. - Higher COD removal at lower hydraulic retention times. - Limited loss of biomass due to support.	- Simple construction and therefore less investment requirements. - Mechanical mixing of digester contents and effluent recycle is not necessary. - Capable of coping with disturbances caused by temperature fluctuations and high loading rates.	- Removal of bed clogging - Low hydraulic head loss and improved hydraulic circulation. - Greater surface area per unit of reactor volume and reduced capital cost due to smaller reactor volume. - Favours the transport of microbial cells from bulk to the surface, enhancing the contact between the microorganisms and the substrate.

Table A-2 (continued): Comparison of commonly used high rate reactors for anaerobic treatment of vinasse.

Configuration	Fixed Film	UASB	Fluidized Bed
Disadvantages	- High reactor volume compared to others due to volume occupied by inert support. - Clogging of reactor due to increase in biofilm thickness and/or high suspended solids concentration in the vinasse.	- Long start up period. - Requires a sufficient amount of seed sludge for faster start-up. - Significant wash-out of sludge during the initial phase of the process. - Requires skilled operation.	- Recycling of effluent may be necessary to achieve bed expansion.

Table A-3: Performance of various anaerobic reactors for molasses-derived vinasse (edited and updated from Satyawali and Balakrishnan, 2008).

Reactor configuration	Size (L)	Operating conditions	HRT (days)	Influent COD (g/L)	COD loading rates (g COD/L.day)	COD removal (%)	References
Downflow fixed film reactor packed with plastic medium	10 000	Mesophilic	3.3 - 2.5	NR	14.2 - 20.4	60 - 73	Bories et al. (1988)
Upflow fixed film reactor with clay brick granules	5.25	Mesophilic	3	66	22	71.8	Seth et al. (1995)
Upflow fixed film reactor with granular activated carbon	5.25	Mesophilic	4	85	21.3	67	Goyal et al. (1996)
UASB	140	Thermophilic		10	Up to 28	36 - 67	Harada et al. (1996)
UASB	100	Mesophilic	2	46	23.3	71.3	Sanchez Riera et al. (1985)
UASB	12.8	Thermophilic	0.3	3	Up to 30	87	Syutsubo et al. (1997)
Fluidized bed reactors with natural zeolite	5.9	Mesophilic	0.46	63	Up to 20	80	Fernández et al. (2008)
UASB	2.3	Mesophilic	3.2	68.9	21.5	58	Espinosa et al. (1995)
UASB	42.5	Mesophilic	10	100	10	67	Driessen et al. (1994)

Table A-3 (continued): Performance of various anaerobic reactors for molasses-derived vinasse (edited and updated from Satyawali and Balakrishnan, 2008).

Reactor configuration	Size (L)	Operating conditions	HRT (days)	Influent COD (g/L)	COD loading rates (g COD/L.day)	COD removal (%)	References
UASB	42.5	Mesophilic	6.8	109	16	67	Driessen et al. (1994)
Two-phase thermophilic system:							
Acidogenic phase	3.6	Thermophilic	2.0	154 - 115	4.6 - 20	1.5 - 3.2	Yeoh (1997)
Methanogenic phase	5.0	Thermophilic	32.7 – 5.6	152 – 111[*]		72.8 - 64.0	

* Methanogenic reactor was fed with acidified substrate from acidogenic reactor (effluent COD from Acidogenic reactor = influent COD to methanogenic reactor).

A.2.2 Aerobic treatment

The anaerobically treated vinasse still has a high organic content, its characteristic dark brown colour, and cannot be discharged. The vinasse, therefore, undergoes a secondary treatment. Solar drying is one option. However, a large land requirement limits this practice. In addition, solar beds become non-functional during the rainy season (Nandy et al., 2002). Aquaculture, constructed wetlands, and biocomposting treatment methods, have also been used for further treatment of anaerobically treated vinasse (Satyawali and Balakrishnan, 2008).

The most common post-anaerobic treatment method is the activated sludge process (aerobic digestion). Several microorganisms such as fungi, white rot fungi, yeast, algae, and bacteria have been reported for use in further treatment and decolourization of vinasse. A consortium of microorganisms is more effective in the treatment, because the maintenance of microorganisms and co-metabolism increase the efficiency of the melanoidin decolourization (Jiranuntipon et al., 2008). Anaerobic treatment using different microorganisms is discussed briefly below.

A.2.2.1 Fungal systems

Fungi consume organic substances in vinasse, thereby reducing the BOD and COD levels. Valuable products are obtained from this process, such as sludge biomass that, due to its high protein content, can be used as an animal feed. A specific metabolite can also be obtained (Pant and Adholeya, 2007). Several fungi have been investigated for their ability to degrade and decolourize vinasse, with *Aspergillus sps*. being one of the most studied. The decolourisation of vinasse is a result of two decomposition mechanisms (Ohmomo et al., 1988). In the first mechanism, melanoidins with lower molecular weight are attached, and in the second mechanism, those with a high molecular weight are attacked. The immobilization of fungi offers the advantage of shorter retention time, easy cell recovery, and increased activity (Pant and Adholeya, 2007). Filamentous fungi have lower sensitivity to variations in temperature, pH, nutrients, and aeration, but are a comparatively, slow-growth species and are more susceptible to infection (Knapp et al., 2001). Yeast has also been investigated for treatment of vinasse. Yeast is characterised by quick growth, is less susceptible to contamination by other microorganisms, and produces biomass with a high nutrient value (Friedrich, 2004). A summary of the various fungi employed for the treatment of molasses-derived vinasse and their performance is summarised in Table A-4.

Table A-4: Fungi employed for the treatment of molasses-derived vinasse (edited and updated from Pant and Adholeya, 2007).

	Fungi	Comments	Colour Removal (%)	COD Removal (%)	Reference
1	*Phanerochaete chrysosporium*	Anaerobically treated vinasse. A readily available carbon source was required for melanoidin decolourization by both fungi. Maximum decolourization was detected in 6.25 % (v/v) vinasse.	53.5	73	Kumar et al. (1998)
	Coriolus versicolor		71.5	90	
2	*Phanerochaete chrysosporium* JAG-40	Decolourized diluted, synthetic melanoidin. Medium supplemented with glucose and peptone.	80	NR	Dahiya et al. (2001)
3	*Trametes versicolor* *	Biologically treated beet vinasse. Satisfactory results observed in the presence of a nutrient source (sucrose and KH_2PO_4)	82	77	Benito et al. (1997)
4	*Coriolus versicolor*	Biologically treated vinasse. Fungus was able to reduce the colour in 8 days. Glucose and peptone was required as an additional nutrient source	53	53	Chopra et al. (2004)
5	*Geotrichum candidum*	Molasses diluted to 40-50 g/l with water. Stable decolourization of molasses was achieved by fungus immobilized on polyurethane foam.	80	NR	Kim and Shoda (1999)
6	*Aspergillus niger* UM2	Immobilized fungus improved decolourization. Initial effluent concentrations was decolourized by up to 50 %.	80	NR	Patil et al. (2003)
7	*Mycelia sterilia*	For the decolourizing activity, the organism required glucose. A lower colour removal was obtained from biologically treated vinasse possibly due to the formation of toxic compounds.	93	NR	Sirianuntapiboon et al. (1988)
8	*Aspergillus niger* *	Biologically treated vinasse. When $MgSO_4$, KH_2PO_4, NH_4NO_3 and a carbon source was added to wastewater maximum colour removal was obtained.	69	75	Miranda et al. (1996)

Table A-4 (continued): Fungi employed for the treatment of molasses-derived vinasse (edited and updated from Pant and Adholeya, 2007).

	Fungi	Comments	Colour Removal (%)	COD Removal (%)	Reference
9	*Rhizoctonia* sp. D-90	Diluted vinasse. When glucose, NaNO₃, KH₂PO₄ and MgSO₄●7H₂O was added to wastewater maximum colour removal was obtained.	90	NR	Sirianuntapiboon et al. (1995)
10	*Coriolus hirsutus* IFO4917	Melanoidins present in heat treatment liquor were subjected to sequencing batch decolourization by the immobilized fungal cells.	45	NR	Fujita et al. (2000)
11	*Trametes* sp. I-62	Maximum decolourization at 20 % (v/v) vinasse.	73	62	González et al. (2000)
12	*Phanerochaete chrysosporium*	Effluent was treated in a RBC using polyurethane foam and scouring web as support.	55	48	Guimarães et al. (2005)
13	*Flavodon flavus*	10 % (v/v) Vinasse was decolourized using the fungus. It also removed 68 % benzo(a)pyrene, a PAH found in the effluent.	80	NR	Raghukumar et al. (2004)
14	*Coriolus versicolor*	30 % (v/v) vinasse. Cotton stalk addition stimulated the decolourization activity of all fungi.	63	49	Kahraman and Yeşilada (2003)
	Funalia trogii		57	62	
	Phanerochaete chrysosporium		37	57	
	Pleurotus pulmonarius		43	34	
15	*Aspergillus niveus*	A litter degrading fungi. A maximum removal of colour and organic matter was achieved in sugarcane bagasse at 1 % (W/v) concentration.	92	37	Angayarkanni et al. (2003)
16	*Aspergillus-UB2*	Results obtained with diluted wastewater.	75	NR	Shayegan et al. (2005)

Table A-4 (continued): Fungi employed for the treatment of molasses-derived vinasse (edited and updated from Pant and Adholeya, 2007).

	Fungi	Comments	Colour Removal (%)	COD Removal (%)	Reference
17	*Coriolus hirsutus*	Colour removal required a large amount of glucose. The decolourizing ability of the fungus was reduced by the addition of peptone.	80	NR	Miyata et al. (2000)
18	*Coriolus versicolor Ps4a*	Sugar-dependent and sugar-independent enzymes, were found to be responsible for the melanoidin decolourizing activity.	80	NR	Ohmomo et al. (1985)
19	*Phanerochaete chrysosporium*	6.25 % (v/v) vinasse. Glucose was added as a nutrient source.	85	NR	Fahy et al. (1997)
20	*Phanerochaete chrysosporium*	10 % (v/v) vinasse was incubated with an appropriate concentration of spores which resulted in the decolourization.	75	NR	Vahabzadeh et al. (2004)
21	*Citeromyces sp. WR-43-6*	Diluted vinasse. Both colour intensity and organic matter experienced high and stable removal efficiencies.	75	Almost 100	Sirianuntapiboon et al. (2004b)
22	*Issatchenkia orientalis*	Anaerobically treated vinasse. The wastewater contained 2.5% glucose, 0.1% NH4Cl, and 0.1% KH2PO4. The pH was adjusted to 5.0 at 30 C.	91.2	80	Tondee et al. (2008)

* Beet molasses; NR = Not reported.

A.2.2.2 Bacterial systems

The bacterial treatment of vinasse results in colour and COD removal. Biomass, CO_2, and volatile acids are produced as final products (Pant and Adholeya, 2007). It has been suggested that the melanoidins are decolourized by the activity of the reactive oxygen species, (O_2^-, H_2O^2), produced by the reactions of enzyme catalysis. Acetogenic bacteria degrade melanoidins by oxidative decomposition, thereby removing low molecular weight compounds in untreated vinasse, and almost all low and high molecular weight compounds in anaerobically treated vinasse (Pant and Adholeya, 2007; Satyawali and Balakrishnan, 2008). Despite the high organic load of anaerobically treated (or dilute) vinasse, there is very little available carbon. A nutrient source is, therefore, often used during treatment by bacteria (Satyawali and Balakrishnan, 2008).

A.2.2.3 Cyanobacterial/Algae systems

Treatment by microalgae removes nutrients, organic matter, and colour from vinasse, while producing oxygen for other organisms. Anaerobically treated vinasse provides satisfactory conditions for microalgae growth. Further cyanobacteria are considered ideal for the treatment of vinasse as they degrade polymers and oxygenate water bodies thereby reducing the BOD and COD levels (Mohana et al., 2009).

A summary of the various bacteria and algae employed for the treatment of molasses-derived vinasse and their performance is summarised in Table A-5 and Table A-6 respectively.

Table A-7 reports a summary of the consortium of microorganisms used for the treatment of vinasse and their performance.

Table A-5: Bacteria employed for the treatment of molasses-derived vinasse (edited and updated from Pant and Adholeya, 2007).

	Bacteria	Comments	Colour Removal (%)	COD Removal (%)	Reference
1	*Xanthomonas fragariae*	Glucose as a carbon source and NH₄Cl as a nitrogen source was required by all three strains. Compared to the immobilized cells, the decolourization efficiency of free cells was better.	76	73	Jain et al. (2002)
2	*Bacillus megaterium*		76	72	
3	*Bacillus cereus*		82	79	
4	*Bacillus smithii*	Decolourization occurred at 55 °C in 20 days under anaerobic conditions. Peptone or yeast extract was used as an added nutrient. Strain could not use vinasse as the sole carbon source.	35.5	NR	Nakajima-Kambe et al. (1999)
5	Lactobacillus hilgardii	Decolourization of the strain under optimal conditions was only 28%. Immobilization of the cells improved the decolourization.	40	NR	Ohmomo et al. (1988)
6	*Acetobacter acetii*	Anaerobically treated vinasse. The organism required glucose for the decolourization. For molasses pigments, the strain obtained a decolourization yield of 76.4%	73.5	NR	Sirianuntapiboon et al. (2004a)
7	*Pseudomonas fluorescens*	Diluted vinasse. Decolourization of 76% was achieved in non-sterile conditions and 90% in sterile conditions at 30°C over a 4 day period. The most effective carrier was found to be cellulose coated with collagen.	94	NR	Dahiya et al. (2001)
8	*Pseudomonas putida*	The organism required glucose as a carbon source which produced hydrogen peroxide and in turn reduced the colour. Vinasse was diluted to 12.5 %	60	44.4	Ghosh et al. (2002)

NR = Not reported.

Table A-6: Algae employed for the treatment of molasses-derived vinasse (edited and updated from Pant and Adholeya, 2007).

	Algae	Comments	Colour Removal (%)	COD Removal (%)	Reference
1	*Chlorella vulgaris*	Anaerobically treated 10% vinasse was further treated using the microalgae Chlorella vulgaris, which removed the organic matter, and macrophyte *Lemna minuscula,* which removed other organic matter, colour and precipitated the algae.	52	61	Valderrama et al. (2002)
2	*Oscillatoria boryana*	The marine filamentous, non- heterocystous cyanobacterium decolorized diluted vinasse (5% v/v). Hydrogen peroxide, hydroxyl ions and molecular oxygen was released by the organism during photosynthesis. Study found that the cyanobacteria was able to use melanoidin as a better nitrogen source than carbon.	60	NR	Kalavathi et al. (2001)
3	*Oscillatoria sp.*	Colour reduction through bio flocculation. The consortium of the three strains showed the maximum decolourization of 98%.	96	NR	Patel et al. (2001)
	Lyngbya sp.		81	NR	
	Synechocystis		26	NR	

NR = Not reported.

Table A-7: Consortium of microorganisms employed for the treatment of molasses-derived vinasse (edited and updated from Pant and Adholeya, 2007).

	Consortium	Comments	Colour Removal (%)	COD Removal (%)	Reference
1	*Pseudomonas aeruginosa* Stenotrophomonas maltophila Proteus mirabilis	Consortium made up of three strains. The anaerobically treated vinasse was decolourized in the presence of basal salts and glucose. Maximum decolourization was achieved at 24 h and maximum COD reduction were achieved at 72 h.	67	51	Mohana et al. (2007)
2	Klebsiella oxytoca *Serratia mercescens* *Citrobacter* sp. Unidentified strain of bacteria	Decolourization on a 20 % (v/v) diluted vinasse was obtained after 2 days and a pH of 4.	17.5		Jiranuntipon et al. (2008)
3	*Phragmites australis* (L.) rhizosphere	15 culturable rhizosphere bacteria collectively brought about the decolourization.	71	86	Chaturvedi et al. (2006)

NR = Not reported.

A.2.3 Physico-chemical treatment

Biological treatment by anaerobic and aerobic methods can still leave vinasse with a BOD of 250 - 500 mg/l (Rais and Sheoran, 2015), as well as its dark colour. Melanoidins are barely affected by the conventional biological treatment (Migo et al., 1993). In fact, anaerobic and aerobic treatment processes can only accomplish the degradation of approximately 6 - 7 % of the melanoidins. Further, the dark colour could intensity if re-polymerisation of melanoidins occurs (Pena et al., 2003). Physico-chemical treatments, such as adsorption, are therefore applied to remove the colour. The majority of physico-chemical methods remove colour by concentrating the colour into sludge, or by partial or complete breakdown of the colour molecules. It is important to note that the use of an individual physico-chemical process, alone, may not result in the adequate treatment of vinasse and often a combination of these processes is necessary to achieve the desired results.

A.2.3.1 Adsorption

Activated carbon (AC) is a widely used adsorbent for the removal of organic pollutants from wastewater. The extended surface area, microporous structure, and high adsorption capacity makes AC very efficient in the adsorption of melanoidins and dark composites in vinasse, however, its high cost restricts its use. AC prepared from different precursors such as bagasse have been investigated. The use of activated carbon as a single process for decolourization of vinasse is inefficient, and combined treatments such as coagulation, followed by adsorption, may result in complete decolourization (Satyawali and Balakrishnan, 2008).

A.2.3.2 Coagulation-flocculation

This treatment involves the addition of a coagulant, such as aluminium or iron salts, which produces a flocculent precipitate that facilitates the separation of the suspended materials in the vinasse.

A.2.3.3 Oxidation process

Ozone is a strong oxidant, capable of oxidizing both biodegradable and non-biodegradable organics. As a result, it is widely used as a disinfectant in the production of drinking water. Ozone is soluble in water, and is readily available for immediate reaction with an organic compound present in the vinasse, without the formation of by-products that need to be removed (Sreethawong and Chavadej,

2008). In the presence of UV radiation and hydrogen peroxide, ozone increases the efficiency of simple ozonation from the generation of free radicals, which are very reactive and oxidizing (Benitez et al., 2003). Oxidation by ozone does not only achieve decolourization of vinasse but also improves the overall biodegradability of the effluent (Satyawali and Balakrishnan, 2008).

A.2.3.4 Membrane treatment

Pre-treatment of vinasse with ceramic membranes prior to anaerobic digestion (Chang et al., 1994), electrodialysis using cation and anion exchange membrane (Neytzell-de Wilde, 1987), and reverse osmosis have all been employed for the treatment of vinasse.

A.2.3.5 Evaporation/combustion

Vinasse containing 4 % solids may be concentrated to a maximum of 40 % solids in a multiple effect evaporation system with thermal recompression (Bhandari et al., 2004). The condensate with a COD of no more than 280 mg/l may be used in fermenters and the concentrated mother liquor is spray dried using hot air, to obtain a desiccated powder, which may be mixed with agriculture waste and burnt in boilers (Satyawali and Balakrishnan, 2008). Combustion is also an effective method, especially for on-site disposal, as it is accompanied by the production of potassium rich ash (Cortez and Brossard Pérez, 1997) that may be used for land application.

A summary of the physico-chemical treatment methods employed for the treatment of vinasse and their performance is summarised in Table A-8.

Table A-8: Summary of various physico-chemical treatment methods used of the treatment of molasses-derived vinasse (edited and updated from Mohana et al., 2009).

Treatment	COD Removal (%)	Colour Removal (%)	Reference
Adsorption			
1) Activated carbon prepared from agro-residues:			
Phosphoric acid carbonized bagasse.	23.6	50.3	Satyawali and Balakrishnan (2007)
2) Commercially available activated carbon:			
AC (ME)	76	93	Satyawali and Balakrishnan (2007)
AC (LB)	88	95	Satyawali and Balakrishnan (2007)
3) Chemically modified bagasse:			
DEAE bagasse	40	51	Mane et al. (2006)
CHPTAC bagasse	25	50	Mane et al. (2006)
4) Chitosan as an anion exchanger	99	98	Lalov et al. (2000)
Coagulation-flocculation			
1) Various inorganic ions were used to carry out flocculation of synthetic melanoidins:			
Polyferric hydroxysulphate (PFS)	NR	95	Migo et al. (1993)
Ferric chloride ($FeCl_3$)	NR	97	
Ferric sulphate ($Fe_2(SO_4)_3$)	NR	96	
Aluminium sulphate ($Al_2(SO_4)_3$)	NR	83	
Calcium oxide (CaO)	NR	78	
Calcium chloride ($CaCl_2$)	NR	47	

Table A-8 (continued): Summary of various physico-chemical treatment methods used of the treatment of molasses-derived vinasse (edited and updated from Mohana et al., 2009).

Treatment	COD Removal (%)	Colour Removal (%)	Reference
2) Different inorganic ions and waste water were used as coagulants. The addition of polyelectrolyte reduced their dosage. Biologically treated vinasse.			
Ferrous sulphate	78	98	Pandey et al. (2003)
Ferric sulphate	77	96	
Iron picking waste water	86	99	
Titanium processing waste water	67	99	
3) Biologically treated vinasse. Bleaching powder followed by aluminium sulfate	97	96	Chandra and Singh (1999)
4) Ferric chloride - anaerobically treated vinasse	55	83	Chaudhari et al. (2007)
5) Aluminium chloride	60	86	Chaudhari et al. (2007)
6) Polyaluminium chloride	72	92	Chaudhari et al. (2007)
7) Commercial inorganic flocculent - polymer of ferric hydroxysulphate. Anaerobically treated vinasse.	NR	87	Migo et al. (1993)
Oxidation processes			
1) Oxidation by ozone of biologically treated vinasse.	15 -25	71-93	Pena et al. (2003)
2) Ozonation-aerobic oxidation-ozonation	79	100	Sangave et al. (2007)
3) Vinasse diluted 20 times. Iron oxide was used as a catalyst to increase the ozonation process	62	87	Sreethawong and Chavadej (2008)

Table A-8 (continued): Summary of various physico-chemical treatment methods used of the treatment of molasses-derived vinasse (edited and updated from Mohana et al., 2009).

Treatment	COD Removal (%)	Colour Removal (%)	Reference
Membrane treatment			
1) Ceramic membranes for pre-treatment of vinasse prior to anaerobic digestion. The efficiency of the anaerobic process was improved by the pre-treatment. The removal of inhibiting substances was probably the reason for this improvement.	50	NR	Chang et al. (1994)
2) Reverse osmosis using thin film composite membranes in spiral wound configuration.	99.9	NR	Nataraj et al. (2006)
3) Hybrid nanofiltration using thin film composite membranes in spiral wound configuration.	97.1	100	Nataraj et al. (2006)

NR = Not reported.

ADDITIONAL HYDRATE LITERATURE

B.1 Comparison of guest molecule sizes and cavities occupied as simple hydrates.
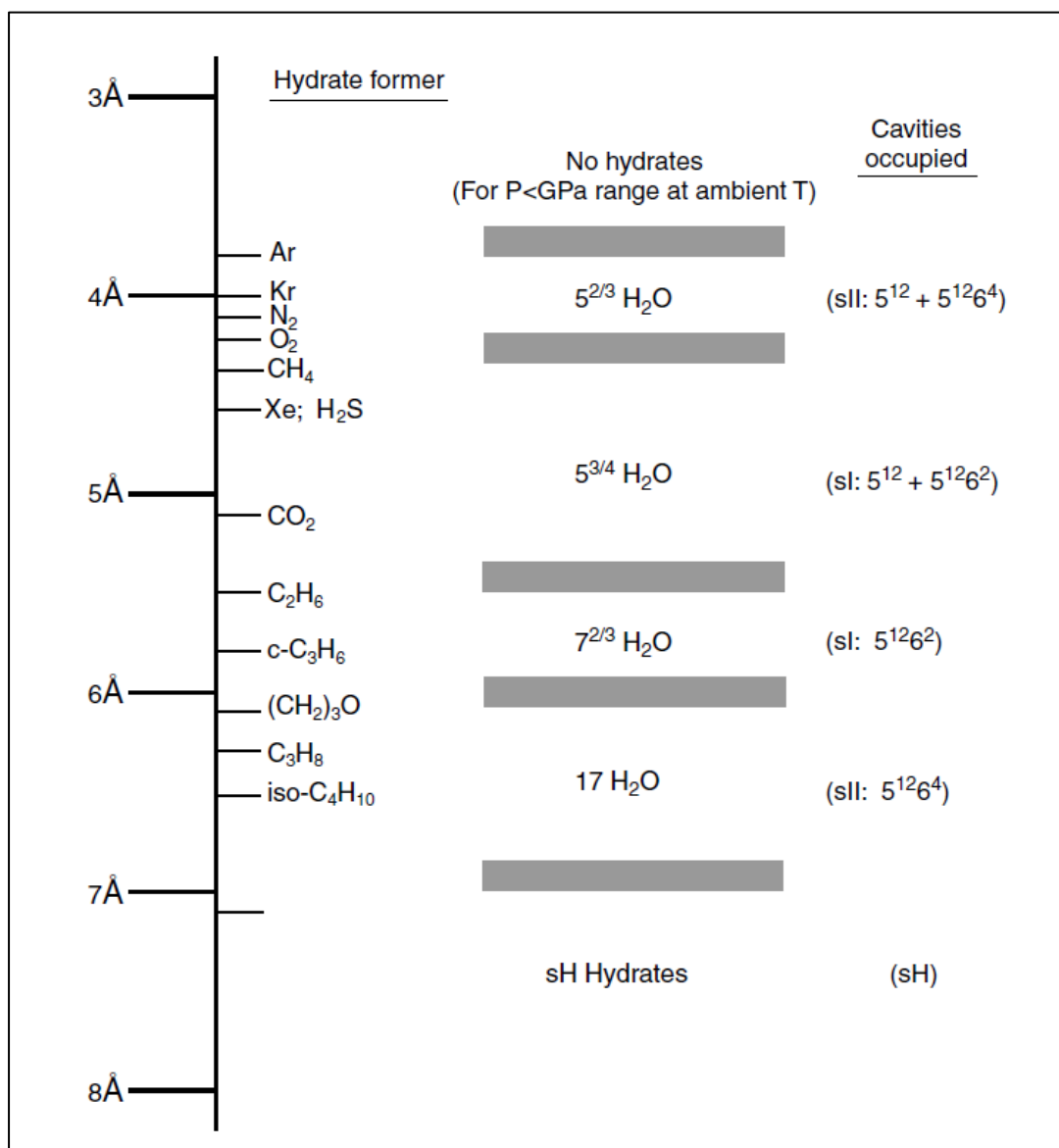
Figure B-1: Relationship between the molecule size of different simple hydrate formers and the corresponding hydrate structures (Sloan and Koh, 2008).

B.2 List of hydrates formers

Table B-1: List of simple sI and sII hydrate formers and their respective structure (Sloan and Koh, 2008).

Guest molecule	sI or sII	Guest molecule	sI or sII
Ar	II	$(CH_3)_3CF$	II
Kr	II	CH_3Cl	I
Xe	I	CH_2Cl_2	II
H_2	II	$CHCl_3$	II
N_2	II	C_2H_3Cl	II
O_2	II	C_2H_5Cl	II
Cl_2	I	CH_3CHCl_2	II
BrCl	I	CH_2ClF	I
CO_2	I	$CHClF_2$	I
N_2O	I	$CHCl_2F$	II
H_2S	I	CCl_2F_2	II
H_2Se	I	CCl_3F	II
SO_2	I	CH_3CClF_2	II
COS	I	CH_3Br	I
CH_4	I	C_2H_5Br	II
C_2H_2	I	CH_3I	II
C_2H_4	I	$CBrF_3$	II
C_2H_6	I	CBr_2F_2	II
Propylene	II	$CBrClF_2$	II
Cyclopropane	I & II	CH_3SH	I
C_3H_8	II	Ethylene oxide	I
iso-butane	II	Dimethyl ether	II
Cyclopentene	II	Propylene oxide	II
Cyclopentane	II	Trimethylene oxide	I & II
CH_3F	I	1,3-Dioxolane	II
CH_2F_2	I	Furan	II
CHF_3	I	2,5-Dihydrofuran	II
CF_4	I	Tetrahydrofuran	II
C_2H_3F	I	Tetrahydropyran	II
C_2H_5F	I	Acetone	II
CH_3CHF_2	I	Cyclobutanone	II

Table B-2: Structure H formers (Sloan and Koh, 2008)

sH formers
methylcyclopentane
ethylcyclopentane
methylcyclohexane
cycloheptane
cyclooctane
2-methylbutane
2,2-dimethylbutane
2,3-dimethylbutane
2,2,3- trimethylbutane
2,2-dimethylpentane
3,3 dimethylpentane

B.3 Phase behaviour of binary and ternary hydrate systems

B.3.1 Binary systems (low critical temperature gases)

The P-T diagram for a binary hydrate system of water and a former gas that has a low critical temperature is shown in Figure B-2. Methane and nitrogen are examples of such gases with low critical temperatures. Methane and nitrogen have critical temperatures of 191 K and 126 K respectively.
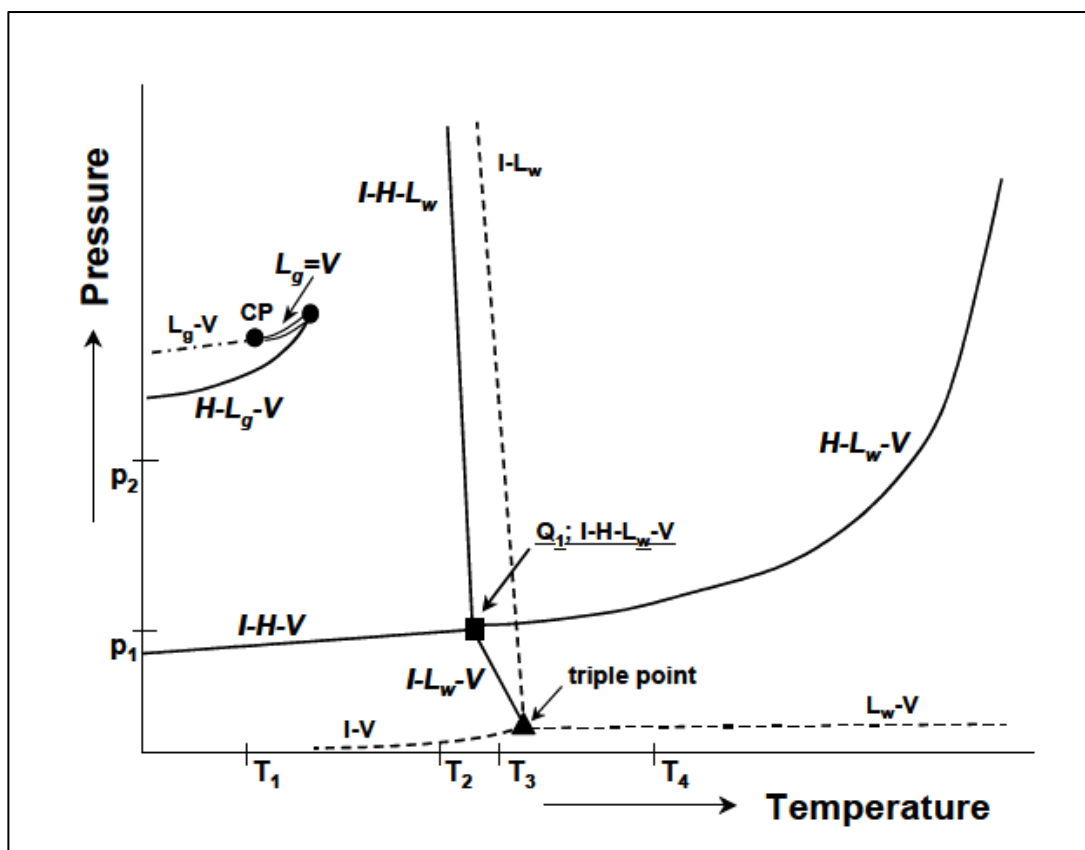
Figure B-2: Pressure-temperature phase diagram for a binary system of water + gas (−). As far as applicable, the phase behavior of the unary system of water (---) and gas (-.-.) is included as a reference. An example of a binary system showing this behavior is water + methane (Mooijer-van den Heuvel, 2004).

A quadruple point (Q_1) is formed at the point where three-phase equilibrium curves intersect. It is the point where four phases coexist, I-H-L_w-V. The equilibrium curves intersecting at Q_1 are H-L_w-V, I-H-V, I-H-L_w and I-L_w-V. The quadruple point temperature approximates 273 K for all hydrate formers however the quadruple pressure varies considerably due to the type of bonds present between the particles (Sloan and Koh, 2008). The triple point of water and Q_1 are connected by the equilibrium curve I-L_w-V. The H-L_w-V equilibrium curve has no upper temperature or pressure limit. This is due to the fact that the V-L critical points for methane and nitrogen are far below the quadruple point (Q_1). Such low critical temperatures prevent intersection of the vapor pressure curves with the H-L_w-V equilibrium line above 273 K to produce an upper quadruple point (Sloan and Koh, 2008). The temperatures and pressures of the H-L_w-V and I-H-V equilibrium curves are the limits of hydrate formation. Hydrates cannot from at higher temperatures or lower pressures on both lines. Hydrate formation can only occur to the left of these lines. The H-L_g-V equilibrium line has a pressure that is slightly lower than that of the vapor pressure for the pure gas component. The H-L_g-V curve thus

terminates at the intersection with the L_g=V critical curve, which in this instance, is located at a much lower temperature than T_{Q1}.

Figures B-3 and B-4 show the effect of composition-pressure or composition-temperature on the equilibrium conditions for the system described above.
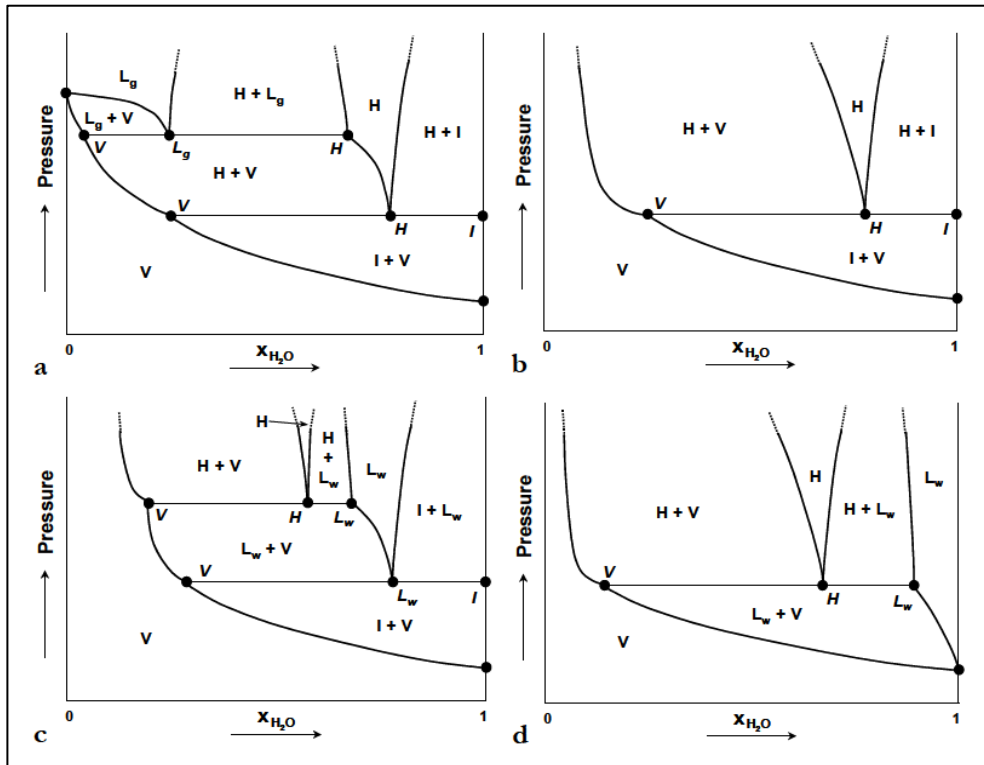
Figure B-3: Pressure-composition phase diagram for a binary system of water + gas at T_1 (a), T_2 (b), T_3 (c) and T_4 (d), as indicated in Figure B-2 (Mooijer-van den Heuvel, 2004).
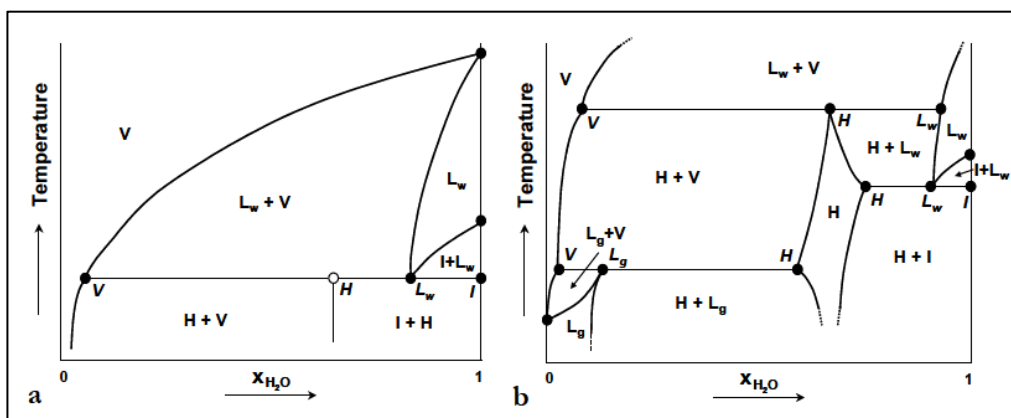
Figure B-4: Temperature-composition phase diagram for a binary system of water + gas at p_1 (a), which is the pressure of Q_1, and p_2 (b), as indicated in Figure B-2 (Mooijer-van den Heuvel, 2004).

B.3.1.1 Application of Gibbs phase rule: binary systems

The application of the Gibbs phase rule for a binary system of water and a gas hydrate-forming component is represented in Table B-3.

Table B-3: Application of Gibbs phase rule for a binary system (Mooijer-van den Heuvel, 2004).

F	N	π	Phase	Representation in Figure 2-4 and B-4
2	2	2	L_w-V, H-L_w, H-I	Region
1	2	3	H-L_w-V, H-L_w-L_g, I-H-V	Curve
0	2	4	I-H-L_w-V, H-L_w-L_g-V	Point

B.3.2 Ternary systems

The appearance of phase diagrams of ternary systems depend on three factors (Mooijer-van den Heuvel, 2004):

- Formation of hydrates in the binary system with water.
- The phase behaviour of the binary system with water and the guest component.
- Presence and size of the regions in which liquid phases will be immiscible.

Based on the above mentioned factors, the phase diagrams for ternary systems consisting of water, guest molecules, and an additive, where both components are present in a hydrate lattice and no structural transition occurs, may be classified as follows (Mooijer-van den Heuvel, 2004):

- Type A: One of the guest components cannot form gas hydrates on its own with water.
- Type B: Both guest components form gas hydrates in binary systems with water. Both components exhibit either gas-like or liquid-like behaviour.
- Type C: Both guest components form gas hydrates in binary systems with water, where the phase behaviour in both the binary systems is different. One component exhibits gas-like phase behaviour, while the other component exhibits liquid-like behaviour.

B.3.2.1 Type A systems

Type A systems are classified by one of the guest components not being able to form hydrates in a binary system with water. These systems are shown in Figure B-5 and B-6. Various assumptions are made for the construction of a type A phase diagram, which are (Mooijer-van den Heuvel, 2004):

- Water and guest components have immiscible L_w and L_g phases and forms hydrates.
- Water and additive components have immiscible L_w and L_a phases. They do not form hydrates.
- Guest and additive components have immiscible L_a and L_g phases.
- Water, guest and additive components have immiscible L_w and L_a phases and form hydrates.

One quintuple point (Q_t) is represented in Figure B-5. This is represented by I-H-L_w-L_a-V. The hydrate instability region is bound by I-H-L_a-V and H-L_w-L_a-V equilibrium curves. Two quintuple points (Q_t) are represented in Figure B-6, which is shown, by I-H-L_w-L_a-V and H-L_w-L_a-L_g-V. The hydrate instability region is bounded by I-H-L_a-V, H-L_w-L_a-V and H-L_w-L_g-V equilibrium curves. The number of quintuple points decreases if the assumptions regarding the immiscibility of L_a and L_g do not apply (Mooijer-van den Heuvel, 2004).
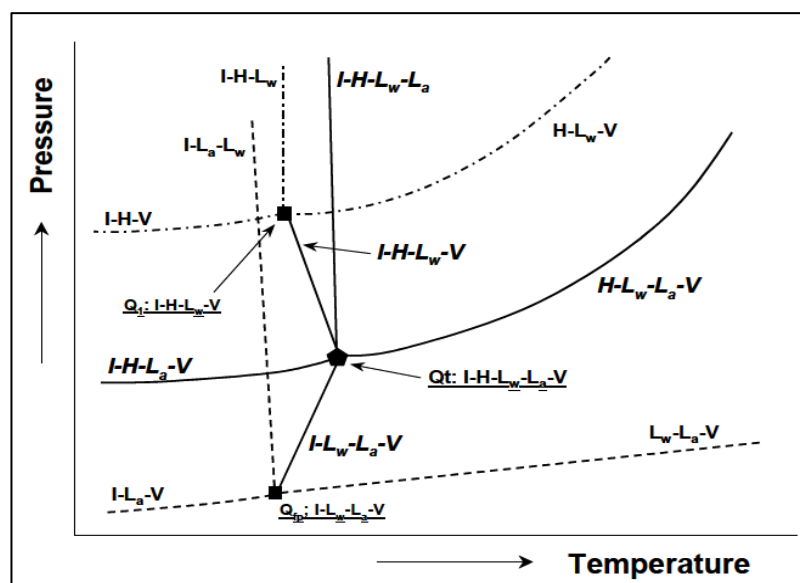
Figure B-5: Pressure-temperature phase diagram for a ternary system showing type A phase behavior. The gaseous component forms clathrate hydrate in the binary system and shows gas-like behavior (-.-.-).The additive does not form clathrate hydrate in the binary system with water (----) (Mooijer-van den Heuvel, 2004).
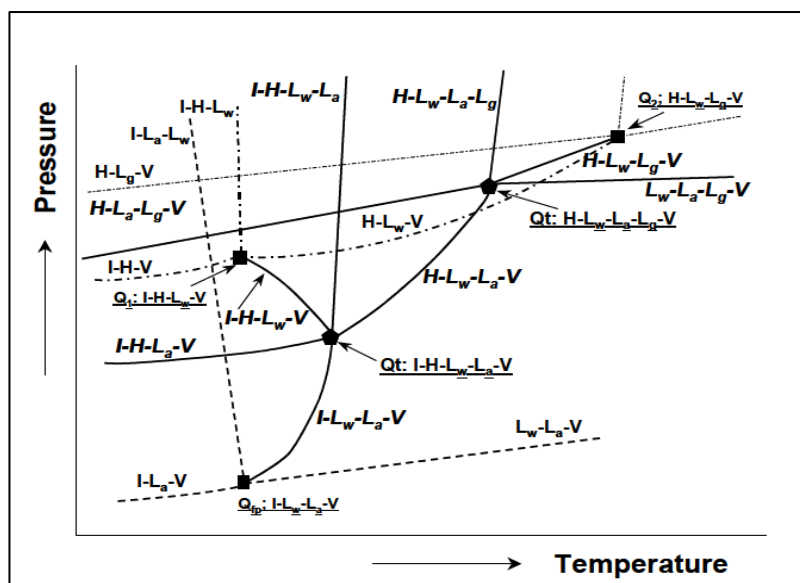
Figure B-6: Pressure-temperature phase diagram for a ternary system showing type A phase behavior. The gaseous component forms clathrate hydrate in the binary system and shows liquid-like behavior (-.-.-). The additive does not form clathrate hydrate in the binary system with water (----). The gaseous and additive components are immiscible (Mooijer-van den Heuvel, 2004).

B.3.2.2 Type B systems

The phase behavior of type B systems is classified by both of the guest components being able to form hydrates in a binary system of water as well as having similar schematic phase diagrams. These are represented in Figures B-7 and B-8. The assumptions made in the construction of these phase diagrams are (Mooijer-van den Heuvel, 2004):

- Water and guest components have immiscible L_w and L_g phases and forms hydrates.
- Water and additive components have immiscible L_w and L_a phases and forms hydrates.
- Guest and additive components have immiscible L_a and L_g phases.
- Water, guest and additive components have miscible L_a and L_g phases and form hydrates.
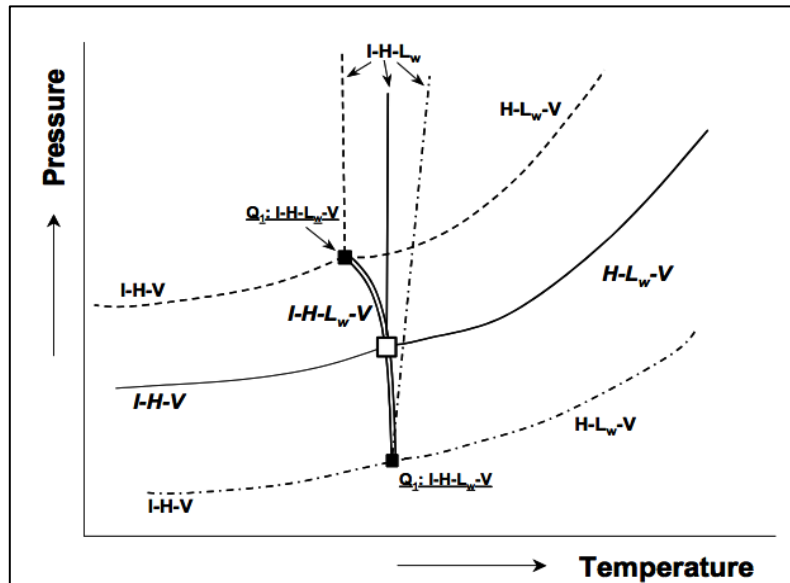
Figure B-7: Pressure-temperature phase diagram for a type B ternary system exhibiting gas-like behavior. (—) phase boundaries for one overall-composition (isopleth); (■) the quadruple point locus I-H-Lw-V; (□) point of intersection of the phase boundaries on the quadruple point locus. In both the binary systems with water, clathrate hydrate is formed and the components show gas-like behavior (-.-.- and ---). An example of a system exhibiting this behavior is H_2O + CH_4 + CF_4 (Mooijer-van den Heuvel, 2004).
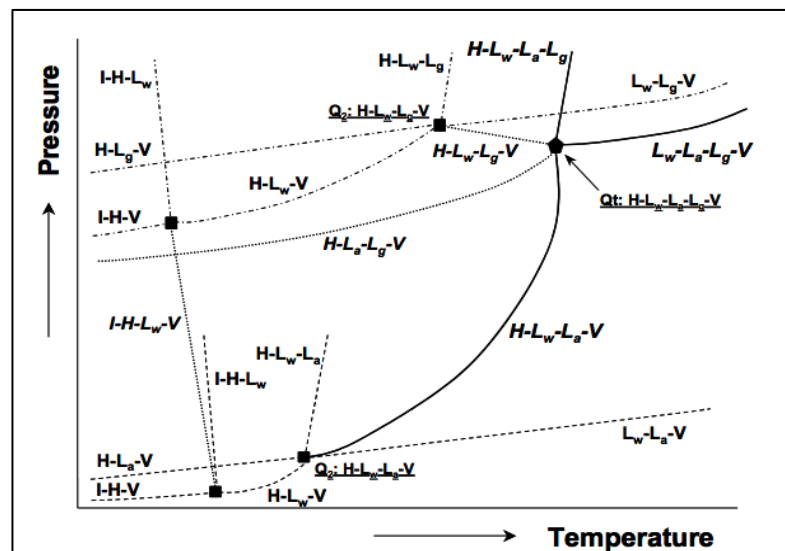
Figure B-8: Pressure-temperature phase diagram for a type B ternary system exhibiting liquid like behavior. (—) phase boundaries for one overall-composition (isopleth). In both the binary systems with water, gas hydrates are formed and the components show liquid-like behavior (-.-.- and ---). An example of a ternary system showing this behavior is H_2O + C_3H_8 + cyclobutanone. Some of the indicated equilibrium (····) may be difficult to determine experimentally (Mooijer-van den Heuvel, 2004).

B.3.2.3 Type C systems

The phase behavior of type C systems is classified by both of the guest molecules forming hydrates; one guest shows gas-like behavior where the other guest shows liquid-like behavior. The phase diagram in Figure B-9 represents this.
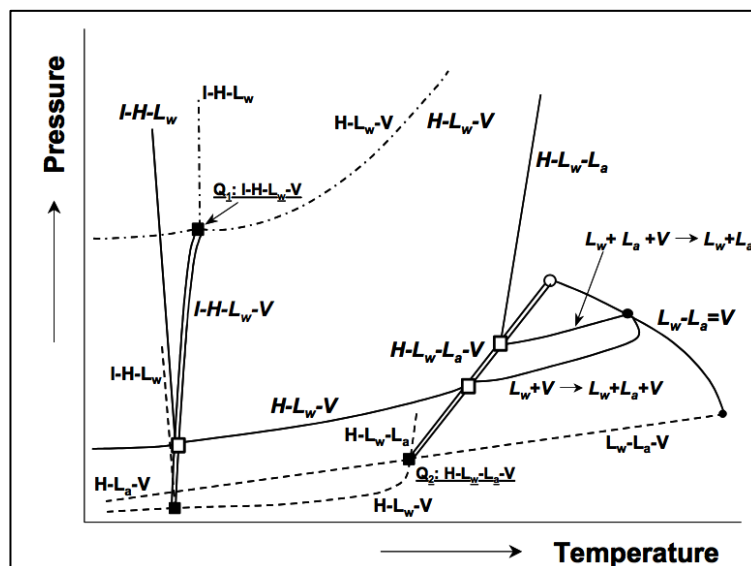
Figure B-9: Pressure-temperature phase diagram for a type C ternary system. Clathrate hydrate is formed in both the binary systems, one showing gas-like (-.-.-) and the other showing liquid-like (---) behavior. The phase boundaries (—), quadruple point loci I-H-L$_w$-V and H-L$_w$-L$_a$-V (■), points of intersection of phase boundaries with the quadruple point loci (□) and critical points (●) are given for a mixture rich in the component showing liquid-like behavior. An example of a ternary system where this behavior can be found is H$_2$O + CH$_4$ + CHF$_3$ (Mooijer-van den Heuvel, 2004).

B.3.2.4 Application of the Gibbs phase rule: ternary systems

The application of the Gibbs phase rule for a ternary system of water, one guest component, and an additive is represented in Table B-4.

Table B-4: Application of Gibbs phase rule for a ternary system (Mooijer-van den Heuvel, 2004).

F	N	π	Phase	Representation in Figure B-5 to B-9
3	3	3	L_w-V, H-L_w, H-I	Region
2	3	3	H-L_w-L_g, H-L_w-L_a	Surface
1	3	2	L_w+L_g = V	Curve
0	3	3	L_w+L_a+L_g = V	Point

B.4 Criteria for potential common hydrate formers

In order to determine the most suitable hydrate formers, a detailed analysis of each property and criteria for each potential former needs to be conducted. This is shown in Table B-5 (common formers) and Table B-7 (fluorinated formers).

Table B-5: Specific criteria used for choosing the most suitable common formers for hydrate formation.

Chemical name	Methane	Ethane	Propane	Carbon dioxide
Chemical formula	CH_4	C_2H_6	C_3H_8	CO_2
Ecological effect	ODP = No Data Available GWP = 25	ODP = 0 GWP = 6	ODP = 0 GWP = 3	ODP = 0 GWP = 1
Toxicity effect	Asphyxiation at high concentrations. Contact with expanding gas or vaporizing liquid may cause burns or frostbite.	Asphyxiation at high concentrations. Contact with expanding gas or vaporizing liquid may cause burns or frostbite.	Asphyxiation at high concentrations. Contact with expanding gas or vaporizing liquid may cause burns or frostbite.	Asphyxiation at high concentrations. Contact with expanding gas or vaporizing liquid may cause burns or frostbite.
Flammability	Flammable	Flammable	Flammable	Non-flammable
Explosive limits % By volume	Lower level = 1.8 % Upper level = 8.4 %	Lower level = 3 % Upper level = 12.5 %	Lower level = 2.2% Upper level = 9.5%	None
Chemical stability	Stable under normal conditions. Unstable at high temperatures outside explosive limits.	Stable under normal conditions. May decompose to form hydrogen at high T and low P.	Stable under normal conditions. Unstable at high temperatures outside explosive limits.	Stable under normal conditions
Compatibility	Incompatible with oxidizing agents.	Incompatible with oxidizing agents.	Incompatible with oxidizing agents	No reaction with any common materials in wet or dry conditions

Table B-5 (continued): Specific criteria used for choosing the most suitable common formers for hydrate formation.

Chemical name	Methane	Ethane	Propane	Carbon dioxide
Structure of unit cell [A]	I	I	II	I
Upper quadruple point [A]	None	287.85 K 3.390 MPa	278.85 K 0.561 MPa	283.05 K 4.499 MPa
Critical point	190.56 K 4.60 MPa	305.55 K 4.87 MPa	369.85 K 4.25 MPa	304.15 K 7.40 MPa
Water solubility	0.0244 g/l	61 mg/l	6.5 % vol/vol at 20 C	0.90 % vol/vol at 20
Availability	Yes	Yes	Yes	Yes

Ref A: Sloan and Koh (2008)

B.5 Commercially available fluorinated formers

Table B-6: Commercially available fluorinated formers (Petticrew, 2011).

Name	Common Name	Formulae	Banned
R11	Trichlorofluoromethane	CCl_3F	Yes
R12	Dichlorodifluoromethane	CCl_2F_2	Yes
R12Br	Bromochlorodifluoromethane	$CBrClF_2$	Yes
R14	Tetrafluoromethane	CF_4	No
R21	Dichlorofluoromethane	$CHCl_2F$	Yes
R22	Chlorodifluoromethane	$CHClF_2$	Yes
R22Br	Bromodifluoromethane	$CHBrF_2$	Yes
R31	Chlorofluoromethane	$CH2ClF$	Yes
R32	Difluoromethane	CH_2F_2	Will be
R116	Hexafluoroethane	C_2F_6	No
R134a	1,1,1,2-Tetrafluoroethane	H_2FC-CF_3	No
R141b	1,1-Dichloro-1-fluoroethane	Cl_2FC-CH_3	Yes
R142b	1-Chloro-1,1-difluoroethane	ClF_2C-CH_3	Yes
R152a	Difluoroethane-1,1	F_2HC-CH_3	No
R218	Octafluoropropane	C_3F_8	No
R404a	Refrigerant blend	52 wt % R143a, 44 wt. % R125, 4 wt % R134a	No
R406a	Refrigerant blend	55 wt % R22, 41 wt % R142b, 4 wt % R600a	Will be
R407c	Refrigerant blend	23 wt % R32, 25 wt % R125, 52 wt % R134a	No
R408a	Refrigerant blend	47 wt % R22, 46 wt % R143a, 7 wt % R125	Will be
R409a	Refrigerant blend	60 wt % R22, 15 wt % R142b, 25 wt % R124	Will be
R410a	Refrigerant blend	50 wt % R125, 50 wt % R32	No
R507a	Refrigerant blend	50 wt % R125, 50 wt % R143a	No

B.6 Criteria for potential fluorinated hydrate formers

Table B-7: Specific criteria to determine commercial fluorinated formers for hydrate formation.

Chemical name	R 14	R 116	R134a	R152a	R 218
Chemical formula	CF_4	C_2F_6	CH_2FCF_3	$CH_2H_4F_2$	C_3F_8
Ecological effect	ODP = 0	OPD = 0	ODP = 0	ODP = 0	OPD = 0
	GWP = 5700	GWP = 12200	GWP = 1370	GWP = 120	GWP = 7000
Toxicity effect	Asphyxiant. Contact with rapidly expanding gas may cause burns or frostbite.	Asphyxiant. Contact with rapidly expanding gas may cause burns or frostbite.	Asphyxiant. Burns or frostbite from expanding gas contact.	Asphyxiation. Contact with expanding gas or may cause burns or frostbite.	Asphyxiation and narcotic effects at high and low concentrations respectively.
Flammability	Non-flammable	Non-flammable	Non-flammable	Extremely flammable.	Non-flammable
Explosion potential	Not applicable	Not applicable	Not applicable	Upper level = 18% Lower level = 3.7%	Not applicable
Chemical stability	Stable under normal conditions. Decomposes at high temperatures.	Stable under normal conditions	Stable. Does not mix with oxygen or air above atmospheric pressure.	Stable under normal conditions.	Stable under normal conditions.

Table B-7 (continued): Specific criteria to determine commercial fluorinated formers for hydrate formation.

Chemical name	R 14	R 116	R134a	R152a	R 218
Compatibility	Incompatible with alkali or alkaline earth metals - powdered Al, Zn, Be	Incompatible with alkali or alkaline earth metals - powdered Al, Zn, Be. Reacts violently with chemical active metals.	Incompatible with alkali metals, alkaline earth metals, powdered metals and powdered metal salts.	Incompatible with oxidizers and moisture. Can form explosive mixture with air.	May react violently with chemically active metals such as Na, K and Ba, powdered Mg, Al and organometallics
Structure of unit cell	I	Not available in examined literature	II	I or II	Not available in examined literature
Upper quadruple point	Not available in examined literature	Not available in examined literature	283.13 K 0.4144 MPa	288 K 0.44 MPa	Not available in examined literature
Critical point	227.65 K 3.74 MPa	292.85 K 2.98 MPa	374.30 K 4.06 MPa	387.15 K 4.76 MPa	345.05 K 2.68 MPa
Water solubility	0.0038 vol/vol (25 ℃, 1atm)	No reliable data available	0.21 vol/vol (25 ℃, 1atm)	No reliable data available	No reliable data available
Availability	Industrially available	Industrially available	Industrially available	Industrially available	Industrially available

Table B-7 (continued): Specific criteria to determine commercial fluorinated formers for hydrate formation.

Chemical name	R404a	R407c	R410a	R 507
Chemical formula	52 wt % R143a, 44 wt % R125, 4 wt % R134a	23 wt % R32, 23 wt % R125, 52 wt % R134a	50 wt % R32, 50 wt % R125	50 wt % R125, 50 wt % R143a
Ecological effect	ODP = 0 GWP = 13922	ODP = 0 GWP = 1774	ODP = 0 GWP = 2088	ODP = 0 GWP = 3800
Toxicity effect	Asphyxiation at high concentrations. Contact with expanding gas or vaporizing liquid may cause burns or frostbite.	Asphyxiation at high concentrations. Contact with expanding gas or vaporizing liquid may cause burns or frostbite.	Asphyxiation at high concentrations. Contact with rapidly expanding gas or vaporizing liquid may cause burns or frostbite	Asphyxiation at high concentrations. Contact with rapidly expanding gas or vaporizing liquid may cause burns or frostbite
Flammability	Non-flammable	Non-flammable	Non-flammable	Non-flammable
Explosion potential	Not applicable	Not applicable	Not applicable	Not applicable
Chemical stability	Stable under normal conditions. Avoid open flames and high temperatures.	Stable under normal conditions. Does not mix with oxygen or air above atmospheric pressure.	Stable under normal conditions.	Stable under normal conditions.
Compatibility	Incompatible with alkali metals, alkaline earth metals, powdered metals (Al, Mg, Zn) and powdered metal salts.	Incompatible with alkali metals, alkaline earth metals, powdered metals (Al, Mg, Zn) and powdered metal salts.	Incompatible with active metals, alkali or alkaline earth metals -powdered Al, Zn, Be, etc.	Incompatible with alkali metals, alkaline earth metals, powdered metals (Al, Mg, Zn) and powdered metal salts.

Table B-7 (continued): Specific criteria to determine commercial fluorinated formers for hydrate formation.

Chemical name	R404a	R407c	R410a	R 507
Structure of unit cell	Not available in examined literature	Not available in examined literature	II	II
Upper quadruple point	Not available in examined literature	Not available in examined literature	Not available in examined literature	Not available in examined literature
Critical point	345.22 K	359.89 K	345.65 K	343.95 K
	3.73 MPa	4.62 MPa	4.86 MPa	3.79 MPa
Water solubility	No reliable data available	Insoluble	430 mg/L	No reliable data available
Availability	Industrially available	Industrially available	Industrially available	Industrially available

B.7 Inhibitors and promoters

Table B-8: List of common thermodynamic inhibitors (Mandal and Laik, 2008; Sloan and Koh, 2008).

Inhibitor
Methanol
Ethanol
Ethylene glycol
Diethylene glycol
Triethylene glycol
Monoethylene glycol
Sodium chloride
Potassium chloride
Calcium chloride
Potassium formate
Hydrogen chloride
Sodium hydroxide
Sodium dodecyl sulfate
Para-toluene sulfonic acid
Sodium dodecyl benzene sulfonate
Potassium oxalate monohydrate

Table B-9: List of known promoters (Reddy, 2013) (work in progress).

Promoter
Acetone
Cyclobutanone
Cycloheptane
Cyclohexane
Cyclopentane
Cyclooctane
Methylcyclohexane
Neopentane
Propylene oxide
TBAB
Tetrahydropyran
THF
2,5-dihydrofuran
3,4-Dihydro-2H-pyran
1,4-dioxane
1,3,5-trioxane
2-Methyl-2-propanol

B.8 Measured HLV equilibrium data

The measured HLV equilibrium data for salt systems containing formers other than CO_2 are presented in Tables B-10 to B-13.

Table B-10 reports the equilibrium data for single salt systems. The table is prepared such that the specific salts are first grouped together and reported for the various formers i.e. the HLV data for NaCl with the various formers is presented first, thereafter, KCl and $CaCl_2$ data etc.

Tale B-11 reports the equilibrium data for mixed salt systems, Table B-12 reports the equilibrium data for organic inhibitor systems, and Table B-13 reports the equilibrium data for mixed thermodynamic inhibitor systems.

Table B-10: Measured HLV equilibrium data for the former (1) + water (2) + single salt (3) systems cited in literature.

System	Temperature Range (K)	Pressure Range (MPa)	Reference
CH_4 (1) + water (2) + 3.00 wt % NaCl (3)	272.7 - 279.4	2.75 - 5.36	Dholabhai et al. (1991)
	276.4 - 283.1	4.00 - 7.90	Maekawa (2001)
CH_4 (1) + water (2) + 5.00 wt % NaCl (3)	274.2 - 283.6	3.58 - 9.60	Mohammadi et al. (2008b)
CH_4 (1) + water (2) + 0.03936 mole fraction wt % NaCl (3)	268.3 - 278.1	2.69 - 7.55	De Roo et al. (1983)
CH_4 (1) + water (2) + 0.05976 mole fraction wt % NaCl (3)	263.4 - 275.0	2.39 - 8.57	De Roo et al. (1983)
CH_4 (1) + water (2) + 0.07785 mole fraction wt % NaCl (3)	261.9 - 272.9	2.94 - 11.00	De Roo et al. (1983)
CH_4 (1) + water (2) + 0.08909 mole fraction wt % NaCl (3)	263.1 - 268.7	4.78 - 9.55	De Roo et al. (1983)
C_2H_6 (1) + water (2) + 5.00 wt % NaCl (3)	272.2 - 284.7	0.540 - 2.90	Mohammadi et al. (2008b)
C_2H_6 (1) + water (2) + 10.00 wt % NaCl (3)	273.7 - 280.4	0.88 - 2.17	Tohidi et al. (1997)
C_2H_6 (1) + water (2) + 15.00 wt % NaCl (3)	272.7 - 277.1	1.08 - 2.15	Tohidi et al. (1997)
C_2H_6 (1) + water (2) + 20.00 wt % NaCl (3)	265.4 - 271.9	0.74 - 1.83	Englezos and Bishnoi (1991)
C_3H_8 (1) + water (2) + 2.50 wt % NaCl (3)	271.0 - 276.6	0.138 - 0.471	Kubota et al. (1984)
C_3H_8 (1) + water (2) + 5.00 wt % NaCl (3)	271.5 - 275.1	0.20 - 0.40	Mohammadi et al. (2008)
C_3H_8 (1) + water (2) + 5.02 wt % NaCl (3)	270.5 - 275.2	0.18 - 0.50	Bishnoi and Dholabhai (1993)
C_3H_8 (1) + water (2) + 9.99 wt % NaCl (3)	268.0 - 271.1	0.18 - 0.34	Bishnoi and Dholabhai (1993)
C_3H_8 (1) + water (2) + 10.02 wt % NaCl (3)	268.0 - 271.0	0.18 - 0.37	Bishnoi and Dholabhai (1993)
C_3H_8 (1) + water (2) + 10.03 wt % NaCl (3)	267.6 - 270.7	0.18 - 0.36	Bishnoi and Dholabhai (1993)
C_3H_8 (1) + water (2) + 14.99 wt % NaCl (3)	263.4 - 265.6	0.16 - 0.25	Bishnoi and Dholabhai (1993)

Table B-10 (continued): Measured HLV equilibrium data for the former (1) + water (2) + single salt (3) systems cited in literature.

System	Temperature Range (K)	Pressure Range (MPa)	Reference
C_3H_8 (1) + water (2) + 15.00 wt % NaCl (3)	263.6 - 267.8	0.15 - 0.37	Bishnoi and Dholabhai (1993)
H_2S (1) + water (2) + 5.00 wt % NaCl (3)	273.7 - 297.4	0.15 - 1.91	Mohammadi and Richon (2009c)
H_2S (1) + water (2) + 10.00 wt % NaCl (3)	274.0 - 295.0	0.18 - 1.80	Mohammadi and Richon (2009)
H_2S (1) + water (2) + 15.00 wt % NaCl (3)	271.7 - 279.6	0.16 - 0.37	Mohammadi and Richon (2012b)
H_2S (1) + water (2) + 20.00 wt % NaCl (3)	272.7 - 280.0	0.23 - 0.55	Mahadev and Bishnoi (1999)
H_2S (1) + water (2) + 22.00 wt % NaCl (3)	268.8 - 274.8	0.19 - 0.36	Mohammadi and Richon (2012)
CH_4-CO_2 (1) + water (2) + 5.02 wt % NaCl (3)	271.6 - 282.0	2.30 - 6.98	Dholabhai and Bishnoi (1994)
CH_4-CO_2 (1) + water (2) + 9.41 wt % NaCl (3)	266.9 - 276.2	1.12 - 3.16	Fan and Guo (1999)
CH_4-CO_2 (1) + water (2) + 9.45 wt % NaCl (3)	267.9 - 277.4	1.24 - 3.75	Fan and Guo (1999)
CH_4-CO_2 (1) + water (2) + 9.99 wt % NaCl (3)	268.5 - 279.0	2.03 - 6.56	Dholabhai and Bishnoi (1994)
CH_4-CO_2 (1) + water (2) + 10.00 wt % NaCl (3)	269.1 - 274.2	1.17 - 2.30	Fan and Guo (1999)
CH_4-CO_2 (1) + water (2) + 15.00 wt % NaCl (3)	264.9 - 277.2	1.86 - 7.31	Dholabhai and Bishnoi (1994)
CH_4-CO_2 (1) + water (2) + 20.00 wt % NaCl (3)	262.0- 270.4	2.12 - 5.42	Dholabhai and Bishnoi (1994)
CH_4-CO_2 (1) + water (2) + 20.01 wt % NaCl (3)	274.31	9.15	Dholabhai and Bishnoi (1994)
CH_4-C_2H_6 (1) + water (2) + 3.00 wt % NaCl (3) (97.9 % CH_4)	277.4 - 283.7	3.80 - 7.60	Maekawa (2001)
CH_4-C_2H_6 (1) + water (2) + 3.00 wt % NaCl (3) (95.2 % CH_4)	280.2 - 287.3	4.00 - 9.50	Maekawa (2001)
CH_4-C_2H_6 (1) + water (2) + 3.00 wt % NaCl (3) (90.2 % CH_4)	281.4 - 288.1	3.70 - 8.40	Maekawa (2001)
CH_4-N_2 (1) + water (2) + 5.00 wt % NaCl (3)	271.2 - 284.5	3.080 - 12.68	Mei et al. (1996)
CH_4-N_2 (1) + water (2) + 10.00 wt % NaCl (3)	272.7 - 281.6	4.330 - 11.41	Mei et al. (1996)

Table B-10 (continued): Measured HLV equilibrium data for the former (1) + water (2) + single salt (3) systems cited in literature.

System	Temperature Range (K)	Pressure Range (MPa)	Reference
CH_4-C_3H_8-CO_2 (1) + water (2) + 5.00 wt % NaCl (3)	280.8 - 288.0	3.269 - 9.849	Bishnoi and Dholabhai (1999)
CH_4-C_3H_8-CO_2 (1) + water (2) + 10.00 wt % NaCl (3)	277.7 - 282.4	2.876 - 5.633	Bishnoi and Dholabhai (1999)
CH_4-C_3H_8-CO_2 (1) + water (2) + 20.00 wt % NaCl (3)	274.2 - 276.9	3.728 - 5.286	Bishnoi and Dholabhai (1999)
CH_4-C_3H_8-CO_2 (1) + water (2) + 20.10 wt % NaCl (3)	279.97	8.874	Bishnoi and Dholabhai (1999)
Natural gas (1) + water (2) + 10.00 wt % NaCl (3)	267.1 - 279.8	0.81 - 3.43	Mei et al. (1998)
Natural gas (1) + water (2) + 20.20 wt % NaCl (3)	276.9 - 282.0	3.22 - 9.29	Bishnoi and Dholabhai (1999)
R134a (1) + water (2) + 5.00 wt % NaCl (3)	274.6 - 280.6	0.10 - 0.38	Petticrew (2011)
	274.6 - 280.6	0.10 - 0.38	Ngema (2014)
R134a (1) + water (2) + 10.00 wt % NaCl (3)	273.3 - 277.1	0.14 - 0.34	Petticrew (2011)
	272.6 - 277.1	0.12 - 0.34	Ngema (2014)
R134a (1) + water (2) + 15.00 wt % NaCl (3)	268.1 - 273.4	0.09 - 0.30	Petticrew (2011)
	268.1 - 273.4	0.09 - 0.30	Ngema (2014)
R134a (1) + water (2) + 0.900 mol/kg NaCl (3)	274.6 - 280.6	0.10 - 0.38	Ngema et al. (2014)
R134a (1) + water (2) + 1.901 mol.kg NaCl (3)	272.6 - 277.1	0.12 - 0.34	Ngema et al. (2014)
R134a (1) + water (2) + 3.020 mol/kg NaCl (3)	268.1 - 273.2	0.09 - 0.30	Ngema et al. (2014)
R152a (1) + water (2) + 2.50 wt % NaCl (3)	272.2 - 286.7	0.06 - 0.41	Kubota et al. (1984)
R152a (1) + water (2) + 3.40 wt % NaCl (3)	271.3 - 286.1	0.06 - 0.40	Kubota et al. (1984)
R152a (1) + water (2) + 5.00 wt % NaCl (3)	271.0 - 285.2	0.06 - 0.39	Kubota et al. (1984)
R410a (1) + water (2) + 0.900 mol/kg NaCl (3)	278.5 - 290.0	0.27 - 1.35	Ngema et al. (2014)

Table B-10 (continued): Measured HLV equilibrium data for the former (1) + water (2) + single salt (3) systems cited in literature.

System	Temperature Range (K)	Pressure Range (MPa)	Reference
R410a (1) + water (2) + 1.901 mol/kg NaCl (3)	276.1 - 288.6	0.24 - 1.27	Ngema et al. (2014)
R507 (1) + water (2) + 0.900 mol/kg NaCl (3)	275.9 - 281.0	0.23 - 0.80	Ngema et al. (2014)
R507 (1) + water (2) + 1.901 mol/kg NaCl (3)	273.9 - 278.0	0.30 - 0.74	Ngema et al. (2014)
R13 (1) + water (2) + 2.50 wt % NaCl (3)	271.7 - 279.7	0.31 - 2.03	Kubota et al. (1984)
R22 (1) + water (2) + 5.00 wt % NaCl (3)	276.2 - 287.3	0.17 - 0.78	Chun et al. (2000)
R22 (1) + water (2) + 10.00 wt % NaCl (3)	275.4 - 284.0	0.21 - 0.71	Chun et al. (2000)
R22 (1) + water (2) + 15.00 wt % NaCl (3)	274.0 - 280.1	0.27 - 0.62	Chun et al. (2000)
R23 (1) + water (2) + 2.00 wt % NaCl (3)	272.6 - 290.6	0.34 - 3.44	Kubota et al. (1984)
R23 (1) + water (2) + 5.00 wt % NaCl (3)	270.4 - 289.2	0.31 - 3.40	Kubota et al. (1984)
CH_4 (1) + water (2) + 5.00 wt % KCl (3)	271.6 - 283.2	2.71 - 8.69	Mohammadi et al. (2008)
CH_4 (1) + water (2) + 10.00 wt % KCl (3)	270.1 - 281.5	2.78 - 8.82	Mohammadi et al. (2008)
C_2H_6 (1) + water (2) + 5.00 wt % KCl (3)	271.4 - 282.3	0.47 - 1.85	Mohammadi et al. (2008)
C_2H_6 (1) + water (2) + 10.00 wt % KCl (3)	270.4 - 281.6	0.50 - 2.11	Mohammadi et al. (2008)
C_2H_6 (1) + water (2) + 12.30 wt % KCl (3)	269.5 - 278.4	0.50 - 1.58	Englezos and Bishnoi (1991)
C_3H_8 (1) + water (2) + 5.00 wt % KCl (3)	271.0 - 275.1	0.17 - 0.41	Bishnoi and Dholabhai (1993)
	272.0 - 276.2	0.18 - 0.46	Mohammadi et al. (2008)
C_3H_8 (1) + water (2) + 10.01 wt % KCl (3)	269.1 - 273.4	0.17 - 0.43	Bishnoi and Dholabhai (1993)
H_2S (1) + water (2) + 5.00 wt % KCl (3)	274.1 - 291.4	0.15 - 0.79	Mohammadi and Richon (2009)
	272.9 - 283.5	0.13 - 0.36	Mohammadi and Richon (2012)

Table B-10 (continued): Measured HLV equilibrium data for the former (1) + water (2) + single salt (3) systems cited in literature.

System	Temperature Range (K)	Pressure Range (MPa)	Reference
H_2S (1) + water (2) + 10.00 wt % KCl (3)	272.8 - 290.3	0.15 - 0.82	Mohammadi and Richon (2009)
H_2S (1) + water (2) + 12.00 wt % KCl (3)	273.6 - 280.5	0.17 - 0.33	Mohammadi and Richon (2012)
CH_4-CO_2 (1) + water (2) + 5.00 wt % KCl (3)	271.4 - 282.0	2.04 - 6.43	Dholabhai and Bishnoi (1994)
CH_4-CO_2 (1) + water (2) + 10.00 wt % KCl (3)	269.2 - 279.0	1.83 - 5.56	Dholabhai and Bishnoi (1994)
CH_4-CO_2 (1) + water (2) + 15.01 wt % KCl (3)	267.0 - 277.1	1.89 - 5.63	Dholabhai and Bishnoi (1994)
Natural gas (1) + water (2) + 10.00 wt % KCl (3)	269.1 - 279.8	0.78 - 2.81	Mei et al. (1998)
R22 (1) + water (2) + 5.00 wt % KCl (3)	275.3 - 287.8	0.14 - 0.79	Chun et al. (2000)
R22 (1) + water (2) + 10.00 wt % KCl (3)	275.8 - 285.6	0.18 - 0.73	Chun et al. (2000)
R22 (1) + water (2) + 15.00 wt % KCl (3)	275.1 - 283.2	0.20 - 0.69	Chun et al. (2000)
CH_4 (1) + water (2) + 5.00 wt % $CaCl_2$ (3)	272.0 - 283.0	2.81 - 8.53	Mohammadi et al. (2008)
CH_4 (1) + water (2) + 15.00 wt % $CaCl_2$ (3)	268.0 - 277.4	3.39 - 9.01	Mohammadi et al. (2008)
C_2H_6 (1) + water (2) + 5.00 wt % $CaCl_2$ (3)	271.5 - 283.3	0.44 - 2.09	Mohammadi et al. (2008)
C_2H_6 (1) + water (2) + 15.00 wt % $CaCl_2$ (3)	267.2 - 275.2	0.57 - 1.61	Englezos and Bishnoi (1991)
	270.0 - 278.5	0.81 - 2.52	Mohammadi et al. (2008)
C_3H_8 (1) + water (2) + 5.00 wt % $CaCl_2$ (3)	271.8 - 276.2	0.18 - 0.46	Mohammadi et al. (2008)
	271.3 - 275.6	0.18 - 0.47	Bishnoi and Dholabhai (1993)
C_3H_8 (1) + water (2) + 9.99 wt % $CaCl_2$ (3)	268.1 - 272.0	0.16 - 0.40	Bishnoi and Dholabhai (1993)
C_3H_8 (1) + water (2) + 15.00 wt % $CaCl_2$ (3)	263.0 - 267.4	0.13 - 0.35	Bishnoi and Dholabhai (1993)
H_2S (1) + water (2) + 5.00 wt % $CaCl_2$ (3)	272.2 - 293.2	0.11 - 0.95	Mohammadi and Richon (2009)

Table B-10 (continued): Measured HLV equilibrium data for the former (1) + water (2) + single salt (3) systems cited in literature.

System	Temperature Range (K)	Pressure Range (MPa)	Reference
H_2S (1) + water (2) + 10.00 wt % $CaCl_2$ (3)	273.0 - 280.3	0.16 - 0.35	Mohammadi and Richon (2012)
H_2S (1) + water (2) + 15.00 wt % $CaCl_2$ (3)	273.1 - 293.0	0.22 - 1.98	Mohammadi and Richon (2009)
H_2S (1) + water (2) + 20.00 wt % $CaCl_2$ (3)	271.8 - 273.8	0.33 - 0.43	Mohammadi and Richon (2012)
CH_4-CO_2 (1) + water (2) + 9.91 wt % $CaCl_2$ (3)	268.6 - 27913	1.96 - 6.08	Dholabhai and Bishnoi (1994)
CH_4-CO_2 (1) + water (2) + 15.00 wt % $CaCl_2$ (3)	266.7 - 276.9	1.88 - 7.09	Dholabhai and Bishnoi (1994)
CH_4-CO_2 (1) + water (2) + 20.00 wt % $CaCl_2$ (3)	263.8 - 273.7	2.89 - 9.46	Dholabhai and Bishnoi (1994)
Natural gas (1) + water (2) + 10.00 wt % $CaCl_2$ (3)	266.7 - 279.7	0.63 - 3.34	Mei et al. (1998)
R134a (1) + water (2) + 3.80 wt % $CaCl_2$ (3)	276.2 - 281.2	0.13 - 0.39	Ngema (2014)
R134a (1) + water (2) + 6.00 wt % $CaCl_2$ (3)	276.4 - 280.1	0.15 - 0.37	Ngema (2014)
R134a (1) + water (2) + 7.50 wt % $CaCl_2$ (3)	276.2 - 279.5	0.17 - 0.36	Ngema (2014)
CH_4 (1) + water (2) + 5.00 wt. % NaBr (3)	272.5 – 285.0	2.85 - 10.12	Mohammadi et al. (2009)
CH_4 (1) + water (2) + 10.00 wt % NaBr (3)	274.0 - 284.5	3.65 - 11.32	Mohammadi et al. (2009)
CH_4 (1) + water (2) + 5.00 wt % KBr (3)	273.1 - 285.5	2.89 - 10.42	Mohammadi et al. (2009)
CH_4 (1) + water (2) + 10.00 wt % KBr (3)	272.8 - 283.7	3.15 - 9.80	Mohammadi et al. (2009)
CH_4 (1) + water (2) + 5.00 wt % $CaBr_2$ (3)	273.6 - 284.8	3.01 - 9.62	Mohammadi et al. (2009)
CH_4 (1) + water (2) + 15.00 wt % $CaBr_2$ (3)	272.9 - 282.8	3.68 - 10.68	Mohammadi et al. (2009)
CH_4 (1) + water (2) + 5.00 wt % K_2CO_3 (3)	273.4 - 284.5	2.95 - 9.55	Mohammadi et al. (2009)
CH_4 (1) + water (2) + 10.00 wt % K_2CO_3 (3)	274.1 - 284.1	3.61 - 10.63	Mohammadi et al. (2009)

Table B-11: Measured HLV equilibrium data for the former (1) + water (2) + mixed salt (3) + (4) + (5) systems cited in literature.

System	Temperature Range (K)	Pressure Range (MPa)	Reference
CH_4 (1) + water (2) + 3.00 wt % NaCl (3) + 3.00 wt % KCl (4)	271.4 - 279.2	2.70 - 5.86	Dholabhai et al. (1991)
CH_4 (1) + water (2) + 3.00 wt % NaCl (3) + 3.00 wt % $CaCl_2$ (4)	270.4 - 281.8	2.50 - 8.16	Dholabhai et al. (1991)
CH_4 (1) + water (2) + 3.00 wt % NaCl (3) + 10.00 wt % $CaCl_2$ (4)	268.8 - 279.7	3.02 - 9.66	Dholabhai et al. (1991)
CH_4 (1) + water (2) + 5.00 wt % NaCl (3) + 5.01 wt % KCl (4)	270.3 - 281.5	2.83 - 9.38	Dholabhai et al. (1991)
CH_4 (1) + water (2) + 5.00 wt % NaCl (3) + 9.98 wt % KCl (4)	267.5 - 279.0	2.57 - 9.05	Dholabhai et al. (1991)
CH_4 (1) + water (2) + 5.02 wt % NaCl (3) + 15.00 wt % KCl (4)	266.3 - 276.2	2.91 - 8.69	Dholabhai et al. (1991)
CH_4 (1) + water (2) + 6.00 wt % NaCl (3) + 3.00 wt % $CaCl_2$ (4)	271.3 - 280.1	3.13 - 7.84	Dholabhai et al. (1991)
CH_4 (1) + water (2) + 6.00 wt % NaCl (3) + 10.00 wt % $CaCl_2$ (4)	268.6 - 277.1	3.69 - 9.51	Dholabhai et al. (1991)
CH_4 (1) + water (2) + 9.97 wt % NaCl (3) + 5.98 wt % $CaCl_2$ (4)	266.0 - 274.3	2.82 - 6.90	Dholabhai et al. (1991)
CH_4 (1) + water (2) + 10.00 wt % NaCl (3) + 3.00 wt % $CaCl_2$ (4)	269.4 - 277.3	3.21 - 7.44	Dholabhai et al. (1991)
CH_4 (1) + water (2) + 10.01 wt % NaCl (3) + 12.00 wt % KCl (4)	264.6 - 274.2	2.99 - 8.82	Dholabhai et al. (1991)
CH_4 (1) + water (2) + 14.99 wt % NaCl (3) + 7.99 wt % KCl (4)	264.4 - 272.1	3.61 - 8.84	Dholabhai et al. (1991)
C_2H_6 (1) + water (2) + 9.93 wt % NaCl (3) + 9.93 wt % KCl (4)	269.2 - 275.1	0.85 - 1.85	Englezos and Bishnoi (1991)
C_2H_6 (1) + water (2) + 10.00 wt % NaCl (3) + 5.00 wt % KCl (4)	267.1 - 276.5	0.49 - 1.69	Englezos and Bishnoi (1991)
C_2H_6 (1) + water (2) + 10.00 wt % NaCl (3) + 5.00 wt % $CaCl_2$ (4)	266.9 - 276.1	0.52 - 1.73	Englezos and Bishnoi (1991)
C_3H_8 (1) + water (2) + 2.03 wt % NaCl (3) + 8.01 wt % $CaCl_2$ (4)	268.1 - 272.2	0.17 - 0.42	Bishnoi and Dholabhai (1993)
C_3H_8 (1) + water (2) + 3.03 wt % NaCl (3) + 3.00 wt % $CaCl_2$ (4)	271.0 - 275.1	0.21 - 0.49	Bishnoi and Dholabhai (1993)
C_3H_8 (1) + water (2) + 4.90 wt % NaCl (3) + 3.80 wt % $CaCl_2$ (4)	270.9 - 273.5	0.23 - 0.44	Tohidi et al. (1997)

Table B-11 (continued): Measured HLV equilibrium data for the former (1) + water (2) + mixed salt (3) + (4) + (5) systems cited in literature.

System	Temperature Range (K)	Pressure Range (MPa)	Reference
C_3H_8 (1) + water (2) + 5.00 wt % NaCl (3) + 5.00 wt % KCl (4)	270.4 - 272.8	0.23 - 0.44	Tohidi et al. (1997)
C_3H_8 (1) + water (2) + 7.98 wt % NaCl (3) + 1.99 wt % $CaCl_2$ (4)	267.7 - 272.3	0.16 - 0.47	Bishnoi and Dholabhai (1993)
H_2S (1) + water (2) + 5.00 wt % NaCl (3) + 5.00 wt % KCl (4)	273.1 - 283.1	0.14 - 0.39	Mohammadi and Richon (2012)
H_2S (1) + water (2) + 5.00 wt % NaCl (3) + 5.00 wt % $CaCl_2$ (4)	274.2 - 282.9	0.16 - 0.40	Mohammadi and Richon (2012)
H_2S (1) + water (2) + 10.00 wt % NaCl (3) + 5.00 wt % KCl (4)	272.2 - 281.4	0.16 - 0.42	Mohammadi and Richon (2012)
H_2S (1) + water (2) + 10.00 wt % NaCl (3) + 5.00 wt % $CaCl_2$ (4)	269.5 - 279.6	0.13 - 0.37	Mohammadi and Richon (2012)
H_2S (1) + water (2) + 10.00 wt % NaCl (3) + 10.00 wt % $CaCl_2$ (4)	275.2 - 284.1	0.32 - 0.89	Mahadev and Bishnoi (1999)
H_2S (1) + water (2) + 10.00 wt % NaCl (3) + 10.00 wt % KCl (4)	275.2 - 286.1	0.27 - 0.85	Mahadev and Bishnoi (1999)
CH_4-CO_2 (1) + water (2) + 5.00 wt % NaCl (3) + 10.00 wt % KCl (4)	265.1 - 281.3	1.66 - 10.4	Dholabhai and Bishnoi (1994)
CH_4-CO_2 (1) + water (2) + 5.01 wt % NaCl (3) + 10.00 wt % $CaCl_2$ (4)	265.5 - 276.7	2.06 - 7.14	Dholabhai and Bishnoi (1994)
CH_4-CO_2 (1) + water (2) + 10.00 wt % NaCl (3) + 5.00 wt % KCl (4)	265.8 - 275.5	1.38 - 4.59	Dholabhai and Bishnoi (1994)
CH_4-CO_2 (1) + water (2) + 10.00 wt % NaCl (3) + 10.00 wt % $CaCl_2$ (4)	264.1 - 270.8	2.15 - 5.16	Dholabhai and Bishnoi (1994)
CH_4-CO_2 (1) + water (2) + 10.17 wt % NaCl (3) + 5.08 wt % $CaCl_2$ (4)	265.5 - 278.7	2.11 - 9.71	Dholabhai and Bishnoi (1994)
CH_4-CO_2 (1) + water (2) + 10.00 wt % KCl (3) + 5.00 wt % $CaCl_2$ (4)	265.1 - 281.6	1.65 - 10.6	Dholabhai and Bishnoi (1994)
C_2H_6 (1) + water (2) + 5.00 wt % $CaCl_2$ (3) + 10.00 wt % KCl (4)	268.1 - 276.4	0.50 - 1.45	Englezos and Bishnoi (1991)
C_3H_8 (1) + water (2) + 7.50 wt % $CaCl_2$ (3) + 7.50 wt % KCl (4)	266.3 - 270.1	0.18 - 0.43	Englezos and Ngan (1993)

Table B-11 (continued): Measured HLV equilibrium data for the former (1) + water (2) + mixed salt (3) + (4) + (5) systems cited in literature.

System	Temperature Range (K)	Pressure Range (MPa)	Reference
C_3H_8 (1) + water (2) + 7.50 wt % KCl (3) + 7.50 wt % NaCl (4)	265.2 - 269.1	0.16 - 0.37	Englezos and Ngan (1993)
CH_4-N_2 (1) + water (2) + 5.00 wt % NaCl (3) + 3.00 wt % $NaHCO_3$ (4)	268.1 - 283.2	2.40 - 10.79	Mei et al. (1996)
CH_4-N_2 (1) + water (2) + 5.00 wt % NaCl (3) + 5.00 wt % $MgCl_2$ (4)	272.1 - 285.2	3.44 - 12.26	Mei et al. (1996)
CH_4-N_2 (1) + water (2) + 10.00 wt % $CaCl_2$ (3) + 5.00 wt % $MgCl_2$ (4)	269.9 - 281.2	3.16 - 11.34	Mei et al. (1996)
CH_4-N_2 (1) + water (2) + 10.00 wt % $CaCl_2$ (3) + 10.00 wt % NaCl (4)	269.9 - 279.8	3.72 - 11.16	Mei et al. (1996)
H_2S (1) + water (2) + 5.00 wt % NaCl (3) + 5.00 wt % KCl (4) + 5.00 wt % $CaCl_2$ (5)	268.6 - 280.5	0.11 - 0.37	Mohammadi and Richon (2012)
C_2H_6 (1) + water (2) + 6.00 wt % NaCl (3) + 3.00 wt % $CaCl_2$ (4) + 5.00 wt % KCl (5)	269.0 - 278.4	0.56 - 1.97	Englezos and Bishnoi (1991)
Synthetic natural gas (1) + water (2) + 2.00 wt % NaCl (3) + 0.50 wt % $CaCl_2$ (4) + 0.50 wt % KCl (5)	270.9 - 281.2	0.60 - 2.75	Mei et al. (1998)
CH_4-N_2 (1) + water (2) + 5.00 wt % NaCl (3) + 5.00 wt % $MgCl_2$ (4) + 5.00 wt % $CaCl_2$ (5)	270.2 - 280.4	2.41 - 10.09	Mei et al. (1996)
C_3H_8 (1) + water (2) + 5.00 wt % $CaCl_2$ (3) + 7.50 wt % NaCl (4) + 7.50 wt % KCl (5)	261.9 - 265.2	0.17 - 0.35	Englezos and Ngan (1993)
CH_4-CO_2 (1) + water (2) + 6.01 wt % NaCl (3) + 5.00 wt % KCl (4) + 3.99 wt % $CaCl_2$ (5)	265.5 - 278.3	1.85 - 7.65	Dholabhai and Bishnoi (1994)

Table B-11 (continued): Measured HLV equilibrium data for the former (1) + water (2) + mixed salt (3) + (4) + (5) systems cited in literature.

System	Temperature Range (K)	Pressure Range (MPa)	Reference
CH_4-CO_2 (1) + water (2) + 6.00 wt % NaCl (3) + 5.00 wt % KCl (4) + 4.00 wt % $CaCl_2$ (5)	266.0 - 275.5	1.45 - 4.46	Dholabhai and Bishnoi (1994)
C_3H_8 (1) + water (2) + 1.98 wt % NaCl (3) + 1.99 wt % KCl (4) + 1.98 wt % $CaCl_2$ (5)	271.0 - 274.5	0.19 - 0.41	Bishnoi and Dholabhai (1993)
H_2S (1) + water (2) + 10.00 wt % NaCl (3) + 5.06 wt % KCl (4) + 5.00 wt % $CaCl_2$ (5)	276.9 - 285.8	0.34 - 0.98	Mahadev and Bishnoi (1999)
CH_4 (1) + water (2) + Synthetic seawater (3) [a]	277.0 - 283.9	4.36 - 9.06	Dholabhai et al. (1991)
C_3H_8 (1) + water (2) + Synthetic seawater (3) [b]	272.0 - 276.1	0.18 - 0.45	Bishnoi and Dholabhai (1993)
C_3H_8 (1) + water (2) + North sea brine (3) [c]	272.7 - 275.9	0.23 - 0.43	Tohidi et al. (1997)
C_3H_8 (1) + water (2) + Forties formation water (3) [d]	270.6 - 273.5	0.24 - 0.45	Tohidi et al. (1997)

[a] Synthetic sea water: 2.394 wt % NaCl + 0.401 wt % Na_2SO_4 + 0.009 wt % NaF + 0.069 wt % KCl + 0.011 wt % KBr + 0.508 wt % $MgCl_2$ + 0.115 wt % $CaCl_2$ + 0.002 wt % $SrCl_2$

[b] Synthetic sea water: 2.6436 wt % NaCl + 0.0740 wt % KCl + 0.3310 wt % Na_2SO4 + 0.2560 wt % $MgCl_2$ + 0.0713 wt % $CaCl_2$ + 0.0020 wt % $SrCl_2$

[c] North sea water: 2.354 wt % NaCl + 0.116 wt % $CaCl_2$ + 0.524 wt % $MgCl_2$ + 0.086 wt % KCl + 0.428 wt % Na_2SO_4

[d] Forties formation water: 6.993 wt % NaCl + 0.735 wt % $CaCl_2$ + 0.186 wt % $MgCl_2$ + 0.066 wt % KCl + 0.099 wt % $SrCl_2$ + 0.036 wt % $BaCl_2$

Table B-12: Measured HLV equilibrium data for the former (1) + water (2) + alcohol/glycol/glycerol (3) systems cited in literature.

System	Temperature Range (K)	Pressure Range (MPa)	Reference
H_2S (1) + water (2) + 10.00 wt % ethylene glycol (3)	276.0 - 287.8	0.17 - 0.55	Mohammadi and Richon (2010a)
H_2S (1) + water (2) + 20.00 wt % ethylene glycol (3)	270.8 - 283.7	0.13 - 0.50	Mohammadi and Richon (2010a)
H_2S (1) + water (2) + 35.00 wt % ethylene glycol (3)	267.8 - 280.5	0.18 - 0.67	Mohammadi and Richon (2010a)
H_2S (1) + water (2) + 50.00 wt % ethylene glycol (3)	262.7 - 274.6	0.28 - 1.02	Mohammadi and Richon (2010a)
H_2S (1) + water (2) + 30.00 wt % methanol (3)	267.5 - 274.8	0.24 - 0.50	Mohammadi and Richon (2012a)
H_2S (1) + water (2) + 50.00 wt % methanol (3)	254.1 - 264.2	0.20 - 0.46	Mohammadi and Richon (2012a)
CH_4 (1) + water (2) + 55.00 wt % methanol (3)	237.3 - 248.4	3.16 - 10.76	Mohammadi and Richon (2010a)
CH_4 (1) + water (2) + 65.00 wt % methanol (3)	234.5 - 240.3	5.19 - 10.31	Mohammadi and Richon (2010a)
CH_4 (1) + water (2) + 5.00 wt % ethanol (3)	273.9 - 280.1	3.45 - 6.20	Mohammadi et al. (2007)
CH_4 (1) + water (2) + 10.00 wt % ethanol (3)	271.1 - 280.2	2.98 - 7.42	Mohammadi et al. (2007)
C_2H_6 (1) + water (2) + 10.00 wt % ethylene glycol (3)	271.1 - 278.5	0.47 - 1.20	Mohammadi and Richon (2010a)
C_2H_6 (1) + water (2) + 20.00 wt % ethylene glycol (3)	267.1 - 275.3	0.41 - 1.18	Mohammadi and Richon (2010a)
C_2H_6 (1) + water (2) + 35.00 wt % ethylene glycol (3)	262.1 - 269.4	0.49 - 1.29	Mohammadi and Richon (2010a)
C_2H_6 (1) + water (2) + 50.00 wt % ethylene glycol (3)	251.6 - 259.0	0.39 - 1.00	Mohammadi and Richon (2010a)
C_2H_6 (1) + water (2) + 5.00 wt % ethanol (3)	273.6 - 280.0	0.59 - 1.34	Mohammadi et al. (2007)
C_2H_6 (1) + water (2) + 10.00 wt % ethanol (3)	274.4 - 282.0	0.59 - 2.23	Mohammadi et al. (2007)
C_3H_8 (1) + water (2) + 5.00 wt % ethanol (3)	272.5 - 276.6	0.20 - 0.51	Mohammadi et al. (2007)
C_3H_8 (1) + water (2) + 10.00 wt % ethanol (3)	272.0 – 275.0	0.20 - 0.50	Mohammadi et al. (2007)

Table B-12 (continued): Measured HLV equilibrium data for the former (1) + water (2) + alcohol/glycol/glycerol (3) systems cited in literature.

System	Temperature Range (K)	Pressure Range (MPa)	Reference
CH_4 (80 mol %) - CO_2 (20 mol %) (1) + water (2) + 10.00 wt % methanol (3)	270.4 - 280.9	2.63 – 8.02	Dholabhai et al. (1997)
CH_4 (80 mol %) - CO_2 (20 mol %) (1) + water (2) + 20.00 wt % methanol (3)	264.3 - 277.3	2.38 - 9.68	Dholabhai et al. (1997)
CH_4 (80 mol %) - CO_2 (20 mol %) (1) + water (2) + 10.00 wt % ethylene glycol (3)	269.6 - 281.2	1.92 - 6.32	Dholabhai et al. (1997)
CH_4 (80 mol %) - CO_2 (20 mol %) (1) + water (2) + 30.00 wt % ethylene glycol (3)	264.8 - 277.2	2.43 - 9.17	Dholabhai et al. (1997)
CH_4 (50 mol %) - CO_2 (50 mol %) (1) + water (2) + 19.99 wt % methanol (3)	264.6 - 275.8	1.88 - 6.73	Dholabhai et al. (1997)

Table B-13: Measured HLV equilibrium data for the former (1) + water (2) + mixed thermodynamic inhibitor (3) + (4) systems cited in literature.

System	Temperature Range (K)	Pressure Range (MPa)	Reference
H_2S (1) + water (2) + 15.00 wt % ethylene glycol (3) + 5.00 wt % NaCl (4)	272.7 - 290.1	0.18 - 1.08	Mohammadi and Richon (2012a)
H_2S (1) + water (2) + 10.00 wt % methanol (3) + 5.00 wt % NaCl (4)	273.4 - 286.8	0.19 - 0.78	Mohammadi and Richon (2012a)
CH_4 (1) + water (2) + 12.00 wt % ethylene glycol (3) + 8.00 wt % $CaCl_2$ (4)	271.6 - 286.1	4.27 - 24.65	Najibi et al. (2009)
CH_4 (1) + water (2) + 13.40 wt % ethylene glycol (3) + 15.30 wt % $CaCl_2$ (4)	265.1 - 283.6	3.97 - 45.44	Masoudi et al. (2005)
CH_4 (1) + water (2) + 14.00 wt % ethylene glycol (3) + 18.00 wt % $CaCl_2$ (4)	261.5 - 279.6	3.91 - 44.84	Masoudi et al. (2005)
CH_4 (1) + water (2) + 20.00 wt % ethylene glycol (3) + 15.00 wt % NaCl (4)	260.0 - 269.0	3.90 - 10.98	Mohammadi and Richon (2009b)
CH_4 (1) + water (2) + 20.00 wt % ethylene glycol (3) + 10.00 wt % KCl (4)	262.4 - 274.1	2.85 - 10.12	Mohammadi and Richon (2009b)
CH_4 (1) + water (2) + 20.00 wt % ethylene glycol (3) + 15.00 wt % $CaCl_2$ (4)	267.7 - 278.0	3.07 - 9.98	Mohammadi and Richon (2009b)
CH_4 (1) + water (2) + 21.30 wt % ethylene glycol (3) + 15.00 wt % $CaCl_2$ (4)	269.4 - 287.8	4.03 - 43.86	Masoudi et al. (2005)
CH_4 (1) + water (2) + 21.30 wt % ethylene glycol (3) + 15.00 wt % NaCl (4)	262.3 - 277.9	5.07 - 46.70	Masoudi et al. (2004a)
CH_4 (1) + water (2) + 23.00 wt % ethylene glycol (3) + 10.00 wt % KCl (4)	265.5 - 283.9	4.16 - 44.51	Masoudi et al. (2004a)
CH_4 (1) + water (2) + 26.00 wt % ethylene glycol (3) + 14.00 wt % $CaCl_2$ (4)	261.6 - 277.9	4.68 - 43.35	Masoudi et al. (2005)
CH_4 (1) + water (2) + 30.00 wt % ethylene glycol (3) + 3.00 wt % NaCl (4)	271.9 - 279.5	7.67 - 20.30	Najibi et al. (2009)

Table B-13 (continued): Measured HLV equilibrium data for the former (1) + water (2) + mixed thermodynamic inhibitor (3) + (4) systems cited in literature.

System	Temperature Range (K)	Pressure Range (MPa)	Reference
CH_4 (1) + water (2) + 30.00 wt % ethylene glycol (3) + 5.00 wt % NaCl (4)	272.7 - 282.1	3.42 - 20.41	Chapoy et al. (2012)
CH_4 (1) + water (2) + 30.80 wt % ethylene glycol (3) + 12.00 wt % NaCl (4)	262.4 - 275.2	6.96 - 46.69	Masoudi et al. (2004a)
CH_4 (1) + water (2) + 35.00 wt % ethylene glycol (3) + 8.00 wt % KCl (4)	259.3 - 277.6	3.93 - 45.05	Masoudi et al. (2004a)
CH_4 (1) + water (2) + 40.00 wt % ethylene glycol (3) + 10.00 wt % NaCl (4)	284.3 - 264.6	1.75 - 10.39	Chapoy et al. (2012)
CH_4 (1) + water (2) + 40.00 wt % ethylene glycol (3) + 10.00 wt % NaCl (4)	284.3 - 264.6	1.75 - 10.39	Chapoy et al. (2012)
Natural gas [a] (1) + water (2) + 23.00 wt % ethylene glycol (3) + 5.00 wt % NaCl (4)	277.4 - 286.7	4.29 - 24.74	Chapoy et al. (2012)
Natural gas [a] (1) + water (2) + 30.00 wt % ethylene glycol (3) + 5.00 wt % NaCl (4)	272.7 - 282.1	3.42 - 20.41	Chapoy et al. (2012)
CH_4 (1) + water (2) + 9.00 wt % methanol (3) + 7.00 wt % KCl (4)	275.9 - 286.3	7.45 - 28.89	Najibi et al. (2009)
CH_4 (1) + water (2) + 9.20 wt % methanol (3) + 8.30 wt % NaCl (4)	273.9 - 283.5	7.83 - 26.34	Najibi et al. (2009)
CH_4 (1) + water (2) + 10.00 wt % methanol (3) + 5.00 wt % $CaCl_2$ (4)	272.1 - 277.5	4.88 - 8.73	Mohammadi and Richon (2009b)
CH_4 (1) + water (2) + 14.00 wt % methanol (3) + 10.00 wt % $CaCl_2$ (4)	274.1 - 280.4	7.83 - 26.34	Najibi et al. (2009)
CH_4 (1) + water (2) + 15.00 wt % methanol (3) + 10.00 wt % KCl (4)	266.2 - 274.4	4.43 - 11.41	Mohammadi and Richon (2009b)
CH_4 (1) + water (2) + 20.00 wt % methanol (3) + 10.00 wt % NaCl (4)	253.9 - 260.1	5.11 - 10.97	Mohammadi and Richon (2009b)
CH_4 (1) + water (2) + 30.00 wt % methanol (3) + 3.00 wt % NaCl (4)	269.3 - 274.4	13.99 - 25.64	Najibi et al. (2009)

Table B-13 (continued): Measured HLV equilibrium data for the former (1) + water (2) + mixed thermodynamic inhibitor (3) + (4) systems cited in literature.

System	Temperature Range (K)	Pressure Range (MPa)	Reference
CH_4 (80 mol %) – CO_2 (20 mol %) (1) + water (2) + 5.00 wt % methanol (3) + 15.00 wt % NaCl (4)	262.4 - 274.9	2.15 - 9.37	Dholabhai et al. (1997)
CH_4 (80 mol %) – CO_2 (20 mol %) (1) + water (2) + 5.00 wt % methanol (3) + 9.97 wt % KCl (4)	267.6 - 280.4	2.17 - 9.71	Dholabhai et al. (1997)
CH_4 (80 mol %) – CO_2 (20 mol %) (1) + water (2) + 5.00 wt % methanol (3) + 9.97 wt % $CaCl_2$ (4)	266.5 - 280.4	2.21 - 10.35	Dholabhai et al. (1997)
CH_4 (80 mol %) – CO_2 (20 mol %) (1) + water (2) + 5.00 wt % methanol (3) + 14.98 wt % $CaCl_2$ (4)	262.2 - 274.8	2.16 - 9.24	Dholabhai et al. (1997)
CH_4 (80 mol %) – CO_2 (20 mol %) (1) + water (2) + 10.00 wt % methanol (3) + 9.98 wt % NaCl (4)	262.2 - 275.2	2.06 - 8.75	Dholabhai et al. (1997)
CH_4 (80 mol %) – CO_2 (20 mol %) (1) + water (2) + 10.00 wt % methanol (3) + 9.96 wt % $CaCl_2$ (4)	262.3 - 276.1	2.03 - 9.36	Dholabhai et al. (1997)
CH_4 (80 mol %) – CO_2 (20 mol %) (1) + water (2) + 5.00 wt % ethylene glycol (3) + 15.03 wt % $CaCl_2$ (4)	264.8 - 276.9	2.27 - 8.87	Dholabhai et al. (1997)
CH_4 (80 mol %) – CO_2 (20 mol %) (1) + water (2) + 20.00 wt % ethylene glycol (3) + 5.02 wt % $CaCl_2$ (4)	269.9 - 276.8	3.38 - 7.66	Dholabhai et al. (1997)

Table B-13 (continued): Measured HLV equilibrium data for the former (1) + water (2) + mixed thermodynamic inhibitor (3) + (4) + (5) + (6) systems cited in literature.

System	Temperature Range (K)	Pressure Range (MPa)	Reference
CH_4 (50 mol %) - CO_2 (50 mol %) (1) + water (2) + 10.02 wt % methanol (3) + 5.00 wt % NaCl (4)	264.5 - 274.0	2.15 - 6.79	Dholabhai et al. (1997)
CH_4 (50 mol %) - CO_2 (50 mol %) (1) + water (2) + 15.00 wt % methanol (3) + 5.00 wt % NaCl (4)	266.1 - 274.1	2.56 - 6.89	Dholabhai et al. (1997)
CH_4 (80 mol %) - CO_2 (20 mol %) (1) + water (2) + 15.00 wt % ethylene glycol (3) + 5.02 wt % NaCl (4) + 4.98 wt % $CaCl_2$ (5)	265.0 - 277.0	2.36 - 9.25	Dholabhai et al. (1997)
CH_4 (80 mol %) - CO_2 (20 mol %) (1) + water (2) + 5.00 wt % methanol (3) + 4.93 wt % NaCl (4) + 4.96 wt % KCl (5) + 5.00 wt % $CaCl_2$ (6)	263.6 - 276.1	2.14 - 9.05	Dholabhai et al. (1997)
CH_4 (50 mol %) - CO_2 (50 mol %) (1) + water (2) + 5.00 wt % methanol (3) + 4.93 wt % NaCl (4) + 4.96 wt % KCl (5) + 5.00 wt % $CaCl_2$ (6)	264.5 - 270.1	1.96 - 3.85	Dholabhai et al. (1997)

[a] Natural gas: 0.8879 mole fraction methane, 0.0530 mole fraction ethane, 0.1550 mole fraction propane, 0.0017 mole fraction i-Butane, 0.0030 mole fraction n-Butane, 0.0007 mole fraction i-Pentane, 0.0010 mole fraction n-Pentane, 0.0168 mole fraction CO_2, and 0.0204 mole fraction nitrogen.

B.9 Literature data for test systems used in this study

Table B-14: Literature data for the test systems used in this study.

System	Reference	Temperature (K)	Pressure (MPa)
CO_2 (1) + water (2)	Deaton and Frost (1946)	282.9	4.32
		282.6	4.13
		281.9	3.71
		281.5	3.53
		280.9	3.21
		279.8	2.76
		279.8	2.79
		278.7	2.43
		278.7	2.41
		277.6	2.08
		277.6	2.08
		277.6	2.10
		276.5	1.85
		275.4	1.61
		274.3	1.39
		274.3	1.42
		274.3	1.42
		273.7	1.32
		273.7	1.32
	Englezos and Hall (1994)	282.7	4.16
		281.6	3.49
		279.2	2.60
		277.7	2.13
		277.1	1.95
		275.1	1.54
	Mohammadi et al. (2005)	282.5	4.02
		282.2	3.84
		277.5	2.05

Table B-14 (continued): Literature data for the test systems used in this study.

System	Reference	Temperature (K)	Pressure (MPa)
CO_2 (1) + water (2) + 5 wt % NaCl (3)	Dholabhai et al. (1993)	280.0	3.77
		278.0	3.00
		275.0	2.02
		273.1	1.60
		271.2	1.31
	Mohammadi et al. (2008b)	280.2	3.73
		278.6	3.01
		274.4	1.83
		271.8	1.37
CO_2 (1) + water (2) + 5 wt % KCl (3)	Dholabhai et al. (1993)	280.5	3.91
		280.4	3.86
		279.4	3.32
		278.6	2.96
		276.0	2.13
		274.1	1.70
		272.1	1.33
CO_2 (1) + water (2) + 5 wt % NaCl (3) + 5 wt % KCl (4)	Dholabhai et al. (1993)	277.3	3.43
		274.1	2.26
		271.7	1.66
		270.0	1.35

ADDITIONAL DATA FOR THERMODYNAMIC MODELLING

C.1 Aspen Plus® flash calculation procedure
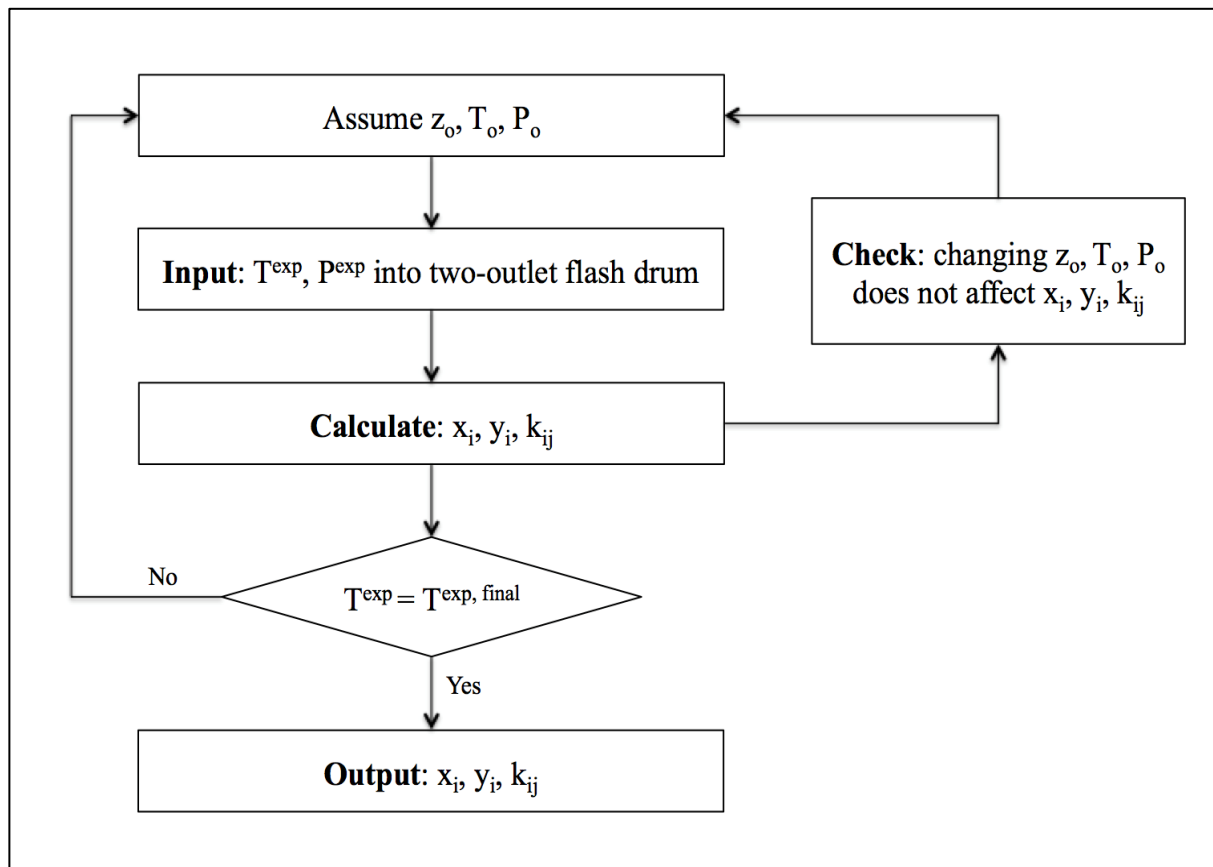
Figure C-1: Computation flow chart for determining the solubility data using Aspen Plus®.

C.2 Model development for the hydrate phase

Numerous models have been developed from the extensions made by Parrish and Prausnitz (1972). Each model attempts to reduce the error between the experimental and predicated equilibrium data, while maintaining the model simplicity for industrial purposes. The model developments can be found in Table C-1 below.

Table C-1: Hydrate model development (updated and edited from Smith, 2015).

Model	Model developed on	Assumptions	Development
Sloan, Khoury and Kobayashi (1976)	Van der Waals and Platteeuw (1959)	Hydrate lattice is composed of pure ice	Fugacity of water in the filled hydrate is related to the difference in chemical potential in the filled and empty hydrate by: $$f_w^H = f_w^{MT} exp\left(\frac{\mu_w^H - \mu_w^{MT}}{RT}\right)$$
Ng and Robinson (1980)	Parrish and Prausnitz (1972)[a] Sloan et al. (1976)[b]		[a] Extended the model for the incorporation of a hydrocarbon liquid former [b] Extended the model to obtaining the f_w^{MT} term. This is demonstrated by using correlative methods from vapour-hydrate data for various components. f_w^{MT} becomes negative for temperatures below 285 K and 287 K for sI and sII respectively.
Sloan, Sparks and Johnson (1987)	Ng and Robinson (1980)	The hydrate partial molar volume is equal to the molar volume and is independent of pressure. P_w^{MT} is in the order of 10^{-3} MPa, therefore $\emptyset_w^{MT} = 1$	Modified the model proposed by Ng and Robinson (1980)by fitting vapour pressure data obtained from H-L-V equilibrium data for various components: $$f_w^{MT} = P_w^{MT} \emptyset_w^{MT} exp \int_{P_w^{MT}}^{P} \frac{V_H^{MT}}{RT} dp$$ $\emptyset_w^{MT}$ is determined using the second viral coefficient, becomes significant at high pressures. This modification, based on the assumptions, can be simplified to: $$f_w^{MT} = P_w^{MT} exp \frac{V_H^{MT}(P - P_w^{MT})}{RT}$$

Table C-1 (continued): Hydrate model development (Updated and edited from Smith, 2015).

Model	Model developed on	Assumptions	Development
Chen and Guo (1998)	Van der Waals and Platteeuw (1959)	Step 1 is based on the assumption that the gas molecules dissolve in the liquid phase, and each guest molecule is surrounded by a cluster of dissolved gas molecules with water molecules.	Developed a model based on a two-step hydrate formation mechanism. First step: the formation of a stoichiometric basic hydrate structures though a quasi-chemical reaction. Second step: The adsorption of dissolved gas molecules into the empty hydrate capitates. This step may only occur for small gas molecules such as N_2, Ar, CH_4 and CO_2. The Langmuir adsorption theory is used to determine this step.
Mohammadi and Richon (2008)	Sloan et al. (1987)	The Poynting correction term, $exp\,\dfrac{V_H^{MT}(P-P_w^{MT})}{RT}=1$, for pressures up to 2 MPa.	The model of Sloan et al. (1987) therefore becomes: $$f_w^{MT}=P_w^{MT}exp\,\frac{V_H^{MT}(P-P_w^{MT})}{RT}$$
Eslamimanesh, Mohammadi and Richon (2011)	Parrish and Prausnitz (1972)	For systems where the dissociation pressure of the hydrate is low, the vapour phase consisting of pure guest molecules is assumed ideal	Based on the assumption, $f_l=P$ The model of Parrish and Prausnitz therefore becomes: $$\frac{\mu_w^H-\mu_w^{MT}}{RT}=\sum_m ln\left(1+\sum_j C_{mj}P\right)^{-\nu_m}$$

DETAILED REVIEW OF EXPERIMENTAL METHODS AND EQUIPMENT

D.1 Experimental methods

D.1.1 Isothermal pressure search method

Two trial-and-error experimentation techniques are available for this method: the visual and non-visual technique. Due to their methodology, both techniques may be time consuming.

Visual technique: The temperature is set to a specific value and kept constant. The pressure in the cell is increased to a value exceeding the predicted equilibrium pressure (Ma et al., 2001). Once a trace amount of hydrate crystals are observed, the pressure is gradually reduced to allow the hydrates to dissociate. After the complete dissociation of the hydrate crystals, the pressure is increased in small increments until hydrate crystals appear once again (Ma et al., 2001). If at the new pressure, the hydrate crystals disappear, the pressure is increased slightly until hydrate crystals reappear. At certain conditions of temperature and pressure, if the hydrates are able to remain intact for 4 - 6 hours, the equilibrium formation pressure at the given temperature is obtained (Mei et al., 1996). To reduce the effect of hysteresis, this process is repeated a number of times for a specific temperature (Englezos and Ngan, 1994).

Non-visual technique: The system temperature is set to a specific value and kept constant. Once the system is stable, hydrate formation occurs. This is indicated by a decrease in pressure. The pressure drop occurs as a result of the encapsulation of the gas molecules in the hydrate phase (Makogon et al., 1996; Mohammadi and Richon, 2010b). When the pressure approaches a near-equilibrium value, the system pressure is decreased below the expected equilibrium value by gas ventilation. The hydrate crystals, which had previously formed, dissociate causing the system pressure to increase and approach the equilibrium value. Once the pressure has stabilized at this new level, the pressure is increased resulting in hydrate formation. This process is repeated until a 2 % error is obtained between the upper and lower equilibrium pressures (Makogon and Sloan, 1994). The arithmetic

average of the upper and lower pressure approximations is taken as the final equilibrium pressure of hydrate formation at the given temperature (Makogon et al., 1996).

D.1.2 Isobaric temperature search method

In isobaric operation, the exchange of gas with an external reservoir maintains the system pressure at a constant value (Sloan and Koh, 2008). The cell is pressurized with the hydrate former and allowed to thermally equilibrate. Once the system is stable, the temperature is decreased until hydrate formation occurs. Upon the formation of gas hydrates, the system pressure decreases and the consumed former is recharged into the system in order to maintain a constant pressure. After hydrate formation, and once the system pressure have reached steady state, the temperature of the cell is slowly increased (a constant pressure is maintained by withdrawing the former) to dissociate the hydrates. The temperature is increased until the last hydrate crystal dissociates (Sloan and Koh, 2008). This point is taken as the equilibrium hydrate dissociation temperature at a constant pressure and may be established visually (Sloan and Koh, 2008).

D.1.3 Isochoric method

In the isochoric method, the equilibrium conditions are established through temperature and pressure measurements, at a constant volume. The isochoric method does not require viewing of the cell contents in order to determine the final hydrate dissociation point. This experimental method was used for the measurements in this study. A pressure-temperature trace depicting the hydrate formation and dissociating conditions during isochoric operation is shown in Figure D-1.
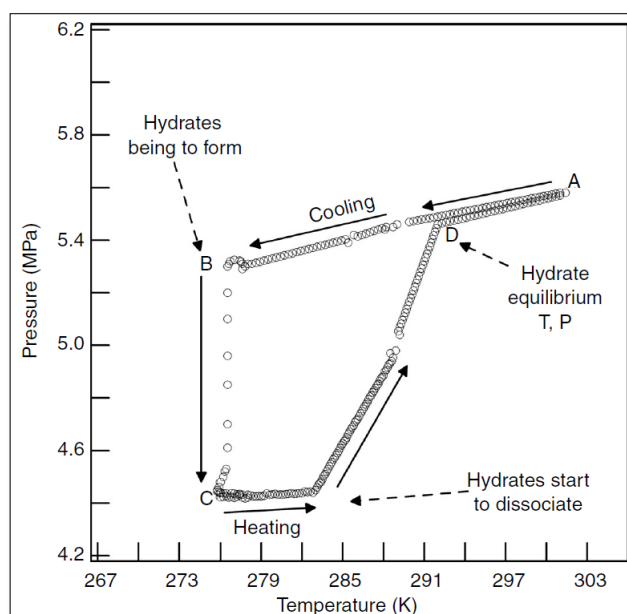
Figure D-1: Pressure-temperature trace for formation of simple hydrates (Sloan and Koh, 2008).

As shown in Figure D-1, measurements begin at temperature and pressure conditions in the hydrate instability region, point A. The temperature of the cell is then reduced. Isochoric cooling of the cell causes the cell pressure to decrease slightly to point B; the conditions for hydrate formation. At point B hydrate crystals form resulting in the pressure to reduce significantly to point C. The extent of the pressure reduction depends on the amount of gas molecules which fill the hydrate cavities as well as other thermodynamic restrictions. Once gas hydrate formation is complete and the system pressure has stabilized, the temperature is slowly increased to dissociate the hydrate crystals. This results in an increase in pressure. Once the hydrates are fully dissociated, all the gas is released from the crystals. According to Sloan and Koh (2008), the hydrate dissociation point is taken at point D, the intersection of the hydrate dissociation trace with the initial cooling trace.

D.2 Experimental equipment

D.2.1 Quartz crystal microbalance (QCM)

Initially, the QCM was developed for the measurement of small changes in mass. It is extremely sensitive; a 1 ng change in mass will result in a 1 Hz change in frequency (Mohammadi et al., 2003). This sensitivity is used to determine the presence or absence of gas hydrate crystals. Figure D-2 shows the set up of a QCM as well as the QCM placed in a high-pressure cell.

The QCM consists of two electrodes, which are separated by a thin quartz disk. Passing an electric current through the electrodes will oscillate the crystal at a specific resonant frequency, which is a function of the properties of the crystal (Sloan and Koh, 2008). A change in the resonant frequency will occur when a mass attaches itself to the surface of the crystal disk. Therefore hydrate formation (the mass) can be detected by the change in resonant frequency.

Initially, a drop of water is added to the surface of the crystal. The crystal is then placed into the high-pressure cell. The temperature of the cell is then decreased in order to freeze the water droplet. The cell is evacuated and the test system is charged into the cell. Favorable conditions of temperature and pressure for hydrate formation are set. The formation of gas hydrates results in a change in mass on the crystal, which causes a significant reduction in resonant frequency. The temperature of the equilibrium cell is then increased in a step wise manner, and the pressure and frequency are recorded at each step (Mohammadi et al., 2003). The point at which the resonant frequency changes (usually the highest frequency) is taken as the hydrate dissociation point.

The key advantage of the QCM method is that is requires small experimental samples (~ drop of water) which results in a significant reduction in the time required for the hydrate phase equilibrium measurements (Sloan and Koh, 2008). Despite its advantages, the QCM requires that the hydrates adhere to the surface of the quartz crystal. In some instances this may fail to occur, resulting in the unfeasibility of these measurements (Sloan and Koh, 2008). It has recently been demonstrated by Lee et al. (2012) that modification of the droplet size yields acceptable results, especially for rapid and practical gas hydrate purposes.
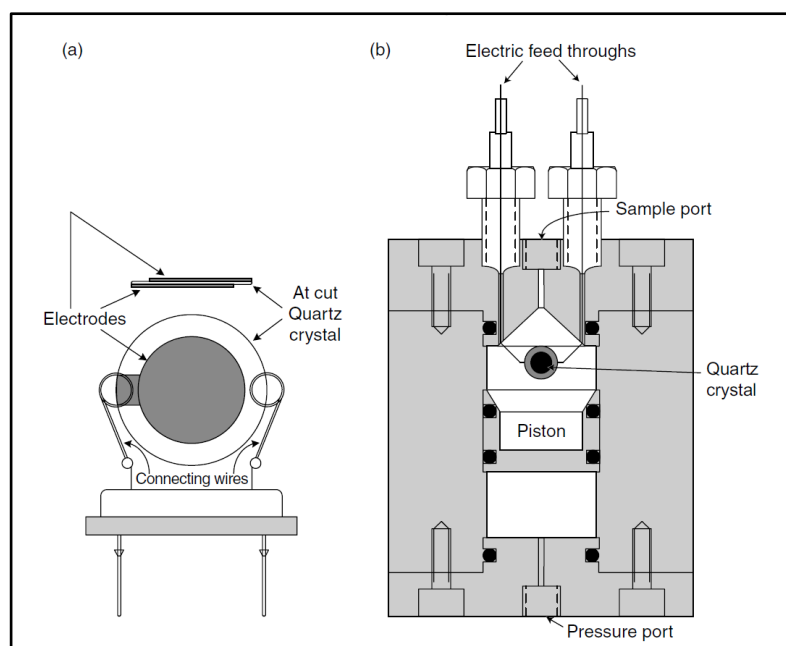
Figure D-2: (a) Schematic illustration of the QCM, and (b) the QCM mounted within a high pressure cell (Mohammadi et al., 2003).

D.2.2 Cailletet

The Cailletet is a high-pressure apparatus. Phase equilibrium conditions can be measured within a pressure and temperature range of 0.35 - 15 MPa and a 250 - 450 K respectively (Peters et al., 1986; Peters et al., 1993; Sabil, 2009). Visual observation is required for the determination of hydrate crystals. The apparatus is schematically shown in Figure D-3.

The heart of the apparatus is a thick-walled Pyrex glass tube of length 500 mm, with an inner and outer diameter of 3 mm and 10 mm respectively (Peters et al., 1993). This tube, known as the Cailletet tube is essentially the equilibrium cell. Only the upper end of the tube is closed. The lower end of the tube has a conical thickening, which enables the tube to be mounted in an autoclave. Experimental samples, which have been prepared according to the synthetic method (known composition), are confined in the top of the tube by using mercury as a sealing and pressure-transmitting fluid. The open end of the tube, which is placed into the autoclave, is always immersed in mercury. A soft iron rod coated with glass stirs the sample in the top of the tube magnetically. The autoclave is connected to a hydraulic oil system. Pressing the oil into the system by means of a screw type hand pump generates pressure. A dead-weight pressure balance is used to measure the equilibrium pressures. A thermostat jacket surrounds the Cailletet tube. The temperature of the sample is kept constant by circulating thermostat liquid through the jacket (Raeissi, 2004). In general, the sample is stirred gently during the measurements and more vigorously at the formation of the hydrate phase. The sample is cooled to form gas hydrates at an elevated pressure, while stirring vigorously. The pressure is kept constant to

prevent changes in the mercury level. The temperature where the gas hydrate crystals disappear is taken as the hydrate dissociation point (Sabil, 2009). From examined literature, even though the Cailletet apparatus boasts experimental work at elevated pressures, it is no longer used as mercury is highly toxic and the apparatus is susceptible to mechanical degradation due to the regular volume adjustments.
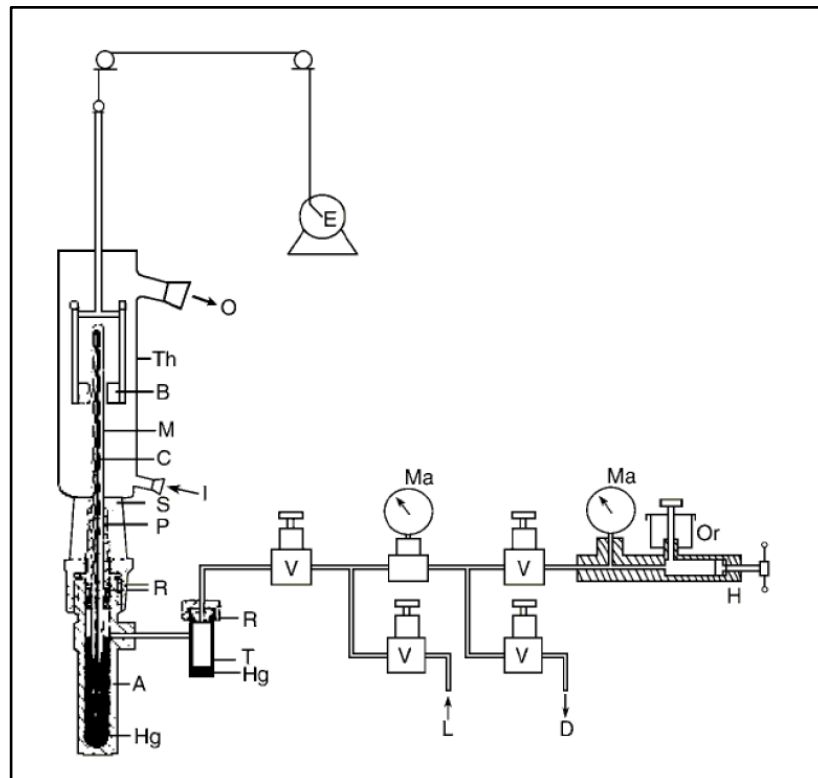
Figure D-3: Cailletet apparatus. (A) autoclave; (B) magnets; (C) Cailletet tube; (D) drain; (E) stirring motor; (H) hydraulic pump; (Hg) mercury; (I) inlet thermostat liquid; (L) connection with dead-weight pressure gauge; (M) sample of mercury; (Ma) manometers; (O) outlet thermostat liquid; (Or) oil reservoir; (P) closing plug; (R) O-rings; (S) silicone rubber stopper; (T) mercury trap; (Th) glass thermostat; (V) valve (Peters et al., 1993; Sabil, 2009).

D.2.3 The high pressure rocking cell

This apparatus consists of a high-pressure equilibrium cell mounted on a horizontal pivot for 180° pneumatic controlled rocking. The rocking of the cell, and consequent movement of the mixing balls within it, ensures adequate mixing of the cell fluids. The rocking rate of the cell is dependent on the degree of mixing required. The cell may be manufactured from sapphire or stainless steel. This allows the apparatus to withstand temperatures in the range of 243.15 - 325.15 K and pressures up to 50.0

MPa (Najibi et al., 2009). The isochoric experimental method is most commonly used and most reliable method for this apparatus (Najibi et al., 2009).

This apparatus allows data to be obtained continuously, allows for temperature cycle instructions to be carried out automatically, and visual observation of hydrate formation however, the setup is no longer used as it is subject to mechanical deterioration due to the continuous rocking motion. The high pressure-rocking cell is schematically shown in Figure D-4.
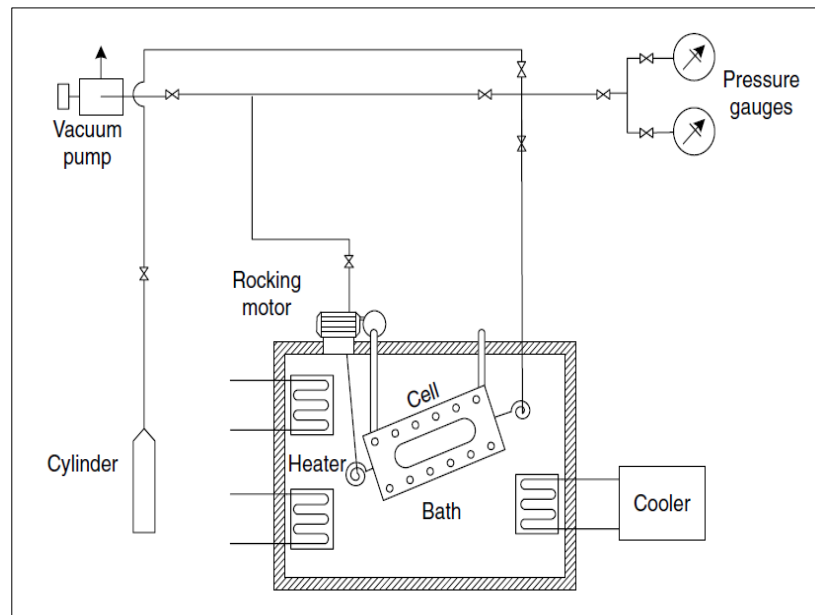
Figure D-4: Rocking hydrate equilibrium apparatus (Sloan and Koh, 2008).

D.2.4 High-pressure differential scanning calorimetry

Recently, the use of high-pressure differential scanning calorimetry (DSC) has been employed for the determination of hydrate phase equilibrium data, as well as gas hydrate thermal property data. Dalmazzone et al. (2002) illustrated the thermodynamic stability boundaries of natural gas and methane hydrates in the presence of various inhibitors by introducing a micro-DSC analyzer, used in conjunction with special high-pressure vessels, namely a High pressure Differential Scanning Calorimetry (HP-DSC).

The DSC apparatus, show in Figure D-5, is equipped with two pressure-controlled cells namely; a sample cell and a reference cell. The sample cell contains the experimental solution and the reference cell remains empty. The sample cell is charged with the experimental system and placed in the furnace and connected to the gas feed line where it is purged to evacuate any air that may be present.

Thereafter the gas pressure is set to the desired value and kept constant for each experimental point (Mayoufi et al., 2009). The isochoric experimental method is used to measure the hydrate dissociation conditions (Martinez et al., 2008; Mayoufi et al., 2009). The hydrate dissociation temperature is the crest of the hydrate progressive dissociation peak of the thermogram, as seen in Figure D-6. The apparatus can operate within a temperature range of 228.15 - 393.15 K. The DSC cells are designed to operate up to a maximum pressure of 40 MPa (Martinez et al., 2008). Due to the nature of the apparatus, no stirring may be used (Martinez et al., 2008).

Studies have shown that DSC is a rapid and easy to operate technique which can be efficiently used for kinetic as well as thermodynamic studies of the formation of high-pressure gas hydrates in complex fluids (such as electrolyte solutions), suspensions and emulsions whilst offering the same level of precision as classical PVT techniques (Le Parlouër et al., 2004). Additional advantages are that the technique is less time-consuming and requires small experimental samples. Despite its advantages, the method of data interpretation that accompanies this apparatus is relatively complex and measurement uncertainty may prove to be too large.
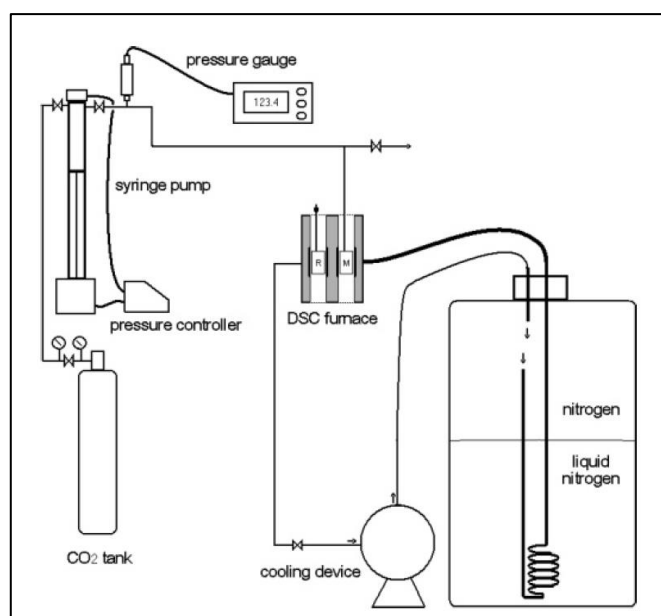
Figure D-5: High pressure differential scanning calorimetry apparatus: (R) reference cell; (M) sample cell (Delahaye et al., 2006).
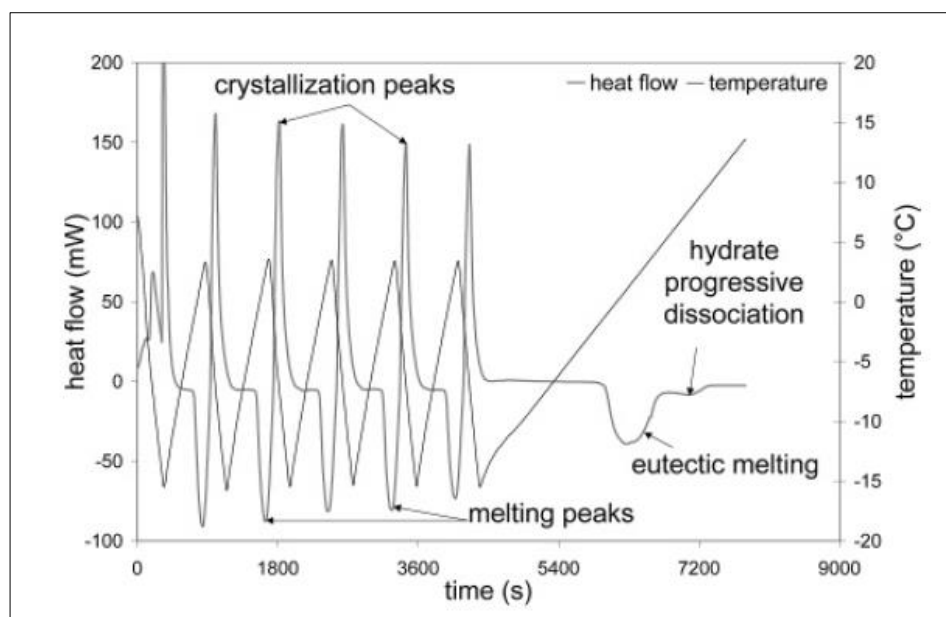
Figure D-6: Thermal cycles of hydrate formation and dissociation for high-pressure differential scanning calorimetry (Delahaye et al., 2006).

D.2.5 Differential thermal analysis

Fournaison et al. (2004) developed an experimental apparatus to characterize the thermal behavior of binary and ternary mixtures, establish the phase diagram of CO_2 hydrate mixtures and measure the heat transfer. The differential thermal analysis (DTA) apparatus is composed of two symmetric transparent glass cells. Like the DSC, one of the cells contains the experimental solution and the other cell contains an inert solution that is used as a reference. The setup is submerged in a temperature-controlled bath. The injection of gas via an injection system sets the initial cells pressures. Temperature and pressure are measured using a thermocouple in each cell and two transducers, respectively. Eight thermocouples connected in series are used to measure the temperature difference between the two cells and to perform the DTA measurements. The apparatus can operate within a temperature range of 250 K - 290 K and a maximum pressure of 4 MPa (Fournaison et al., 2004). The apparatus is schematically represented in Figure D-7.

Hydrate dissociation conditions may be measured using the isobaric temperature search method (Fournaison et al., 2004). The cells are subjected to cyclic decreasing and increasing temperature changes, at constant pressure, in order to obtain the cooling and heating rates. A stirring device is used in order to aid hydrate crystallization (Fournaison et al., 2004). The DTA signal (Figure D-8) is attained from the difference between the temperatures of the two cells. The increasing peaks indicate the formation of crystals while the decreasing peaks indicate hydrate dissociation. The temperature at

the crest of the dissociation peak is taken as the hydrate dissociation temperature at the experimental pressure (Delahaye et al., 2006). This apparatus is quite complex in its setup and has the potential for misinterpreting results.
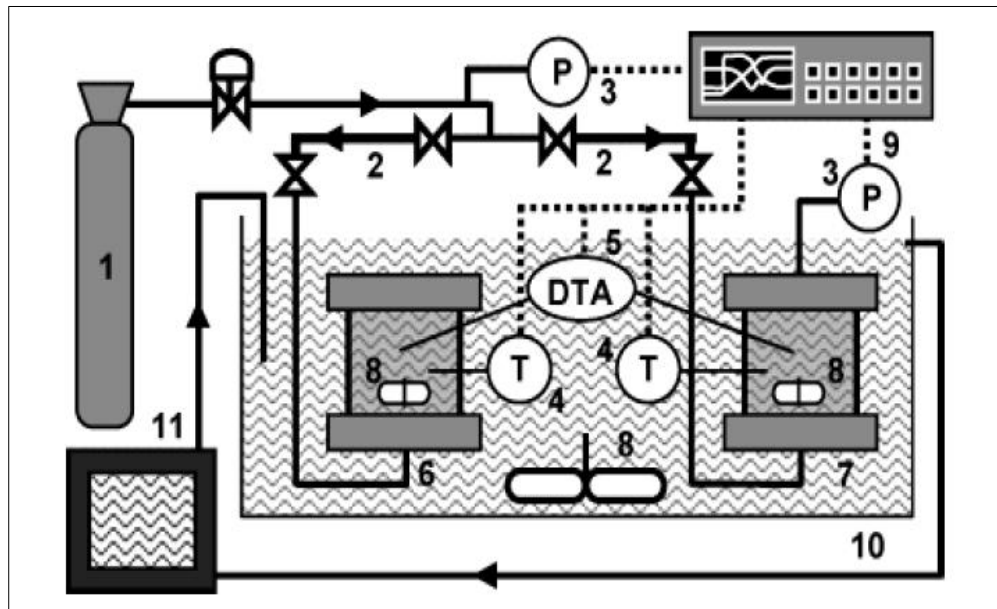
Figure D-7: Differential thermal analysis equipment. (1) Gas cylinder; (2) injection tank; (3) pressure gauge; (4) thermocouples; (5) differential thermal analyzer; (6) reference cell; (7) measuring cell; (8) stirrer; (9) acquisition interface; (10) temperature controlled bath; (11) cooling/heating unit (Fournaison et al., 2004).
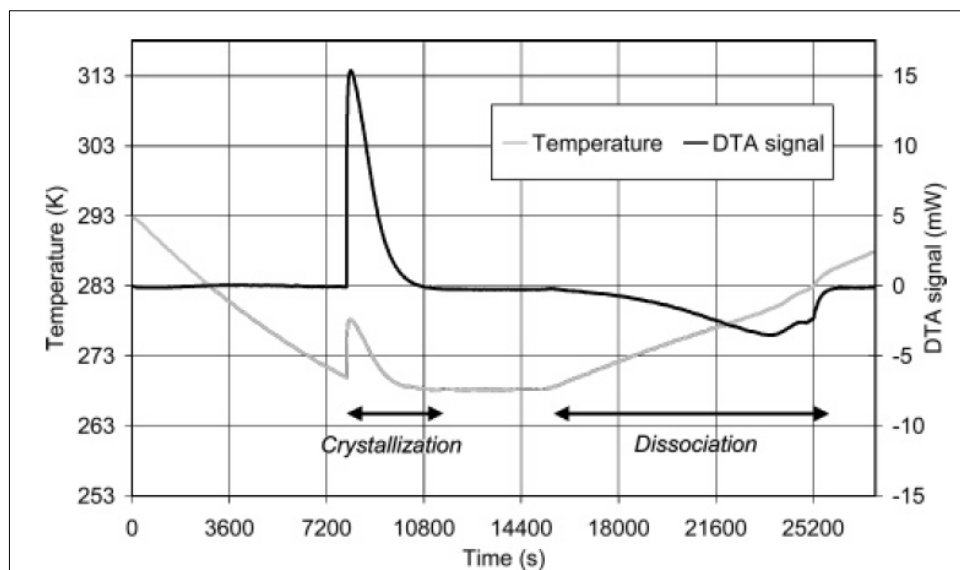
Figure D-8: Temperature and DTA signal history of a hydrate formation and dissociation for differential thermal analysis (Delahaye et al., 2006).

D.2.6 High pressure autoclave

Apparatus which includes a high-pressure autoclave with temperature and pressure control, are the most commonly used equipment for measuring gas hydrate equilibrium conditions (Zhang et al., 2007; Duc et al., 2007; Herri et al., 2011; Javanmardi et al., 2012). The core of the apparatus is a high-pressure cylindrical cell. These high-pressure cells may be constructed of either sapphire or 316 stainless steel. The cell can have a volume between 30 and 2000 cm^3 (Kang et al., 1998; Herri et al., 2011; Petticrew, 2011). The autoclave cell may be visual or non-visual in nature. For visual cells sapphire or Plexiglas windows are fitted into the cell for direct observation. A magnetic or mechanical stirrer generally achieves cell agitation. In cases where vortex formation is possible, baffles may be used to reduce the effect (Lee et al., 2005). The high-pressure cell is immersed in a thermostat bath for temperature control. The type of solution used in the bath is dependent on the temperature range required. Due to their heat capacity, ethanol is generally used for low temperatures, ethylene glycol-water mixture for moderate temperatures, and silicon oil for high temperatures. Any of the experimental methods described in section D.1 can be used to determine the hydrate dissociation conditions.

A few of the advantages of this setup are: simple construction and operation, capable of sampling cell contents if required, compatible with many chemicals, allows for the use of any of the three most common experimental methods, and fittings and O-rings are easily available for replacement.

CALIBRATION CONFIRMATION
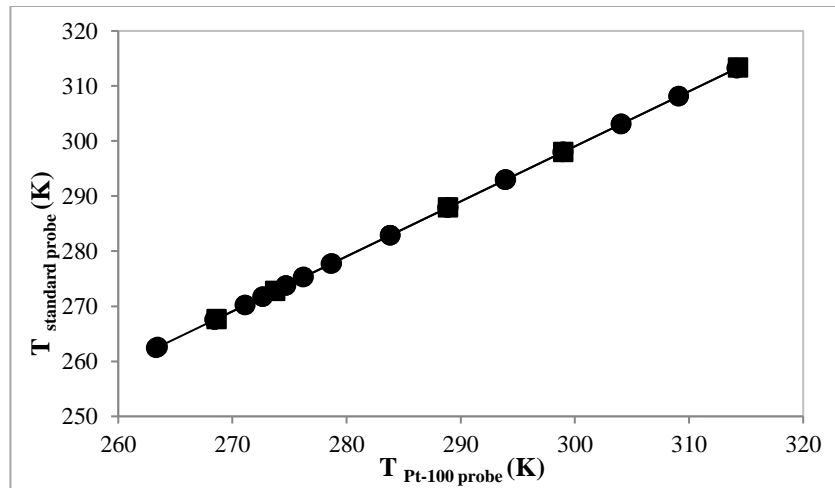
Figure E-1: Confirmation of the calibration performed on the Pt-100 temperature probe used in this study. (●) Calibration performed in June 2016; (■) confirmation of the calibration, performed in December 2016.
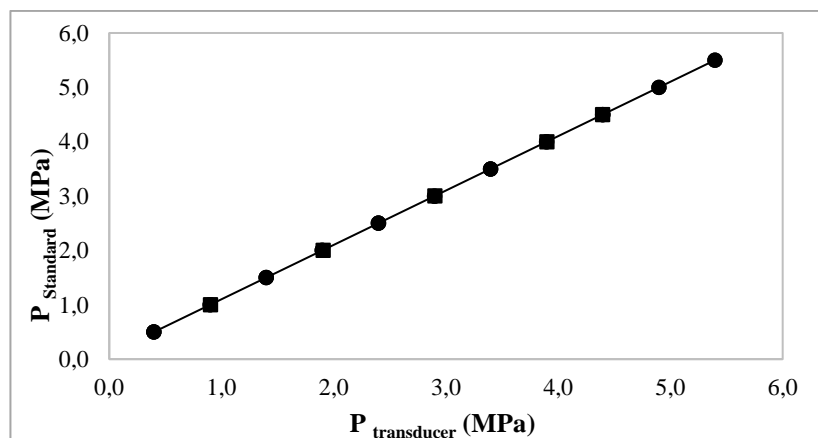
Figure E-2: Confirmation of the calibration performed on the 1 - 10 MPa WIKA pressure transducer used in this study. (●) Calibration performed in June 2016; (■) confirmation of the calibration, performed in December 2016.

CONCEPTUAL DESIGN AND ECONOMIC EVALUATION

The conceptual design performed in this study was based on the CO_2 (1) + water (2) + 5 wt % NaCl (3) + 5 wt % KCl (4) system as this exhibited the greatest temperature shift from the CO_2 (1) + water (2) system.

F.1 Mass balance

The mass balance performed in this study, for the proposed process, was based on a basis of 1000 tons of potable water produced per day. The detailed calculation procedure is presented below.

The selected basis of potable water produced per day, in standard units is:

$$Amount\ of\ potable\ water\ produced = 1000\frac{ton}{day} = 41666,66\frac{kg}{hr} \tag{F-1}$$

Assuming 30% yield,

$$Vinasse\ feed\ rate = \frac{Amount\ of\ potable\ water\ produced}{yield} \tag{F-2}$$

$$Vinasse\ feed\ rate = \frac{1000}{0.3}$$

$$Vinasse\ feed\ rate = 3333,33\frac{ton}{hr} = 138889\frac{kg}{hr}$$

Therefore:

$$Brine\ produced = Vinasse\ feed\ rate - Amount\ of\ potable\ water\ produced \tag{F-3}$$

$$Brine\ produced = 3333,33 - 1000\frac{ton}{hr}$$

$$Brine\ produced = 2333,33\frac{ton}{hr} = 97222,67\frac{kg}{hr}$$

For the vinasse feed rate, the required amount of CO_2 is calculated as:

$$Amount\ of\ CO_2\ required = \ Amount\ of\ potable\ water\ produced\frac{L}{hr} \times 0.264\frac{kg}{L} \qquad \text{(F-4)}$$

Using a simple conversion, the amount of potable water produced in L/hr. is:

$$Amount\ of\ potable\ water\ produced = \ 41666{,}66\frac{kg}{hr} \approx 41666{,}66\frac{L}{hr}$$

Therefore:

$$Amount\ of\ CO_2\ required = 41666{,}66 \ \times \ 0.264$$
$$Amount\ of\ CO_2\ required = 11000\frac{kg}{hr}$$

Assuming 200 % excess CO_2:

$$Amount\ of\ CO_2\ required = 11000 \ \times \frac{200\ \%}{100\ \%} \qquad \text{(F-5)}$$
$$Amount\ of\ CO_2\ required = 22000\frac{kg}{hr}$$

Using a simple conversion, the total amount of CO_2 required in kmol/hr. is therefore:

$$Amount\ of\ CO_2\ required = 22000\frac{kg}{hr} \times \frac{1}{MM_{CO_2}} \qquad \text{(F-6)}$$
$$Amount\ of\ CO_2\ required = 22000 \times \frac{1}{44}$$
$$Amount\ of\ CO_2\ required = 499.89\frac{kmol}{hr}$$

In order to convert the required amount (basis) of potable water produced in kmol/hr., the average molar mass of the potable water stream is needed. The average molar mass of the potable water stream was determined from the following equation:

$$\frac{1}{MM_{avg}} = \frac{X_a}{MM_a} + \cdots + \frac{X_i}{MM_i} \qquad \text{(F-7)}$$

where X represents the weight fraction of component and MM represents the molar mass of component.

It was assumed that 80 % of the salts present in the vinasse stream are present in the brine. Therefore 20 % of the salts are still present in the potable water stream. Based on the selected hydrate system on which the design was based, the vinasse feed stream is comprised of 90 % water, 5 % NaCl, and 5 % KCl:

$$Amount\ water\ in\ feed = x_{water,feed} \times Vinasse\ feed\ rate \qquad \text{(F-8)}$$

$$Amount\ water\ in\ feed = 0.9 \times 138889\frac{kg}{hr}$$

$$Amount\ water\ in\ feed = 125\ 000\frac{kg}{hr} = 3000\ \frac{ton}{day}$$

Similarly, the amount of NaCl present in the feed:

$$Amount\ NaCl\ in\ feed = x_{NaCl,feed} \times Vinasse\ feed\ rate \qquad \text{(F-9)}$$

$$Amount\ NaCl\ in\ feed = 0.05 \times 138889\frac{kg}{hr}$$

$$Amount\ NaCl\ in\ feed = 6944.44\frac{kg}{hr} = 166,67\ \frac{ton}{day}$$

Since the weight percentage of NaCl is the same as the weight percentage of KCl, the amount of KCl in the feed is:

$$Amount\ KCl\ in\ feed = 6944.44\frac{kg}{hr} = 166,67\ \frac{ton}{day}$$

Based on 20 % of the salts still present in the potable water:

$$Amount\ of\ NaCl\ in\ potable\ water = 0.2 \times Amount\ of\ NaCl\ in\ feed \qquad \text{(F-10)}$$

$$Amount\ of\ NaCl\ in\ potable\ water = 0.2 \times 6944.44\frac{kg}{hr}$$

$$Amount\ of\ NaCl\ in\ potable\ water = 1388.88\ \frac{kg}{hr} = 33.33\ \frac{ton}{day}$$

Similarly, the amount of KCl in potable water is 1388.88 kg/hr (33.33 ton/day). By using the total flow rate of the potable water stream and the amounts of NaCl and KCl present in the stream; the

amount of water in the potable water stream is 38888.75 kg/hr (933.33 ton/day). The results of the mass balance were used in Aspen Plus® in order to perform the conceptual design.

F.2 Aspen Plus® simulation results

The flow diagram from the simulation performed in Aspen Plus® is shown in Figure F-1. The simulation results are reported in Table F-1.
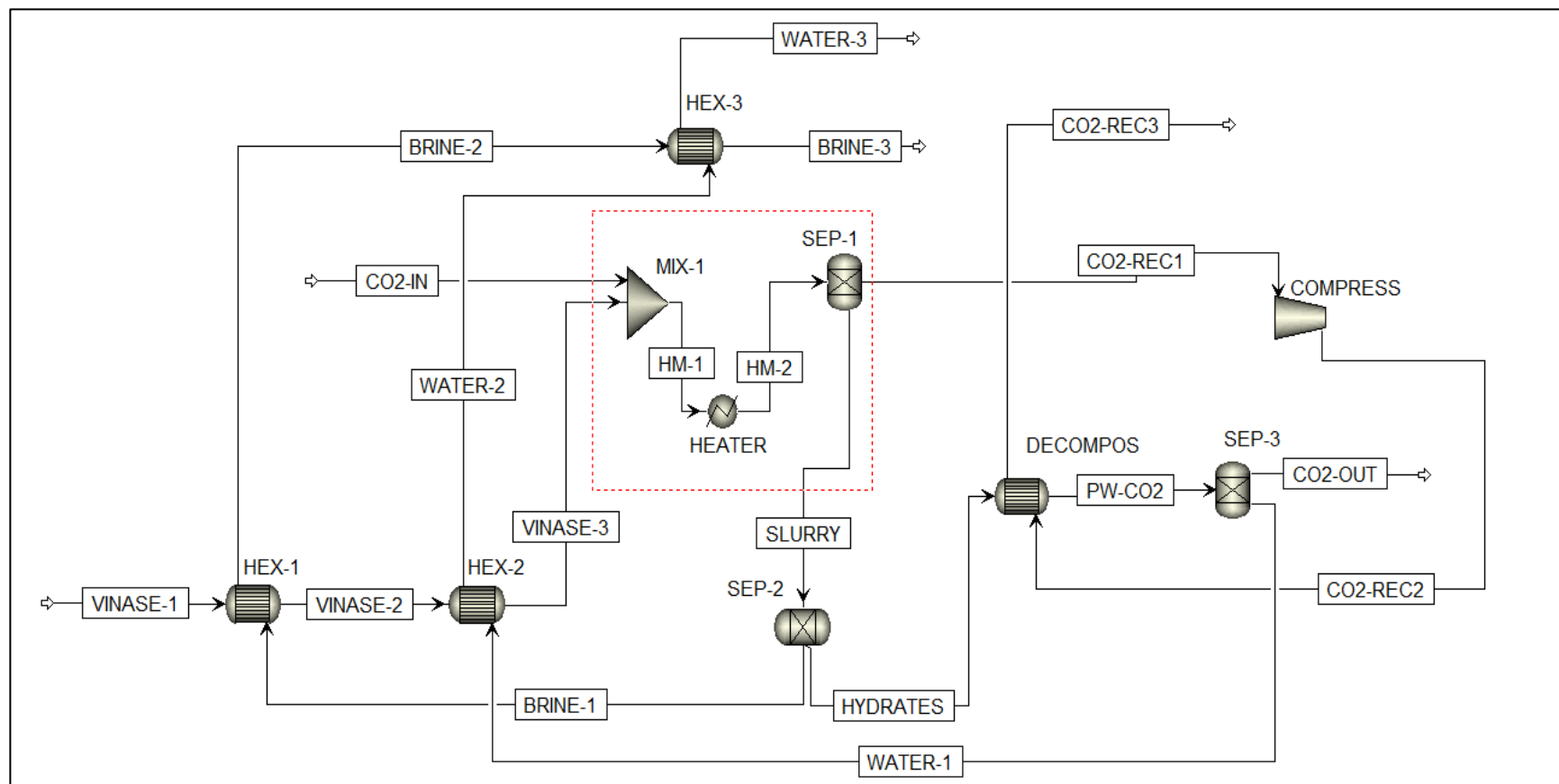
Figure F-1: Flow diagram from the Aspen Plus® simulation performed in this study, for the proposed process. The - - - - square around MIX-1, SEP-1, and HEATER units represent the units that were used to model the reactor.

Table F-1: Results of the Aspen Plus® simulation.

Streams		VINASE-1	VINASE-2	VINASE-3	CO2-IN	HM-1	HM-2	SLURRY
From			HEX-1	HEX-2		MIX-1	HEATER	SEP-01
To		HEX-1	HEX-2	MIX-1	MIX-1	HEATER	SEP-01	SEP-02
Phase:		Liquid	Liquid	Liquid	Vapor	Mixed	Mixed	Mixed
Component Mole Flow								
Water	kmol/hr	6938.55	6938.55	6938.55	0.00	0.33	0.16	0.11
CO_2	kmol/hr	0.00	0.00	0.00	499.89	497.99	498.33	346.96
KCl	kmol/hr	93.15	93.15	93.15	0.00	0.00	0.00	0.00
NaCl	kmol/hr	118.83	118.83	118.83	0.00	0.00	0.00	0.00
Component Mole Fraction								
Water		0.970	0.970	0.970	0.000	0.001	0.000	0.000
CO_2		0.000	0.000	0.000	1.000	0.999	1.000	1.000
KCl		0.013	0.013	0.013	0.000	0.000	0.000	0.000
NaCl		0.017	0.017	0.017	0.000	0.000	0.000	0.000
Component Mass Flow								
Water	kg/hr	125000.00	125000.00	125000.00	0.00	125000.00	125000.00	125000.00
CO_2	kg/hr	0.00	0.00	0.00	22000.00	22000.00	22000.00	15338.40
KCl	kg/hr	6944.44.	6944.44	6944.44	0.00	6944.44	6944.44	6944.44
NaCl	kg/hr	6944.44	6944.44	6944.44	0.00	6944.44	6944.44	6944.44

Table F-1 (continued): Results of the Aspen Plus® simulation.

Streams		VINASE-1	VINASE-2	VINASE-3	CO2-IN	HM-1	HM-2	SLURRY
From			HEX-1	HEX-2		MIX-1	HEATER	SEP-01
To		HEX-1	HEX-2	MIX-1	MIX-1	HEATER	SEP-01	SEP-02
Component Mass Fraction								
Water		0.90	0.90	0.90	0.00	0.78	0.78	0.81
CO₂		0.00	0.00	0.00	1.00	0.14	0.14	0.10
KCl		0.05	0.05	0.05	0.00	0.04	0.04	0.05
NaCl		0.05	0.05	0.05	0.00	0.04	0.04	0.05
Mole Flow	kmol/hr	7150.53	7150.53	7150.53	499.89	7650.42	7650.42	7499.05
Mass Flow	kg/hr	138888.89	138888.89	138888.89	22000.00	160888.89	160888.89	154227.29
Volume Flow	L/min	2185.54	2176.52	2175.05	3970.71	6536.06	6099.38	4903.05
Temperature	°C	25.00	17.84	16.66	5.00	15.94	4.49	4.49
Pressure	Bar	30.00	30.00	30.00	34.66	34.66	34.66	34.66
Vapour Fraction		0.00	0.00	0.00	1.00	0.14	0.14	0.10
Liquid Fraction		1.00	1.00	1.00	0.00	0.86	0.86	0.90
Solid Fraction		0.00	0.00	0.00	0.00	0.00	0.00	0.00
Molar Enthalpy	Cal/mol	-69410.82	-69545.85	-69568.15	-94655.14	-71207.37	-71420.13	-70951.05
Mass Enthalpy	Cal/GM	-3573.53	-3580.49	-3581.63	-2150.77	-3385.98	-3396.09	-3449.88
Enthalpy Flow	Cal/sec	-137867810.16	-138136030.34	-138180315.20	-13143619.60	-151323934.80	-151776073.20	-147796018.56
Molar Entropy	Cal/Mol-K	-39.30	-39.76	-39.83	-8.20	-37.77	-38.52	-39.14

Table F-1 (continued): Results of the Aspen Plus® simulation.

Streams		VINASE-1	VINASE-2	VINASE-3	CO2-IN	HM-1	HM-2	SLURRY
From			HEX-1	HEX-2		MIX-1	HEATER	SEP-01
To		HEX-1	HEX-2	MIX-1	MIX-1	HEATER	SEP-01	SEP-02
Mass Entropy	Cal/GM-K	-2.02	-2.05	-2.05	-0.19	-1.80	-1.83	-1.90
Molar Density	Mol/CC	0.05	0.05	0.05	0.00	0.02	0.02	0.03
Mass Density	GM/CC	1.06	1.06	1.06	0.09	0.41	0.44	0.52
Average Molecular Weight		19.42	19.42	19.42	44.01	21.03	21.03	20.57

Table F-1 (continued): Results of the Aspen Plus® simulation.

Streams		BRINE-1	BRINE-2	BRINE-3	HYDRATES	PW-CO2	CO2-OUT	CO2-REC1
From		SEP-2	HEX-1	HEX-3	SEP-2	DECOMPOS	SEP-3	SEP-1
To		HEX-1	HEX-3		DECOMPOS	SEP-3		COMPRESS
Phase:		Liquid	Liquid	Liquid	Mixed	Mixed	Vapor	Vapor
Component Mole Flow								
Water	kmol/hr	4779.90	4779.90	4779.90	0.11	0.16	0.00	0.00
CO₂	kmol/hr	0.01	0.01	0.01	348.03	347.98	348.51	151.37
KCl	kmol/hr	74.52	74.52	74.52	0.00	0.00	0.00	0.00
NaCl	kmol/hr	95.06	95.06	95.06	0.00	0.00	0.00	0.00
Component Mole Fraction								
Water		0.966	0.966	0.966	0.000	0.000	0.000	0.000
CO₂		0.000	0.000	0.000	1.000	1.000	1.000	1.000
KCl		0.015	0.015	0.015	0.000	0.000	0.000	0.000
NaCl		0.019	0.019	0.019	0.000	0.000	0.000	0.000
Component Mass Flow								
Water	kg/hr	86111.25	86111.25	86111.25	38888.75	38888.75	0.00	0.00
CO₂	kg/hr	0.44	0.44	0.44	15337.96	15337.96	15337.96	6661.60
KCl	kg/hr	5555.55	5555.55	5555.55	1388.89	1388.89	0.00	0.00
NaCl	kg/hr	5555.55	5555.55	5555.55	1388.89	1388.89	0.00	0.00

Table F-1 (continued): Results of the Aspen Plus® simulation.

Streams		BRINE-1	BRINE-2	BRINE-3	HYDRATES	PW-CO2	CO2-OUT	CO2-REC1
From		SEP-2	HEX-1	HEX-3	SEP-2	DECOMPOS	SEP-3	SEP-1
To		HEX-1	HEX-3		DECOMPOS	SEP-3		COMPRESS
Component Mass Fraction								
Water		0.89	0.89	0.89	0.68	0.68	0.00	0.00
CO_2		0.00	0.00	0.00	0.27	0.27	1.00	1.00
KCl		0.06	0.06	0.06	0.02	0.02	0.00	0.00
NaCl		0.06	0.06	0.06	0.02	0.02	0.00	0.00
Mole Flow	kmol/hr	4949.49	4949.49	4949.49	2549.56	2549.56	348.51	151.37
Mass Flow	kg/hr	97222.80	97222.80	97222.80	57004.49	57004.49	15337.96	6661.60
Volume Flow	L/min	1504.63	1513.03	1512.98	3407.97	3554.14	2898.33	1196.20
Temperature	°C	4.49	14.85	14.79	4.49	9.87	9.87	4.49
Pressure	Bar	34.66	34.66	34.66	34.66	34.66	34.66	34.66
Vapour Fraction		0.00	0.00	0.00	0.27	0.27	1.00	1.00
Liquid Fraction		1.00	1.00	1.00	0.73	0.73	0.00	0.00
Solid Fraction		0.00	0.00	0.00	0.00	0.00	0.00	0.00
Molar Enthalpy	Cal/mol	-69901.90	-69706.81	-69707.87	-72988.08	-72888.97	-94587.96	-94662.37
Mass Enthalpy	Cal/GM	-3558.62	-3548.69	-3548.74	-3264.44	-3260.00	-2149.25	-2150.94
Enthalpy Flow	Cal/sec	-96105234.51	-95837014.33	-95838472.65	-51690994.93	-51620800.40	-9156965.14	-3980192.20
Molar Entropy	Cal/Mol-K	-40.52	-39.83	-39.83	-36.46	-36.11	-7.96	-8.22

Table F-1 (continued): Results of the Aspen Plus® simulation.

Streams		BRINE-1	BRINE-2	BRINE-3	HYDRATES	PW-CO2	CO2-OUT	CO2-REC1
From		SEP-2	HEX-1	HEX-3	SEP-2	DECOMPOS	SEP-3	SEP-1
To		HEX-1	HEX-3		DECOMPOS	SEP-3		COMPRESS
Mass Entropy	Cal/GM-K	-2.06	-2.03	-2.03	-1.63	-1.61	-0.18	-0.19
Molar Density	Mol/CC	0.05	0.05	0.05	0.01	0.01	0.00	0.00
Mass Density	GM/CC	1.08	1.07	1.07	0.28	0.27	0.09	0.09
Average Molecular Weight		19.64	19.64	19.64	22.36	22.36	44.01	44.01

Table F-1 (continued): Results of the Aspen Plus® simulation.

Streams		CO2-REC2	CO2-REC3	WATER-1	WATER-2	WATER-3
From		COMPRESS	DECOMPOS	SEP-3	HEX-2	HEX-3
To		DECOMPOS		HEX-2	HEX-3	
Phase:		Vapor	Mixed	Liquid	Liquid	Liquid
Component Mole Flow						
Water	kmol/hr	0.00	0.00	2158.65	2158.65	2158.65
CO_2	kmol/hr	151.37	47.25	0.00	0.00	0.00
KCl	kmol/hr	0.00	0.00	18.63	18.63	18.63
NaCl	kmol/hr	0.00	0.00	23.77	23.77	23.77
Component Mole Fraction						
Water		0.000	0.000	0.981	0.981	0.981
CO_2		1.000	1.000	0.000	0.000	0.000
KCl		0.000	0.000	0.008	0.008	0.008
NaCl		0.000	0.000	0.011	0.011	0.011
Component Mass Flow						
Water	kg/hr	0.00	0.00	38888.75	38888.75	38888.75
CO_2	kg/hr	6661.60	6661.60	0.00	0.00	0.00
KCl	kg/hr	0.00	0.00	1388.89	1388.89	1388.89
NaCl	kg/hr	0.00	0.00	1388.89	1388.89	1388.89

Table F-1 (continued): Results of the Aspen Plus® simulation.

Streams		CO2-REC2	CO2-REC3	WATER-1	WATER-2	WATER-3
From		COMPRESS	DECOMPOS	SEP-3	HEX-2	HEX-3
To		DECOMPOS		HEX-2	HEX-3	
Component Mass Fraction						
Water		0.00	0.00	0.93	0.93	0.93
CO_2		1.00	1.00	0.00	0.00	0.00
KCl		0.00	0.00	0.03	0.03	0.03
NaCl		0.00	0.00	0.03	0.03	0.03
Mole Flow	kmol/hr	151.37	151.37	2201.05	2201.05	2201.05
Mass Flow	kg/hr	6661.60	6661.60	41666.53	41666.53	41666.53
Volume Flow	L/min	919.10	306.88	659.39	661.05	661.10
Temperature	°C	37.31	14.86	9.87	13.66	13.79
Pressure	Bar	50.66	50.66	34.66	34.66	34.66
Vapour Fraction		1.00	0.31	0.00	0.00	0.00
Liquid Fraction		0.00	0.69	1.00	1.00	1.00
Solid Fraction		0.00	0.00	0.00	0.00	0.00
Molar Enthalpy	Cal/mol	-94467.41	-96136.87	-69454.60	-69382.17	-69379.79
Mass Enthalpy	Cal/GM	-2146.51	-2184.44	-3668.96	-3665.14	-3665.01
Enthalpy Flow	Cal/sec	-3971994.54	-4042189.07	-42464713.36	-42420428.50	-42418970.18
Molar Entropy	Cal/Mol-K	-8.10	-13.84	-40.57	-40.31	-40.31

Table F-1 (continued): Results of the Aspen Plus® simulation.

Streams		CO2-REC2	CO2-REC3	WATER-1	WATER-2	WATER-3
From		COMPRESS	DECOMPOS	SEP-3	HEX-2	HEX-3
To		DECOMPOS		HEX-2	HEX-3	
Mass Entropy	Cal/GM-K	-0.18	-0.31	-2.14	-2.13	-2.13
Molar Density	Mol/CC	0.00	0.01	0.06	0.06	0.06
Mass Density	GM/CC	0.12	0.36	1.05	1.05	1.05
Average Molecular Weight		44.01	44.01	18.93	18.93	18.93

Table F-2: Aspen Plus® results for equipment in the proposed process

Equipment	Key for Figure F-1	Result
Compressor	COMPRESS	bhp = 34.32 kW
Decomposer	DECOMPOS	Area = 37.81 m^2 (406.98 ft^2)
Heat exchanger I	HEX-1	Area = 113.12 m^2 (1217.60 ft^2)
Heat exchanger II	HEX-2	Area = 40.54 m^2 (436.36 ft^2)
Heat exchanger III	HEX-3	Area = 6.56 m^2 (71.58 ft^2)
Reactor	HEATER	Area = 941.87 m^2 (10138.21 ft^2)

F.3 Assumptions for deriving economic equations

The assumptions made by Douglas (1988) in the derivation of the shortcut method equations used in the economic evaluation of the proposed process are shown in Table F-3.

Table F-3: Assumptions made by Douglas (1988) in deriving the economic evaluation equations.

Equation	**Tot.Inv. = 2.36 (Onsite)**
Assumptions	Start-up costs ∼ 0.1 (Fixed capital costs)
	Working capital ∼ 0.15 (Total investment)
	Offsite ∼ 0.45 (Onsite costs)
	Owner's Cost ∼ 0.05 (Onsite + Offsite)
	Contingencies and fees ∼ 0.20 (Onsite + Offsite)
Equation	**O&M = 1.031 (Raw matl. + Util.) + 0.186 (Onsite) + 2.13 (Operating labour) + 0.0256 (Revenue)**
Assumptions	General expenses (SARE) ∼ 0.025 (Revenue)
	Maintenance (Maint.) costs = 0.04 (Fixed capital)
	Supply = 0.15 (Maint.)
	Royalty = 0.03 (Total product costs)
	Tax = Insurance = 0.03 (Fixed capital costs)
	Interest = 0
	Rent = 0

F.4 Parameters used in the economic evaluation

F.4.1 Compressors

Design type F_d	Factor
Centrifugal, motor	1.00
Reciprocating, steam	1.07
Centrifugal, turbine	1.15
Reciprocating, motor	1.29
Reciprocating, gas engine	1.82

Figure F-2: Correction factors for compressors used in equation (6-3) (Guthrie, 1969).

F.4.2 Heat exchangers

Design type	F_d	Design pressure, psi	F_p
Kettle, reboiler	1.35	Up to 150	0.00
Floating head	1.00	300	0.10
U-tube	0.85	400	0.25
Fixed-tube sheet	0.80	800	0.52
		1000	0.55

Figure F-3: Correction factors for heat exchangers used in equation (6-4) (Guthrie, 1969).

Surface area, ft^2	CS/ CS	CS/ Brass	CS/ MO	CS/ SS	SS/ SS	CS/ Monel	Monel/ Monel	CS/ T_i	T_i/ T_i
1000 to 5000	1.00	1.30	2.15	2.81	3.75	3.10	4.25	8.95	13.05

Figure F-4: Parameters for shell and tube material, Fm, used in equation (6-4) (Guthrie, 1969).

F.5 Economic evaluation

The detailed calculation for the economic evaluation is presented below. The shortcut method put forward by Douglas (1988) was used to perform the economic evaluation. The economic evaluation involved determining the total capital investment, which was dependent on the total sum of the installed equipment cost, and the operation and maintenance cost. The cost correlations proposed by Guthrie (1969) were used to determine the installed equipment costs. The parameters needed for the determination of the installed costs for each piece of equipment can be found in Table F-2 (Aspen Plus® results) and Figures F-2 to F-4 (correction factors for the correlations proposed by Guthrie (1969)).

F.5.1 Total capital investment

The total capital investment is associated with the sum of the installed cost of the equipment. From the design simulation performed in Aspen Plus®, the bhp of the compressor and the area of the heat exchangers were obtained.

Compressor installed cost:

$$Compressor = \left(\frac{M\&S}{280}\right)(517.5)(bhp)^{0.82}(2.11 + F_c) \tag{F-11}$$

Using a centrifugal compressor $F_c = 1$. Since the bhp was determined to be 34.32 kW (Table F-2) $F_c = F_d$. Therefore:

$$Compressor = \left(\frac{1501.35}{280}\right)(517.5)(34.32)^{0.82}(2.11 + 1)$$

$$Compressor = \$\ 156\ 734.22$$

Decomposer:

$$Decomp = \left(\frac{M\&S}{280}\right)(101.3)(A)^{0.65}\left(2.29 + \left((F_d + F_p)F_m\right)\right) \tag{F-12}$$

From Table F-2, the area for the decomposer is 406.98 ft². Using stainless steel as the material of construction, $F_m = 2.81$. The selected reactor operating pressure and the decomposer discharge pressure is 3.00 and 4.50 MPa respectively. Therefore $F_p = 0.52$ was selected (800 psi = 5.51 MPa). Choosing a fixed-tube sheet, $F_d = 0.8$.

Therefore,

$$Decomposer = \left(\frac{1501.35}{280}\right)(101.3)(406.98)^{0.65}\left(2.29 + \left((0.8 + 0.52) \times 2.81\right)\right)$$

$$Decomposer = \$\,161\,904.17$$

Heat exchanger I (HEX-1):

From Table F-2, the area for heat exchanger I is 1217.60 ft^2. Using the same assumptions used for the costing of the decomposer for correction factors F_d, F_p and F_m, the cost of heat exchanger I is:

$$HEX - I = \left(\frac{M\&S}{280}\right)(101.3)(A)^{0.65}\left(2.29 + \left((F_d + F_p)F_m\right)\right) \tag{F-13}$$

$$HEX - I = \left(\frac{1501.35}{280}\right)(101.3)(1217.60)^{0.65}\left(2.29 + \left((0.8 + 0.52) \times 2.81\right)\right)$$

$$HEX - I = \$\,330\,069.27$$

Similarly for heat exchangers II and III, the areas are 436.36 ft^2 and 71.58 ft^2 respectively (Table F-2). The costs for heat exchanger II (HEX-2) and heat exchanger III (HEX-3) was calculated as \$ 169 398.06 and \$ 51 874.11 respectively. The area of the reactor (which was designed as a heat exchanger) is 10138.21 ft^2. Using the same correction factors used in the determining of the decomposer and heat exchangers I to III, the cost of the reactor was calculated as \$ 1 143 354.54.

Once the installed costs for all pieces of equipment had been determined, the total onsite cost was determined by the following:

$$Onsite = \sum Installed\ cost \tag{F-14}$$

where:

$$\sum Installed\ cost = Compressor + Decomposer + \tag{F-15}$$
$$HEX - 1 + HEX - 2 + HEX - 3 + Reactor$$

Therefore:

$$\sum Installed\ cost = 156\,734.22 + 161\,904.17 + 330\,069.27 +$$
$$169\,398.06 + 51\,874.11 + 1\,143\,354.54$$
$$Onsite = \$\,2\,013\,334.37$$

The total capital investment is therefore:

$$Tot.Inv. = 2.36\,(Onsite) \tag{F-16}$$
$$Tot.Inv. = 2.36\,(2\,013\,334.37)$$
$$Tot.Inv. = \$4\,751\,469.11 = M\$\,4.75$$

F.5.2 Operation and maintenance cost

The operation and maintenance (O&M) cost associated with the operating and maintaining the hydrate-based desalination processing equipment was determined using the following equation:

$$O\&M = 1.031(Raw\;matl. + Util.) + 0.186(Onsite) \tag{F-17}$$
$$+\; 2.13(Operating\;labor) + 0.0256(Revenue)$$

The operating labor component was calculated from:

$$Operating\;labor = \exp(2.791 + 0.234\ln(capacity)) \tag{F-18}$$

Capacity is based on the processing capacity of the plant i.e. the vinasse feed rate per day.

$$Operating\;labor = \exp(2.791 + 0.234\ln(3333.33))$$
$$Operating\;labor = 108.76$$

The cost of the raw materials (Raw matl.), the utilities (Util.), and revenue were all taken as zero. The reasons for selecting zero were discussed in section 6.9. Dividing the onsite cost by the plant useful life of 20 years in equation (F-16) and substituting the operating labor in the equation, the O&M cost is:

$$O\&M = 1.031(Raw\;matl. + Util.) + 0.186\left(\frac{2\,013\,334.37}{20}\right) + 2.13(Operating\;labor)$$
$$+\; 0.0256(Revenue)$$
$$O\&M = 1.031(0 + 0) + 0.186(Onsite) + 2.13(108.76) + 0.0256(0)$$
$$O\&M = \$\,18\,955.67/day$$

F.5.3 Amortized total capital investment

The amortized total capital investment was dependent on four variables: the plant capacity, the total capital investment, economic plant life (20 years) and continuous discount rate (8 %).

The amortized total capital investment was therefore calculated as follows:

$$Amortized\ tot.inv. = \frac{\left(\frac{\exp(0.08 \times 20)}{\sum_{i=0}^{19} \exp(0.08 \times i)}\right)}{365 \times capacity} \times Tot.inv. \tag{F-19}$$

In equation (F-19), 0.08 represents the continuous discount rate of 8 %.
The summation within the brackets is:

$$\sum_{i=0}^{19} \exp(0.08 \times i) = 0.104$$

Therefore

$$Amortized\ tot.inv. = \frac{\left(\frac{\exp(0.08 \times 20)}{0.104}\right)}{365 \times 3333.33} \times 4\,751\,469.11$$

$$Amortized\ tot.inv. = \$\,0.41/ton$$

F.5.4 Amortized operating and maintenance costs

The amortized O&M costs were determined from equation F-20. The capacity is the vinasse feed rate in ton/day.

$$Amortized\ O\&M = \frac{O\&M}{Capacity} \tag{F-20}$$

$$Amortized\ O\&M = \frac{18\,955.67}{3333.33}$$

$$Amortized\ O\&M = \$\,5.69/ton$$

F.5.5 Total product cost

The total product cost was determined from equation F-21.

$$Total\ product\ cost = Amortized\ tot.inv. + Amortized\ O\&M \tag{F-21}$$
$$Total\ product\ cost = 0.41 + 5.69$$
$$Total\ product\ cost = \$\ 6.09/ton$$